DISS. ETH NO. 24435

Modelling Global Water–Food–Environment–Trade Nexus in the Context of Agricultural Intensification

A thesis submitted to attain the degree of

DOCTOR OF SCIENCES of ETH ZURICH
(Dr. sc. ETH Zurich)

presented by

WENFENG LIU
M.Eng. in Hydrology and Water Resources, Beijing Normal University

born on 01.03.1988

citizen of China

accepted on the recommendation of

Prof. Dr. Rainer Schulin, ETH Zurich, examiner
Prof. Dr. Hong Yang, Eawag, co-examiner
Dr. Karim C. Abbaspour, Eawag, co-examiner
Dr. Michael Obersteiner, IIASA, co-examiner

2017

TO MY GRANDMA

NO PAIN IN THE HEAVEN

Contents

Summary

Modern agriculture is facing a trilemma in the context of population growth and social–economic development: increasing food supply and nutritional quality, reducing resource requirements, and minimizing negative environmental consequences. Current research tackling challenges in agriculture often focuses on one or two aspects of the trilemma and/or is limited to providing a general picture of the challenges. Therefore, there is a need to develop a systematic research framework for investigating trade-offs in the trilemma and to develop pathways to sustain the increasing food supply while mitigating negative impacts of agricultural production.

Grid-based large-scale crop models have been developed as a useful tool to address a variety of agricultural issues, e.g. simulating crop–water–nutrient relations, projecting crop yields under certain agronomic conditions, and quantifying climate change impacts. However, large-scale crop models are rarely used to investigate the water–nutrient–food–environment nexus. Meanwhile, few studies have addressed the role of global food trade in redistributing agricultural resources and environmental impacts in the context of the nexus. Against this background, the present study aimed to develop a large-scale crop model and enhance its capabilities in modelling the global water–food–environment–trade nexus under several agricultural intensification scenarios. Knowledge derived from the study on the nexus is useful in supporting the development of global strategies for addressing the agricultural trilemma.

For this purpose, a grid-based Environmental Policy Integrated Climate was programmed under a Python environment: PEPIC. The PEPIC model was first used to investigate uncertainties derived from an important resource, i.e. the choice of different potential evapotranspiration (PET) estimation methods, on simulating the crop–water relations of maize. The simulations demonstrated substantial differences in PET by using different estimation methods, even in the same climate zone, leading to large uncertainties in simulating crop–water relations in terms of crop water productivity. However, the uncertainties showed varied patterns for different variables, i.e. more significant on water-related variables while less on crop yields. Water availability played an important role in the uncertainties. This information highlights the significance of considering the impacts of different PET methods in crop model application. By using the Penman–Monteith estimation method, the PEPIC model provided the best crop yield estimates and relatively reasonable simulations of evapotranspiration in different climate zones. Therefore, the Penman–

Monteith method was recommended for global crop modelling in the situation of a whole set of required climate variables being available. It was also used in the following sections of this study.

The PEPIC model was then applied to assess global nitrogen (N) losses and trade-offs with yields from three most produced crops – maize, rice, and wheat – by using state-of-the-art crop-specific N input datasets. The simulations showed that a large amount of N was lost to the environment from the three crops, reaching 44 Tg N yr^{-1}. N losses were particularly high in the eastern and southern Asia mainly due to high N inputs there. The N loss intensity, defined as a ratio of N losses to yields, was proposed to reflect trade-offs between N losses and yields. It presented high variations for different countries, indicating diverse environmental impacts for producing the same level of yields. The results also demonstrated that redistributing global N input patterns and improving N fertilization schedules could reduce N losses and yield trade-offs.

Grey water footprint (GWF) is defined as the volume of water that is required to assimilate a load of pollutants to a freshwater body based on existing ambient water quality standards. It is an indicator of water pollution intensity. N and phosphorus (P) losses from global maize cultivation simulated by the PEPIC model were used to investigate the water pollution intensity caused by N and P losses. Some major limitations regarding the assessment of GWF were addressed and ways towards its improvement were proposed. The results showed that GWF relating to N and P loads into water caused by maize production alone had already exceeded the local water availability in many parts of the world. Grey water stress, a ratio of GWF to water availability, showed a more critical situation at the grid level (on finer spatial resolution) than at the watershed level because the former represents the local concentration whereas the latter gives the average situation of the whole watershed.

Agricultural input intensification is an essential option to achieve higher crop production for feeding the ever growing and increasingly affluent world population. In order to identify the appropriate intensification strategies in terms of priority regions and efficient pathways, PEPIC was used to determine N losses and yield trade-offs under five input intensification scenarios considering a range of irrigation and N managements in addition to the baseline. Incremental N losses and yields in response to increased N inputs and irrigated areas presented high spatial variations and negative relationships. Regions where a high level of climatic yield potential has already been achieved had only minor yield benefits but had large N loss potentials under the intensification scenarios. It was found that avoiding intensification in regions with baseline yields higher than 75% of yield potentials, relative increases in N losses can be reduced by 3–193% globally, while compromises in relative yield increases range only between 1% and 23%.

In the final step of the study, the PEPIC model was combined with the Global Trade Analysis Project (GTAP) model to investigate impacts of global food trade on resource

conservation and N loss reduction of the three major crops under the baseline and an intensification scenario regarding enhanced N and irrigation inputs. The results showed that substantial natural resources were conserved with values of 85 km^3 yr^{-1}, 105 km^3 yr^{-1}, and 2333 Gg N yr^{-1} for blue water use, total water use, and N inputs, respectively. The resource conservation was particularly high for blue water use, accounting for more than half of total blue water use of the three crops. Also, a large amount of N losses were avoided through global food trade. These achievements, however, also posed significant pressures on the major food exporting countries in terms of resource losses and export-associated pollution. The study found both resource conservation and N loss reduction would decline under the intensification scenario, although crop yields could largely increase in low agricultural inputs and low yields countries. Therefore, there are double challenges to international food trade: 1) balancing global benefits and environmental impacts on major exporters and 2) balancing the relationship between enhancing country-specific food supply and enlarging global food trade benefits.

In conclusion, the entire analytical framework developed in this study provides an integrated approach for investigating the global water–food–environment–trade nexus in the context of agricultural intensification. This systematic framework is useful for supporting the development of strategies to attenuate the agricultural trilemma. There are high potentials to address agricultural challenges through altering N input patterns, improving N fertilization schedules, efficient input (N and irrigation) intensification, and global food trade.

Zusammenfassung*

Die moderne Landwirtschaft befindet sich bezüglich Bevölkerungswachstum und sozioökonomischer Entwicklung in einem trilateralen Spannungsfeld folgender Ziele: Erhöhung der Lebensmittelversorgung und –qualität, Reduzierung des Ressourcenverbrauchs und Minimierung der negativen Auswirkungen auf die Umwelt. Die aktuelle Forschung konzentriert sich meist auf einen oder zwei der genannten Aspekte oder beschränkt sich auf ein generelles, ganzheitliches Bild des Spannungsfelds. Deshalb bedarf es der Entwicklung systematischer Forschungsmethoden, um die Zielkonflikte innerhalb dieses trilateralen Spannungsfeldes zu analysieren, den wachsenden Lebensmittelbedarf zu decken und gleichzeitig negative Auswirkungen der landwirtschaftlichen Produktion zu vermeiden.

Grossskalige, pixelbasierte Landwirtschaftsmodelle haben sich als nützlich erwiesen für das Simulieren von Beziehungen zwischen Ertrag, Wasser und Nährstoffen, Vorhersage von Ernteerträgen und Quantifizierung von Effekten des Klimawandels. Dennoch werden grossskalige Landwirtschaftsmodelle bisher kaum eingesetzt in der Erforschung des Zusammenhangs zwischen Wasser, Nährstoffen, Lebensmitteln und der Umwelt. Ähnlich wenige Studien befassen sich mit der Rolle des globalen Lebensmittelhandels in der Verteilung landwirtschaftlicher Ressourcen und Auswirkungen auf die Umwelt. Vor diesem Hintergrund hat die vorliegende Arbeit zum Ziel, ein grossskaliges, pixelbasiertes Landwirtschaftsmodell zu entwickeln und dessen Funktionalitäten zur Abbildung des globalen Zusammenhangs zwischen Wasser, Nahrungsmitteln, Umwelt und Handel unter mehreren Szenarien intensivierter landwirtschaftlicher Entwicklungen zu erweitern. Die Analyse dieser Zusammenhänge trägt zur Entwicklung von globalen Strategien bei, um das Spannungsfeld, in dem sich die Landwirtschaft befindet, zu entschärfen.

Zu diesem Zweck wurde ein pixelbasiertes „Environmental Policy Integrated Climate“-Modell (PEPIC) in Python entwickelt. Mit dem PEPIC-Modell wurden die Unsicherheiten des Verhältnisses von Ertrag zu Wasserverbrauch von Mais abgeschätzt, die durch die Wahl verschiedener Methoden zur Schätzung der potentiellen Evapotranspiration (PET) entstehen. Die Simulationen wiesen sogar in klimatisch ähnlichen Gebieten erhebliche Unterschiede in der PET-Abschätzung auf, was zu grossen Unsicherheiten in dem Ertrag-Wasserverbrauch-Verhältnis führt.

* Translated by Lorenz Ammann from Eawag and Dr. Christian Folberth from IIASA

Die Unsicherheiten waren allerdings nicht in allen Variablen gleich gross; sie waren beispielsweise erheblich grösser für Variablen die direkt mit Wasser in Verbindung stehen als für die Ernteerträge. Auch die Wasserverfügbarkeit spielte eine grosse Rolle für die Unsicherheiten. Dies zeigt wie wichtig es ist, die Auswirkungen verschiedener PET-Methoden in Landwirtschaftsmodellen zu berücksichtigen. Die Penman-Monteith-Methode (PM) erlaubte – eingebettet in PEPIC – die zuverlässigsten Schätzungen der Ernteerträge und realistische Schätzungen der Evapotranspirationsraten in verschiedenen Klimazonen. Deshalb wurde die PM-Methode zur Modellierung von globalen Ernteerträgen empfohlen, für den Fall, dass Daten zu den benötigten Klimavariablen zur Verfügung stehen. Die PM-Methode wurde somit auch in den folgenden Abschnitten dieser Arbeit verwendet.

Das PEPIC-Modell wurde verwendet um die globalen Stickstoffverluste (N-Verluste) abzuschätzen und einen Kompromiss zwischen N-Verlust und Ernteerträgen für die drei Hauptgetreidesorten Mais, Reis und Weizen zu ermitteln. Dafür wurden Daten zu globalen Stickstoffgaberaten verwendet, die dem neusten Wissensstand entsprechen. Die Simulationen zeigen, dass – alle drei Getreidesorten zusammengenommen – grosse Mengen an Stickstoff (N) in die Umwelt gelangen, insgesamt 44 Tg pro Jahr. Die N-Verluste waren besonders hoch in Ost- und Südasien, was vor allem auf die hohen N-Einträge in diesen Regionen zurückzuführen ist. Das quantitative Verhältnis zwischen N-Verlust und Ernteertrag wurde vorgeschlagen um den Kompromiss zwischen diesen beiden Grössen besser abzubilden. Dieses Verhältnis unterschied sich stark in verschiedenen Nationen, was darauf hindeutet, dass ähnliche Ernteerträge mit grossen Unterschieden in den Auswirkungen auf die Umwelt einhergehen können. Diese Resultate zeigen auch, dass eine Umverteilung der globalen N-Gaben und eine Verbesserung der Düngungspläne den Zielkonflikt zwischen einem möglichst hohen Ertrag und einem möglichst kleinen N-Verlust entschärfen könnten.

Der Grauwasserfussabdruck (GWF) ist definiert als das Volumen Wasser, das benötigt wird, um eine bestimmte Fracht an Schadstoffen zu verdünnen, so dass bestehende Wasserqualitätsstandards gerade noch eingehalten werden können. Der GWF ist also ein Indikator für die Intensität der Wasserverschmutzung. Abschätzungen der N- und Phosphor-(P)-Verluste aus Maisanbauflächen weltweit durch das PEPIC-Modell wurden verwendet, um die Intensität der Wasserverschmutzung, verursacht durch N und P, abzuschätzen. Die Verwendung des GWF wurde kritisch untersucht und es wurden Verbesserungsvorschläge für die Verwendung des GWF angeführt. Die Resultate zeigen, dass in vielen Regionen der Welt der GWF, der allein durch die N- und P-Einträge des Maisanbaus verursacht wird, die lokale Wasserverfügbarkeit übersteigt. Die Grauwasserbelastung, also das Verhältnis zwischen GWF und Wasserverfügbarkeit, war

höher auf der Pixelskala als auf der Ebene von Einzugsgebieten, weil erstere die tatsächliche lokale Konzentrationen abbildet, während letztere die Werte über das Einzugsgebiete mittelt.

Die Intensivierung der Bewässerung und der Nährstoffgabe ist eine wichtige Möglichkeit zur Erreichung höherer Ernteerträge, um den steigenden Nahrungsmittelbedarf einer stetig wachsenden und zunehmend vermögenderen Weltbevölkerung zu decken. Um die geeignetsten Strategien zur Intensivierung zu wählen, wurde das Spannungsfeld zwischen N-Verlusten und Ernteerträgen unter fünf verschiedenen Intensivierungsszenarien mit PEPIC untersucht. Die Zunahme der N-Verluste und der Erträge mit höherer N-Gabe und zunehmender Bewässerung zeigten deutliche räumliche Unterschiede und negative Korrelationen. Regionen in denen die klimatisch möglichen Erträge bereits annähernd erreicht wurden, zeichneten sich aus durch geringe Zunahmen der Erträge bei hohen zusätzlichen N-Verlusten in allen Szenarien. Es wurde gezeigt, dass, falls keine Intensivierung erfolgt in Gebieten in denen die Erträge höher als 75% des maximal möglichen Ertrags sind, die relative Zunahme der globalen N-Verluste um 3–193% reduziert werden kann, während die relative Zunahme der globalen Erträge um lediglich 1–23% reduziert wird.

Im letzten Teil der vorliegenden Arbeit wurde das PEPIC-Modell mit einem globalen Handelsmodell, Global Trade Analysis Project (GTAP), kombiniert um den Einfluss des globalen Handels mit Nahrungsmitteln auf die Erhaltung von Ressourcen und Reduzierung von Umweltbelastungen abzuschätzen. Dies wurde für die drei Hauptgetreidesorten unter dem Basisszenario umgesetzt, sowie den Intensivierungsszenarien, die ausgeglichenere Düngergabe im Vergleich zum Basisszenario annehmen. Die Resultate zeigen, dass substantielle Einsparungen beim Ressourcenverbrauch erreicht werden können: der Verbrauch blauen Wassers wurde um 85 $km^3\ yr^{-1}$, der totale Wasserverbrauch um 105 $km^3\ yr^{-1}$ und die N-Gabe um 2333 Gg N yr^{-1} reduziert. Die Einsparungen waren besonders hoch im Falle von blauem Wasser und beliefen sich auf mehr als die Hälfte des totalen Verbrauchs an blauem Wasser für die drei Getreidesorten. Der globale Handel vermochte auch eine grosse Menge an Umweltverschmutzung zu verhindern. Diese Errungenschaften erhöhten jedoch auch den Druck auf die lebensmittelexportierenden Länder im Zusammenhang mit Ressourcenverbrauch und exportbedingten N-Verlusten. Im Falle von ausgeglicheneren Szenarien der Inputintensivierung würde der Ressourcenerhalt abnehmen und die Umweltverschmutzung würde weniger rasch reduziert werden, obwohl die Erträge in Ländern mit geringen Düngergaben und niedrigen Erträgen grösstenteils zunehmen könnten. Hierauf basierend gibt es folgende zwei Herausforderungen im internationalen Lebensmittelhandel: 1) Ausgleich zwischen dem globalen Nutzen und den Umweltauswirkungen der Hauptexporteure und 2) Ausgleich zwischen der Zunahme des länderspezifischen Nahrungsmittelangebots und des Nutzens des globalen Lebensmittelhandels.

Zusammenfassend lässt sich sagen, dass die analytischen Werkzeuge, die in dieser Studie entwickelt wurden, einen ganzheitlichen Ansatz darstellen, mit dem der globale Zusammenhang zwischen Wasser, Nahrungsmitteln, Umwelt und Handel im Kontext der landwirtschaftlichen Intensivierung beurteilt werden kann. Diese Werkzeuge sind nützlich, um Strategien für die Entschärfung des landwirtschaftlichen trilateralen Spannungsfeldes zu entwerfen. Die Veränderung der Muster des Stickstoffeintrags, die Verbesserung von Düngungsplänen, effiziente Intensivierung der Produktionsmittel (N und Bewässerung) und der globale Nahrungsmittelhandel sind vielversprechende Methoden, um die landwirtschaftlichen Herausforderungen zu adressieren.

Chapter 1

Introduction

1.1 Background and motivation

1.1.1 Agricultural trilemma in the 21st century

Global food security is facing great challenges due to population growth, a shift to more animal-based diets, and expanding areas of biofuel crops (Bodirsky et al., 2015; Tilman et al., 2011). However, resources required as inputs for agricultural production such as water, fertile land, and nutrients are not limitless. Moreover, crop production is causing substantial environmental problems, particularly due to nitrogen (N) and phosphorus (P) losses to the environment (Erisman et al., 2013; Galloway et al., 2003; Galloway et al., 2008; Sutton et al., 2013) and excessive water consumption for irrigation (Gleeson et al., 2012; Rodell et al., 2009), but also due to greenhouse gas (GHG) emissions, soil degradation and biodiversity loss. Therefore, modern agriculture is facing a trilemma as it strives to increase the quantity and nutritional quality of crop plant production, to limit the consumption of resources such as water and nutrients for plant production, and to minimize adverse environmental impacts (Figure 1-1).

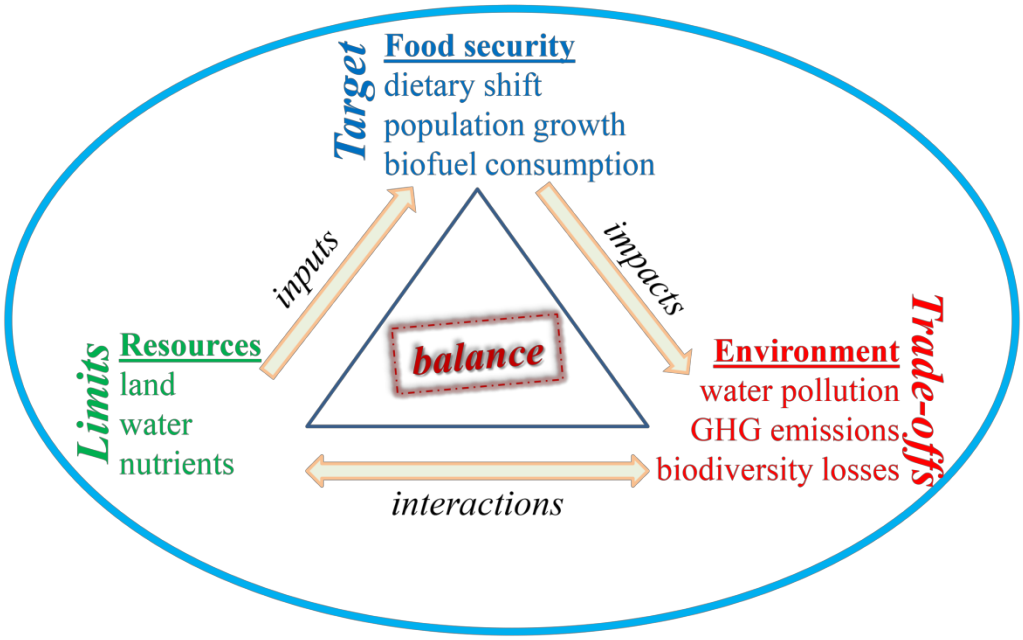

Figure 1-1. Description of agricultural trilemma in the 21st century.

In order to meet the food requirements of feeding 9 billion people by 2050 (Godfray et al., 2010), global food production was expected to be doubled relative to the situation around 2000 (Bodirsky et al., 2015; Tilman et al., 2011). However, several studies indicated that the trend of crop yield improvements had stagnated in some major food-producing regions in the world (Iizumi et al., 2014; Ray et al., 2013; Ray et al., 2012). The continuation of the global trend could mean that increasing amounts of agricultural inputs are poured into the croplands but the returns will diminish.

On the other hand, agricultural production has already consumed a large amount of resources and also caused major impacts on environment and ecosystems (Foley et al., 2005; Foley et al., 2011). An important example is global water consumption. As the largest water user, agriculture consumes about 85% of global freshwater withdrawals (Shiklomanov, 2003). Agricultural water consumption has posed significant pressures on water resources (Oki and Kanae, 2006). Indeed, water scarcity is already a critical worldwide concern (Fedoroff et al., 2010). Substantial water consumption for irrigation in many areas, notably India, Pakistan, China, and the USA, has been exacerbating groundwater depletion (Dalin et al., 2017; Gleeson et al., 2012; West et al., 2014).

Nitrogen is another important resource essential for crop growth. About 120 Tg N yr^{-1} (Tg = 10^{12} g) N fertilizer was applied to global croplands in 2010 (Fowler et al., 2013). Although it seems that unlimited amounts of N can be produced using the Haber–Bosch processes (Erisman et al., 2008), the energy requirements for it may set an upper limit, as about 2% of global energy use has already been consumed for the production of reactive N (Sutton et al., 2013). More seriously, the excessive application of N in the farmlands for agricultural production has led to a large amount of N losses. It was estimated that about half of total N inputs to croplands were lost to the environment in 2000 (Liu et al., 2010) and about 80 Tg N yr^{-1} was transported to the ocean in 2010 (Fowler et al., 2013). N losses have already significantly transgressed the safe planetary boundary for N (Rockström et al., 2009; Steffen et al., 2015), which is resulting in substantial environmental problems, e.g. serious eutrophication and wide-spreading dead zones of marine ecosystems (Conley et al., 2009; Diaz and Rosenberg, 2008), biodiversity losses (Clark and Tilman, 2008), soil acidification in croplands (Liu et al., 2013), and enlarged global GHG emissions from agricultural production (Bouwman et al., 2013a).

To address the great challenges of the agricultural trilemma in the 21st century, it is important to develop an integrated approach to simultaneously consider the interplays among agricultural resources, crop yields, and environmental consequences. A better understanding of the interactions can help design effective pathways towards sustainable agricultural development (Galloway et al., 2008).

1.1.2 Application of large-scale crop models and the challenges

Agronomic crop models are a useful research tool for understanding the interactions among resource uses, food production, and environmental impacts. Models can represent the complex processes linking crop growth processes, including evapotranspiration (ET), photosynthesis and carbon assimilation, with environmental processes, including carbon cycling, nutrient turnover and hydrological processes, and agricultural management schemes. Many crop models have been developed and widely applied, e.g. APSIM (Keating et al., 2003), CropSyst (Stockle et al., 2003), EPIC (Williams et al., 1984), DSSAT (Jones et al., 2003), STICS (Brisson et al., 2003), and WOFOST (Vandiepen et al., 1989). All these models were originally site-based models. In order to address the agricultural water–food–environmental nexus with a global perspective, grid-based and spatially explicit large-scale crop models are required.

Since the late 1990s, coupling spatial analytical tools (such as Geographic Information System and other computer programing methods) with site-based crop models to improve the spatial representation and visualization ability on large scales has drawn growing attention. So far, many spatially explicit crop models have been developed, e.g. GEPIC (Liu et al., 2007), LPJmL (Müller and Robertson, 2014), pAPSIM and pDSSAT (Elliott et al., 2014), and PEGASUS (Deryng et al., 2011). Until now, large-scale crop models have been mainly used to simulate crop yields (Müller et al., 2017), to investigate crop–water relations (Liu, 2009), and to quantify the impacts of climate change (Deryng et al., 2016; Rosenzweig et al., 2014) including extreme events (Schauberger et al., 2017), among others. However, there are still significant challenges to using the large-scale crop models to address the global agricultural trilemma. Assessment of environmental impacts, e.g. N losses, using crop models was mostly implemented at local or regional scales (Molina-Herrera et al., 2016; Qiu et al., 2011). There are only a few applications of large-scale crop models for investigating the environmental consequences of global crop production (Del Grosso et al., 2009). A comprehensive evaluation of the water–food–environmental nexus by using large-scale crop models is still absent on a global scale with high spatial resolution.

Agricultural pollutants entering water bodies can deteriorate water quality. It can also intensify water scarcity by making the available water not useable due to poor quality. The grey water footprint (GWF) measures the water required to dilute these pollutants to meet the ambient water quality standards (Hoekstra et al., 2011). It is an indicator of water pollution intensity. Large-scale crop models have been used to assess global GWF related to crop production (Wu et al., 2012). However, there are some shortcomings in the existing literature on GWF concerning the selection of water quality standards (Franke et al., 2013), multiple pollutants (Liu et al., 2012),

and geographical scales (Mekonnen and Hoekstra, 2014). A proper assessment of the environmental impact measured with GWF is required to address these limitations.

There are many studies on uncertainties associated with large-scale crop simulations from different resources, e.g. soil datasets (Folberth et al., 2016), model parameters (Xiong et al., 2016), spatial resolution (Folberth et al., 2012), and model structures (Müller et al., 2017). However, an important factor contributing to the uncertainties of large-scale simulations, i.e. the choice of different potential ET (PET) estimation methods, has received little attention (Balkovič et al., 2013). A detailed investigation of the impacts of different PET methods on global crop simulation is required, as it is one of the most fundamental processes regulating crop growth (Sau et al., 2004).

1.1.3 Strategies for addressing the agricultural trilemma

Facing the great challenges in agriculture, there have been many studies addressing the problems and proposing solutions. They mainly concern three aspects: improving resources use efficiency, agricultural intensification, and global virtual water trade.

Limited available water resources and tremendous N losses require that these resources are used in a more efficient way. There are many studies on improving water use efficiency (Brauman et al., 2013; Jagermeyr et al., 2016) and N use efficiency (Cui et al., 2014; Zhang, 2017; Zhang et al., 2015). However, previous studies often only included one input variable, either water or N, but rarely considered their interactions. An important example considering the interactions was conducted by the Global Landscapes Initiative group at the University of Minnesota (Mueller et al., 2012; West et al., 2014). A yield-response model was developed for different climate zones and then used to quantify the attainable yields and the associated multiple resources requirements (e.g. water and N) to close yield gaps for each zone (Mueller et al., 2012). They proposed reallocating global N inputs for the purpose of reducing N surplus in the excessive application regions and improving N use efficiency (Mueller et al., 2017; Mueller et al., 2014). However, they only focused on investigating the water–nutrient–food relations, but ignored the environment impacts involved.

Given the major concerns about the future food supply to feed the expected 9 billion people by 2050, most previous studies have concentrated on quantifying potential yields, as well as how to close yield gaps through genotypes/breeding and plant protection, as well as water and nutrients management, i.e. agricultural intensification (Garnett et al., 2013). In the past, a doubling of crop production was achieved with a 4- to 5-fold increase in fertilizer application (especially N fertilizer by 7- to 8-fold) and a 2-fold increase in the area of irrigated croplands and number of agricultural machines (Pretty, 2008). Agricultural intensification will remain the major

way to increase food production in the future (Foley et al., 2011) due to the limitation of land resources. Whereas, continuing agricultural intensification can have great impacts on the planet's environment and ecosystems (Phelps et al., 2013). For instance, the CO_2–C equivalent GHG emissions from agriculture were projected to reach ~3 Gt y^{-1} by 2050 if the current intensification trend is unchanged (Tilman et al., 2011). In addition, global cropping systems demonstrated different scopes for improving efficiency and also presented diverse nutrient imbalances in the course of agricultural development and intensification (Carberry et al., 2013; Vitousek et al., 2009). It implies that some regions may not be suitable for intensification due to high marginal increase in N losses and low marginal increase in yields. Therefore, it is important to identify priority regions for implementing efficient agricultural intensification practices. This is particularly important for achieving global food security while alleviating environmental impacts (Chen et al., 2014; Lu et al., 2015).

Due to the uneven spatial distribution of global water resources and increasing water scarcity in many regions in the world, the concept of "virtual water" has been put forward as a strategy to attenuate water stress for food importing countries (Allan, 1993; Allan, 1998). Virtual water refers to the amount of water involved in the production of a good or service. Through international or interregional food trade, water is exported from exporting countries to importing countries in a virtual form, i.e. embodied in the traded commodity. Besides this, it was demonstrated that virtual water trade also saved a large amount of global water resources through increasing overall water use efficiency (Chapagain et al., 2005; Konar et al., 2013; Yang et al., 2006). In addition to water, other agricultural resources, e.g. crop land and N inputs, and environmental impacts, e.g. water pollution, are also involved in and affected by international food trade. However, previous studies have intensively focused on water but less on other agricultural elements (Dalin and Rodriguez-Iturbe, 2016; Oita et al., 2016). There are only a few integrated assessments of the impacts of food trade on the environment that simultaneously take several agricultural resources and environmental impacts into account (Martinez-Melendez and Bennett, 2016). A main constraint on the study at the global level is the lack of crop-specific data on resource consumption and pollution emission with a high spatial resolution, apart from water. For instance, global agricultural N and P inputs and the associated losses were largely evaluated by considering the agricultural sector as a whole (Bouwman et al., 2013b). There is a need to conduct crop-specific assessments of agricultural resources consumption and related environmental impacts to provide detailed information for evaluating the overall impacts of global food trade.

1.2 Objectives of the research

The overall objective of this study was to assess the water–food–environment–trade nexus in the context of agricultural input intensification by developing and applying a systematic modelling framework. The specific tasks were:

- To develop a grid-based large-scale crop model—Python-based Environmental Policy Integrated Climate (PEPIC) and to investigate the impacts of the choice of different PET estimation methods on simulating crop–water relations;
- To use the PEPIC model for assessing crop-specific trade-offs between N losses and yields from major crop cultivations on a global scale;
- To address agricultural N and P water pollution intensity measured by GWF and propose enhanced approaches for the assessment of agricultural GWF;
- To explore pathways towards crop yields improvements with reduced environmental pollution in the context of agricultural input intensification;
- To explore the overall impacts of global food trade on resource conservation and pollution reduction by combining PEPIC with a global trade model—Global Trade Analysis Project (GTAP) in the analysis.

1.3 Contents of the dissertation

Following this introduction, the dissertation consists of five research chapters (Chapters 2–6) and a general conclusion chapter (Chapter 7).

Chapter 2 introduces the PEPIC model and applies it to investigate the impacts of five PET estimation methods, i.e. Baier–Robertson, Hargreaves, Penman, Penman–Monteith and Priestley–Taylor, on simulating crop yields, crop water use, and crop water productivity of maize globally at a spatial resolution of 30 arc minutes. Performance in modelling the crop–water relations by using the five PET estimation methods is evaluated.

Chapter 3 extends the PEPIC model for estimating N losses from the cultivation of three major crops, i.e. maize, rice, and wheat, by using state-of-the-art crop-specific N input datasets. An indicator—N loss intensity—is put forward to assess the trade-offs between N losses and crop yields. Mitigation scenarios in terms of spatial redistribution of N inputs and improved N fertilization are proposed to reduce the trade-offs.

Chapter 4 quantifies the agricultural pollution intensity measured by GWF due to N and P losses to water from global maize cultivation. Some major limitations in the literature related to the assessment of GWF are addressed and ways towards its improvement are proposed.

Chapter 5 compares five agricultural input intensification scenarios regarding irrigated cultivation areas and N inputs. Hotspots with high improvements in crop yields and/or high increases in N losses under different intensification scenarios are identified. The relationship between incremental yields and incremental N losses relative to incremental N inputs is determined. A strategy to improving crop yields with reduced N losses is proposed based on the determined relationship.

Chapter 6 combines the PEPIC model with the global trade model GTAP to assess the environmental impacts of global food trade in the context of agricultural intensification. Conservation in agricultural resources (blue water use, total water use, and N inputs) and reduction in environmental pollution (N losses) are estimated for the baseline year 2000 and an intensification scenario.

Chapter 7 draws the conclusions of the entire study regarding pathways to address the agricultural trilemma through better understanding the water–food–environment–trade nexus. An outlook is also provided pointing out the significance of further studies on enhancing the water–nutrient–food–environment benefits on a global scale.

1.4 References

Allan, J., 1993. Fortunately there are substitutes for water otherwise our hydro-political futures would be impossible, In: Priorities for water resources allocation and management, ODA, London, pp. 13–26.

Allan, J.A., 1998. Virtual water: A strategic resource global solutions to regional deficits. Ground Water, 36(4): 545–546.

Balkovič, J. et al., 2013. Pan-European crop modelling with EPIC: Implementation, up-scaling and regional crop yield validation. Agric. Syst., 120: 61–75.

Bodirsky, B.L. et al., 2015. Global food demand scenarios for the 21st century. PLoS One, 10(11): e0139201.

Bouwman, A.F. et al., 2013a. Global trends and uncertainties in terrestrial denitrification and N2O emissions. Philos. Trans. R. Soc. London, Ser. B, 368(1621): 20130112.

Bouwman, L. et al., 2013b. Exploring global changes in nitrogen and phosphorus cycles in agriculture induced by livestock production over the 1900–2050 period. Proc. Natl. Acad. Sci. U.S.A., 110(52): 20882–20887.

Brauman, K.A., Siebert, S. and Foley, J.A., 2013. Improvements in crop water productivity increase water sustainability and food security—a global analysis. Environ. Res. Lett., 8(2): 024030.

Brisson, N. et al., 2003. An overview of the crop model STICS. Eur. J. Agron., 18(3–4): 309–332.

Carberry, P.S. et al., 2013. Scope for improved eco-efficiency varies among diverse cropping systems. Proc. Natl. Acad. Sci. U.S.A., 110(21): 8381–8386.

Chapagain, A.K., Hoekstra, A.Y. and Savenije, H.H., 2005. Saving water through global trade. Value of water research report series no. 17. UNESCO-IHE Institute for Water Education, Delft.

Chen, X. et al., 2014. Producing more grain with lower environmental costs. Nature, 514(7523): 486–9.

Clark, C.M. and Tilman, D., 2008. Loss of plant species after chronic low-level nitrogen deposition to prairie grasslands. Nature, 451(7179): 712–715.

Conley, D.J. et al., 2009. Controlling eutrophication: nitrogen and phosphorus. Science, 323(5917): 1014–1015.

Cui, Z.L. et al., 2014. Closing the N-use efficiency gap to achieve food and environmental security. Environ. Sci. Technol., 48(10): 5780–5787.

Dalin, C. and Rodriguez-Iturbe, I., 2016. Environmental impacts of food trade via resource use and greenhouse gas emissions. Environ. Res. Lett., 11(3): 035012.

Dalin, C., Wada, Y., Kastner, T. and Puma, M.J., 2017. Groundwater depletion embedded in international food trade. Nature, 543(7647): 700–704.

Del Grosso, S.J. et al., 2009. Global scale DAYCENT model analysis of greenhouse gas emissions and mitigation strategies for cropped soils. Global Planet. Change, 67(1–2): 44–50.

Deryng, D. et al., 2016. Regional disparities in the beneficial effects of rising CO2 concentrations on crop water productivity. Nat. Clim. Change, 6(8): 786–790.

Deryng, D., Sacks, W.J., Barford, C.C. and Ramankutty, N., 2011. Simulating the effects of climate and agricultural management practices on global crop yield. Global Biogeochem. Cycles, 25: GB2006.

Diaz, R.J. and Rosenberg, R., 2008. Spreading dead zones and consequences for marine ecosystems. Science, 321(5891): 926–929.

Elliott, J. et al., 2014. The parallel system for integrating impact models and sectors (pSIMS). Environ. Modell. Software, 62: 509–516.

Erisman, J.W. et al., 2013. Consequences of human modification of the global nitrogen cycle. Philos. Trans. R. Soc. London, Ser. B, 368(1621): 20130116.

Erisman, J.W., Sutton, M.A., Galloway, J., Klimont, Z. and Winiwarter, W., 2008. How a century of ammonia synthesis changed the world. Nat. Geosci., 1(10): 636–639.

Fedoroff, N.V. et al., 2010. Radically rethinking agriculture for the 21st century. Science, 327(5967): 833–834.

Folberth, C. et al., 2016. Uncertainty in soil data can outweigh climate impact signals in global crop yield simulations. Nat. Commun., 7: 11872.

Folberth, C., Yang, H., Wang, X.Y. and Abbaspour, K.C., 2012. Impact of input data resolution and extent of harvested areas on crop yield estimates in large-scale agricultural modeling for maize in the USA. Ecol. Modell., 235: 8–18.

Foley, J.A. et al., 2005. Global consequences of land use. Science, 309(5734): 570–573.

Foley, J.A. et al., 2011. Solutions for a cultivated planet. Nature, 478(7369): 337–342.

Fowler, D. et al., 2013. The global nitrogen cycle in the twenty-first century. Philos. Trans. R. Soc. London, Ser. B, 368(1621): 20130164.

Franke, N., Hoekstra, A. and Boyacioglu, H., 2013. Grey water footprint accounting: Tier 1 supporting guidelines. Value of water research report series No. 17. UNESCO-IHE Institute for Water Education, Delft.

Galloway, J.N. et al., 2003. The nitrogen cascade. Bioscience, 53(4): 341–356.

Galloway, J.N. et al., 2008. Transformation of the nitrogen cycle: Recent trends, questions, and potential solutions. Science, 320(5878): 889–892.

Garnett, T. et al., 2013. Sustainable intensification in agriculture: Premises and Policies. Science, 341(6141): 33–34.

Gleeson, T., Wada, Y., Bierkens, M.F.P. and van Beek, L.P.H., 2012. Water balance of global aquifers revealed by groundwater footprint. Nature, 488(7410): 197–200.

Godfray, H.C. et al., 2010. Food security: the challenge of feeding 9 billion people. Science, 327(5967): 812–8.

Hoekstra, A.Y., Chapagain, A.K., Aldaya, M.M. and Mekonnen, M.M., 2011. The water footprint assessment manual: Setting the global standard. Earthscan, London, UK.

Iizumi, T. et al., 2014. Historical changes in global yields: major cereal and legume crops from 1982 to 2006. Global Ecol. Biogeogr., 23(3): 346–357.

Jagermeyr, J. et al., 2016. Integrated crop water management might sustainably halve the global food gap. Environ. Res. Lett., 11(2): 025002.

Jones, J.W. et al., 2003. The DSSAT cropping system model. Eur. J. Agron., 18(3–4): 235–265.

Keating, B.A. et al., 2003. An overview of APSIM, a model designed for farming systems simulation. Eur. J. Agron., 18(3–4): 267–288.

Konar, M., Hussein, Z., Hanasaki, N., Mauzerall, D.L. and Rodriguez-Iturbe, I., 2013. Virtual water trade flows and savings under climate change. Hydrol. Earth Syst. Sci., 17(8): 3219–3234.

Liu, C., Kroeze, C., Hoekstra, A.Y. and Gerbens-Leenes, W., 2012. Past and future trends in grey water footprints of anthropogenic nitrogen and phosphorus inputs to major world rivers. Ecol. Indic., 18: 42–49.

Liu, J., 2009. A GIS-based tool for modelling large-scale crop–water relations. Environ. Modell. Software, 24(3): 411–422.

Liu, J., Williams, J.R., Zehnder, A.J.B. and Yang, H., 2007. GEPIC – modelling wheat yield and crop water productivity with high resolution on a global scale. Agric. Syst., 94(2): 478–493.

Liu, J. et al., 2010. A high-resolution assessment on global nitrogen flows in cropland. Proc. Natl. Acad. Sci. U.S.A., 107(17): 8035–8040.

Liu, X. et al., 2013. Enhanced nitrogen deposition over China. Nature, 494(7438): 459–62.

Lu, Y. et al., 2015. Addressing China's grand challenge of achieving food security while ensuring environmental sustainability. Sci. Adv., 1(1): e1400039.

Martinez-Melendez, L.A. and Bennett, E.M., 2016. Trade in the US and Mexico helps reduce environmental costs of agriculture. Environ. Res. Lett., 11(5): 055004.

Mekonnen, M.M. and Hoekstra, A.Y., 2014. Water footprint benchmarks for crop production: A first global assessment. Ecol. Indic., 46: 214–223.

Molina-Herrera, S. et al., 2016. A modeling study on mitigation of N2O emissions and NO3 leaching at different agricultural sites across Europe using LandscapeDNDC. Sci. Total Environ., 553: 128–140.

Mueller, N.D. et al., 2012. Closing yield gaps through nutrient and water management. Nature, 490(7419): 254–257.

Mueller, N.D. et al., 2017. Declining spatial efficiency of global cropland nitrogen allocation. Global Biogeochem. Cycles, 31(2): 245–257.

Mueller, N.D. et al., 2014. A tradeoff frontier for global nitrogen use and cereal production. Environ. Res. Lett., 9(5): 054002.

Müller, C. et al., 2017. Global gridded crop model evaluation: benchmarking, skills, deficiencies and implications. Geosci. Model Dev., 10(4): 1403–1422.

Müller, C. and Robertson, R.D., 2014. Projecting future crop productivity for global economic modeling. Agr. Econ., 45(1): 37–50.

Oita, A. et al., 2016. Substantial nitrogen pollution embedded in international trade. Nat. Geosci., 9(2): 111–115.

Oki, T. and Kanae, S., 2006. Global hydrological cycles and world water resources. Science, 313(5790): 1068–1072.

Phelps, J., Carrasco, L.R., Webb, E.L., Koh, L.P. and Pascual, U., 2013. Agricultural intensification escalates future conservation costs. Proc. Natl. Acad. Sci. U.S.A., 110(19): 7601–6.

Pretty, J., 2008. Agricultural sustainability: concepts, principles and evidence. Philos. Trans. R. Soc. London, Ser. B, 363(1491): 447–465.

Qiu, J.J. et al., 2011. GIS-model based estimation of nitrogen leaching from croplands of China. Nutr. Cycling Agroecosyst., 90(2): 243–252.

Ray, D.K., Mueller, N.D., West, P.C. and Foley, J.A., 2013. Yield trends are insufficient to double global crop production by 2050. PLoS One, 8(6): e66428.

Ray, D.K., Ramankutty, N., Mueller, N.D., West, P.C. and Foley, J.A., 2012. Recent patterns of crop yield growth and stagnation. Nat. Commun., 3: 1293.

Rockström, J. et al., 2009. A safe operating space for humanity. Nature, 461(7263): 472–476.

Rodell, M., Velicogna, I. and Famiglietti, J.S., 2009. Satellite-based estimates of groundwater depletion in India. Nature, 460(7258): 999–1002.

Rosenzweig, C. et al., 2014. Assessing agricultural risks of climate change in the 21st century in a global gridded crop model intercomparison. Proc. Natl. Acad. Sci. U.S.A., 111(9): 3268–3273.

Sau, F., Boote, K.J., Bostick, W.M., Jones, J.W. and Minguez, M.I., 2004. Testing and improving evapotranspiration and soil water balance of the DSSAT crop models. Agron. J., 96(5): 1243–1257.

Schauberger, B. et al., 2017. Consistent negative response of US crops to high temperatures in observations and crop models. Nat. Commun., 8: 13931.

Shiklomanov, I.A., 2003. World water resources at the beginning of the 21st century. Cambridge University Press, Cambridge.

Steffen, W. et al., 2015. Sustainability. Planetary boundaries: guiding human development on a changing planet. Science, 347(6223): 1259855.

Stockle, C.O., Donatelli, M. and Nelson, R., 2003. CropSyst, a cropping systems simulation model. Eur. J. Agron., 18(3–4): 289–307.

Sutton, M.A. et al., 2013. Our Nutrient World: the challenge to produce more food and energy with less pollution. Centre for Ecology and Hydrology (CEH).

Tilman, D., Balzer, C., Hill, J. and Befort, B.L., 2011. Global food demand and the sustainable intensification of agriculture. Proc. Natl. Acad. Sci. U.S.A., 108(50): 20260–20264.

Vandiepen, C.A., Wolf, J., Vankeulen, H. and Rappoldt, C., 1989. WOFOST – a simulation model of crop production. Soil Use Manage., 5(1): 16–24.

Vitousek, P.M. et al., 2009. Nutrient imbalances in agricultural development. Science, 324(5934): 1519–1520.

West, P.C. et al., 2014. Leverage points for improving global food security and the environment. Science, 345(6194): 325–328.

Williams, J.R., Jones, C.A. and Dyke, P.T., 1984. A modeling approach to determining the relationship between erosion and soil productivity. T. ASAE, 27(1): 129–144.

Wu, M., Chiu, Y. and Demissie, Y., 2012. Quantifying the regional water footprint of biofuel production by incorporating hydrologic modeling. Water Resour. Res., 48: W10518.

Xiong, W. et al., 2016. Calibration-induced uncertainty of the EPIC model to estimate climate change impact on global maize yield. J. Adv. Model. Earth Syst., 8(3): 1358–1375.

Yang, H., Wang, L., Abbaspour, K.C. and Zehnder, A.J.B., 2006. Virtual water trade: an assessment of water use efficiency in the international food trade. Hydrol. Earth Syst. Sci., 10(3): 443–454.

Zhang, X., 2017. BIOGEOCHEMISTRY A plan for efficient use of nitrogen fertilizers. Nature, 543(7645): 322–323.

Zhang, X. et al., 2015. Managing nitrogen for sustainable development. Nature, 528(7580): 51–59.

Chapter 2

Global investigation of impacts of PET methods on simulating crop–water relations for maize

Based on

Global investigation of impacts of PET methods on simulating crop–water relations for maize. Agricultural and Forest Meteorology, 221: 164–175. (2016)

Authors

Wenfeng Liu[a], Hong Yang[a,b], Christian Folberth[c,d], Xiuying Wang[e], Qunying Luo[f], Rainer Schulin[g]

[a]*Eawag, Swiss Federal Institute of Aquatic Science and Technology, Ueberlandstrasse 133, CH-8600 Duebendorf, Switzerland*

[b]*Faculty of Sciences, University of Basel, Petersplatz 1, CH-4003 Basel, Switzerland*

[c]*International Institute for Applied Systems Analysis (IIASA), Ecosystem Services and Management Program, Schlossplatz 1, A-2361 Laxenburg, Austria*

[d]*Department of Geography, Ludwig Maximilian University, Munich, Germany*

[e]*Blackland Research and Extension Center, Temple, TX 76502, USA*

[f]*Plant Functional Biology and Climate Change Cluster, University of Technology Sydney, Po Box 123, Broadway 2007, NSW, Australia*

[g]*ETH Zürich, Institute of Terrestrial Ecosystems, Universitätstr. 16, CH-8092 Zürich, Switzerland*

Abstract

Crop models are commonly used to investigate crop–water relations over different spatial scales. Estimating potential evapotranspiration (PET) is a basis for this investigation. Most crop models have built-in PET estimation methods. Using different methods can lead to very different PET estimates; but little is known about the sensitivity of large-scale crop model predictions on the choice of the PET estimation methods. In the work reported here, we used PEPIC, a grid-based EPIC (Environmental Policy Integrated Climate) model with a Python environment, to investigate the impacts of five different PET methods on estimated crop–water relations for maize on a global scale at a resolution of 30 arc min. Results show that the estimated PET varied largely among different PET methods for the same climate zones, leading to uncertainties in estimating crop–water relations. Uncertainties in water-related variables such as growing season evapotranspiration (GSET) and irrigation water requirement were more relevant than uncertainties in crop yields. Water availability played an important role in the uncertainties. All PET methods showed similar performance with respect to simulations of GSET for rainfed maize cultivation in low-rainfall regions, while there were large differences for regions with high rainfall. For irrigated agriculture, the estimated irrigation water requirement varied widely among the five PET methods, with a factor of 2 between the smallest and the largest estimates. Overall, using the Priestley–Taylor method led to lowest yield but highest GSET estimates. The Baier–Robertson and Hargreaves methods produced rather high GSET estimates for tropical and humid regions. The Penman–Monteith method gave the best yield estimates, compared to agricultural statistics. The results highlight the importance of considering the uncertainties resulting from the selection of PET estimation methods in investigating crop–water relations, particularly in predicting impacts of future climate change and in formulating appropriate water management strategies.

Keywords

PET; PEPIC; Maize; Crop–water relations; Modelling uncertainties; Global scale

Abbreviations

AET, actual evapotranspiration; APT, actual plant transpiration; ASE, actual soil evaporation; CWP, crop water productivity; CWU, crop water use; EPIC, Environmental Policy Integrated Climate; ET, evapotranspiration; GSET, growing season evapotranspiration; PEPIC, a grid-based EPIC model with a Python environment; PET, potential evapotranspiration; PHU, potential heat units; PPT, potential plant transpiration; PSE, potential soil evaporation.

2.1 Introduction

Agriculture consumes the largest proportion (85%) of global water withdrawals (Shiklomanov, 2003). In the context of climate change and dietary shifts caused by socio-economic development, agriculture is facing the dual challenges of ameliorating water scarcity while increasing crop production (Elliott et al., 2014; Liu et al., 2013). Realistic estimates of global crop water use (CWU) and associated crop production are essential for policy makers to address these challenges.

Crop models are increasingly used to project large-scale historical CWU and crop production trends into the future (Elliott et al., 2015; Rosenzweig et al., 2013). There are considerable uncertainties in such predictions, however, originating in particular from inadequate input data, model structure, and parameter estimation methods. There are many studies on how to best identify and reduce these uncertainties in the calibration of these models. Folberth et al. (2012b) discussed the impacts of grid resolution on simulating maize yields in America. Liu et al. (2013) and Rosenzweig et al. (2014) investigated the uncertainties relating to future climate change by using different climate data inputs (e.g. General Circulation Models with different climate scenarios). Folberth et al. (2012a) explored the influences of potential heat units (PHU) and planting dates on the estimation of maize yields in Sub-Saharan Africa and the effects of crop management on climate change impact estimates in the same region (Folberth et al., 2014). Studies addressing similar issues include Balkovič et al. (2014), Xiong et al. (2014) and Yin et al. (2014). However, uncertainties related to the choice of method for the estimation of potential evapotranspiration (PET) have not been assessed and compared in large-scale modelling of CWU and crop production.

PET determines the maximum rate of crop soil water use under conditions of unlimited water availability. An accurate estimation of PET is essential for crop water modelling, since it directly influences the estimation of CWU and irrigation water requirement. It also affects the simulation of crop yields, as crops depend on water to take up nutrients, reduce heat stresses through transpiration, and maintain crop assimilation, among others. Many methods have been introduced to estimate PET (Jensen et al., 1990). We reviewed the PET options in 29 crop models found in the literature (Table S2-1). Often, crop models provide several methodological options to simulate the PET process. For example, five PET methods are available in the EPIC (Environmental Policy Integrated Climate) model (Williams, 1995; Williams et al., 1984), i.e. the Baier–Robertson (BR) (Baier and Robertson, 1965), Hargreaves (H) (Hargreaves and Samani, 1985), Penman (P) (Penman, 1948), Penman–Monteith (PM) (Monteith, 1965), and Preistly–Taylor (PT) (Priestley and Taylor, 1972). The DSSAT (Decision Support System for Agrotechnology Transfer) model provides three of these options: PT, P and PM (Jones et al., 2003). Recently, Palosuo et al. (2011)

compared eight crop models for their ability to simulate wheat yields at eight different sites in Europe, while Bassu et al. (2014) analysed 23 crop models for simulating maize yields at four sites across the world. In both studies, the PET methods were explicitly specified. However, they did not explore the influences of different PET methods on yield estimates. We also reviewed the PET methods used in 20 large-scale crop modelling work (Table S2-2). Surprisingly, many of them did not specify the PET methods that were employed.

Some earlier studies have shown that different PET estimation methods can have impacts on model results. For instance, Benson et al. (1992) evaluated how the five PET estimation methods in EPIC can influence simulated soil water balances for five locations in America and pointed out the importance of selecting an appropriate PET method. Roloff et al. (1998) assessed how EPIC prediction of wheat yield in a crop rotation experiment field in Canada depended on the method of PET estimation and found that the BR method was the most suitable method. Balkovič et al. (2013) compared the performance of the five PET estimation methods in reproducing crop yields in Europe with an EPIC-based model and found that BR and H performed best. Sau et al. (2004) compared the PT, P and some PM-based methods in simulating soil water balances at some sites in Spain using the DSSAT model and concluded that the PM-based methods were the most reliable, while P showed the poorest performance, and PT, though still reasonable, tended to overestimate evapotranspiration (ET). Anothai et al. (2013) compared the PT and PM methods in combination with the DSSAT model for an experimental site in Colorado, USA, and also found PM to perform better than PT. These studies show how important a proper choice of the PET estimation methods is and that this choice depends on site, especially climate conditions. To be able to make an informed choice it is of significance to know from where the uncertainties in different PET methods come and for which conditions various methods perform best. However, previous works comparing different PET methods were mostly conducted on regional scale and focused on either yields or crop soil water use. Such kind of research is rare for large-scale simulations. A comprehensive assessment of impacts of different PET estimation methods on crop yields and water use in rainfed and irrigated systems on a global scale with specification of climate zones has been absent.

EPIC is one of the most widely used crop models (Balkovič et al., 2013; Folberth et al., 2012a, 2014; Liu et al., 2007; Tan and Shibasaki, 2003) due to its good performance in a large variety of applications throughout the world (Gassman et al., 2005). The five PET estimation methods offered in EPIC were developed for applications in different climate regions and for different situations of climate data availability. The H method was often used for large-scale simulations in cases of limited climate data availability (Folberth et al., 2013; Liu, 2009; Liu et al., 2013). However, after global gridded climate datasets (e.g. Hempel et al. (2013); Elliott et al.

(2015)) have become available recently, it is now possible also to use the other PET estimation methods in large-scale simulations with EPIC.

Here, we used PEPIC, a grid-based EPIC model with a Python environment, to compare how the choice of the PET estimation methods would influence global scale simulations of maize growth and to identify error sources for different climate zones. In addition to PET, we analysed growing season evapotranspiration (GSET), yields, CWU, crop water productivity (CWP), and total maize production, which are all related to PET. To our best knowledge, this is the first study exploring the influences of PET estimation methods on simulating crop growth and water consumption on a global scale.

2.2 Simulation framework

2.2.1 Methodologies

The EPIC model and PET methods

The EPIC model was initially introduced by Williams et al. (1984) to evaluate the impacts of soil erosion on soil productivity. Since its first release, it has been continuously improved and expanded by integrating some major components from other models, such as CREAMS (Knisel, 1980), GLEAMS (Leonard et al., 1987), Century (Parton et al., 1994), and ALMANAC (Kiniry et al., 1992). EPIC can be used to simulate a large number of complex soil, water, climate, crop development and agricultural management processes (Williams et al., 1984). EPIC simulates crop growth at a daily step based on the concept of energy–biomass conversion. Daily potential biomass increase is the product of intercepted solar radiation and a crop-specific biomass–energy ratio. The potential increase in biomass is reduced each day in response to the dominating plant stress (water, nutrient, temperature, aeration, and salinity) to obtain the actual biomass. The crop yield is estimated by the product of the harvest index and actual biomass accumulation (Williams, 1995).

In EPIC, PET can be calculated using one of the following five functions:

$$PET_{BR} = 0.288 * T_{max} - 0.144 * T_{min} + 0.139 * RAMX - 4.931 \quad (2\text{-}1)$$

$$PET_{H} = 0.0032 * (RAMX/(2.501 - 0.0022 * T)) * (T + 17.8) * (T_{max} - T_{min})^{0.6} \quad (2\text{-}2)$$

$$PET_{P} = (RN * \delta/(2.501 - 0.0022 * T) + \gamma * (2.7 + 1.63 * U) * EA(1 - RH))/(\delta + \gamma) \quad (2\text{-}3)$$

$$PET_{PM} = (RN * \delta + 86.66 * AD * EA(1 - RH) * U/350)/((2.501 - 0.0022 * T) * (\delta + \gamma)) \quad (2\text{-}4)$$

$$PET_{PT} = 1.28 * (RN * (1.0 - AB)/(2.501 - 0.0022 * T)) * (\delta/(\delta + \gamma)) \quad (2\text{-}5)$$

where PET_{BR}, PET_H, PET_P, PET_{PM}, and PET_{PT} are the PET [mm d^{-1}] estimates obtained by using the BR, H, P, PM and PT methods, respectively; T_{max} and T_{min} are the daily maximum and minimum temperatures [°C]; $RAMX$ is the clear day solar radiation at the surface [MJ m^{-2} d^{-1}] and can be calculated based on day of the year and latitude; T is the daily mean air temperature [°C]; RN is the net radiation [MJ m^{-2} d^{-1}]; δ is the slope of the saturation vapour pressure curve [kPa $°C^{-1}$]; γ is the psychrometer constant [kPa $°C^{-1}$]; U is the daily mean wind speed [m s^{-1}]; EA is the saturation vapour pressure at mean air temperature [kPa]; RH is the daily mean relative humidity; AD is the air density [Kg m^{-3}]; and AB is the soil albedo.

With P, PT, H and BR, potential plant transpiration (PPT) is estimated by using an approach similar to Ritchie (1972) as following :

$$\begin{cases} PPT = PET * LAI/3 & 0 \le LAI \le 3 \\ PPT = PET & LAI > 3 \end{cases} \quad (2\text{-}6)$$

where LAI is the leaf area index. With PM, PPT is calculated as:

$$PPT = \frac{RN*\delta+86.66*AD*\frac{EA(1-RH)}{AR}}{(2.501-0.0022*T)*(\delta+\gamma(1+CR/AR))} \quad (2\text{-}7)$$

where AR is the aerodynamic resistance for heat and vapour transfer [s m^{-1}]; CR is the canopy resistance for vapour transfer [s m^{-1}], which can be calculated as:

$$CR = p_1/(LAI * g_0 * (1.4 - 0.00121 * CO_2)) \quad (2\text{-}8)$$

where p_1 is a parameter used in EPIC to adjust PPT estimation ranging between 1.0 and 2.0 and a default value of 1 was used in this study; g_0 is the leaf conductance [m s^{-1}] and CO_2 is the carbon dioxide concentration [ppm].

Potential soil evaporation (PSE) is calculated as:

$$PSE = \max\{(PET - I) * SCI, 0\} \quad (2\text{-}9)$$

where I is the rainfall interception [mm d^{-1}]; SCI is a soil cover index varying between 0 and 1, which can be calculated as:

$$SCI = \exp\{-\max(0.4 * SMLA, 0.1 * (CV + 0.1))\} \quad (2\text{-}10)$$

where $SMLA$ is the sum of the LAI and CV is the weight of all above ground plant material [t ha^{-1}]. When $PET < I$, both actual plant transpiration (APT) and soil evaporation (ASE) are set to 0. Otherwise, they are estimated as:

$$APT = \min\{(PET - I), PPT\} \quad (2\text{-}11)$$

$$ASE = \min\{PSE, PSE * (PET - I)/(PSE + APT)\} \quad (2\text{-}12)$$

Actual evapotranspiration (AET) is the sum of APT and ASE. The climate variables required as input for each PET method are listed in Table 2-1.

The PEPIC model

PEPIC runs the EPIC (the latest version v0810) model within a Python-based framework. The whole study domain is firstly categorized into a number of subareas depending on the study purposes (e.g. administrative boundaries, climate regions, watersheds). Input data (e.g. elevation, slope, climate, soil, and management practice information) need to be specified for each grid cell, which has a spatial resolution of 30 arc min. After simulation is complete for all grids cells, PEPIC extracts the results and presents the spatial distribution of desired variables for a given time period. In this study, we simulated crop growth processes separately for irrigated and rainfed maize cultivation. To get combined outputs for each grid cell, values from irrigated and rainfed cultivation were aggregated using area-weighted averaging as described by Liu et al. (2007).

Table 2-1. Description of potential evapotranspiration (PET) methods and associated climate variables.

Method	Abbr.	Solar radiation (RN)	Temperature (T, T_{min}, T_{max})	Relative humidity (RH)	Wind speed (U)	Reference
Baier–Robertson	BR		Yes			Baier and Robertson (1965)
Hargreaves	H		Yes			Hargreaves and Samani (1985)
Penman	P	Yes	Yes	Yes	Yes	Penman (1948)
Penman–Monteith	PM	Yes	Yes	Yes	Yes	Monteith (1965)
Priestley–Taylor	PT	Yes	Yes			Priestley and Taylor (1972)

2.2.2 Data description

The input data for the PEPIC model include latitude, longitude, elevation, slope, climate, soil properties, nitrogen and phosphorus fertilizer as well as irrigation application rates, cropland use areas for irrigated and rainfed cultivation, planting dates, harvesting dates, and PHU.

Climate data required to run PEPIC include solar radiation, maximum and minimum air temperature, precipitation, relative humidity, wind speed, and CO_2 concentration. In this study, the Global Annual Mean CO_2 Dataset provided by Goddard Institute for Space Studies (GISS) of National Aeronautics and Space Administration (NASA) was used. The other climate variables were obtained from the Global Gridded Crop Model Intercomparison (GGCMI) Project (Elliott et al., 2015). This dataset is based on WFDEI (Weedon et al., 2014) ERA-Interim historical re-analysis data that have been bias corrected on a monthly scale against the Climate Research Unit (CRU) data (Mitchell and Jones, 2005). It spans the time period of 1979–2012, which is also the simulation period in this study. Soil properties of layer depth, pH, bulk density, organic carbon

content, % sand, and % silt, etc. were extracted from the ISRIC–WISE (Batjes, 2006). This soil dataset was spatially linked to the FAO Digital Soil Map (FAO, 1995).

The fertilizer application rates of N and P around 2000 were derived from the FertiStat (FAO, 2007). This dataset is only available at the country level. Application rates were assumed to be the same for the different grid cells within a given country in this study. Because of the available data on irrigation rates were not sufficiently complete, an automatic irrigation schedule with a maximum total volume of 1,000 mm for the whole growing season was employed to guarantee enough water for crop growth. Besides, the minimum and maximum single application volumes were set to 1 and 500 mm. This kind of irrigation strategy is commonly assumed in large scale crop modelling (Rosenzweig et al., 2014). Harvested maize areas for irrigated and rainfed cultivation were obtained from the MIRCA2000 dataset (Portmann et al., 2010), which provides the irrigated and rainfed areas for 26 crops within the period of 1998–2002.

The required data on planting dates and harvesting dates were obtained from the Center for Sustainability and the Global Environment (SAGE) (Sacks et al., 2010). The SAGE dataset includes the beginning, medium, end of planting/harvesting dates for 19 crops. Medium values were used in our study. PHU was calculated by using the PHU Calculator of the Blackland Research Center based on the input data of planting dates, harvesting dates and temperature.

Besides the grid-based analyses, also an updated version of the Köppen–Geiger classification of climate zones (Peel et al., 2007) was used to compare the results. The Köppen–Geiger classification divides the whole world into five major categories (Table 2-2), i.e. A (tropical), B (arid), C (temperate), D (cold) and E (polar) based on global temperature and precipitation information. Details about the Köppen–Geiger classification can be found at http://www.hydrol-earth-syst-sci.net/11/1633/2007/hess-11-1633-2007-supplement.zip. The Köppen–Geiger classification has been widely used as a basis for regionalisation of climatic variables such as in GGCMI (Elliott et al., 2015). Table 2-2 shows the climate zones and the irrigated and rainfed maize areas in each zone.

Table 2-2. Definition of the Köppen–Geiger climate zones and harvest areas in irrigated and rainfed systems of maize.

Zone	Definition	Irrigated		Rainfed		Combined		Percent of irrigated and rainfed area	
		Harvest area (ha)	Percent in the total irrigated area (%)	Harvest area (ha)	Percent in the total rainfed area (%)	Harvest area (ha)	Percent in the total mixed area (%)	Irrigated (%)	Rainfed (%)
Af	Tropical rainforest	123,627	0.43	3,820,347	3.23	3,943,974	2.68	3.13	96.87
Am	Tropical monsoon	253,565	0.87	3,881,438	3.28	4,135,003	2.81	6.13	93.87
Aw	Tropical Savannah	1,326,765	4.56	24,270,654	20.53	25,597,419	17.38	5.18	94.82
BWh	Arid desert hot	1,387,463	4.77	328,925	0.28	1,721,057	1.17	80.62	19.11
BWk	Arid desert cold	910,677	3.13	44,427	0.04	956,655	0.65	95.19	4.64
BSh	Arid steppe hot	1,075,022	3.70	4,072,646	3.44	5,147,970	3.49	20.88	79.11
BSk	Arid Steppe cold	1,722,430	5.92	624,599	0.53	2,347,029	1.59	73.39	26.61
Csa	Temperate dry and hot summer	182,738	0.63	69,399	0.06	252,212	0.17	72.45	27.52
Csb	Temperate day and warm summer	78,896	0.27	21,706	0.02	100,602	0.07	78.42	21.58
Cwa	Temperate dry winter and hot summer	304,081	1.05	2,215,906	1.87	2,519,987	1.71	12.07	87.93
Cwb	Temperate dry winter and warm summer	42,648	0.15	1,300,172	1.10	1,342,820	0.91	3.18	96.82
Cwc	Temperate dry winter and cold summer	6	0.00	1,116	0.00	1,122	0.00	0.53	99.47
Cfa	Temperate no dry season hot summer	7,458,669	25.65	22,468,226	19.00	29,927,094	20.32	24.92	75.08
Cfb	Temperate no dry season warm summer	1,879,087	6.46	9,527,090	8.06	11,406,177	7.74	16.47	83.53
Cfc	Temperate no dry season cold summer	3,855	0.01	3,179	0.00	7,034	0.00	54.81	45.19
Dsa	Cold dry and hot summer	1,447	0.00	1,483	0.00	2,930	0.00	49.39	50.61
Dsb	Cold dry and warm summer	2,878	0.01	956	0.00	3,834	0.00	75.07	24.93
Dsc	Cold dry and cold summer	0	0.00	30	0.00	30	0.00	0.00	100.00
Dwa	Cold dry winter and hot summer	987,116	3.39	1,214,479	1.03	2,201,595	1.49	44.84	55.16
Dwb	Cold dry winter and warm summer	804,639	2.77	866,153	0.73	1,670,792	1.13	48.16	51.84
Dwc	Cold dry winter and cold summer	93,082	0.32	164,158	0.14	257,240	0.17	36.18	63.82
Dwd	Cold dry winter and very cold summer	0	0.00	7	0.00	7	0.00	0.00	100.00
Dfa	Cold no dry season hot summer	8,954,943	30.79	27,410,705	23.19	36,365,648	24.69	24.62	75.38
Dfb	Cold no dry season warm summer	1,425,208	4.90	15,598,072	13.19	17,023,280	11.56	8.37	91.63
Dfc	Cold no dry season cold summer	44,914	0.15	281,278	0.24	326,192	0.22	13.77	86.23
ET	Polar tundra	19,102	0.07	37,535	0.03	56,637	0.04	33.73	66.27

2.2.3 Description of estimated variables

GSET is the accumulated AET from planting date to harvesting date. Irrigation is automatically triggered when water stress factor (ratio between daily plant water use and daily potential water use) is lower than 0.9. Irrigation rate is determined by the minimum of the maximum single application volume and the volume required to fill the soil moisture to field capacity. Irrigation water requirement in this study is defined as the total applied irrigation rates during the whole growing season for irrigated maize cultivation. CWU was calculated by multiplying GSET with crop harvest areas at the grid cell level and then summing over all grid cells. For irrigated cultivation, CWU was separated into blue and green CWU, where green CWU refers to the CWU derived from soil moisture and precipitation, while blue CWU is the CWU originating from irrigation. We adopted the methods introduced in Liu et al. (2009) to separate blue and green CWU. Crop water productivity (CWP) is defined as the ratio between maize yield and GSET (Liu et al., 2007). For consistency with MIRCA2000 data and fertilizer inputs, results in this study were averaged between 1998 and 2002.

2.3 Results

2.3.1 Estimation of potential evapotranspiration (PET)

The five PET estimation methods compared here produced quite different annual PET distributions (Figure 2-1a). Only H and BR gave similar results. With H more grid cells fell into the high range (>2000 mm) than with BR, while with BR more cells fell into the low range (<1000 mm). Major differences were found among PM, P and PT methods. The PM method produced a large fraction of low values (<1000 mm) and the smallest fraction of high values (>1600 mm), whereas estimates obtained with P and PT were dominated by high values (>1600 mm). With PT more than half of all grid cells had annual PET values >2000 mm. The largest differences were found for the tropical and arid regions, southwestern part of America, Mexico, and southeastern part of China.

Large differences in estimated annual PET were also evident at the level of the Köppen–Geiger climate zones (Figure 2-1b). The lowest annual PET values were obtained with the PM method for the Af, Am, Aw, Cwa, Cwb, Cfa, Cfb and Cfc zones. For other zones, BR estimated the lowest annual PET values. In contrast, PT estimates were the highest in all Köppen–Geiger zones except in the arid regions Bwh, BWk and BSh, where P gave the highest values. As for the grid cells, the H method produced a similar pattern to that of BR, but with higher values. Different climate variables used in different PET estimation methods contribute to the variations in PET

estimations in a given climate zone. For example, the P and PM methods consider relative humidity and wind speed in PET estimation, which are not considered in the other PET methods.

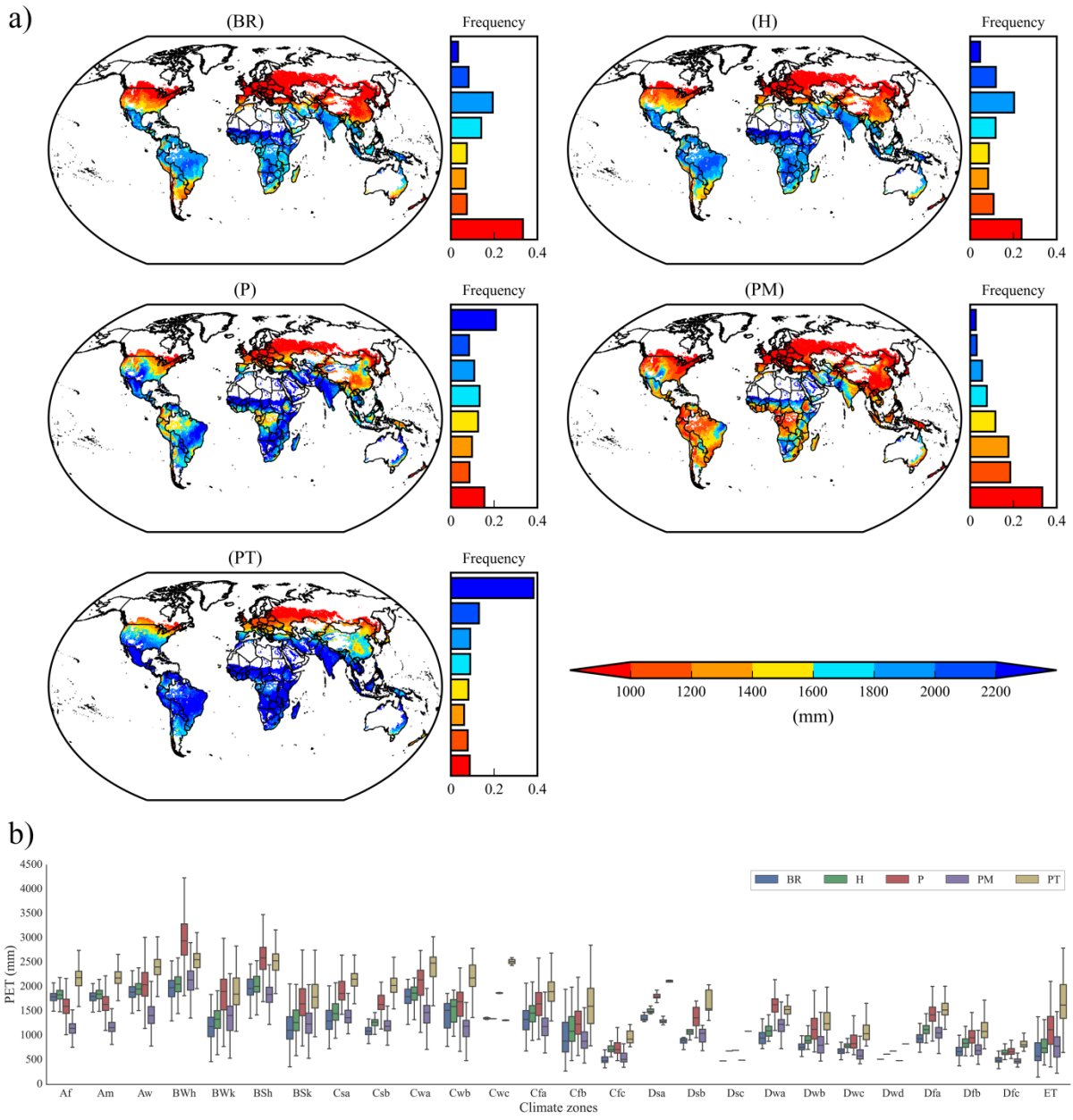

Figure 2-1. Spatial patterns of annual potential evapotranspiration (PET) estimates obtained using different PET methods at the (a) grid and (b) Köppen–Geiger levels.

2.3.2 Estimation of growing season evapotranspiration (GSET)

Irrigated maize cultivation

Generally, the differences in GSET estimates (Figure 2-2) obtained with the different PET estimation methods were smaller than those shown in PET values (Figure 2-1). This is because GSET is also related to other crop growth factors, especially the development of LAI. The PT method produced higher GSET values than the other PET methods, as shown with more grid cells

falling into the range of >600 mm and few grid cells falling into the range of <300 mm GSET (Figure 2-2a). In contrast, the BR and H methods gave relatively low GSET values, with more grid cells falling into the range of <400 mm and less grid cells into the range of >700 mm than with the other methods. The PM and P produced comparable spatial patterns and frequency distributions of grid cells. Also at the Köppen–Geiger level, the variation of GSET estimates was not as significant as in PET estimates (Figures 2-1b and 2-2b). The PT method resulted in the highest GSET for all regions, with the exception of Bwh, Bwk, Bsh and BSk, where the PM method led to the highest values. On the other hand, PM produced low values in many other regions, especially in the Af, Am, Aw, Cwa, Cwb, Cfa, Cfb and Cfc regions. BR and H showed again similar performance with low GSET estimates especially for arid and cold regions and high GSET estimates for the Af, Am, Aw, Cwa, Cwb, and Cfc regions (Figure 2-2b).

Rainfed maize cultivation

The differences among GSET estimates obtained with the five PET estimation methods were relatively small also for rainfed maize cultivation (Figure 2-3). Rather large differences only occurred between PM and PT estimates (Figure 2-3a). PM resulted in low GSET values (<300 mm) for the majority of grid cells (>50%), while PT produced much higher values (>500 mm) for most grid cells. Furthermore, PT, H and BR methods led to high GSET values for tropical regions, in contrast to P and PM. At the Köppen-Geiger level, similar GSET values were obtained with all the five PET estimation methods except for the Af, Am, Aw, Cwa, Cwb, Cfa, Cfb and Cfc regions (Figure 2-3b). In the latter eight regions, PT, H and BR estimates of PET produced higher GSET values than the other two methods, while PM estimates produced the lowest GSET values.

2.3.3 Estimation of maize yields

The performance of different PET methods was evaluated against the reported yields for individual countries. Country-specific reported yield data were downloaded from FAO (Food and Agriculture Organization of the United Nations) database (http://faostat3.fao.org/home/E). For consistency with the estimated yields, FAO reported yields were also averaged for 1998 and 2002. Generally, the PEPIC model performed well in estimating yields for all the countries by using the five PET methods (Figure S2-1). However, biases can be found for minor maize producers. In order to show the overall trends more clearly, Figure 2-4 presents the respective results only for the 21 major maize producing countries, i.e. the countries with cropland area used for maize cultivation larger than 0.8% of the global total maize cultivation areas. These 21 countries account for more than 80% of the global areas used for maize production. The slopes of the regression lines between estimated and reported maize yields were 0.90, 0.87, 0.83, 0.90, and 0.74 for the simulations based on PET estimation with the BR, H, P, PM, and PT methods, respectively. The slopes for P and PT were significantly different from 1 at the 95% statistical level. The intercepts

of the regression lines were 1.00, 0.94, 0.88, 0.76, and 0.99 (all significantly different from 0 at the 95% statistical level), respectively, and the R^2 values ranged between 0.82 and 0.90, demonstrating that PEPIC performed relatively well in estimating maize yields for the major maize-producing countries.

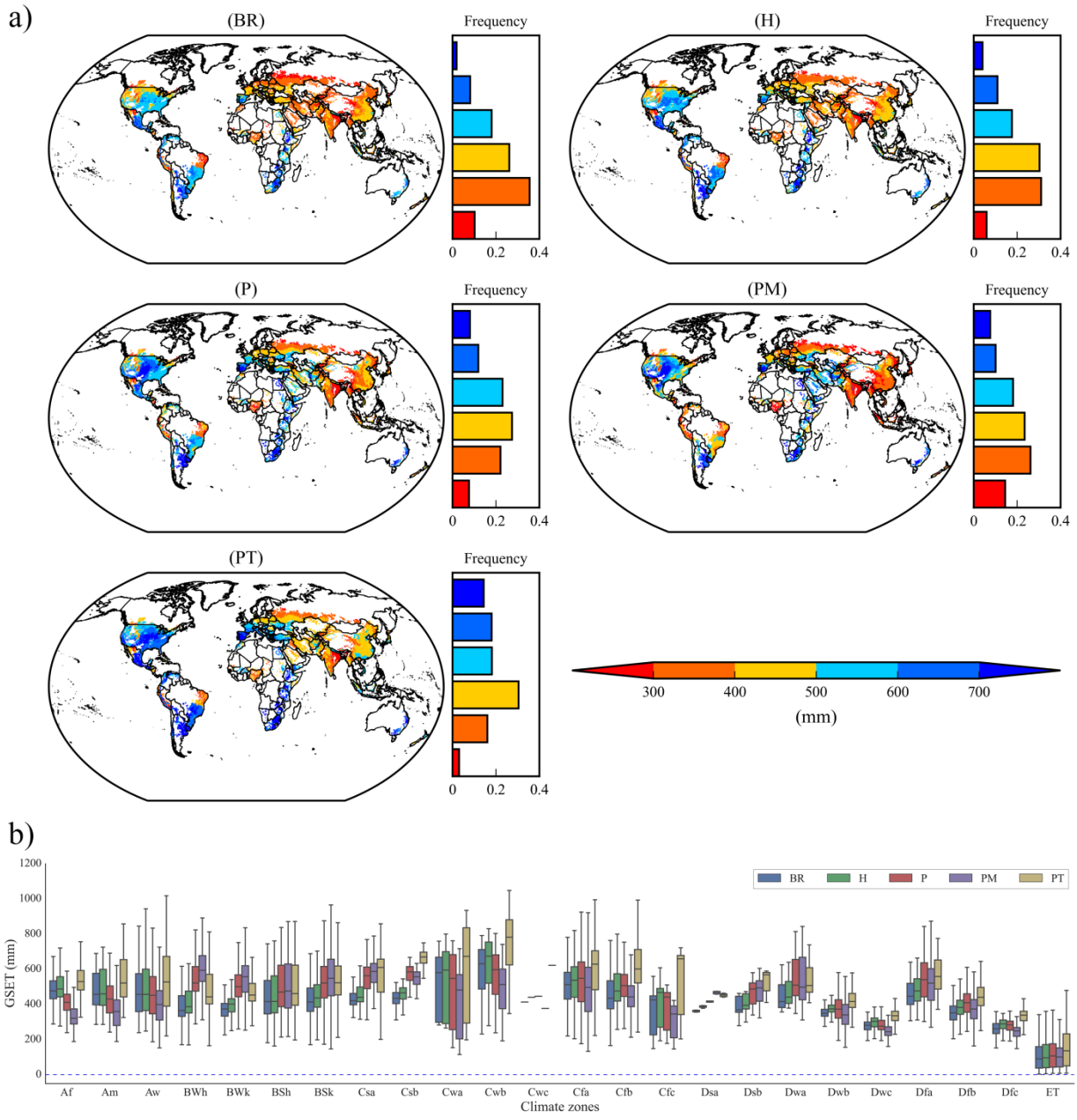

Figure 2-2. Spatial patterns of growing season evapotranspiration (GSET) estimates obtained using different PET estimation methods for irrigated maize cultivation at the (a) grid and (b) Köppen–Geiger levels.

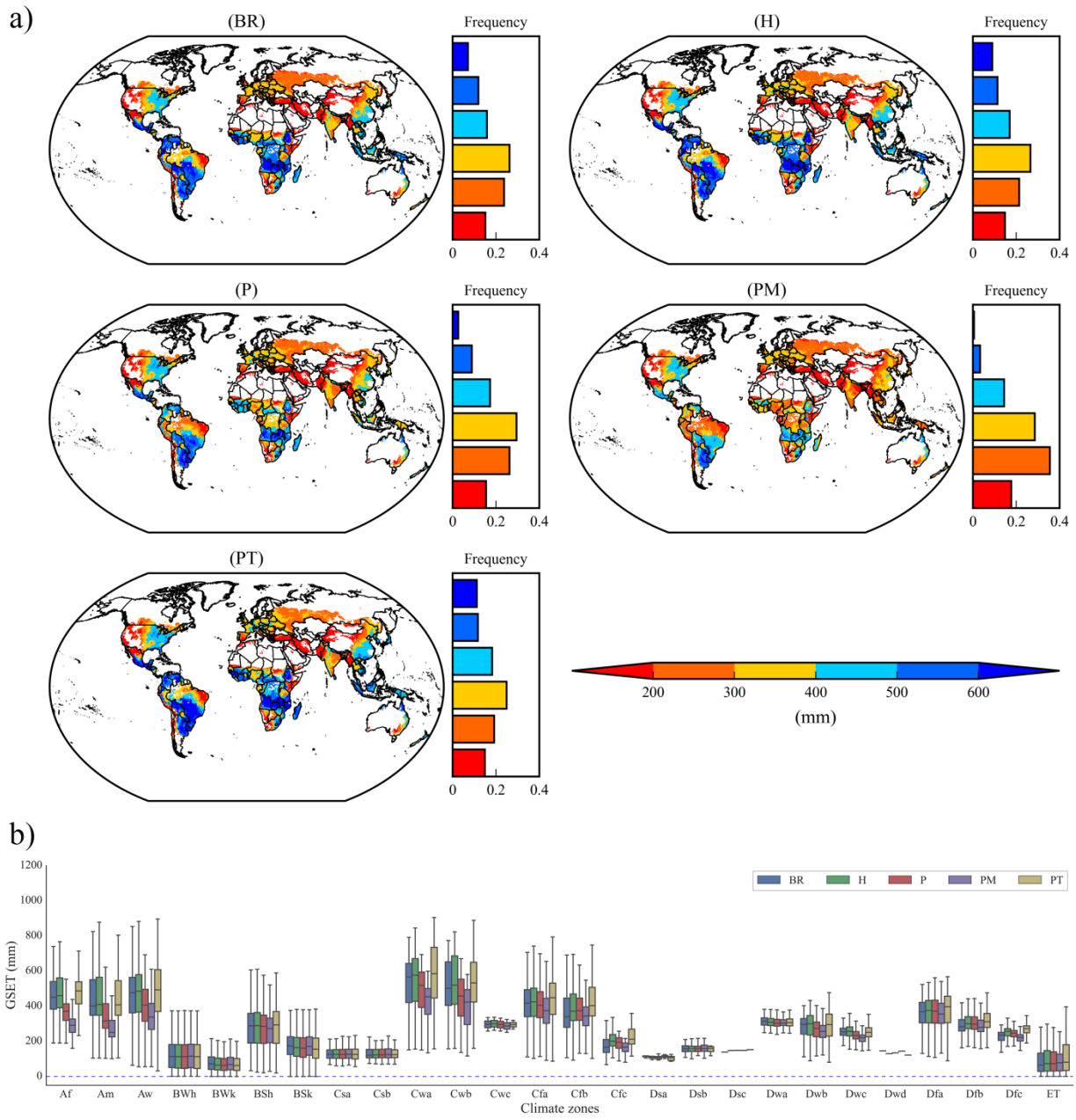

Figure 2-3. Spatial patterns of growing season evapotranspiration (GSET) estimates obtained using different PET estimation methods for rainfed maize cultivation at the (a) grid and (b) Köppen–Geiger levels.

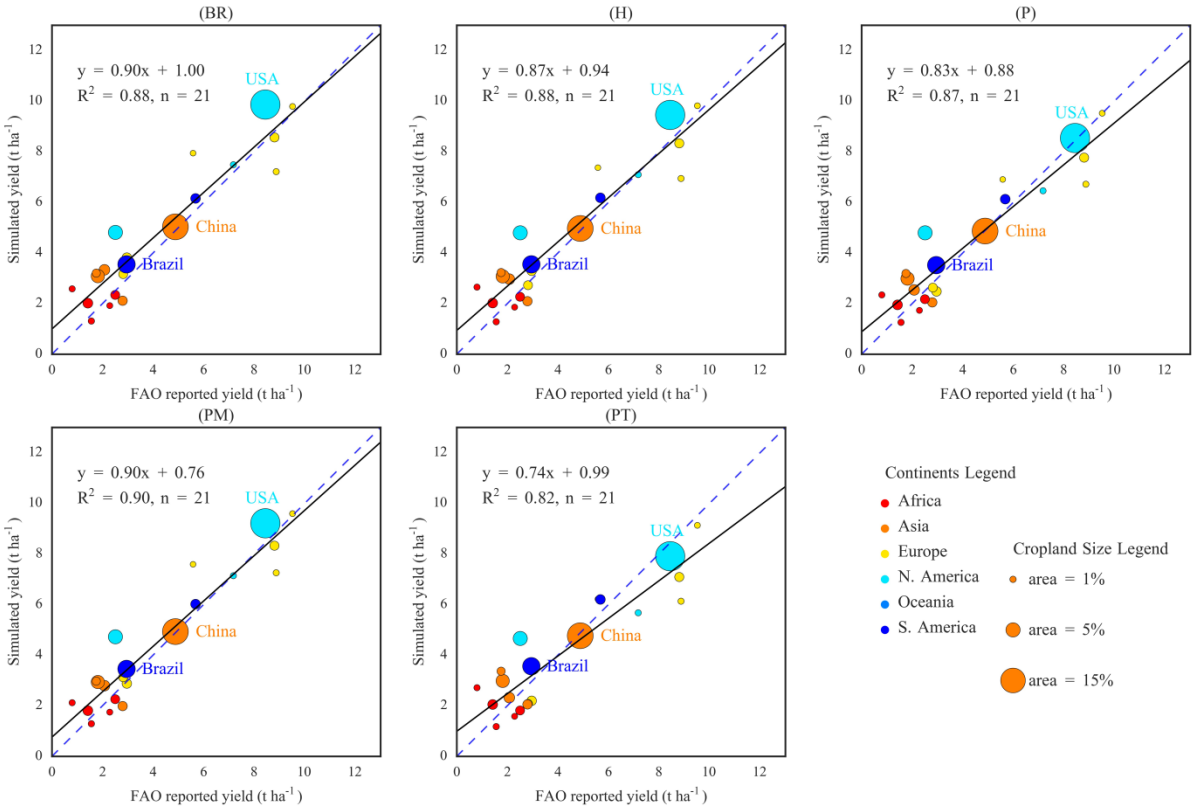

Figure 2-4. Comparisons between reported and estimated yields using different PET estimation methods for major maize-producing countries. Colours represent continents, and the areas of the circles represent the areas of land used for maize production in the respective countries relative to the total area used for maize cultivation worldwide.

The best performance (large slope and R^2, low intercept) of the five PET estimation methods was found for PM, but BR and H performed almost as well, while the poorest performance was found for PT (Figure 2-4). Using PT, PEPIC tended to underestimate high yields (e.g. >6 t ha^{-1}) more than using the other PET estimation methods. The differences in yield estimates related to the choice of the PET estimation method mainly resulted from differences in yield simulations for rainfed maize cultivation, while there was little variation related to the PET estimation methods for irrigated maize cultivation (Figures 2-5 and S2-2). Also in rainfed maize cultivation there were only small differences relating to PET estimation for regions of Af, Am, Aw, Cwa, Cwb, and Cfc, whereas differences were more notable for regions of such as Csa, Csb, Dwa, Dfa, and Dfb (Figure 2-5b).

2.3.4 Estimation of irrigation water requirement and crop water productivity (CWP)

The highest irrigation water requirement occurred in the regions of BWh, BWk, BSh and BSk, Csa, and Csb (Figure 2-6). For regions with generally high irrigation demand, the BR and H

methods of PET estimation generally predicted the lowest demand. On the other hand, the PT method with few exceptions tended to predict the highest irrigation water requirement.

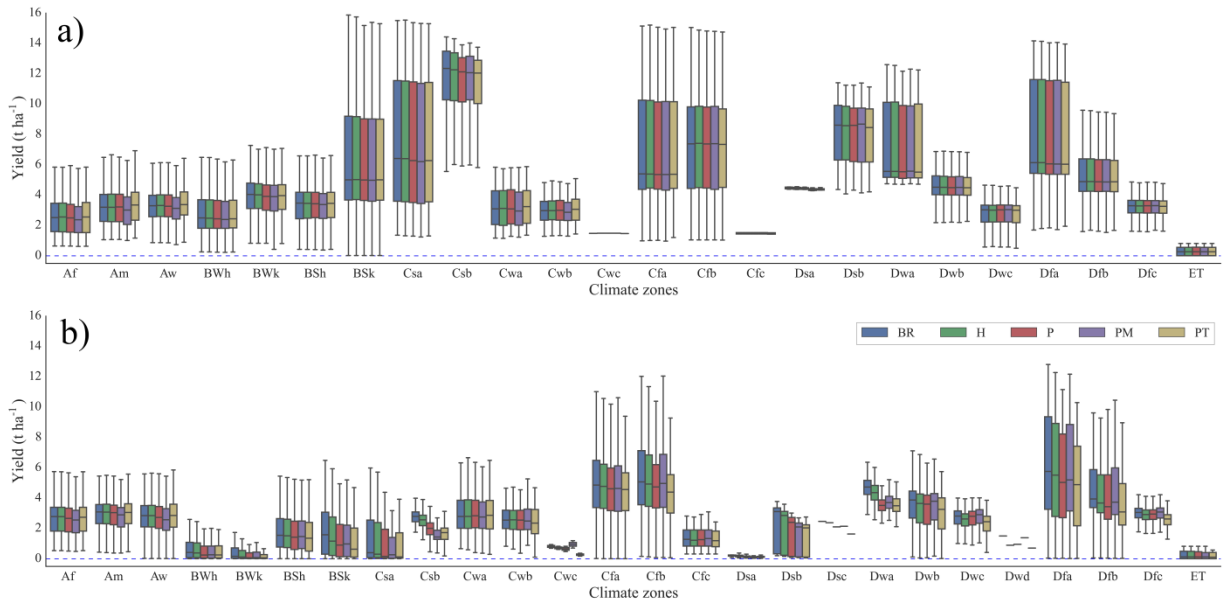

Figure 2-5. Simulated maize yields at the Köppen–Geiger level for (a) irrigated and (b) rainfed cultivation.

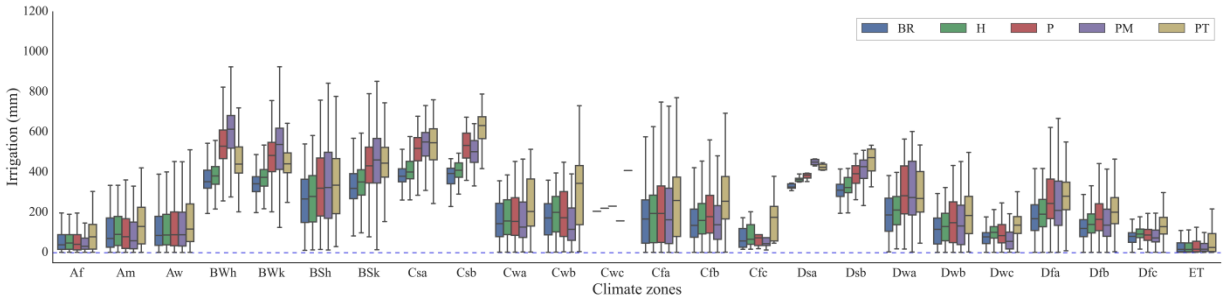

Figure 2-6. Simulated irrigation water requirement at the Köppen–Geiger level.

In most cases BR estimation of PET resulted in the highest CWP values for irrigated maize cultivation (Figure 2-7a). Only in the tropical areas (Af, Am, Aw) and in the Cwa, Cwb, Cfa, Cfb and Cfc regions the highest values were produced using the PM method. On the other hand, PT method produced the lowest values except for the arid areas (BWh, BWk, BSk and BSk) and for Csa and Dsb, where PM led to the lowest CWP estimates. The patterns for rainfed maize were similar to the irrigated system (Figure 2-7b).

2.3.5 Global aggregated CWU, production and CWP

Using PT to estimate PET produced the highest total CWU in both irrigated (158.80×10^9 m^3) and rainfed (537.86×10^9 m^3) maize cultivation, while PM produced the lowest total CWU

(442.90 × 10^9 m^3) for rainfed cultivation and BR the lowest total CWU (129.68 × 10^9 m^3) for irrigated cultivation (Table 2-3). When separating the total CWU for irrigated cultivation into blue and green CWU, the PM method produced the lowest green CWU (88.29 × 10^9 m^3), while BR resulted in the lowest blue CWU (35.68 × 10^9 m^3). Also for rainfed and irrigated cultivation combined , the PM-based CWU estimates were the lowest.

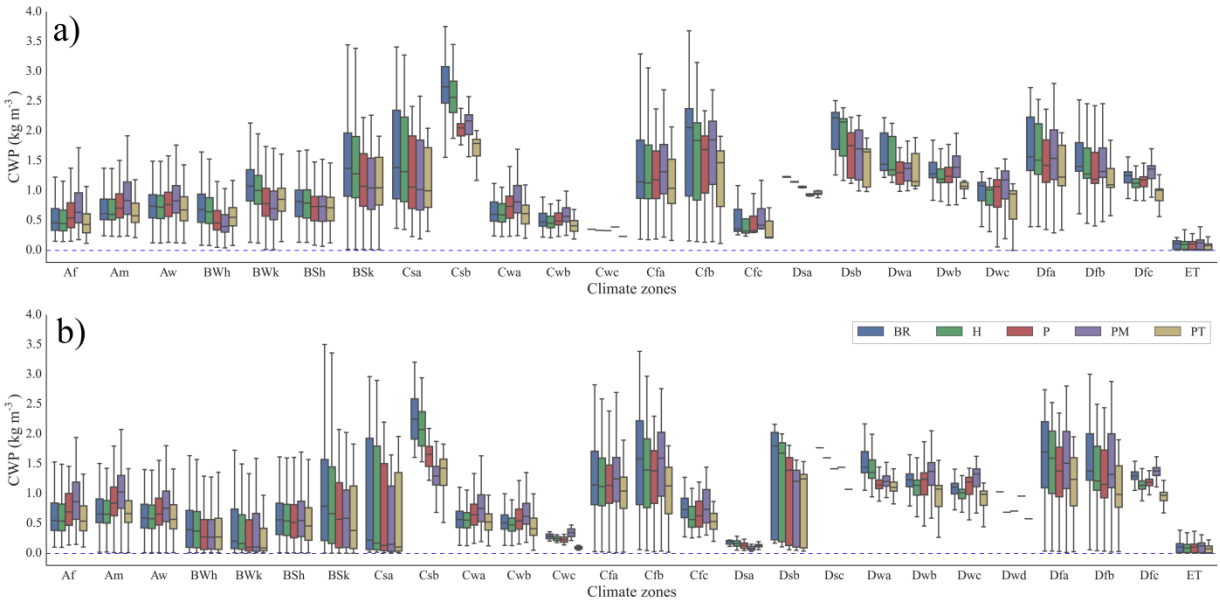

Figure 2-7. Simulated (a) irrigated and (b) rainfed maize crop water productivity (CWP) at the Köppen–Geiger level.

In accordance with the results for the yields, the estimates of total rainfed maize production were quite sensitive to the choice of the PET estimation methods, while there was little sensitivity for irrigated maize production (Table 2-3). PT gave the lowest (512.47 × 10^6 t) and BR the highest (610.63 × 10^6 t) estimates for rainfed maize production. For irrigated maize, H-based simulation estimated the highest and PM-based simulations the lowest production, but the difference between them was only 2.8 × 10^6 t. The estimates of global total maize production for both systems combined decreased with the choice of PET estimation methods in the order BR, H, PM, P, PT. The difference of 99.15 × 10^6 t between maximum and minimum productions was almost equivalent to China's total maize production in 2000 (106× 10^6 t).

The estimated global average CWP varied between 1.17 and 1.44 kg m^{-3} for irrigated maize cultivation and between 0.95 and 1.29 kg m^{-3} for rainfed maize cultivation (Table 2-3). While the lower bounds of these range resulted from PET estimates based on the PT method in both cases, the upper value resulted for irrigated production from using the BR method and for rainfed production from using the PM method.

2.4 Discussion

2.4.1 Comparison of CWU and CWP with other studies

The green CWU of maize was two times the blue CWU for irrigated maize cultivation in the study of Mekonnen and Hoekstra (2011). Our study obtained similar results with much higher green CWU than blue CWU for irrigated maize (Table 2-3). Total volumes of blue CWU in global irrigated maize production reported in the literatures varied between 51×10^9 and 72.4×10^9 m^3 (Fader et al., 2011; Mekonnen and Hoekstra, 2011; Siebert and Döll, 2010). Our estimates of blue CWU by using P, PM and PT for estimating PET were within this range, while the estimates based on BR and H methods were lower. The total CWU for maize production was previously reported to range between 548.39×10^9 and 657.7×10^9 m^3 (Chapagain and Hoekstra, 2004; Fader et al., 2011; Mekonnen and Hoekstra, 2011; Siebert and Döll, 2010). The estimates obtained in this study were all within this range, except for the PT method, which tended to overestimate CWU. Ranging between 1.00 and 1.30 the CWP values estimated in this study were of the same magnitude as the value estimated by Chapagain and Hoekstra (2004), but higher than the values estimated by Mekonnen and Hoekstra (2011) and Siebert and Döll (2010).

Table 2-3. Comparison of global aggregated crop water use (CWU, in 10^9 m^3), crop production (in 10^6 t), and crop water productivity (CWP, in kg m^{-3}) for maize based on different PET methods in the EPIC model and comparison with literatures.

Variable	This study					Chapagain and Hoekstra (2004)	Fader et al. (2011)	Mekonnen and Hoekstra (2011)	Siebert and Döll (2010)
	BR	H	P	PM	PT	PM	PT	PM	PM
Irrigated blue CWU	35.68	40.98	55.81	53.19	60.35		66.38	51	72.4
Irrigated green CWU	94.01	94.86	92.70	88.29	98.45			104	
Rainfed CWU	498.29	512.33	486.32	442.90	537.86			493	
Total CWU	627.97	648.17	634.83	584.37	696.67	548.39	592.67	648	657.7
Irrigated production	186.57	187.04	185.16	184.25	185.56				
Rainfed production	610.63	588.23	545.47	573.73	512.47				
Mixed production	797.21	775.29	730.66	757.99	698.06				
Irrigated CWP	1.44	1.38	1.25	1.30	1.17			1.125	
Rainfed CWP	1.23	1.15	1.12	1.29	0.95			0.924	
Combined CWP	1.27	1.20	1.15	1.30	1.00	1.1		0.973	0.919

2.4.2 Influences of water availability on GSET and yield estimates

For irrigated maize cultivation, the variation of GEST estimates was considerable with PET estimation methods in all climate regions. However, the variation of GSET estimates presented different patterns at the Köppen–Geiger level for rainfed maize cultivation, with high variation in some regions (e.g. Af, Am, Aw, Cwa, Cwb, Cfa, Cfb, and Cfc), but quite low variation in the other regions (Figure 2-3b). This is mainly due to the influence of the spatial pattern of annual precipitation. We found that the average annual precipitation in the aforementioned eight climate

regions was greater than 800 mm, especially in the tropical areas (Figure S2-3). High annual precipitation leads to less limit on GSET in these regions. However, the GSET estimates were strongly constrained by water availability in the rainfall limited regions, leading to low variation. This finding is consistent with Wang and Dickinson (2012). It suggests the important role of water availability on the variation of GSET estimation with different PET methods.

The yield estimates showed little variation with PET estimation methods for irrigated maize cultivation (Figure 2-5a). This is mainly attributable to the fact that irrigation was set automatically to a level that is sufficient for crop needs in PEPIC independent of PET estimation methods. The major differences of yield estimates were found in the limited water availability regions for rainfed maize cultivation (Figure 2-5b), especially for the regions of Dfa and Dfb, which had high fractions of total rainfed cropland areas (Table 2-2). This is because the effects of PET methods on yields will only show up when water availability is limited. Consequently, the global total maize production varied largely for rainfed maize cultivation (Table 2-3).

2.4.3 Assessment of the performance of different PET methods

In this study, the PT method produced the highest annual PET estimates, and consequently also the highest GSET estimates for both irrigated and rainfed maize cultivation and the lowest maize yield estimates for rainfed maize. Also the PT method tends to underestimate yields for high-yield countries (compared with the reported yields) (Figures 2-4 and S2-1). The main reason for underestimating yields may be related to its overestimation of water stress (Figure S2-4) stemmed from overestimation of PET.

The BR method was developed in Canada (Baier and Robertson, 1965). It was designed to estimate PET in cold regions, where it is generally low. In this study, we found that annual PET estimates obtained with the BR method were low for cold regions, but high for tropical regions (Figure 2-1). Consequently, GSET estimates obtained with the BR method for cold regions were also lower than estimates using the other methods for irrigated maize production (Figure 2-2b). On the other hand, the BR-based GSET estimates were quite high for the Af, Am, Aw, Cwa and Cwb regions (Figures 2-2b and 2-3b), which suggests that BR may be less suitable for these areas because it was initially developed and tested for cold regions. As for production, BR led to the highest estimate of total maize production for rainfed cultivation (Table 2-3). We attribute this to the lowest crop water stress estimated with BR (Figure S2-4). Given that BR led to the largest overestimation of yields (Figure 2-5b), crop water stress probably tended to be underestimated with this method for rainfed cultivation.

The H method was developed for semi-arid and arid regions (Hargreaves and Allen, 2003). It led to low annual PET estimates for arid regions in our study compared with the other PET

methods, whereas the estimated annual PET was relatively high for tropical regions (Figure 2-1). As a consequence, the GSET estimates were also small for arid regions, but quite high for Af, Am, Aw, Cwa and Cfb regions, where annual precipitation for both irrigated and rainfed maize cultivation is sufficiently high (Figures 2-2 and 2-3). This implies that H tends to overestimate GSET in humid regions. The higher GSET estimates for humid regions were consistent with findings by other studies Yoder et al. (2005), Trajkovic, (2007), and Saghravani et al. (2009). Trajkovic (2007) proposed an exponential index of 0.424 in Eq. 2 instead of 0.6 for humid regions. Moreover, using H led to the highest maize production estimates for irrigated cultivation (Table 2-3), which implies that H is likely to overestimate crop yields under sufficient water supplying conditions.

The P method was once recommended as the reference PET method by FAO (Doorenbos, 1977). However, it was replaced by PM, because it overestimated PET for a wide range of environmental conditions (Allen et al., 1998). Sau et al. (2004) even recommended to delete the P option from the DSSAT model because of its poor performance compared with other options in DSSAT. We also found that the estimates of annual PET and GSET obtained with the P method were higher than those obtained with PM method (Figures 2-1–2-3). Considering the better agreement between estimated and reported yields with PM- than P-based PET estimates and that both require the same climate input data, we suggest to use PM instead of P in simulating maize growth on a global scale. Besides, the estimation of PPT with PM considers LAI and CO_2 in calculating canopy resistance coefficient for the whole crop growing period. This is one of major differences of PM from the other PET methods and could be part of the reason that PM performed more reliably for yield estimation. Therefore, if input data are not the major limitation, we recommend PM to be used for global crop simulation.

2.5 Conclusions

Large-scale crop models are major tools used to investigate the global water–food relations, the impacts of climate change on food production and irrigation demand, and to assess water management strategies for alleviating water scarcity and enhancing food security. This study demonstrates that different PET methods can lead to large uncertainties in the estimation of crop–water relations, which could impair sound decision making for policy makers.

The differences in annual PET estimates obtained with different PET methods were significant. Their impacts on predictions of water related variables (e.g. GSET, irrigation water requirement, and CWU) were more substantial than on yields. At the same time, also water availability played an important role for predictions of GSET and yields. Overall, PT tended to

estimate high GSET and to underestimate yields. H and BR tended to estimate high GSET for rainfall sufficient regions. In rainfall-limited regions, all the PET methods performed consistently, except the overestimation of maize yield with BR due to its lower estimation of water stress. Globally, PM was more reliable in yield estimation than the other PET methods and has more reasonable implementation in estimating PPT by considering the effects of LAI and CO_2 on canopy resistance coefficient, thus should be considered with priority. However, PM requires more climate variables than H, BR, and PT. In contrast, H and BR only require temperature. However, BR tended to overestimate maize yield for rainfed cultivation, where H performed reasonably well for most regions except for high-rainfall regions. If obtaining whole set of climate data is a major challenge, H is a valid alternative option for all other regions except for high-rainfall regions.

2.6 References

Allen, R.G., Pereira, L.S., Raes, D. and Smith, M., 1998. Crop evapotranspiration—Guidelines for computing crop water requirements. FAO Irrigation and drainage paper 56. FAO, Rome.

Anothai, J., Soler, C.M.T., Green, A., Trout, T.J. and Hoogenboom, G., 2013. Evaluation of two evapotranspiration approaches simulated with the CSM–CERES–Maize model under different irrigation strategies and the impact on maize growth, development and soil moisture content for semi-arid conditions. Agric. For. Meteorol., 176: 64–76.

Baier, W. and Robertson, G.W., 1965. Estimation of Latent Evaporation from Simple Weather Observations. Can. J. Plant. Sci., 45(3): 276–284.

Balkovič, J., et al., 2013. Pan-European crop modelling with EPIC: Implementation, up-scaling and regional crop yield validation. Agric. Syst., 120: 61–75.

Balkovič, J., et al., 2014. Global wheat production potentials and management flexibility under the representative concentration pathways. Global Planet. Change, 122: 107–121.

Bassu, S., et al., 2014. How do various maize crop models vary in their responses to climate change factors? Global Change Biol., 20(7): 2301–20.

Batjes, N.H., 2006. ISRIC–WISE derived soil properties on a 5 by 5 arc-minutes global grid (version 1.1), ISRIC – World Soil Infromation, Wageningen.

Benson, V., Potter, K., Bogusch, H., Goss, D. and Williams, J., 1992. Nitrogen leaching sensitivity to evapotranspiration and soil water storage estimates in EPIC. J. Soil Water Conserv., 47(4): 334–337.

Chapagain, A.K. and Hoekstra, A.Y., 2004. Water footprints of nations. Research Report Series No. 16. UNESCO-IHE, Delft.

Doorenbos, J., 1977. Guidelines for predicting crop water requirements. FAO irrigation and drainage paper, 24: 15–29.

Elliott, J., et al., 2014. Constraints and potentials of future irrigation water availability on agricultural production under climate change. Proc. Natl. Acad. Sci. U.S.A., 111(9): 3239–3244.

Elliott, J., et al., 2015. The Global Gridded Crop Model Intercomparison: data and modeling protocols for Phase 1 (v1. 0). Geosci. Model Dev., 8(2): 261–277.

Fader, M., et al., 2011. Internal and external green–blue agricultural water footprints of nations, and related water and land savings through trade. Hydrol. Earth Syst. Sci., 15(5): 1641–1660.

FAO, 1995. Digital Soil Map of the World Map. FAO, Rome.

FAO, 2007. FertiSTAT–Fertilizer Use Statistics. FAO, Rome.

Folberth, C., Gaiser, T., Abbaspour, K.C., Schulin, R. and Yang, H., 2012a. Regionalization of a large-scale crop growth model for sub-Saharan Africa: Model setup, evaluation, and estimation of maize yields. Agric. Ecosyst. Environ., 151: 21–33.

Folberth, C., Yang, H., Gaiser, T., Abbaspour, K.C. and Schulin, R., 2013. Modeling maize yield responses to improvement in nutrient, water and cultivar inputs in sub-Saharan Africa. Agric. Syst., 119: 22–34.

Folberth, C., et al., 2014. Effects of ecological and conventional agricultural intensification practices on maize yields in sub-Saharan Africa under potential climate change. Environ. Res. Lett., 9(4): 044004.

Folberth, C., Yang, H., Wang, X.Y., Abbaspour, K.C., 2012b. Impact of input data resolution and extent of harvested areas on crop yield estimates in large-scale agricultural modeling for maize in the USA. Ecol. Model., 235: 8–18.

Gassman, P.W., et al., 2005. Historical development and applications of the EPIC and APEX Models Iowa State University, Center for Agricultural and Rural Development. Working Paper 05-WP 397, Ames, Iowa.

Hargreaves, G.H. and Allen, R.G., 2003. History and evaluation of Hargreaves evapotranspiration equation. J. Irrig. Drain. Eng., 129(1): 53–63.

Hargreaves, G.H. and Samani, Z.A., 1985. Reference crop evapotranspiration from temperature. Appl. Eng. Agric., 1(2): 96–99.

Hempel, S., Frieler, K., Warszawski, L., Schewe, J. and Piontek, F., 2013. A trend-preserving bias correction – the ISI-MIP approach. Earth Syst. Dyn., 4(2): 219–236.

Jensen, M.E., Burman, R.D. and Allen, R.G., 1990. Evapotranspiration and Irrigation Water Requirements. ASCE Manual of Practice No. 70. ASCE, New York.

Jones, J.W., et al., 2003. The DSSAT cropping system model. Eur. J. Agron., 18(3–4): 235–265.

Kiniry, J.R., Williams, J.R., Gassman, P.W. and Debaeke, P., 1992. A general, process-oriented model for two competing plant species. Trans. ASABE, 35(3): 801–810.

Knisel, W.G., 1980. CREAMS: A field-scale model for chemicals, runoff and erosion from agricultural management systems. Conservation Research Report No. 26, Washington D.C.

Leonard, R.A., Knisel, W.G. and Still, D.A., 1987. GLEAMS: Groundwater loading effects of agricultural management systems. Trans. ASABE, 30(5): 1403–1418.

Liu, J., 2009. A GIS-based tool for modelling large-scale crop–water relations. Environ. Modell. Software, 24(3): 411–422.

Liu, J., et al., 2013. A global and spatially explicit assessment of climate change impacts on crop production and consumptive water use. PLoS One, 8(2): e57750.

Liu, J., Williams, J.R., Zehnder, A.J.B. and Yang, H., 2007. GEPIC – modelling wheat yield and crop water productivity with high resolution on a global scale. Agric. Syst., 94(2): 478–493.

Liu, J., Zehnder, A.J.B. and Yang, H., 2009. Global consumptive water use for crop production: The importance of green water and virtual water. Water Resour. Res., 45(5): W05428.

Mekonnen, M.M. and Hoekstra, A.Y., 2011. The green, blue and grey water footprint of crops and derived crop products. Hydrol. Earth Syst. Sci., 15(5): 1577–1600.

Mitchell, T.D. and Jones, P.D., 2005. An improved method of constructing a database of monthly climate observations and associated high-resolution grids. Int. J. Climatol., 25(6): 693–712.

Monteith, J., 1965. Evaporation and environment. Symp. Soc. Exp. Biol, 19, 205–234.

Palosuo, T., et al., 2011. Simulation of winter wheat yield and its variability in different climates of Europe: A comparison of eight crop growth models. Eur. J. Agron., 35(3): 103–114.

Parton, W.J., et al., 1994. A general model for soil organic matter dynamics: sensitivity to litter chemistry, texture and management. Soil Science Society of America Inc., Minneapolis, Minnesota, USA, pp. 147–167.

Peel, M.C., Finlayson, B.L. and McMahon, T.A., 2007. Updated world map of the Köppen–Geiger climate classification. Hydrol. Earth Syst. Sci., 11(5): 1633–1644.

Penman, H.L., 1948. Natural Evaporation from Open Water, Bare Soil and Grass. Proc. R. Soc. London, Ser. A, 193(1032): 120–145.

Portmann, F.T., Siebert, S. and Doll, P., 2010. MIRCA2000 – Global monthly irrigated and rainfed crop areas around the year 2000: A new high-resolution data set for agricultural and hydrological modeling. Global Biogeochem. Cycles, 24: GB1011.

Priestley, C. and Taylor, R., 1972. On the assessment of surface heat flux and evaporation using large-scale parameters. Mon. Weather Rev., 100(2): 81–92.

Ritchie, J.T., 1972. Model for predicting evaporation from a row crop with incomplete cover. Water Resour. Res., 8(5): 1204–1213.

Roloff, G., Jong, R.d., Zentner, R., Campbell, C. and Benson, V., 1998. Estimating spring wheat yield variability with EPIC. Can. J. Soil Sci., 78(3): 541–549.

Rosenzweig, C., et al., 2014. Assessing agricultural risks of climate change in the 21st century in a global gridded crop model intercomparison. Proc. Natl. Acad. Sci. U.S.A., 111(9): 3268–3273.

Rosenzweig, C., et al., 2013. The Agricultural Model Intercomparison and Improvement Project (AgMIP): Protocols and pilot studies. Agric. For. Meteorol., 170: 166–182.

Sacks, W.J., Deryng, D., Foley, J.A. and Ramankutty, N., 2010. Crop planting dates: an analysis of global patterns. Global Change Biol., 19(5): 607–620.

Saghravani, S.R., ari Mustapha, S., Ibrahim, S. and Randjbaran, E., 2009. Comparison of daily and monthly results of three evapotranspiration models in tropical zone: A case study. Am. J. Environ. Sci., 5(6): 698–705.

Sau, F., Boote, K.J., Bostick, W.M., Jones, J.W. and Minguez, M.I., 2004. Testing and improving evapotranspiration and soil water balance of the DSSAT crop models. Agron. J., 96(5): 1243–1257.

Shiklomanov, I.A., 2003. World water resources at the beginning of the 21st century. Cambridge University Press, Cambridge.

Siebert, S. and Döll, P., 2010. Quantifying blue and green virtual water contents in global crop production as well as potential production losses without irrigation. J. Hydrol., 384(3–4): 198–217.

Tan, G.X. and Shibasaki, R., 2003. Global estimation of crop productivity and the impacts of global warming by GIS and EPIC integration. Ecol. Modell., 168(3): 357–370.

Trajkovic, S., 2007. Hargreaves versus Penman–Monteith under humid conditions. J. Irrig. Drain. Eng., 133(1): 38–42.

Wang, K.C. and Dickinson, R.E., 2012. A Review of Global Terrestrial Evapotranspiration: Observation, Modeling, Climatology, and Climatic Variability. Rev. Geophys., 50: RG2005.

Weedon, G.P., et al., 2014. The WFDEI meteorological forcing data set: WATCH Forcing Data methodology applied to ERA-Interim reanalysis data. Water Resour. Res., 50(9): 7505–7514.

Williams, J.R., 1995. The EPIC model. In: V.P. Singh (Editor), Computer Models of Watershed Hydrology. Water Resources Publications, Highlands Ranch, Colo.

Williams, J.R., Jones, C.A. and Dyke, P.T., 1984. A modeling approach to determining the relationship between erosion and soil productivity. Trans. ASABE, 27(1): 129–144.

Xiong, W., et al., 2014. A calibration procedure to improve global rice yield simulations with EPIC. Ecol. Modell., 273: 128–139.

Yin, Y.Y., et al., 2014. GEPIC-V-R model: A GIS-based tool for regional crop drought risk assessment. Agric. Water Manage., 144: 107–119.

Yoder, R.E., Odhiambo, L.O. and Wright, W.C., 2005. Evaluation of methods for estimating daily reference crop evapotranspiration at a site in the humid Southeast United States. Appl. Eng. Agric., 21(2): 197–202.

Supplementary Information for

Global investigation of impacts of PET methods on simulating crop–water relations for maize

Figure S2-1 shows the comparison between FAO reported country maize yields (averaged over 1998–2002) and estimated yields for all the maize-producing countries (a total of 141) (also averaged over 1998–2002). The slopes of the regression line are 0.68, 0.68, 0.65, 0.69, and 0.60 for BR, H, P, PM, and PT, respectively. The intercepts are 1.60, 1.60, 1.57, 1.47, and 1.67, respectively. The R^2 varied between 0.54 and 0.62. It is clear that there are some overestimations for the low yield countries and underestimations for the high yield countries. Generally, these unmatched countries are the minor producers of maize in terms of global total maize harvest areas.

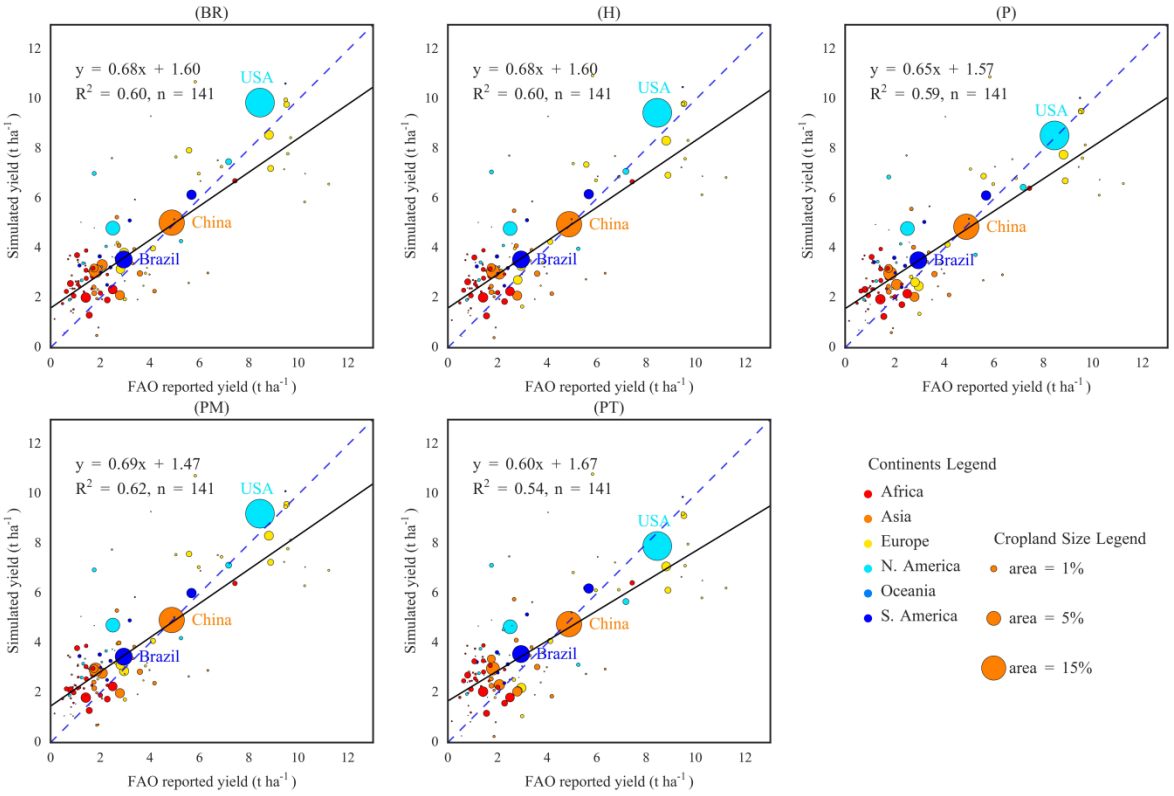

Figure S2-1. Comparisons between reported and estimated yields using different PET estimation methods for all maize-producing countries. Colours represent continents, and the areas of the circles represent the areas of land used for maize production in the respective countries relative to the total area used for maize cultivation worldwide.

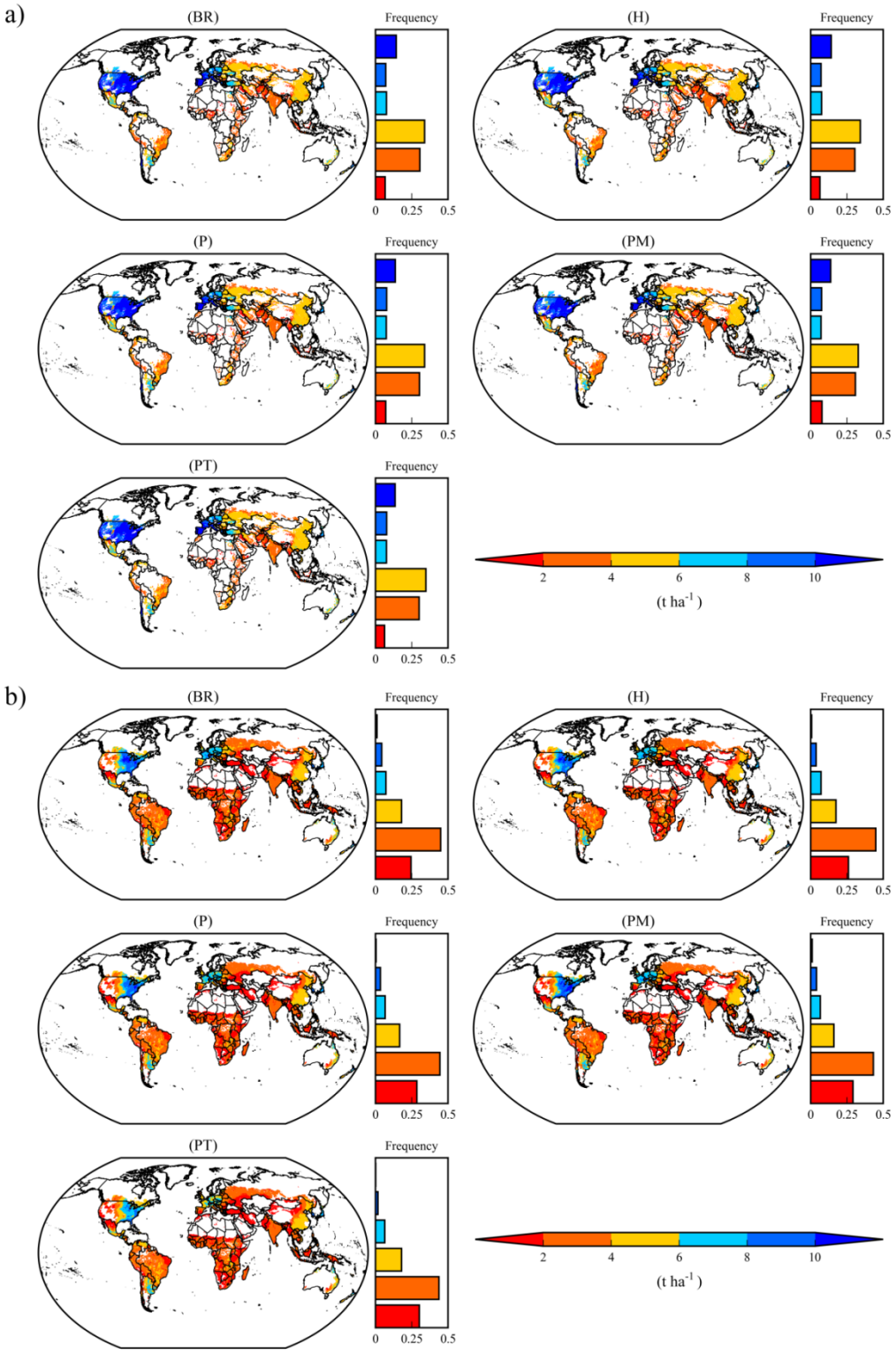

Figure S2-2. Spatial patterns of yield estimates obtained using different PET estimation methods at the grid level for irrigated (a) and rainfed (b) maize cultivation.

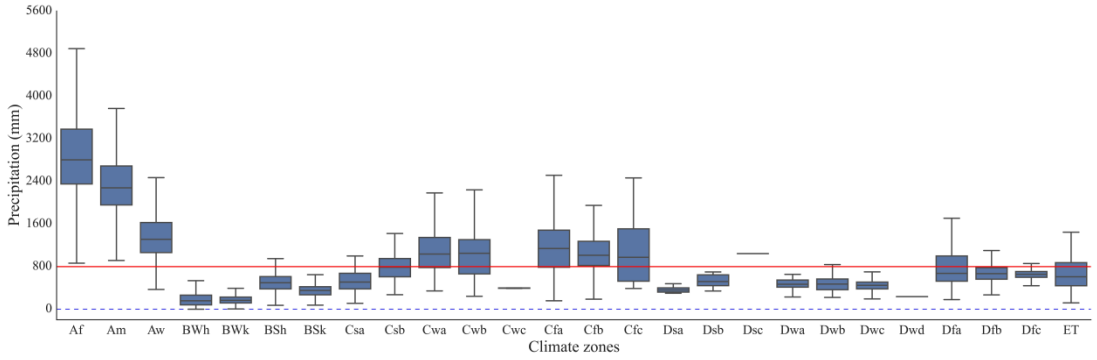

Figure S2-3. Global annual precipitation in different Köppen–Geiger climate zones.

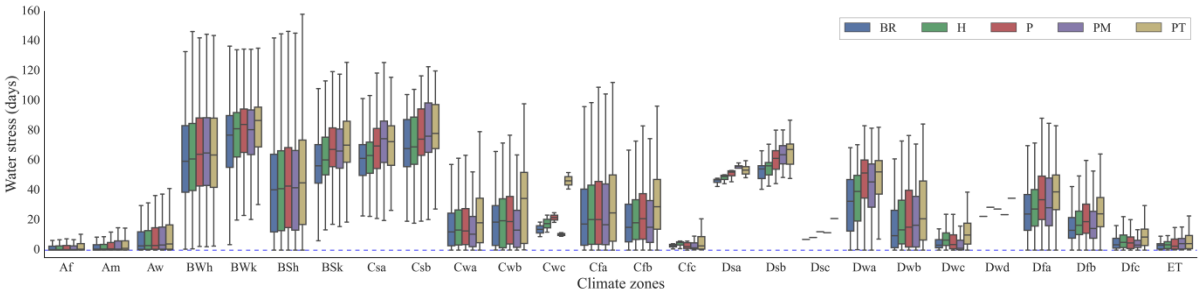

Figure S2-4. Estimated days of water deficit (water stress) at the Köppen–Geiger level.

Table S2-1. PET methods comparison between different crop models.

Model	PET options	Reference	Comments
APES	H, P, PM, PT	Donatelli et al. (2010)	Only PM, PT, H mentioned in the model reference
APSIM	PT, PM	Keating et al. (2003)	PM or PT are only used for calculating soil evaporation, while transpiration is calculated by using a transpiration efficiency approach based on dry matter growth.
AquaCrop	PM	Steduto et al. (2009)	
CropWat	PM	Smith (1992)	
CropSyst	PT, PM	Stockle et al. (2003)	Potential biomass accumulation is based on potential transpiration and crop intercepted solar radiation.
Daisy	PM	Hansen et al. (2012)	
DayCent	PM	Stehfest et al. (2007)	
DSSAT	P, PT, PM	Jones et al. (2003)	
EPIC	BR, H, P, PT, PM	Williams et al. (1989)	
Expert-N	P, PM, Haude, Ritchie	Stenger et al. (1999)	
FASSET	Makkink	Berntsen et al. (2003)	
GLAM	PT	Challinor et al. (2004)	
H08	Bulk formula	Hanasaki et al. (2008)	
HERMES	PM, Haude, TW	Kersebaum (2007)	Only Haude and TW mentioned in reference
HYBRID-maize	PM	Yang et al. (2004)	Not specified in the literature
InfoCrop	PT, PM	Aggarwal et al. (2006)	
IXIM	PT, PM	Lizaso et al. (2011)	Only PT mentioned in the model reference
LINPAC	PM	Jing et al. (2012)	
LPJmL	PT, PM	Bondeau et al. (2007)	
MAIZSIM	P	Kim et al. (2012)	
MCWLA	PM	Tao et al. (2009)	
MONICA	PM	Nendel et al. (2011)	
MSB	PT	Muchow et al. (1990)	Not specified in the reference
PEGASUS	PT	Deryng et al. (2011)	
PlantSys 1.0	P, PM	Jongschaap (2007)	Only PM mentioned in the model reference
SALUS	PT	Basso et al. (2010)	
SARRAH	PM	Baron et al. (2005)	
STICS	P, PT, SW	Brisson et al. (2003)	
WOFOST	P	Vandiepen et al. (1989)	

PET methods: BR: Barier–Robertson (Baier and Robertson, 1965); H: Hargreaves (Hargreaves and Samani, 1985); Haude (Haude ,1955); Makkink (Makkink, 1957); Ritchie (Ritchie, 1972); P: Penman (Penman, 1948); PM: Penman–Monteith (Monteith, 1965); PT: Priestley–Taylor (Priestley and Taylor, 1972); SW: Shuttleworth and Wallace (Shuttleworth and Wallace, 1985); TW: Turc–Wendling (Wendling et al., 1991)

Table S2-2. PET methods used in some large-scale crop modelling works.

Model	PET method	Reference	Study area
CLM-Crop	no information	Drewniak et al. (2013)	Global
EPIC-IIASA	no information	Balkovič et al. (2014)	Global
EPIC-IIASA	H	Balkovič et al. (2013)	Europe
DayCent	PM	Stehfest et al. (2007)	Global
GEPIC	H	Folberth et al. (2012)	Sub-Saharan Africa
GEPIC	H	Liu et al. (2007)	Global
GIS-based EPIC	no information	Tan and Shibasaki (2003)	Global
GLAM	PT	Osborne et al. (2007)	Global
Grid-Parallel-APSIM	no information	Zhao et al. (2013)	Australia
iGAEZ	PM	Tatsumi et al. (2011)	Global
LPJ-GUESS	no information	Lindeskog et al. (2013)	Africa
LPJmL	no information	Bondeau et al. (2007)	Global
LPJmL	no information	Gerten et al. (2011)	Global
MCWLA	PM	Tao and Zhang (2013)	China
ORCHIDEE-STICS	no information	Valade et al. (2014)	Brazil, Australia and La Réunion Island
pAPSIM	no information	Elliott et al. (2014)	Africa
pDSSAT	no information	Elliott et al. (2014)	Africa
PEGASUS	PT	Deryng et al., (2014); Deryng et al., (2011)	Global
WOFOST	P	Boogaard et al. (2013)	European Union

References

Aggarwal, P.K., et al., 2006. InfoCrop: a dynamic simulation model for the assessment of crop yields, losses due to pests, and environmental impact of agro-ecosystems in tropical environments. II. Performance of the model. Agric. Syst., 89(1), 47–67.

Baier, W. and Robertson, G.W., 1965. Estimation of latent evaporation from simple weather observations. Can. J. Plant. Sci., 45(3), 276–284.

Balkovič, J., et al., 2013. Pan-European crop modelling with EPIC: implementation, up-scaling and regional crop yield validation. Agric. Syst., 120, 61–75.

Balkovič, J., et al., 2014. Global wheat production potentials and management flexibility under the representative concentration pathways. Global Planet. Change, 122, 107–121.

Baron, C., et al., 2005. From GCM grid cell to agricultural plot: scale issues affecting modelling of climate impact. Philos. Trans. R. Soc. London, Ser. B, 360(1463), 2095–2108.

Basso, B., Cammarano, D., Troccoli, A., Chen, D.L. and Ritchie, J.T., 2010. Long-term wheat response to nitrogen in a rainfed Mediterranean environment: field data and simulation analysis. Eur. J. Agron., 33(2), 132–138.

Berntsen, J., Petersen, B.M., Jacobsen, B.H., Olesen, J.E. and Hutchings, N.J., 2003. Evaluating nitrogen taxation scenarios using the dynamic whole farm simulation model FASSET. Agric. Syst., 76(3), 817–839.

Bondeau, A., et al., 2007. Modelling the role of agriculture for the 20th century global terrestrial carbon balance. Global Change Biol., 13(3), 679–706.

Boogaard, H., Wolf, J., Supit, I., Niemeyer, S. and van Ittersum, M., 2013. A regional implementation of WOFOST for calculating yield gaps of autumn-sown wheat across the European Union. Field Crops Res., 143, 130–142.

Brisson, N., et al., 2003. An overview of the crop model STICS. Eur. J. Agron., 18(3–4), 309–332.

Challinor, A.J., Wheeler, T.R., Craufurd, P.Q., Slingo, J.M. and Grimes, D.I.F., 2004. Design and optimisation of a large-area process-based model for annual crops. Agric. For. Meteorol., 124(1–2), 99–120.

Deryng, D., Conway, D., Ramankutty, N., Price, J. and Warren, R., 2014. Global crop yield response to extreme heat stress under multiple climate change futures. Environ. Res. Lett., 9(3): 034011.

Deryng, D., Sacks, W.J., Barford, C.C. and Ramankutty, N., 2011. Simulating the effects of climate and agricultural management practices on global crop yield. Global Biogeochem. Cycles, 25: GB2006.

Donatelli, M., et al., 2010. A component-based framework for simulating agricultural production and externalities. Environmental and Agricultural Modelling. Springer, pp. 63–108.

Drewniak, B., Song, J., Prell, J., Kotamarthi, V.R. and Jacob, R., 2013. Modeling agriculture in the Community Land Model. Geosci. Model Dev., 6(2), 495–515.

Elliott, J., et al., 2014. The parallel system for integrating impact models and sectors (pSIMS). Environ. Modell. Software, 62, 509–516.

Folberth, C., Gaiser, T., Abbaspour, K.C., Schulin, R. and Yang, H., 2012. Regionalization of a large-scale crop growth model for sub-Saharan Africa: model setup, evaluation, and estimation of maize yields. Agric. Ecosyst. Environ., 151, 21–33.

Gerten, D., et al., 2011. Global water availability and requirements for future food production. J. Hydrometeorol., 12(5), 885–899.

Hanasaki, N., et al., 2008. An integrated model for the assessment of global water resources part 1: model description and input meteorological forcing. Hydrol. Earth Syst. Sci., 12(4), 1007–1025.

Hansen, S., Abrahamsen, P., Petersen, C.T. and Styczen, M., 2012. Daisy: model use, calibration, and validation. Trans. ASABE, 55(4), 1315–1333.

Hargreaves, G.H. and Samani, Z.A., 1985. Reference crop evapotranspiration from temperature. Appl. Eng. Agric., 1(2), 96–99.

Haude, W., 1955. Zur Bestimmung der Verdunstung auf möglichst einfache Weise. Mitt Dt Wetterd 11, 1–24.

Jing, Q., Conijn, S.J.G., Jongschaap, R.E.E. and Bindraban, P.S., 2012. Modeling the productivity of energy crops in different agro-ecological environments. Biomass Bioenergy, 46, 618–633.

Jones, J.W., et al., 2003. The DSSAT cropping system model. Eur. J. Agron., 18(3–4), 235–265.

Jongschaap, R.E.E., 2007. Sensitivity of a crop growth simulation model to variation in LAI and canopy nitrogen used for run-time calibration. Ecol. Modell., 200(1–2), 89–98.

Keating, B.A., et al., 2003. An overview of APSIM, a model designed for farming systems simulation. Eur. J. Agron., 18(3–4), 267–288.

Kersebaum, K.C., 2007. Modelling nitrogen dynamics in soil-crop systems with HERMES. Nutr. Cycling Agroecosyst., 77(1), 39–52.

Kim, S.H., et al., 2012. Modeling temperature responses of leaf growth, development, and biomass in maize with MAIZSIM. Agron. J., 104(6), 1523–1537.

Lindeskog, M., et al., 2013. Implications of accounting for land use in simulations of ecosystem carbon cycling in Africa. Earth Syst. Dyn., 4(2), 385–407.

Liu, J., Williams, J.R., Zehnder, A.J.B. and Yang, H., 2007. GEPIC – modelling wheat yield and crop water productivity with high resolution on a global scale. Agric. Syst., 94(2), 478–493.

Lizaso, J.I., et al., 2011. CSM-IXIM: A new maize simulation model for DSSAT version 4.5. Agron. J., 103(3), 766–779.

Makkink, G.F., 1957. Testing the Penman formula by means of lysimeters. J. Int. Water Eng., 11, 277–288.

Monteith, J., 1965. Evaporation and environment. Symp. Soc. Exp. Biol, 19, 205–234.

Muchow, R.C., Sinclair, T.R. and Bennett, J.M., 1990. Temperature and solar-radiation effects on potential maize yield across locations. Agron. J., 82(2), 338–343.

Nendel, C., et al., 2011. The MONICA model: testing predictability for crop growth, soil moisture and nitrogen dynamics. Ecol. Modell., 222(9), 1614–1625.

Osborne, T.M., Lawrence, D.M., Challinor, A.J., Slingo, J.M. and Wheeler, T.R., 2007. Development and assessment of a coupled crop-climate model. Global Change Biol., 13(1), 169–183.

Penman, H.L., 1948. Natural evaporation from open water, bare soil and grass. Proc. R. Soc. London, Ser. A, 193(1032), 120–145.

Priestley, C. and Taylor, R., 1972. On the assessment of surface heat flux and evaporation using large-scale parameters. Mon. Weather Rev., 100(2), 81–92.

Ritchie, J.T., 1972. Model for predicting evaporation from a row crop with incomplete cover. Water Resour. Res., 8(5): 1204–1213.

Shuttleworth, W.J. and Wallace, J., 1985. Evaporation from sparse crops – an energy combination theory. Q. J. R. Meteorolog. Soc., 111(469), 839–855.

Smith, M., 1992. CROPWAT: A computer program for irrigation planning and management. FAO Irrigation and drainage paper 46, 46. FAO, Rome.

Steduto, P., Hsiao, T.C., Raes, D. and Fereres, E., 2009. AquaCrop – The FAO Crop Model to Simulate Yield Response to Water: I. Concepts and Underlying Principles. Agron. J., 101(3), 426–437.

Stehfest, E., Heistermann, M., Priess, J.A., Ojima, D.S. and Alcamo, J., 2007. Simulation of global crop production with the ecosystem model DayCent. Ecol. Modell., 209(2–4), 203–219.

Stenger, R., Priesack, E., Barkle, G. and Sperr, G., 1999. Expert-N, a tool for simulating nitrogen and carbon dynamics in the soil-plant atmosphere system, Proceedings of the technical session, pp. 19–28.

Stockle, C.O., Donatelli, M. and Nelson, R., 2003. CropSyst, a cropping systems simulation model. Eur. J. Agron., 18(3–4), 289–307.

Tan, G.X. and Shibasaki, R., 2003. Global estimation of crop productivity and the impacts of global warming by GIS and EPIC integration. Ecol. Modell., 168(3), 357–370.

Tao, F., Yokozawa, M. and Zhang, Z., 2009. Modelling the impacts of weather and climate variability on crop productivity over a large area: a new process-based model development, optimization, and uncertainties analysis. Agric. For. Meteorol., 149(5), 831–850.

Tao, F. and Zhang, Z., 2013. Climate change, high-temperature stress, rice productivity, and water use in eastern China: a new superensemble-based probabilistic projection. J. Appl. Meteor. Climatol., 52(3), 531–551.

Tatsumi, K., et al., 2011. Estimation of potential changes in cereals production under climate change scenarios. Hydrol. Processes, 25(17), 2715–2725.

Valade, A., et al., 2014. Modeling sugarcane yield with a process-based model from site to continental scale: uncertainties arising from model structure and parameter values. Geosci. Model Dev., 7(3), 1225–1245.

Vandiepen, C.A., Wolf, J., Vankeulen, H. and Rappoldt, C., 1989. WOFOST – a simulation model of crop production. Soil Use Manage., 5(1), 16–24.

Wendling, U., Schellin, H.G. and Thomä, M., 1991. Bereitstellung von täglichen Informationen zum Wasserhaushalt des Bodens für die Zwecke der agrarmeteorologischen Beratung. Zeitschrift für Meteorologie, 41(6), 468–475.

Williams, J.R., Jones, C.A., Kiniry, J.R. and Spanel, D.A., 1989. The EPIC crop growth model. Trans. ASABE, 32(2), 497–511.

Yang, H.S., et al., 2004. Hybrid-maize–a maize simulation model that combines two crop modeling approaches. Field Crops Res., 87(2–3), 131–154.

Zhao, G., et al., 2013. Large-scale, high-resolution agricultural systems modeling using a hybrid approach combining grid computing and parallel processing. Environ. Modell. Software, 41, 231–238.

Chapter 3

Global assessment of nitrogen losses and trade-offs with yields from major crop cultivations

Based on

Global assessment of nitrogen losses and trade-offs with yields from major crop cultivations. Science of the Total Environment, 572: 526–537. (2016)

Authors

Wenfeng Liu[a], Hong Yang[a,b], Junguo Liu[c], Ligia B. Azevedo[d], Xiuying Wang[e], Zongxue Xu[f], Karim C. Abbaspour[a], Rainer Schulin[g]

[a]*Eawag, Swiss Federal Institute of Aquatic Science and Technology, Ueberlandstrasse 133, CH-8600 Duebendorf, Switzerland*

[b]*Department of Environmental Sciences, University of Basel, Petersplatz 1, CH-4003 Basel, Switzerland*

[c]*School of Environmental Science and Engineering, South University of Science and Technology of China, Shenzhen, 518055, China*

[d]*International Institute for Applied Systems Analysis (IIASA), Ecosystem Services and Management Program, Schlossplatz 1, A-2361 Laxenburg, Austria*

[e]*Blackland Research and Extension Center, Temple, TX 76502, USA*

[f]*College of Water Sciences, Beijing Normal University, Beijing 100875, China*

[g]*ETH Zürich, Institute of Terrestrial Ecosystems, Universitätstr. 16, CH-8092 Zürich, Switzerland*

Abstract

Agricultural application of reactive nitrogen (N) for fertilization is a cause of massive negative environmental problems on a global scale. However, spatially explicit and crop-specific information on global N losses into the environment and knowledge of trade-offs between N losses and crop yields are largely lacking. We use a crop growth model, Python-based Environmental Policy Integrated Climate (PEPIC), to determine global N losses from three major food crops: maize, rice, and wheat. Simulated total N losses into the environment (including water and atmosphere) are 44 Tg N yr^{-1}. Two thirds of these, or 29 Tg N yr^{-1}, are losses to water alone. Rice accounts for the highest N losses, followed by wheat and maize. The N loss intensity (NLI), defined as N losses per unit of yield, is used to address trade-offs between N losses and crop yields. The NLI presents high variation among different countries, indicating diverse N losses to produce the same amount of yields. Simulations of mitigation scenarios indicate that redistributing global N inputs and improving N management could significantly abate N losses and at the same time even increase yields without any additional total N inputs.

Keywords

N losses; Global assessment; NLI; Trade-offs; Major crops; PEPIC

Graphical Abstract

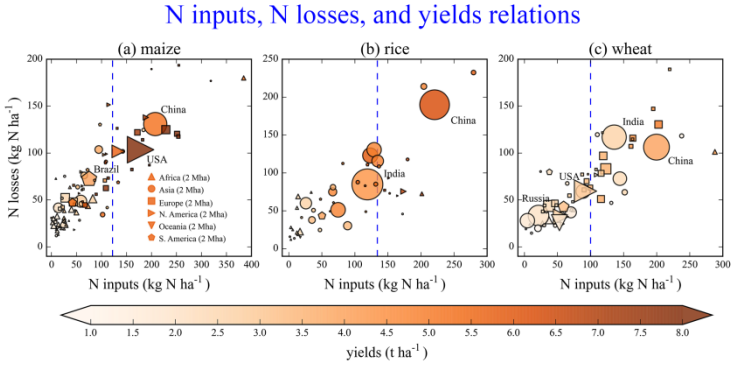

Highlights

We simulate N losses of major cereal crops by using a global crop model.

N losses are focused on several main producers, where more attentions should be paid.

NLI is a useful indicator for assessing trade-offs between N losses and yields.

Mitigation scenarios show that N losses can be reduced without compromising yields.

3.1 Introduction

Anthropogenic activities are the major driver of changes in the global nitrogen (N) cycle (Fowler et al., 2013). Terrestrial N flows resulting from anthropogenic activities have increased to > 3.3-fold of those resulting from natural processes by 2010 (Fowler et al., 2013; Galloway et al., 2014). As a consequence, the global N cycle is now 3.5 times above what is considered as a safe threshold (Rockstrom et al., 2009). Agriculture is the largest consumer (63%) of annual terrestrial reactive N (Sutton et al., 2013). Global industrial N fertilizer application increased 9-fold from 1960 to 2010 (Ladha et al., 2016; Sutton et al., 2013), with N fertilizer inputs to croplands reaching 120 Tg N yr^{-1} (Tg = 10^{12} g) at the end of that period (Fowler et al., 2013). This unprecedented increase in N flows was made possible by the development of industrial fixation of atmospheric N (Haber–Bosch process) and the associated mineral N fertilizer use (Galloway et al., 2008). The drivers of this development are the need to supply food for an increasing global population, dietary shift towards more meat and dairy products consumption, and growing biofuel demand (Foley et al., 2011). On the downside, this development is associated with increasing agricultural N losses into the environment, causing stratospheric ozone depletion, eutrophication and acidification of water and soil, as well as losses in the diversity of ecosystems (Babbin and Ward, 2013; Clark and Tilman, 2008; Conley et al., 2009; Davidson, 2009; Diaz and Rosenberg, 2008; Erisman et al., 2013; Foley et al., 2005; Foley et al., 2011; Guo et al., 2010; Liu et al., 2013b; Sutton et al., 2013). Many studies have found that N use efficiency (NUE, defined as the ratio of crop harvested N to total N inputs) is low in major food producing regions. On global average, it is only about 0.42 in 2010 (Zhang et al., 2015). Without emission reductions, global N losses are expected to further increase and reach levels higher than 150% of the 2010 values by 2050 (Bodirsky et al., 2014).

To control N emissions, it is important to quantify and identify the main pathways and major contribution regions of N emissions. Previous studies of N losses performed at a global scale were mainly based on mass balance methods. On this basis, Liu et al. (2010) found that about half of global total N inputs into croplands were lost to the environment. Bouwman et al. (2013) estimated that around 93 Tg N yr^{-1} was lost from arable lands and 45 Tg N yr^{-1} from grasslands. Lassaletta et al. (2014) investigated the relationship between crop yields and N inputs based on FAO (Food and Agriculture Organization of the United Nations) data from 124 countries and concluded that about 53% of N added to croplands was lost to the environment. Zhang et al. (2015) built a global N budget database and the total N losses to the environment were estimated at about 100 Tg N yr^{-1} in 2010. However, all of these studies require crop yields as data inputs to quantify harvested N. Consequently, interactions between N dynamics and crop growth cannot be represented, which are essential to explore the trade-offs of N losses and yield benefits for future

N management. Mass balance method applies the same empirical equations to calculate N fluxes over a large scale without explicitly considering the spatial variability (e.g. site-, climate- and management-specific differences). Besides, most of these global N balance assessment studies focus on total N fluxes aggregated from different crops (and grasses) with much less attention on crop-specific disparity, which is important to guide N fertilization management, especially from the major cereal crop cultivations. Therefore, it is critical to explicitly investigate crop-specific N losses and the related trade-offs with yields in order to provide suggestions for controlling N emissions.

While biophysical crop growth models nowadays have the ability to account for site- and crop-specific interactions between plant growth and N turnover, only few studies so far have made use of this ability in assessing agricultural N losses on a large scale. Examples are the studies of van der Velde et al. (2009) who used the Environmental Policy Integrated Climate (EPIC) model (Williams, 1995; Williams et al., 1984) to estimate N losses through leaching for rapeseed cultivation in Europe; and the study of Del Grosso et al. (2009) who used the DAYCENT model to study global N losses from maize, soybean, and wheat cultures. In addition, the spatial resolution in the simulations by Del Grosso et al. (2009) is quite coarse (1.9 arcdeg), and no crop-specific information on N fertilizer use and N leaching is given. Another example is the study of Qiu et al. (2011) who applied the GIS-based DNDC (Denitrification–Decomposition) model to simulate N leaching from croplands at the county level in China, but did not give site- and crop-specific information on N losses. None of these studies include rice. Three major cereal crops, i.e. maize, rice, and wheat, together consume about 60% of global N fertilizer application (Ladha et al., 2005) and provide about 57% of the dietary calories produced by agriculture (Tilman et al., 2011). In order to identify the hotspots of N losses from crop cultivations, it is important to conduct a high spatial resolution assessment of N losses by focusing on these three major crops.

The concept of NUE is generally used in N management. Achieving high NUE is one of the major targets for modern agriculture (Conant et al., 2013; Cui et al., 2014; Lassaletta et al., 2014; Zhang et al., 2015). However, this concept cannot be directly used for N loss assessment due to soil N imbalance, either N accumulation or N depletion (Liu et al., 2010). For example, Liu et al. (2010) estimated NUE based on the ratio of crop harvested N to total N inputs to be 0.59 on global average, however the ratio of total N losses to total N inputs was 0.49 other than 0.41 based on their estimations. This imbalance stemmed from the difference between total N losses and total N inputs minus total crop harvested N. The former considers the soil N imbalance and the latter does not. Taking into consideration the soil N balance is important for understanding the global N budget and for N management. In low input countries, typically African countries, soil N

depletion is prevalent (Sanchez, 2002). In high N input countries, such as China, soil N accumulation may be significant (Zhou et al., 2016).

Here, we use PEPIC, a grid-based EPIC model developed in a Python environment, to determine global N losses from the cultivations of the three major crops at a high spatial resolution of 30´ (about 50 km at the equator). The EPIC model adopts the Century model (Parton et al., 1994), which is widely used to simulate soil carbon and N dynamics (Bhattacharyya et al., 2010; Cong et al., 2014), to model carbon and N turnover (Izaurralde et al., 2006). Coupled with spatial analysis tools, EPIC has been widely applied to estimate impacts of agronomic practices and climate change on crop yields (Balkovič et al., 2014; Folberth et al., 2014; Liu et al.,2013a; among others). Due to its integration with Python, PEPIC can be easily applied at different spatial scales. It has been successfully applied to simulate global maize growth (Liu et al., 2016). In addition, its performance on simulating growth of the other two crops is also quite robust (Figure S3-1). Given that N leaching to water is a major source of water pollution, we also consider the losses to water alone, in addition to total losses to the environment which includes water and atmosphere. To address the trade-offs between N losses and yields, we propose a concept as N loss intensity (NLI) which measures N losses per unit of yield. Finally, in order to demonstrate the feasibility of reducing N losses while still maintaining or increasing global production of the three target crops, the trade-offs between N losses and crop yields under three proposed N fertilization scenarios are also investigated.

3.2 Methods

3.2.1 Model and input data

The EPIC model (Williams, 1995; Williams et al., 1984) simulates crop growth and soil nutrient dynamics. In this study, the PEPIC model was used for the global simulation at a resolution of 30´ (Liu et al., 2016). Default parameters of the EPIC model were used for global application, as it is difficult to adjust model parameters at specific regions on such a large scale. Additionally, the estimated N losses were compared with previous studies.

Soil N inputs considered in EPIC include fertilizer (N_{fer}) and manure (N_{man}) application, crop residue decomposition (N_{dec}), and rainfall deposition (N_{dep}). Soil N outputs are N up taking by crops (N_{up}), N losses into the atmosphere via volatilization of ammonia (N_{av}) and denitrification of nitrate (N_{ad}) and exports of dissolved or particle-bound N into water with soil erosion (N_{ws}), surface runoff (N_{wr}) and leaching (N_{wl}). To close the soil N cycle, change of soil N stock (ΔN) is also considered. Soil N budget is expressed as following:

$$N_{fer} + N_{man} + N_{dec} + N_{dep} = N_{up} + N_{av} + N_{ad} + N_{ws} + N_{wr} + N_{wl} + \Delta N \quad (3\text{-}1)$$

In this study, we focused on N losses into the total and aquatic (water) environment:

$$N_t = N_{av} + N_{ad} + N_{ws} + N_{wr} + N_{wl} \quad (3\text{-}2)$$

$$N_w = N_{ws} + N_{wr} + N_{wl} \quad (3\text{-}3)$$

where N_t and N_w are N losses into the total and the aquatic (water) environment, respectively. All these fluxes are calculated in units of kg N ha^{-1}. In EPIC, N_{ad} is a function of soil temperature and water content, while N_{av} is calculated based on soil temperature and wind speed. N_{wr} and N_{wl} are calculated by the products of nitrate-N concentration and soil surface runoff and seepage water. N_{ws} is calculated by considering soil erosion, organic N concentration in the top soil layer, and enrichment ratio of N in sediment. It should be noted that, while N_w is N export from agricultural fields with water flows, this export may not end up entirely in water bodies. Also, a portion of N losses to water bodies can flow to the sea, imposing the environmental impacts on coastal waters instead of the areas where they are initially generated. However, quantifying N losses reaching the coastal waters requires hydrological models to simulate the transport of nutrient in the water channels, which is beyond the scope of this study. One of the main purposes of this study is to explore the possible N losses from the farmlands and identify the global hotspots of losses. We do not trace further the fate of the N that is lost to water bodies. More details about N routines in EPIC can be found in Williams (1995) and Izaurralde et al. (2006).

Crop-specific N inputs with application of mineral fertilizers and manure (N_{fer} + N_{man}, N_{in} hereafter) were obtained from EarthStat (http://www.earthstat.org). Mineral N, phosphorus, and potassium fertilizer inputs are based on Mueller et al. (2012), while N, phosphorus, and potassium inputs from manure are based on West et al. (2014), which considers 36% of manure being volatilized before reaching croplands. These data are currently the most up-to-date crop-specific datasets on global agricultural N inputs. N deposition from precipitation was estimated by EPIC based on annual precipitation and N concentration in rainfall. The sources of other input datasets can be found in SI. As both land-use (1998–2002) and fertilizer data relate to the years around 2000, this also holds for the model outputs (averaging between 1998 and 2002). Simulation results are presented at four levels, i.e. grid, country, continent, and globe. Average N_{in}, N_t, N_w, and crop yields at country, continent, and global levels were calculated as area-weighted averages of each variable at the corresponding levels. Total N_{in}, total N_t, total N_w, and crop production were calculated by multiplying average values of N_{in}, N_t, N_w, and yields by corresponding cropland areas calculated by using Eqs. (3-4) – (3-7):

$$TN_{in} = N_{in} * A_i \quad (3\text{-}4)$$

$$TN_t = N_t * A_i \quad (3\text{-}5)$$

$$TN_w = N_w * A_i \quad (3\text{-}6)$$

$$P = Y * A_i \quad (3\text{-}7)$$

where A is cropland areas at the country, continental, and global levels; TN_{in} [Gg N yr^{-1}], TN_t [Gg N yr^{-1}], and TN_w [Gg N yr^{-1}] are total N_{in}, N_t, and N_w at each spatial level, respectively; P [Tg yr^{-1}] is the crop production and Y [t ha^{-1}] is the yield.

In order to reflect the trade-offs between N losses and yields, we used the NLI defined as:

$$NLI = N_t/Y \quad (3\text{-}8)$$

The NLI quantifies the N losses associated with the production of a unit mass (1 t) of yield. Lower values of NLI mean less N losses for producing the same amount of food.

3.2.2 Crop management parameters

The model was separately applied to rainfed and irrigated cultivations. For irrigated crops, we assumed that drip irrigation was applied when water stress exceeded 10% on a given day up to a maximum annual supply of 1000 mm. This is a common practice in crop modelling when there is no information on the actual irrigation schedules and the amounts of water applied over time in different regions (Balkovič et al., 2014; Folberth et al., 2012; Liu and Yang, 2010; Liu et al., 2016; Rosenzweig et al., 2014). After simulation of both rainfed and irrigated cultivations, aggregated outputs from both cultivation systems were calculated for each grid cell by using area-weight averaging (Liu et al., 2007). Based on Del Grosso et al. (2009), we assumed that 25% of the crop residues are left on field. Furthermore, we assumed that phosphorus and potassium fertilizers were applied immediately before planting (Balkovič et al., 2014), as we found no global-scale dataset on fertilization schedules. Tillage was implemented before planting. Previous studies proposed various schedules for N application. For example, Folberth et al. (2014) applied 1/3 of N inputs before planting, and the rest one month after germination in sub-Saharan Africa. Stehfest et al. (2007) applied equal amounts of N four times globally. Other studies, not aiming at N loss assessment, used an automatic application schedule (Balkovič et al., 2013; Folberth et al., 2012; Liu et al., 2007). In this study, we tested three different N fertilization schedules: FixN1, FixN2, and FixN3 (Table 3-1). While N_t predictions were quite similar for all three schedules (Figure 3-5), we found that the predicted country-specific yields agreed best with the FAO reported yields for wheat simulation when we used the FixN3 schedule and that there were only minor differences to reported yields for maize and rice with this schedule (SI and Figure S3-1). Therefore, we selected FixN3 as the baseline for the analysis of the three N mitigation scenarios: FixN3E, AutoN, and AutoNE as defined in Table 3-1. Briefly, FixN3E distributes world N inputs evenly using the FixN3 schedule. AutoN stands for automatic N fertilization with current value of N inputs, which means N application is dependent on crop demands before reaching the current

application rates. AutoN can be also used as baseline of efficient N fertilization, as the needed amount of N is applied at the time when it is needed. AutoNE stands for automatic N fertilization, but puts limits on the maximum application amounts evenly with global average N_{in} of maize, rice, and wheat. It should be noted that in all different N fertilization schedules and scenarios, we did not consider different types of N fertilizers due to unavailable data. This simplification has been widely used in large-scale crop modelling (Balkovič et al., 2014; Folberth et al., 2014; Rosenzweig et al., 2014; van der Velde et al., 2009).

Table 3-1. Description of different nitrogen (N) fertilization schedules and scenarios.

	Application time			Application rates
	1st	2nd	3rd	
Schedules				
FixN1	3 days before planting			Applying N inputs once
FixN2	3 days before planting	35 days after planting		One-second of N inputs for each time
FixN3	3 days before planting	35 days after planting	65 days after planting	One-third of N inputs for each time
Scenarios				
FixN3E	3 days before planting	35 days after planting	65 days after planting	One-third of 122, 134, 100 kg N ha^{-1} for maize, rice, and wheat for each time[a]
AutoN	Dynamic			Applying N when crop needs with a cap set at the current level of N inputs
AutoNE	Dynamic			Applying N when crop needs with a maximum amount of 122, 134, 100 kg N ha^{-1} for maize, rice, and wheat[a]

[a] Global average N inputs for maize, rice, and wheat are 122, 134, and 100 kg N ha^{-1}, respectively.

3.2.3 Uncertainty analysis

We applied the Latin Hypercube Sampling (LHS) method to explore model uncertainties derived from model parameters (Mckay et al., 1979). LHS first divides the parameters into indicated number of segments. Then the parameter segments are randomized, and finally a random sample is chosen in each segment. It is more efficient than Monte Carlo (Mckay et al., 1979) and also used in the SWAT-CUP software (Abbaspour, 2011) to calibrate SWAT (Soil and Water Assessment Tool) model parameters (Abbaspour et al., 2007; Schuol et al., 2008; Yang et al., 2008). Parameters associated with N, phosphorus, and carbon routines in EPIC and their possible ranges for uncertainty analysis were carefully selected based on Della Peruta et al. (2014) and Wang et al. (2012) (Table S3-2). In this study, we considered 100 parameter segments for each crop based on the LHS method.

3.3 Results

3.3.1 Nitrogen loss assessment

The simulations identified some regions with particularly high N losses (Figure 3-1), to which more attentions should be paid. As Figure S3-2 suggests, the high losses in these regions are mainly related to high N inputs, and also Figure 3-2 shows a clear trend that N losses increase with increasing N inputs. For maize cultivation, the model predicted particularly high levels of N_t in the eastern parts of China, South Korea, Japan, Indonesia, western Europe, the northeastern parts of the USA, and southern Mexico (Figure 3-1a). Predicted N_w show similar spatial patterns as N_t (Figure 3-1b). The USA and China are two major maize producers and also produced quite high N_t, especially in China (Figure 3-2a). Consequently, these two countries together accounted for 52% of global TN_t for maize (Table 3-2). On the other hand, N_t is also relatively high for some countries with low N_{in} (e.g. <50 kg N ha^{-1}), especially in Africa. In some cases, the simulations indicate that the ratio of N_t to N_{in} was even higher than 1. Such high ratios in combination with low total N inputs suggest that soil N depletion should be considered a major factor. The relationship between N_w and N_{in} is not as clear as that between N_t and N_{in}, as shown in Figure 3-2 the linear relationship and coefficient of determination (R^2). We found that the total volume of growing season precipitation (GSP) and irrigation water also affects N losses, with low volume of GSP and irrigation tending to have low values of N losses at the country level (Figure S3-3). These effects can also be observed in different climate regions. For example, N_t of maize is highest where the total volume of GSP and irrigation water is higher than 600 mm in temperate regions, although N_{in} is not highest in these regions (Figure S3-4). The global TN_t and TN_w were calculated to be 12,414 and 6,777 Gg N yr^{-1} (Gg = 10^9 g) (Table 3-2). Asia and North America produced the highest total N losses. Together they accounted for 71% and 74% of the global TN_t and TN_w, respectively. While predicted total environmental N losses were similar in Asia and North America, with North America having much higher maize yields (Table 3-2).

For rice cultivation, high levels of N_t and N_w were found in China, South Korea, Japan, Vietnam, Bangladesh, and Indonesia (Figures 3-1c and 3-1d). India and China have the largest rice cultivation areas. Together the two countries accounted for two thirds of global total N losses, both to the total environment as well as to water alone (Table 3-2). As Figure 3-2 shows, the higher N losses in China are related to correspondingly higher inputs of N fertilizers compared to India. The total volume of GSP and irrigation water for rice cultivation is much higher than that for maize and wheat cultivation, particularly for wheat (Figure S3-3). This difference may partially explain the higher N losses for rice in addition to its high N inputs than the other two crops. At the same time, high levels of total GSP and irrigation are associated with high levels of N losses from rice cultivation in various climate regions (Figure S3-4). The predicted global TN_t

and TN_w are 17,129 and 13,531 Gg N yr^{-1} from rice cultivation (Table 3-2). Asia on the whole produced about 92% of the global rice harvests in 2000, and also played an overwhelming role in contributing to total N losses. It alone accounted for 96% of the global total N released from rice fields into the total environment and for 97% of the global N released form rice fields into water.

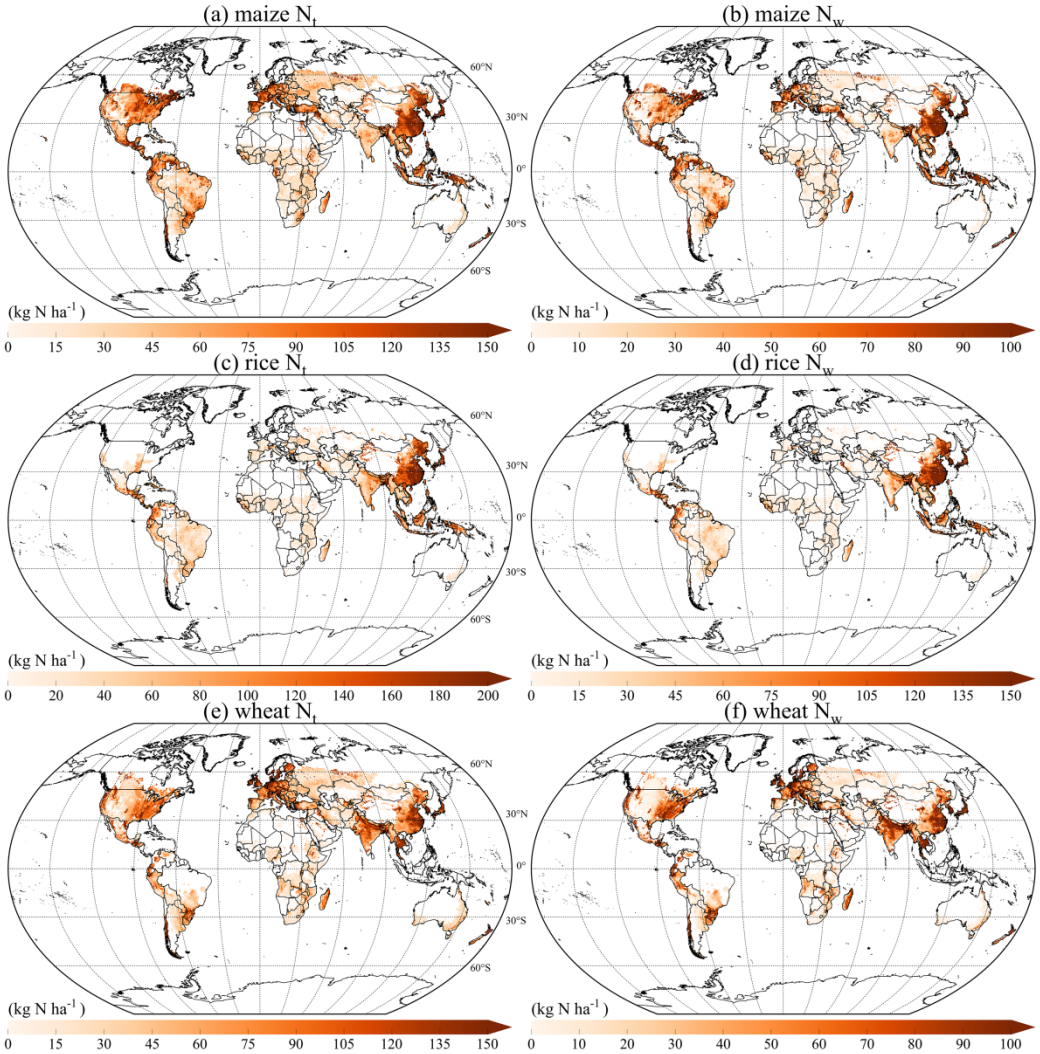

Figure 3-1. Global maps of nitrogen losses into the environment (N_t) and water (N_w) for maize (a, b), rice (c, d), and wheat (e, f).

For wheat cultivation, high level of N losses were predicted for large parts of southeastern China, northern India, South Korea, Japan, Thailand, southeastern USA, and central Europe (Figures 3-1e and 3-1f). India and China are also the largest wheat producers and together contributed 44% and 55% of global TN_t and TN_w for wheat, respectively (Figures 3-2e and 3-2f). In contrast, the USA and Russia, another two major wheat producers, produced much less N losses, but also applied much less N inputs, especially Russia. The global TN_t and TN_w were 14,253 and 8,584 Gg N yr^{-1} (Table 3-2). Asia produced 45% of global wheat harvests, but contributed 60% and 69% of global TN_t and TN_w, respectively. Following Asia, Europe presented

the second highest total N losses, accounting for 20% and 18% of global TN_t and TN_w, respectively.

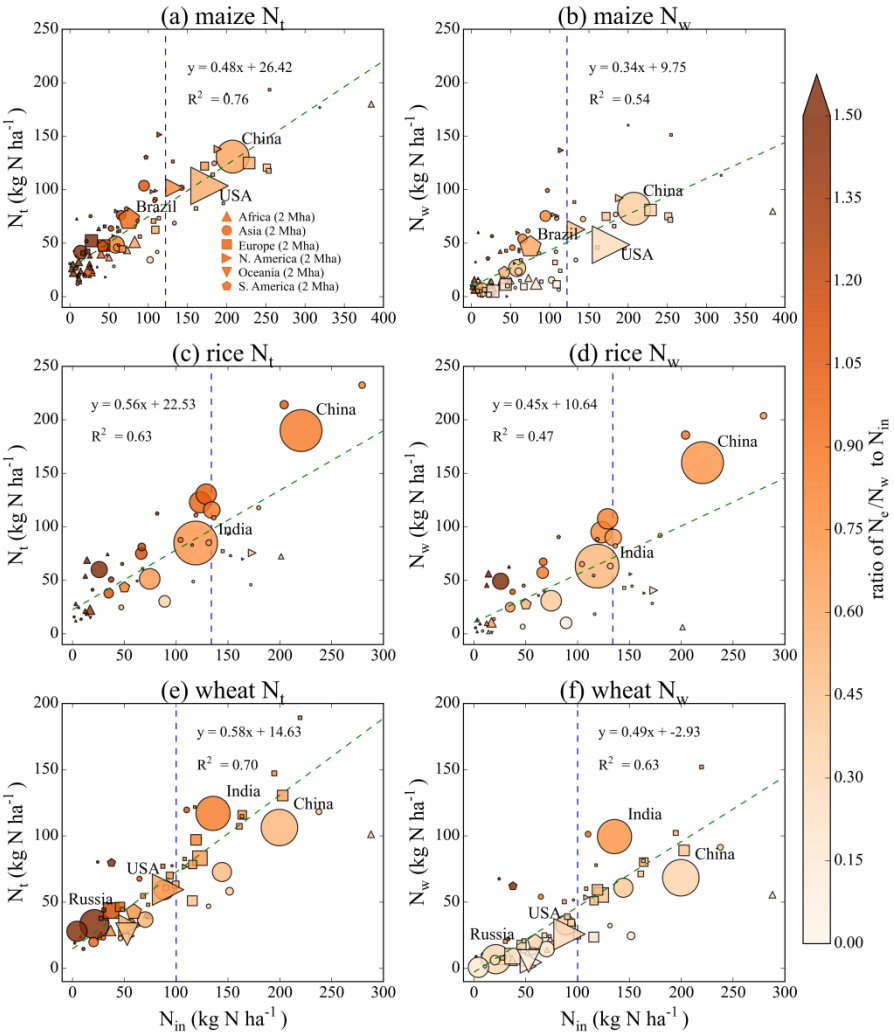

Figure 3-2. Nitrogen inputs (N_{in}) and nitrogen losses into the environment (N_t) and water (N_w) for maize (a, b), rice (c, d), and wheat (e, f) at country level. Countries with the smallest areas (for a total of 1% of global total cropland areas of each crop) are discarded; different shapes represent different continents; sizes represent cropland areas for each country; colours present ratio of N losses (N_t and N_w) to N_{in}; dashed blue vertical line represents the world average N_{in} for each crop; dashed green line represents linear regression between N_t and N_{in} (a, c, e) and between N_w and N_{in} (b, d, f); equation represents the linear relationship; R^2 is the coefficient of determination of equation.

3.3.2 Intensity of nitrogen losses in relation to yields

Generally, yields increase with N inputs as long as N is limiting crop plant growth, but with increasing N inputs also N losses increase (Figures 3-2 and 3-3). In order to demonstrate the complex relationship among N_{in}, yields, and N_t more clearly, we use the concept of NLI. The NLI presents quite high variation, indicating some countries perform better, in terms of low N losses,

to produce the same amount of yields, while the other countries do not (Figure 3-3). For maize cultivation, NLI is around 8–30 kg N t^{-1} (Figure 3-3a). High N inputs can be associated with high NLI, as in the case of China, as well as with low NLI, as in the case of the USA, where N is obviously more efficiently used to produce high yield and thus less N is wasted. Vice versa, also low N inputs can be associated with quite high NLI due to low yields and relatively high N loses compared to N inputs. For example, the variation of NLI in Africa is between 6 and 45 kg N t^{-1} despite very small N inputs. For rice cultivation, predicted NLI were around 10–40 kg N t^{-1} (Figure 3-3b). China has NLI about 30 kg N t^{-1}, while India around 20 kg N t^{-1}. For wheat cultivation, NLI is higher compared with the other two crops, around 10–50 kg N t^{-1} (Figure 3-3c). Among the major wheat producers, India has the highest NLI, followed by China, the USA, and Russia.

Table 3-2. Total nitrogen losses and crop production globally, continentally, and in the top 10 producing countries for maize, rice, and wheat in 2000. TN_{in}, TN_t, and TN_w are total nitrogen inputs (only including mineral fertilizer and manure), total nitrogen losses into the environment, and total nitrogen losses into water (in Gg N yr^{-1}), respectively; P is crop production (in Tg yr^{-1}).

Maize					Rice					Wheat				
Regions	TN_{in}	TN_t	TN_w	P	Regions	TN_{in}	TN_t	TN_w	P	Regions	TN_{in}	TN_t	TN_w	P
Global	17816	12414	6777	780	Global	20332	17129	13531	677	Global	20859	14253	8583	517
Africa	1001	852	322	54	Africa	204	245	136	17	Africa	559	298	120	15
Asia	6363	4364	2728	190	Asia	19492	16432	13107	624	Asia	12899	8560	5893	232
Europe	2223	1629	721	115	Europe	37	26	11	3	Europe	3598	2893	1542	130
N. America	7013	4386	2267	347	N. America	299	153	91	12	N. America	2704	1714	658	95
Oceania	7	5	3	0	Oceania	2	2	0	0	Oceania	618	304	69	20
S. America	1209	1179	737	74	S. America	298	271	186	21	S. America	483	484	301	25
USA	5649	3286	1540	289	India	5126	3660	2729	188	China	6002	3197	2057	118
China	5048	3184	2002	128	China	8744	7533	6345	178	India	3594	3100	2636	36
Brazil	851	817	527	44	Indonesia	1271	1270	980	61	USA	2054	1324	576	65
Mexico	958	731	450	40	Thailand	713	491	296	46	Russia	408	643	134	39
India	381	318	175	19	Bangladesh	1209	1224	1007	45	Australia	610	298	64	20
Russia	57	174	27	9	Vietnam	831	715	557	30	Canada	580	340	48	29
Nigeria	88	92	39	8	Myanmar	152	353	289	16	Kazakhstan	41	261	7	16
Argentina	146	164	79	19	Philippines	267	91	31	10	Turkey	771	517	285	20
Ukraine	91	174	17	8	Pakistan	199	225	171	14	Pakistan	1190	600	502	6
France	694	379	246	27	Brazil	140	121	77	11	Argentina	348	251	117	19

3.3.3 Mitigation scenarios

Based on the FixN3E mitigation scenario, which evenly distributes the globally available N fertilizers, the global production of maize, rice, and wheat could increase by 29, 62, and 45 Tg yr^{-1} without any additional N inputs (Table 3-3). At the same time, it would lead to significant decreases in total N_t and N_w, especially for rice and wheat cultivations according to our

simulations. Maize yields and environmental N losses are predicted to decline in some European countries and the USA, while only N_t but not yield would decrease in China (Figure 3-4a). Large increases in maize yields but also in N losses would be expected in South America and Africa (Table 3-3). Some countries such as Brazil would be expected to show a substantial increase in yield with only a negligible increase N_t compared to a large increase in N_{in} (from 75 to 122 kg N ha^{-1}). For rice, a major decrease in N losses would be expected for China, while yield could be maintained at today's level (Figure 3-4b). For wheat, China would see a large decrease in N_t with a small decrease in yield, while India would only experience a decrease in N_t (Figure 3-4c). In the contrary, Russia shows a high potential to increase yield (about 1 t ha^{-1}) with a minor increase in N_t.

In the AutoN mitigation scenario, crop yields would not increase significantly (at least for maize and rice), but as much less N inputs would be needed (Figures 3-4d–3-4f), it would result in a significant reduction in global N losses with more efficient N fertilization (Table 3-3). For maize and rice cultivation, China shows a dominant decrease in N_t (Figures 3-4d and 3-4e). For wheat, China and India would see large decreases in N_t, while many countries in Europe would decrease N_t and simultaneously increase wheat yields (Figure 3-4f).

Compared with the FixN3E scenario, the impacts on yields are similar for maize and rice cultivations by adopting the AutoNE mitigation scenario with more efficient N management (Figures 3-4g and 3-4h). Further decreases of N_t in China and the USA from maize cultivation and in China from rice cultivation are predicted. As for wheat, the influence is more positive with more countries moving into a condition where increasing yields and decreasing average N_t happen simultaneously, especially in Europe (Figure 3-4i). Besides, the increases of N_t are less significant in the rising N losses countries under the FixN3E scenario; while the decreases of N_t in China and India would be further enhanced.

3.3.4 Uncertainties

Generally, the range of uncertainty for N_t derived from parameters is relatively small for maize, rice, and wheat either globally, continentally, or for the top 10 producing countries (Figure 3-5). The results calculated by using model default parameters are very close to the median values for all the three crops, which, in another way and to some degree, reflect the reasonable estimations of N losses by using the constructed simulation framework in this study. Furthermore, differences in N losses between simulations comparing the three fertilization schedules, i.e. FixN1, FixN2, and FixN3, were also small (Figure 3-5).

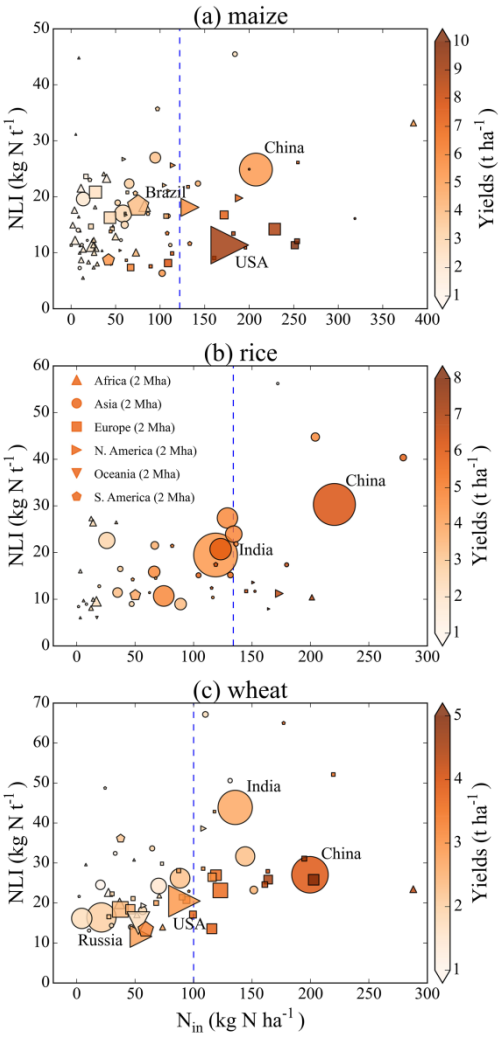

Figure 3-3. Intensity of nitrogen losses (NLI) into the environment in relation to yields against nitrogen inputs (N_{in}) at country level. Countries with the smallest areas (for a total of 1% of global total cropland areas of each crop) are discarded; shapes represent different continents; sizes represent cropland areas for each country; colours present crop yields; FAO reported yields are used for China for rice cultivation and for India and Pakistan for wheat cultivation because of their underestimated yields, more details see SI; dashed vertical line represents the world average N_{in} for each crop.

3.4 Discussion

3.4.1 Comparisons with other studies

We compared our results with previous studies, which investigated large-scale N losses from the whole agricultural sector, to check the reliability of our simulations. The ratio of N_t to N_{in} ranged between 0.76 and 0.85 in such studies (Bouwman et al., 2009; Bouwman et al., 2013; Liu et al., 2010; Mekonnen and Hoekstra, 2015; Sutton et al., 2013) (Table 3-4). The ratio found in

our study is just slightly below this range. No legume crops were considered in this study as other studies did; this might contribute to the slight difference. Generally, even though much less soil N excess over crop plant demand can be expected to occur in legume crops compared to the major cereal crops investigating here, some N losses do also occur from legume crop cultivations. On the other hand, the ratio of N_w to N_{in} is 0.49 in our study, which is within the range of 0.22–0.55 as reported by these previous studies. The reported variation of N_w/N_t is quite high (0.26–0.70), implying the large uncertainties to separate N_w and N losses into atmosphere from N_t. Our estimation is also within this range. These comparisons thus indicate that our simulations produced plausible results.

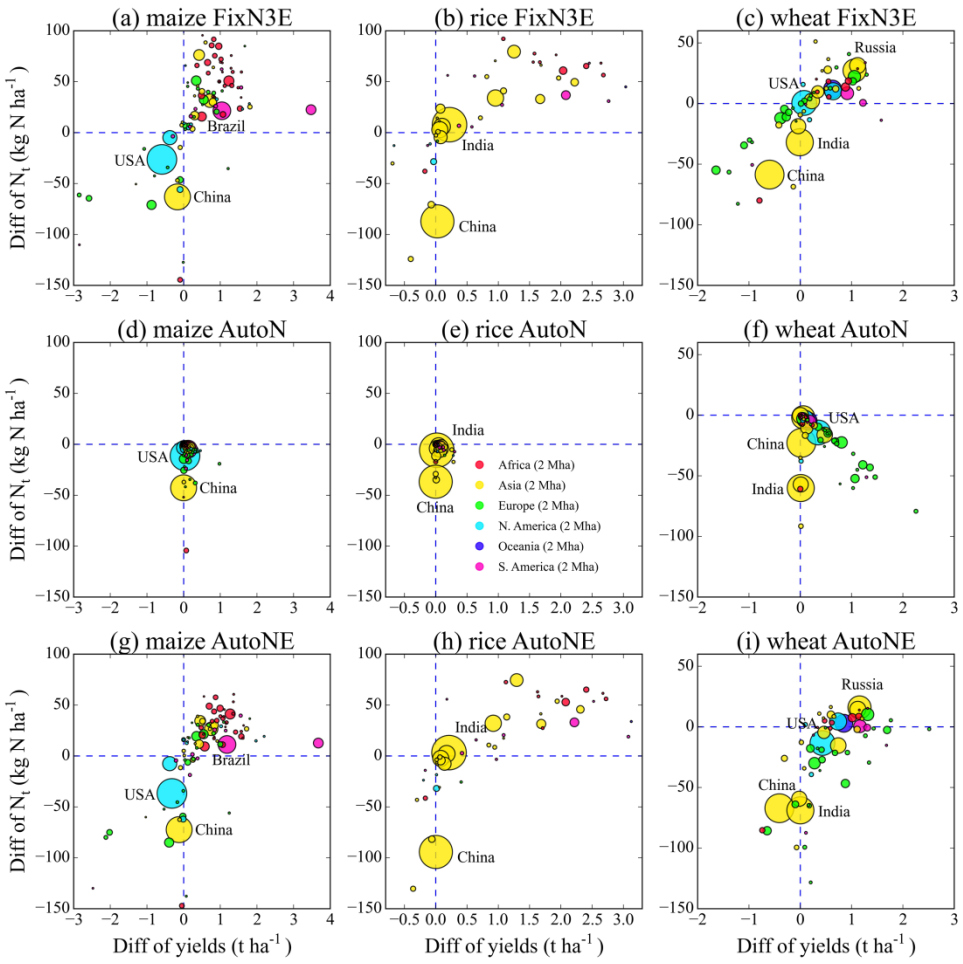

Figure 3-4. Differences of yields and nitrogen losses into the environment (N_t) between different mitigation scenarios and base scenario for maize (a, d, g), rice (b, e, h), and wheat (c, f, i). Countries with smallest areas (for a total of 1% of global total cropland areas of each crop) are discarded; sizes represent cropland areas for each country; colours represent different continents.

It should be noted that the difference between 1 and N_t/N_{in} in Table 3-4 cannot be directly compared with the previously reported NUE, e.g. in Lassaletta et al. (2014) and Zhang et al. (2015). This is because N_{in} in this table only includes N_{fer} and N_{man}, while NUE was generally

estimated by considering the whole N inputs (including N_{fer}, N_{man}, N_{dep}, N_{dec}, etc.). Another reason is that N_t estimated in this study also takes into account the changes of soil N stock, whereas the calculation of NUE only focuses on crop N_{up}.

Table 3-3. Differences of total nitrogen inputs (TN_{in}, in Gg N yr^{-1}), total nitrogen losses into the environment (TN_t, in Gg N yr^{-1}) and into water (TN_w, in Gg N yr^{-1}), and crop production (P, in Tg yr^{-1}) between mitigation scenarios and base scenario.

Region	Scenario	Maize				Rice				Wheat			
		TN_{in}	TN_t	TN_w	P	TN_{in}	TN_t	TN_w	P	TN_{in}	TN_t	TN_w	P
Global	FixN3E	0	−411	−627	29	0	−1586	−1892	62	0	−1723	−2158	45
	AutoN	−1625	−1898	−1418	7	−2045	−2011	−1708	3	−4008	−4432	−4015	42
	AutoNE	−1134	−2182	−1801	46	−1026	−2505	−2397	64	−2471	−5351	−5148	95
Africa	FixN3E	1675	959	679	19	628	353	299	11	199	28	−2	4
	AutoN	−152	−100	−62	1	−24	−12	−2	0	−113	−78	−63	0
	AutoNE	1269	555	357	20	558	290	253	11	161	−38	−46	5
Asia	FixN3E	−1120	−992	−989	6	−957	−2080	−2290	42	−2521	−2177	−2158	4
	AutoN	−1210	−1123	−966	1	−2020	−1986	−1709	3	−3795	−3096	−2950	7
	AutoNE	−1473	−1431	−1247	8	−1895	−2886	−2721	42	−4822	−4357	−4091	17
Europe	FixN3E	448	167	69	−1	36	18	13	1	804	139	−32	12
	AutoN	−88	−213	−139	2	0	−3	−1	0	−26	−780	−674	23
	AutoNE	195	−234	−238	2	31	9	7	1	764	−694	−704	36
N. America	FixN3E	−1901	−913	−629	−21	−42	−33	−27	0	628	108	−14	9
	AutoN	−148	−385	−205	1	−1	−1	6	0	−70	−374	−273	9
	AutoNE	−1955	−1263	−796	−12	−48	−43	−32	0	558	−274	−269	18
Oceania	FixN3E	4	0	−1	0	16	7	4	0	534	134	41	7
	AutoN	0	−1	0	0	0	0	0	0	−2	−57	−25	2
	AutoNE	3	−1	−1	0	14	5	3	0	513	31	−11	10
S. America	FixN3E	893	369	244	25	319	149	109	8	356	44	8	8
	AutoN	−26	−77	−45	2	1	−9	−1	0	−1	−46	−30	1
	AutoNE	827	191		27	314	119	93	8	355	−19	−26	10

3.4.2 Environmental impacts associated with high nitrogen losses

Nitrogen losses are associated with significant environmental impacts, especially in the high emissions regions (Erisman et al., 2013). Our study identified four hotspots of N losses: China, India, eastern parts of the USA, and Central Europe (Figure 3-1). Considerable environmental consequences have already been detected in these regions. Because of much higher N inputs than crop demands, China has experienced significant N deposition enhancement (Liu et al., 2013b), which has led to substantial soil acidification in major croplands (Guo et al., 2010). It was reported that N imbalance also resulted in significant nitrate accumulation in Chinese croplands, even at soil depth bellow 4 m (Zhou et al., 2016). Downstream, large amounts of N have been discharged into coastal water bodies and caused severe eutrophication (Tong et al., 2015). Eastern parts of the USA and India experienced similar N deposition patterns as China (Erisman et al.,

2013). Furthermore, Diaz and Rosenberg (2008) identified 415 eutrophic and hypoxic coastal water systems around the world mostly located in the northern Gulf of Mexico, Chesapeake Bay, and Baltic and North Seas. The eutrophic conditions in these regions were mainly due to N losses in the Mississippi river basin and respective catchment in the eastern parts of the USA and central Europe. These regions were detected in our study as high N loss regions.

3.4.3 Assessment of nitrogen loss conditions

Generally, our results show three patterns of N loss conditions: a) high N inputs associated with high N losses due to N overuse, thus decreasing N_{in} is required; b) low N inputs associated with low yields due to insufficient availability of N inputs, thus increasing N_{in} is needed but appropriate fertilization management should be considered when intensifying these croplands; c) high yields associated with low NLI, indicating that the right amount of N inputs is applied. We will focus on several major crop producers to discuss these patterns below.

China showed the largest overuse of N for all the three crops, especially for rice cultivation (Figure 3-4). Decreasing its N inputs for the three crops to the respective world averages would not affect yields, except for a small decrease in wheat yield. This action in China alone would avoid about 7.5 Tg N yr^{-1} of environmental N losses from the three crops. This finding is consistent with Mueller et al. (2012), who also found that China has a particularly high potential to reduce N_{in}. Similar as China, also India shows a high potential to decrease N inputs for wheat cultivation and thus to reduce environmental N losses.

Many countries in Africa and South America, on the other hand, should increase N inputs to increase yields. In our simulations, food production in Africa increased by between 30 and 65% when N inputs were increased to the world average (Table 3-3). But also N losses increased. Therefore, appropriate N fertilization is needed when increasing N inputs. For example, yield was predicted to increase by 1.0 t ha^{-1} and N_t by 21 kg N ha^{-1} in the FixN3E scenario for maize production in Brazil, while yield increased by 1.2 t ha^{-1} and N_t by only 11 kg N ha^{-1} in the AutoNE scenario (Figures 3-4a and 3-4g). Similarly in Russia for wheat cultivation, an increase of yield rising from 1.1 to 1.2 t ha^{-1} is obtained with increase of N_t declining from 27 to 16 kg N ha^{-1} when N fertilization scenario changes from FixN3E to AutoNE (Figures 3-4c and 3-4i).

In the USA, maize cultivation belongs to the third pattern of N loss conditions (Figure 3-4). The current average N application rate in the USA in maize cultivation is 178 kg N ha^{-1}. In the AutoN scenario, we identified a value of 174 kg N ha^{-1}, which is only slightly lower than the actual value. In addition, N_t differs only slightly between FixN3 and AutoN. This suggests that in average the N input amounts applied in the USA in maize cultivation are just matching the demand of the crop. This may also partially explain why we found much better performance for

the USA in maize cultivation than for China in terms of NLI (Figure 3-3). Although the USA and China are the major N loss contributors of maize cultivation, with appropriate N fertilization and higher yields, the NLI obtained for the USA was only 46% of that for China.

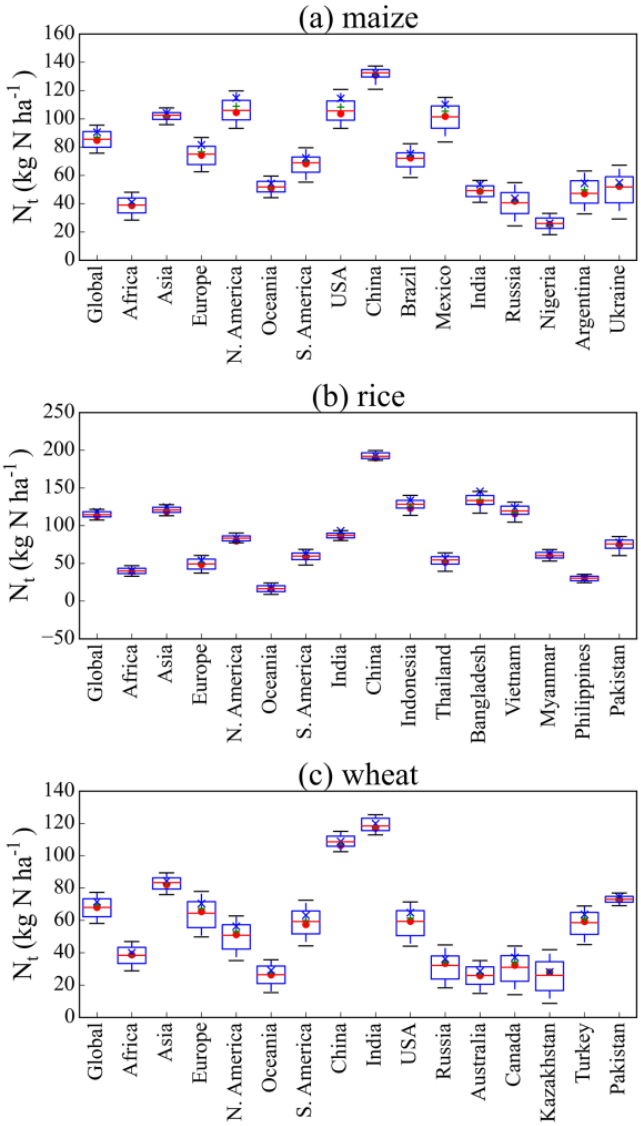

Figure 3-5. Uncertainties of nitrogen losses into the environment (N_t) globally, continentally, and for the top 10 producing countries of maize (a), rice (b), and wheat (c). Lines from top to bottom are 95th, 75th, 50th, 25th, and 5th percentiles, respectively. Red cycles represent results with default parameters by using FixN3 fertilization schedule; green pluses represent results with default parameters by using FixN2 fertilization schedule; blue crosses represent results with default parameters by using FixN1 fertilization schedule.

3.4.4 Current progress

Due to limitations in available input data, our results relate to the situation around the year 2000. How this situation has developed since the year 2000 can be inferred from the trend in

global total N fertilizer consumption. Generally, global total N consumption increased by 25% from 2002 to 2013 (Figure S3-5), implying an increase in total N losses. In particular, total N fertilizer consumption in India increased by > 60% in this period. Considering that N losses were already high in 2000 according to our simulation, the need to reduce N pollution appears to be even more urgent today. During the same period, the total N fertilizer consumption in China has only increased by 10%. This is mainly related to China's effort to find ways to improve its nutrient management. For example, an integrated soil–crop system management was introduced in China to produce more grains with less fertilizer use at lower environmental costs (Chen et al., 2014; Chen et al., 2011; Ju et al., 2009). The success achieved in China may be extended to other N overuse countries and countries planning to increase N fertilizer inputs (Zhang et al., 2013). Total N consumption in Brazil and Russia, which showed high potential to improve yields by increasing N inputs in our study, almost doubled in this period. Similar increasing trends were also observed in some other insufficient-N countries, e.g. Nigeria, Paraguay, Ukraine, etc. In Kenya, for example, maize yield almost tripled from 0.8 ton ha^{-1} in 2005 to 2.2 ton ha^{-1} in 2007, after farmers were subsidized to buy 100 kg fertilizer per farm in 2005 (Sanchez, 2010). With the development of better N management under the pressure to give more attentions to environmental protection, N inputs decreased in many western European countries (Figure S3-5), and N losses were considerably reduced without compromising yields (Sutton et al., 2011; Velthof et al., 2014). However, their potential to reduce N_{in} without yield losses is not fully exhausted yet. For example, Van Grinsven et al. (2013) performed a cost–benefit assessment and concluded that N application could be further lowered on average by around 50 kg N ha^{-1} in northwestern Europe.

Table 3-4. Comparison of estimated global total nitrogen losses into the environment (TN_t, in Tg N yr^{-1}) and water (TN_w, in Tg N yr^{-1}), and ratio of total nitrogen losses to total nitrogen inputs (TN_{in}, in Tg N yr^{-1}) with results from previous studies.

	(Bouwman et al., 2009)	(Bouwman et al., 2013)	(Liu et al., 2010)	(Mekonnen and Hoekstra, 2015)	(Sutton et al., 2013)	Current study
Time period	2000	2000	2000	2002–2010	2000–2010	2000
TN_{in} (Tg N yr^{-1})[a]	184	175	85	134	177	59
TN_t (Tg N yr^{-1})	157	138	67	109	135	44
TN_w (Tg N yr^{-1})	41	57	47	53	95	29
TN_t/TN_{in}	0.85	0.79	0.79	0.81	0.76	0.74
TN_w/TN_{in}	0.22	0.33	0.55	0.40	0.54	0.49
TN_w/TN_t	0.26	0.41	0.70	0.49	0.70	0.66

[a]Only nitrogen inputs from fertilizer and manure are considered here.

3.4.5 Limitations

Because of the unavailability of data on fertilizer application timing, assumptions have been made for the fertilizer application schedules in the model simulation. As we do not know how well these assumptions match reality, there will be some errors in the results, although the overall

differences of N_t among the three N fertilization schedules are small. We only considered uncertainties derived from the possible ranges of model parameters. The impacts of cross- and spatial-corrections of these model parameters could also be important (Kros et al., 2012). Besides, uncertainties in other management practices (e.g. planting and harvesting dates, residue management, tillage, etc.), N inputs, and soil inputs were not addressed. These factors may also play important roles in N fluxes (Molina-Herrera et al., 2016). Estimating these uncertainties is out of the scope in this study, but should be the subject of future studies.

3.5 Conclusions

In this study, we applied a spatially explicit crop model, PEPIC, to quantify N losses and to explore the trade-offs with yields from three major cereal crop cultivations, i.e. maize, rice, and wheat, on a global scale with high spatial resolution. Without requiring yields as input data, this method can be used to determine the N losses and yields relations under different N mitigation scenarios, which is the major advantage of large-scale crop modelling for assessing N losses compared to empirical mass balances.

Global total N losses were 44 Tg N yr^{-1} for the three crops, with rice contributing the most. These losses were concentrated in a few regions, for example in China and the USA for maize cultivation, and China and India for rice and wheat cultivations. This concentration of N losses calls for more attention to N management in these countries. With the simultaneous consideration of N losses and yields, we were able to assess trade-offs between them using an N loss index: NLI. The NLI showed high variations among different countries, indicating diverse performance in terms of N losses associated with the production of the same amount of yield. This variation suggests that there is still considerable potential to improve the efficiency of N use in cereal production in many countries without compromising yields. The analysis of mitigation scenarios also shows that N losses can be significantly reduced and yields at the same time increased by transferring N from currently high application countries to countries with low application. Furthermore, there is also still much potential to increase yields by using more efficient N fertilization schemes in low N application countries. The findings of this study are useful for policy makers to guide better N management and reduce N emissions.

3.6 References

Abbaspour, K.C., 2011. SWAT-CUP: SWAT calibration and uncertainty programs. Eawag, Dübendorf, Switzerland.

Abbaspour, K.C., Yang, J., Maximov, I., Siber, R., Bogner, K., Mieleitner, J., Zobrist, J., Srinivasan, R., 2007. Modelling hydrology and water quality in the pre-ailpine/alpine Thur watershed using SWAT. J. Hydrol., 333: 413–430.

Babbin, A.R., Ward, B.B., 2013. Controls on nitrogen loss processes in Chesapeake Bay sediments. Environ. Sci. Technol., 47: 4189–4196.

Balkovič, J., van der Velde, M., Schmid, E., Skalsky, R., Khabarov, N., Obersteiner, M., Sturmer, B., Xiong, W., 2013. Pan-European crop modelling with EPIC: implementation, up-scaling and regional crop yield validation. Agric. Syst., 120: 61–75.

Balkovič, J., van der Velde, M., Skalsky, R., Xiong, W., Folberth, C., Khabarov, N., Smirnov, A., Mueller, N.D., Obersteiner, M., 2014. Global wheat production potentials and management flexibility under the representative concentration pathways. Global Planet. Chang., 122: 107–121.

Bhattacharyya, T., Pal, D.K., Williams, S., Telpande, B.A., Deshmukh, A.S., Chandran, P., et al., 2010. Evaluating the Century C model using two long-term fertilizer trials representing humid and semi-arid sites from India. Agric. Ecosyst. Environ., 139: 264–272.

Bodirsky, B.L., Popp, A., Lotze-Campen, H., Dietrich, J.P., Rolinski, S., Weindl, I., Schmitz, C., Muller, C., Bonsch, M., Humpenoder, F., Biewald, A., Stevanovic, M., 2014. Reactive nitrogen requirements to feed the world in 2050 and potential to mitigate nitrogen pollution. Nat. Commun., 5: 3858.

Bouwman, A.F., Beusen, A.H.W., Billen, G., 2009. Human alteration of the global nitrogen and phosphorus soil balances for the period 1970–2050. Global Biogeochem. Cy., 23: GB0A04.

Bouwman, L., Goldewijk, K.K., Van Der Hoek, K.W., Beusen, A.H., Van Vuuren, D.P., Willems, J., Rufino, M.C., Stehfest, E., 2013. Exploring global changes in nitrogen and phosphorus cycles in agriculture induced by livestock production over the 1900–2050 period. Proc. Natl. Acad. Sci. U. S. A., 110: 20882–20887.

Chen, X., Cui, Z., Fan, M., Vitousek, P., Zhao, M., Ma, W., Wang, Z., Zhang, W., Yan, X., Yang, J., Deng, X., Gao, Q., Zhang, Q., Guo, S., Ren, J., Li, S., Ye, Y., Wang, Z., Huang, J., Tang, Q., Sun, Y., Peng, X., Zhang, J., He, M., Zhu, Y., Xue, J., Wang, G., Wu, L., An, N., Wu, L., Ma, L., Zhang, W., Zhang, F., 2014. Producing more grain with lower environmental costs. Nature, 514: 486–489.

Chen, X., Cui, Z., Vitousek, P.M., Cassman, K.G., Matson, P.A., Bai, J., Meng, Q., Hou, P., Yue, S., Romheld, V., Zhang, F., 2011. Integrated soil-crop system management for food security. Proc. Natl. Acad. Sci. U. S. A., 108: 6399–6404.

Clark, C.M., Tilman, D., 2008. Loss of plant species after chronic low-level nitrogen deposition to prairie grasslands. Nature, 451: 712–715.

Conant, R.T., Berdanier, A.B., Grace, P.R., 2013. Patterns and trends in nitrogen use and nitrogen recovery efficiency in world agriculture. Global Biogeochem. Cy., 27: 558–566.

Conley, D.J., Paerl, H.W., Howarth, R.W., Boesch, D.F., Seitzinger, S.P., Havens, K.E., Lancelot, C., Likens, G.E., 2009. ECOLOGY controlling eutrophication: nitrogen and phosphorus. Science, 323: 1014–1015.

Cong, R., Wang, X., Xu, M., Ogle, S.M., Parton, W.J., 2014. Evaluation of the CENTURY model using long-term fertilization trials under corn–wheat cropping systems in the typical croplands of China. PLoS One, 9: e95142.

Cui, Z., Wang, G., Yue, S., Wu, L., Zhang, W., Zhang, F., Chen, X., 2014. Closing the N-use efficiency gap to achieve food and environmental security. Environ. Sci. Technol,. 48: 5780–5787.

Davidson, E.A., 2009. The contribution of manure and fertilizer nitrogen to atmospheric nitrous oxide since 1860. Nat. Geosci., 2: 659–662.

Del Grosso, S.J., Ojima, D.S., Parton, W.J., Stehfest, E., Heistemann, M., DeAngelo, B., Rose, S., 2009. Global scale DAYCENT model analysis of greenhouse gas emissions and mitigation strategies for cropped soils. Global Planet. Chang., 67: 44–50.

Della Peruta, R., Keller, A., Schulin, R., 2014. Sensitivity analysis, calibration and validation of EPIC for modelling soil phosphorus dynamics in Swiss agro-ecosystems. Environ. Model. Softw., 62: 97–111.

Diaz, R.J., Rosenberg, R., 2008. Spreading dead zones and consequences for marine ecosystems. Science, 321: 926–929.

Erisman, J.W., Galloway, J.N., Seitzinger, S., Bleeker, A., Dise, N.B., Petrescu, A.M.R., Leach, A.M., de Vries, W., 2013. Consequences of human modification of the global nitrogen cycle. Philos. Trans. R. Soc. B, 368: 20130116.

Folberth, C., Gaiser, T., Abbaspour, K.C., Schulin, R., Yang, H., 2012. Regionalization of a large-scale crop growth model for sub-Saharan Africa: model setup, evaluation, and estimation of maize yields. Agric. Ecosyst. Environ., 151: 21–33.

Folberth, C., Yang, H., Gaiser, T., Liu, J., Wang, X., Williams, J., Schulin, R., 2014. Effects of ecological and conventional agricultural intensification practices on maize yields in sub-Saharan Africa under potential climate change. Environ. Res. Lett., 9: 044004.

Foley, J.A., Defries, R., Asner, G.P., Barford, C., Bonan, G., Carpenter, S.R., Chapin, F.S., Coe, M.T., Daily, G.C., Gibbs, H.K., Helkowski, J.H., Holloway, T., Howard, E.A., Kucharik, C.J., Monfreda, C., Patz, J.A., Prentice, I.C., Ramankutty, N., Snyder, P.K., 2005. Global consequences of land use. Science, 309: 570–574.

Foley, J.A., Ramankutty, N., Brauman, K.A., Cassidy, E.S., Gerber, J.S., Johnston, M., Mueller, N.D., O'Connell, C., Ray, D.K., West, P.C., Balzer, C., Bennett, E.M., Carpenter, S.R., Hill, J., Monfreda, C., Polasky, S., Rockstrom, J., Sheehan, J., Siebert, S., Tilman, D., Zaks, D.P.M., 2011. Solutions for a cultivated planet. Nature, 478: 337–342.

Fowler, D., Coyle, M., Skiba, U., Sutton, M.A., Cape, J.N., Reis, S., Sheppard, L.J., Jenkins, A., Grizzetti, B., Galloway, J.N., Vitousek, P., Leach, A., Bouwman, A.F., Butterbach-Bahl, K., Dentener, F., Stevenson, D., Amann, M., Voss, M., 2013. The global nitrogen cycle in the twenty-first century. Philos. Trans. R. Soc. B, 368: 20130164.

Galloway, J.N., Townsend, A.R., Erisman, J.W., Bekunda, M., Cai, Z.C., Freney, J.R., Martinelli, L.A., Seitzinger, S.P., Sutton, M.A., 2008. Transformation of the nitrogen cycle: recent trends, questions, and potential solutions. Science, 320: 889–892.

Galloway, J.N., Winiwarter, W., Leip, A., Leach, A.M., Bleeker, A., Erisman, J.W., 2014. Nitrogen footprints: past, present and future. Environ. Res. Lett., 9: 115003.

Guo, J., Liu, X., Zhang, Y., Shen, J., Han, W., Zhang, W., Christie, P., Goulding, K.W., Vitousek, P.M., Zhang, F., 2010. Significant acidification in major Chinese croplands. Science, 327: 1008–1010.

Izaurralde, R.C., Williams, J.R., McGill, W.B., Rosenberg, N.J., Jakas, M.C.Q., 2006. Simulating soil C dynamics with EPIC: model description and testing against long-term data. Ecol. Model., 192: 362–384.

Ju, X., Xing, G., Chen, X., Zhang, S., Zhang, L., Liu, X., Cui, Z., Yin, B., Christie, P., Zhu, Z., Zhang, F., 2009. Reducing environmental risk by improving N management in intensive Chinese agricultural systems. Proc. Natl. Acad. Sci. U. S. A., 106: 3041–3046.

Kros, J., Heuvelink, G.B.M., Reinds, G.J., Lesschen, J.P., Ioannidi, V., De Vries, W., 2012. Uncertainties in model predictions of nitrogen fluxes from agro-ecosystems in Europe. Biogeosciences, 9: 4573–4588.

Ladha, J.K., Pathak, H., Krupnik, T.J., Six, J., van Kessel, C., 2005. Efficiency of fertilizer nitrogen in cereal production: Retrospects and prospects. Adv. Agron., 87: 85–156.

Ladha, J.K., Tirol-Padre, A., Reddy, C.K., Cassman, K.G., Verma, S., Powlson, D.S., van Kessel, C., Richter, D.D., Chakraborty, D., Pathak, H., 2016. Global nitrogen budgets in cereals: a 50-year assessment for maize, rice, and wheat production systems. Sci. Rep., 6: 19355.

Lassaletta, L., Billen, G., Grizzetti, B., Anglade, J., Garnier, J., 2014. 50 year trends in nitrogen use efficiency of world cropping systems: the relationship between yield and nitrogen input to cropland. Environ. Res. Lett., 9: 105011.

Liu, J., Folberth, C., Yang, H., Rockstrom, J., Abbaspour, K., Zehnder, A.J., 2013a. A global and spatially explicit assessment of climate change impacts on crop production and consumptive water use. PLoS One, 8: e57750.

Liu, J., Williams, J.R., Zehnder, A.J.B., Yang, H., 2007. GEPIC – modelling wheat yield and crop water productivity with high resolution on a global scale. Agric. Syst., 94: 478–493.

Liu, J., Yang, H., 2010. Spatially explicit assessment of global consumptive water uses in cropland: green and blue water. J. Hydrol., 384: 187–197.

Liu, J., You, L., Amini, M., Obersteiner, M., Herrero, M., Zehnder, A.J., Yang, H., 2010. A high-resolution assessment on global nitrogen flows in cropland. Proc. Natl. Acad. Sci. U. S. A., 107: 8035–8040.

Liu, W., Yang, H., Folberth, C., Wang, X., Luo, Q., Schulin, R., 2016. Global investigation of impacts of PET methods on simulating crop–water relations for maize. Agric. For. Meteorol., 221: 164–175.

Liu, X., Zhang, Y., Han, W., Tang, A., Shen, J., Cui, Z., Vitousek, P., Erisman, J.W., Goulding, K., Christie, P., Fangmeier, A., Zhang, F., 2013b. Enhanced nitrogen deposition over China. Nature, 494: 459–462.

Mckay, M.D., Beckman, R.J., Conover, W.J., 1979. A comparison of three methods for selecting values of input variables in the analysis of output from a computer code. Technometrics, 21: 239–245.

Mekonnen, M.M., Hoekstra, A.Y., 2015. Global gray water footprint and water pollution levels related to anthropogenic nitrogen loads to fresh water. Environ. Sci. Technol., 49: 12860–12868.

Molina-Herrera, S., Haas, E., Klatt, S., Kraus, D., Augustin, J., Magliulo, V., Tallec, T., Ceschia, E., Ammann, C., Loubet, B., Skiba, U., Jones, S., Brummer, C., Butterbach-Bahl, K., Kiese, R., 2016. A modeling study on mitigation of N2O emissions and NO3 leaching at different agricultural sites across Europe using LandscapeDNDC. Sci. Total Environ., 553: 128–140.

Mueller, N.D., Gerber, J.S., Johnston, M., Ray, D.K., Ramankutty, N., Foley, J.A., 2012. Closing yield gaps through nutrient and water management. Nature, 490: 254–257.

Parton, W.J., Ojima, D.S., Cole, C.V., Schimel, D.S., 1994. A general model for soil organic matter dynamics: Sensitivity to litter chemistry, texture and management. In: Quantitative Modeling of Soil Forming Processes, SSSA Spec. Public No. 39, Madison, WI, pp. 147–167.

Qiu, J., Li, H., Wang, L., Tang, H., Li, C., Van Ranst, E., 2011. GIS-model based estimation of nitrogen leaching from croplands of China. Nutr. Cycl. Agroecosys., 90: 243–252.

Rockstrom, J., Steffen, W., Noone, K., Persson, A., Chapin, F.S., Lambin, E.F., Lenton, T.M., Scheffer, M., Folke, C., Schellnhuber, H.J., Nykvist, B., de Wit, C.A., Hughes, T., van der Leeuw, S., Rodhe, H., Sorlin, S., Snyder, P.K., Costanza, R., Svedin, U., Falkenmark, M., Karlberg, L., Corell, R.W., Fabry, V.J., Hansen, J., Walker, B., Liverman, D., Richardson, K., Crutzen, P., Foley, J.A., 2009. A safe operating space for humanity. Nature, 461: 472–475.

Rosenzweig, C., Elliott, J., Deryng, D., Ruane, A.C., Muller, C., Arneth, A., Boote, K.J., Folberth, C., Glotter, M., Khabarov, N., Neumann, K., Piontek, F., Pugh, T.A.M., Schmid, E., Stehfest, E., Yang, H., Jones, J.W., 2014. Assessing agricultural risks of climate change in the 21st century in a global gridded crop model intercomparison. Proc. Natl. Acad. Sci. U. S. A., 111: 3268–3273.

Sanchez, P.A., 2002. Ecology – Soil fertility and hunger in Africa. Science, 295: 2019–2020.

Sanchez, P.A., 2010. Tripling crop yields in tropical africa. Nat. Geosci., 3: 299–300.

Schuol, J., Abbaspour, K.C., Yang, H., Srinivasan, R., Zehnder, A.J.B., 2008. Modeling blue and green water availability in Africa. Water Resour. Res., 44: W07406.

Stehfest, E., Heistermann, M., Priess, J.A., Ojima, D.S., Alcamo, J., 2007. Simulation of global crop production with the ecosystem model DayCent. Ecol. Model., 209: 203–219.

Sutton, M.A., Bleeker, A., Howard, C., Bekunda, M., Grizzetti, B., Vries, W.d., Van Grinsven, H., Abrol, Y., Adhya, T., Billen, G., 2013. Our nutrient world: the challenge to produce more food and energy with less pollution. Centre for Ecology and Hydrology (CEH).

Sutton, M.A., Howard, C.M., Erisman, J.W., Billen, G., Bleeker, A., Grennfelt, P., van Grinsven, H., Grizzetti, B., 2011. The European nitrogen assessment: sources, effects and policy perspectives. Cambridge University Press.

Tilman, D., Balzer, C., Hill, J., Befort, B.L., 2011. Global food demand and the sustainable intensification of agriculture. Proc. Natl. Acad. Sci. U. S. A., 108: 20260–20264.

Tong, Y., Zhao, Y., Zhen, G., Chi, J., Liu, X., Lu, Y., et al., 2015. Nutrient loads flowing into coastal waters from the main rivers of China (2006–2012). Sci. Rep., 5: 16678.

van der Velde, M., Bouraoui, F., Aloe, A., 2009. Pan-European regional-scale modelling of water and N efficiencies of rapeseed cultivation for biodiesel production. Global Chang. Biol., 15: 24–37.

Van Grinsven, H.J.M., Holland, M., Jacobsen, B.H., Klimont, Z., Sutton, M.A., Willems, W.J., 2013. Costs and benefits of nitrogen for Europe and implications for mitigation. Environ. Sci. Technol., 47: 3571–3579.

Velthof, G.L., Lesschen, J.P., Webb, J., Pietrzak, S., Miatkowski, Z., Pinto, M., Kros, J., Oenema, O., 2014. The impact of the nitrates directive on nitrogen emissions from agriculture in the EU-27 during 2000–2008. Sci. Total Environ., 468: 1225–1233.

Wang, X., Williams, J.R., Gassman, P.W., Baffaut, C., Izaurralde, R.C., Jeong, J., Kiniry, J.R., 2012. EPIC and APEX: model use, calibration, and validation. T. ASABE, 55: 1447–1462.

West, P.C., Gerber, J.S., Engstrom, P.M., Mueller, N.D., Brauman, K.A., Carlson, K.M., Cassidy, E.S., Johnston, M., MacDonald, G.K., Ray, D.K., Siebert, S., 2014. Leverage points for improving global food security and the environment. Science, 345: 325–328.

Williams, J.R., 1995. The EPIC model, in: Singh, V.P. (Ed.), Computer Models of Watershed Hydrology. Water Resources Publications, Highlands Ranch, Colo.

Williams, J.R., Jones, C.A., Dyke, P.T., 1984. A modeling approach to determining the relationship between erosion and soil productivity. T. ASAE, 27: 129–144.

Yang, J., Reichert, P., Abbaspour, K.C., Xia, J., Yang, H., 2008. Comparing uncertainty analysis techniques for a SWAT application to the Chaohe Basin in China. J. Hydrol., 358: 1–23.

Zhang, F., Chen, X., Vitousek, P., 2013. Chinese agriculture: an experiment for the world. Nature, 497: 33–35.

Zhang, X., Davidson, E.A., Mauzerall, D.L., Searchinger, T.D., Dumas, P., Shen, Y., 2015. Managing nitrogen for sustainable development. Nature, 528: 51–59.

Zhou, J., Gu, B., Schlesinger, W.H., Ju, X., 2016. Significant accumulation of nitrate in Chinese semi-humid croplands. Sci. Rep., 6: 25088.

Supplementary information for

Global assessment of nitrogen losses and trade-offs with yields from major crop cultivations

Simulation framework

The EPIC (Environmental Policy Integrated Climate) model was initially developed to simulate impacts of soil erosion on soil productivity (Williams et al., 1984). It can be used to simulate a variety of complex soil–water–climate–management processes, e.g. crop growth, soil temperature, hydrology, nutrient, management, erosion, tillage, etc. (Williams, 1995). EPIC simulates crop growth at a daily step. Potential biomass increase is estimated by the product of intercepted solar radiation and biomass–energy ratio. Actual biomass is then calculated by multiplying potential biomass increase with a dominant crop stress. Finally, crop yield is obtained by the product of accumulated biomass and a harvest index (Williams et al., 1984).

EPIC simulates the coupled carbon and nitrogen (N) routines in soil organic matters by adopting the Century model (Parton et al., 1994). Soil organic matters are divided into three compartments: microbial, slow, and passive. These three compartments differ in size, function, and turnover times (Izaurralde et al., 2006). Organic residues added to soil, e.g. roots and crop residues, are split into metabolic and structural litter compartments based on their lignin and N contents. More details about the N routine in EPIC can be found in Izaurralde et al. (2006).

EPIC is a site-based biophysical model, which is not convenient for a global simulation. Whereas, the Python configuration of EPIC, or PEPIC performed the simulation within a spatial domain (Liu et al., 2016). PEPIC spatially runs the EPIC model at each grid cell (at a spatial resolution of 30 arc minutes in this study) for the whole world, with the ability to prepare the input data for each grid cell before simulation, to extract results, and to show the spatial patterns of desired variables after the completion of simulation for all grid cells. In this study, we considered both irrigated and rainfed cultivations. First, we run the model for irrigated and rainfed cultivations separately. Then, we used crop harvest areas of irrigated and rainfed cultivations to get the area-weighted average for that grid following the methods in Liu et al. (2007). We applied the same method to aggregate crop yields and N losses at the national, continental, and global levels.

Validation of simulated yields

Generally, the PEPIC model performed well in representing FAO reported yields (Figure S3-1). The simulated yields show acceptable agreements with FAO reported yields for maize and rice

by applying the FixN1, FixN2, FixN3 schedules. Additionally, the differences of simulated yields for maize and rice cultivation by using the three fixed N fertilization schedules are quite small. However, we found the rice yield of China was underestimated, which may be because we used the same crop growth parameters (e.g. harvest index) for the whole world, while China applied high-yield rice cultivar. This underestimation in China for rice simulation was also found in Xiong et al. (2014). While differences for wheat simulation can be found by using the FixN1, FixN2, FixN3 schedules, using the FixN3 fertilization schedule demonstrated the best estimation among these three schedules. Besides, there are some underestimations for high-yield countries and for India and Pakistan. Regarding the underestimation for high-yield countries, we found that it was improved if we applied automatic fertilization (Figure S3-1). The underestimation of wheat yields for high-yield countries was also found by Balkovic et al. (2014) when they applied N with an automatic fertilization schedule. As for the underestimation of India and Pakistan, we found this is mainly because the growing season period provided by Sacks et al. (2010) in the border regions between India and Pakistan is much shorter than other regions in the two counties. The estimated yields in these regions was lower than other regions in these two countries.

Given the importance of China in rice production and India and Pakistan in wheat production, we used FAO reported yields for China's rice yield and India and Pakistan's wheat yields when we calculated the nitrogen loss intensity in Figure 3-3.

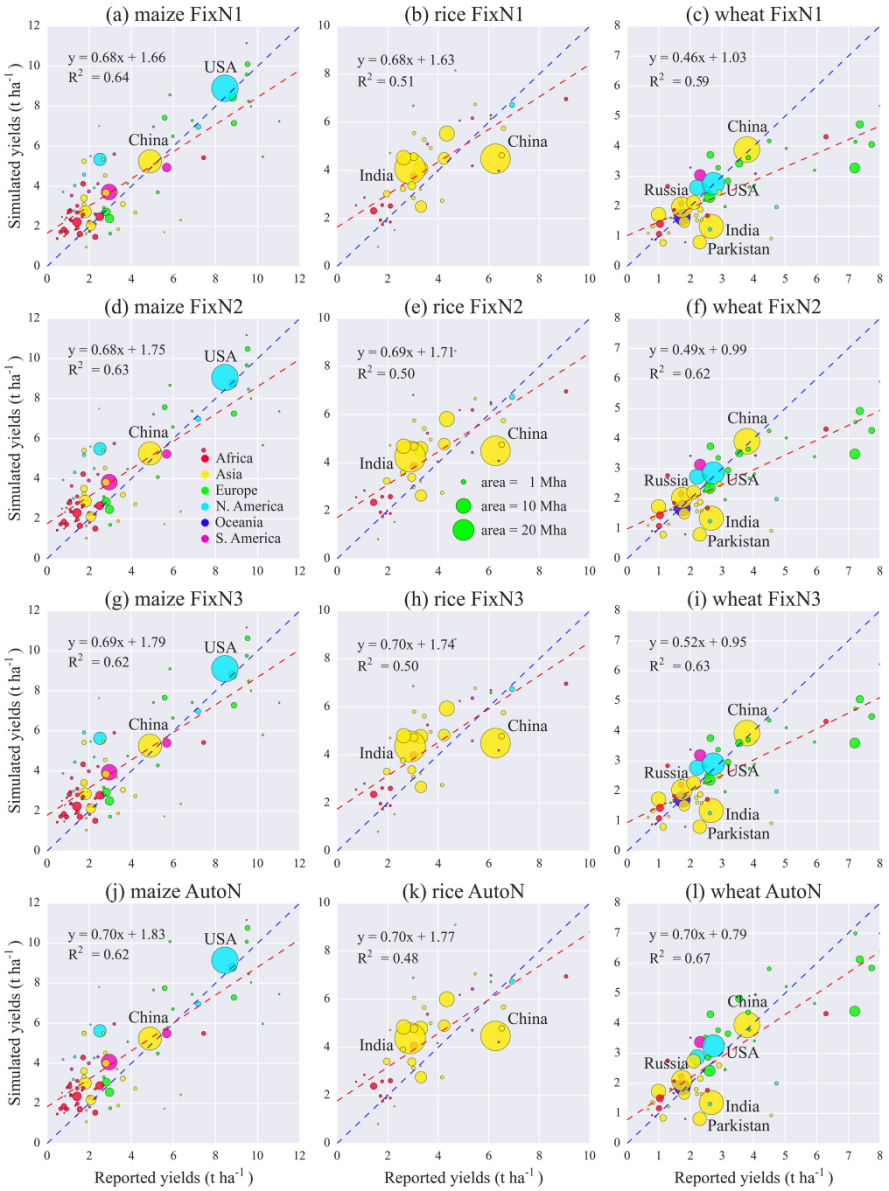

Figure S3-1. Comparison between reported and estimated yields under the FixN1, FixN2, FixN3, and AutoN nitrogen fertilization schedules. Countries with the smallest areas (for a total of 1% of global total cropland areas of each crop) are discarded; colours represent different continents; sizes represent cropland areas for each country; dashed blue line is the 1:1 line; dashed red line is the regression line; functions represent linear relationship between reported and estimated yields; R^2 is the coefficient of determination of the regression line.

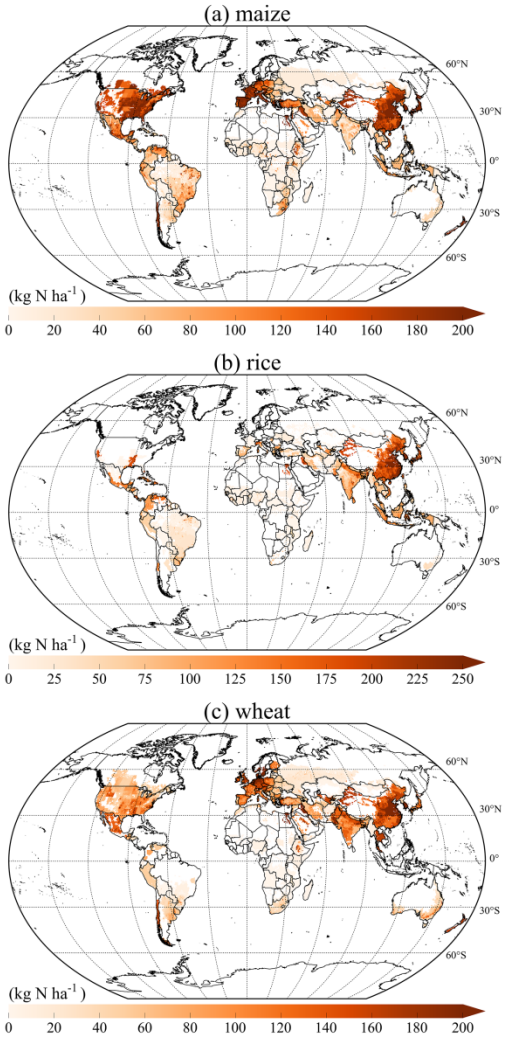

Figure S3-2. Global maps of nitrogen inputs (N_{in}) for maize (a), rice (b), and wheat (c).

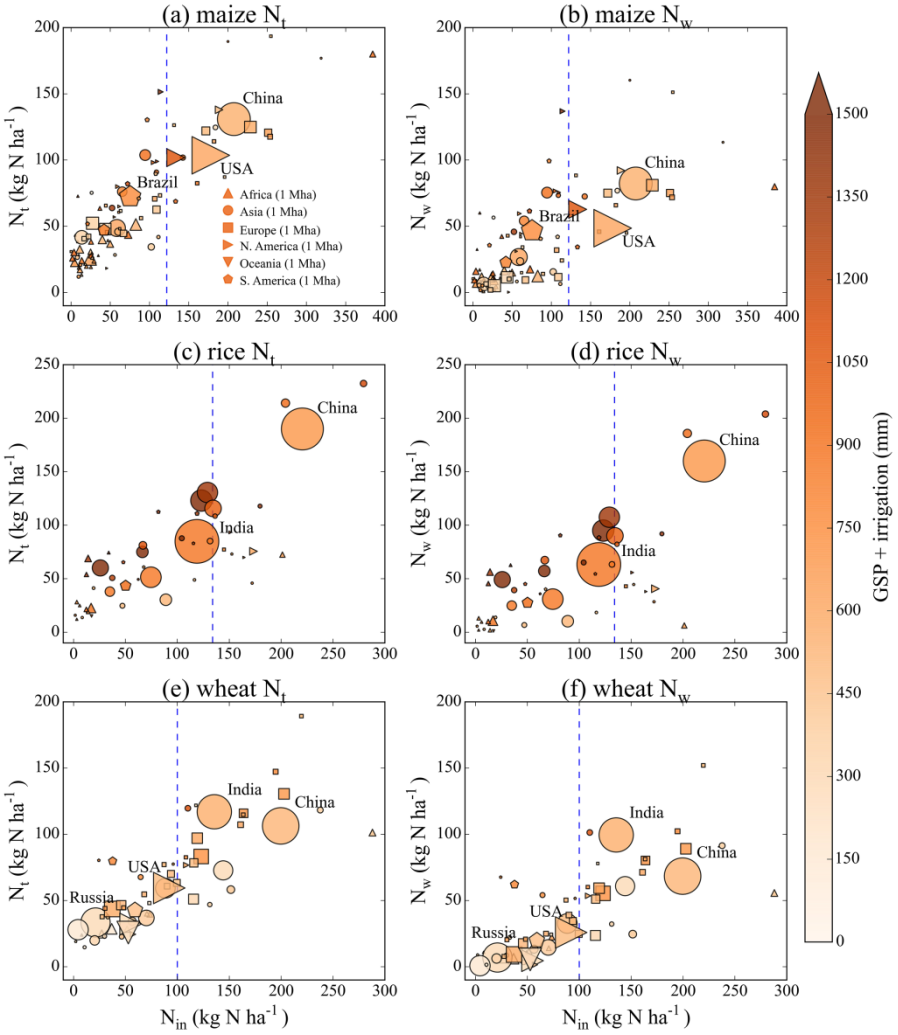

Figure S3-3. Nitrogen inputs (N_{in}) and nitrogen losses into the environment (N_t) and waters (N_w) for maize (a, b), rice (c, d), and wheat (e, f) at country level. Countries with the smallest areas (for a total of 1% of global total cropland areas of each crop) are discarded; shapes represent different continents; sizes represent cropland areas for each country; colours present total growing season precipitation (GSP) and irrigation water; dashed vertical lines represent the world average N_{in} for each crop.

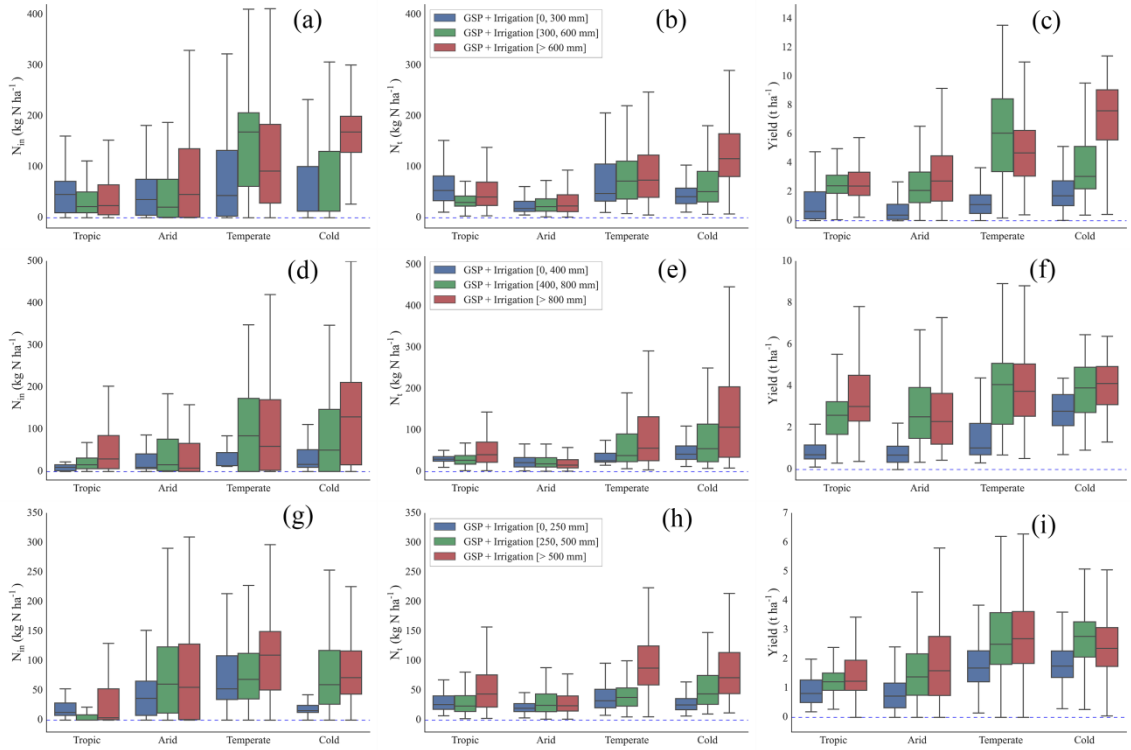

Figure S3-4. Nitrogen inputs (N_{in}), nitrogen losses into the environment (N_l), and yield for maize (a, b, c), rice (d, e, f), and wheat (g, h, i) in four climate regions with different levels of total growing season precipitation (GSP) and irrigation water.

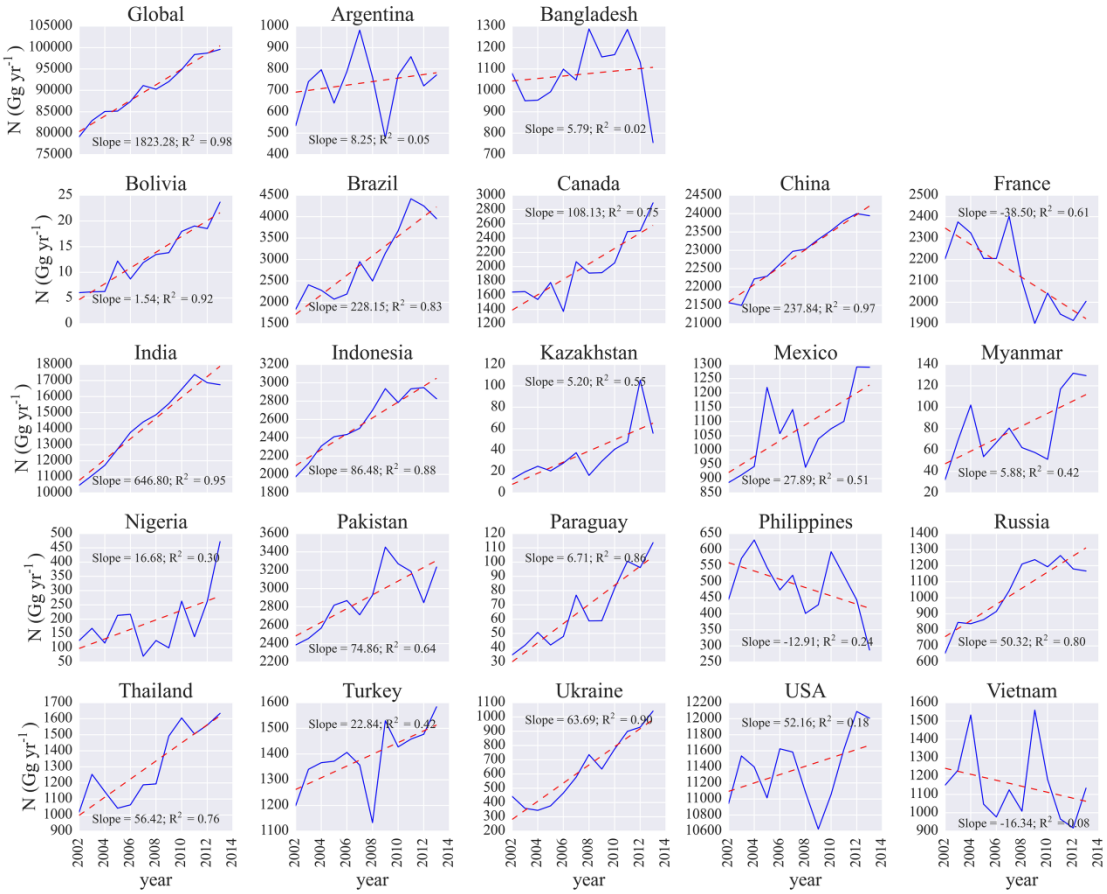

Figure S3-5. Total nitrogen fertilizer consumption (N) of the whole agricultural sector globally and for major crop producing countries between 2002 and 2013. Data downloaded from FAOSTAT (http://faostat3.fao.org/home/E); dashed red lines are the linear trend lines; Slope (in Gg N yr^{-1}) is the slope of trend line; R^2 is the coefficient of determination of the trend line.

Table S3-1. Description of input datasets and their sources.

Data set	Description	Source	Comments
Elevation	Digital Elevation Model	USGS/NASA	
Slope	Hill slope; derived from DEM	USGS/NASA	
Soil	Most important soil properties for top and sub soil	World Inventory of Soil Emission Potentials (WISE) (Batjes, 2006)	layer depth, pH, bulk density, organic carbon content, % sand, and % silt, etc.
Climate	ERA-Interim corrected by Climate Research Unit (CRU) data	WFDEI (Weedon et al., 2014)	solar radiation, air temperature, precipitation, relative humidity, as well wind speed
Land use	Rain-fed and irrigated areas in each grid cell around 2000	MIRCA, Frankfurt University (Portmann et al., 2010)	Land use data for 26 crops between 1998 and 2002
Fertilizer	Nitrogen, phosphorus, and potassium fertilizer and manure around 2000	EarthStat	This dataset is based on literatures (Mueller et al., 2012; West et al., 2014)
Planting dates	Julian day of crop planting	SAGE, University of Wisconsin (Sacks et al., 2010)	This dataset provides the earliest, medium and latest value of planting dates. The medium value was used.
Harvesting dates	Julian day of crop harvesting	SAGE, University of Wisconsin (Sacks et al., 2010)	This dataset provides the earliest, medium and latest value of harvesting dates. The medium value was used.
Reported yield	Country-specific reported yields between 1998 and 2002	FAOSTAT (http://faostat3.fao.org/home/E)	Average between 1998 and 2002 was used for model validation.

Table S3-2. Parameter description for uncertainty analysis and their boundaries.

Parameter	Description	Unit	Lower limit	Upper limit	Default value
PRM04	Denitrification rate constant	-	0.01	2	0.05
PRM08	Soluble P runoff coefficient	-	10	20	10
PRM14	Nitrate leaching ratio	-	0.1	1	0.5
PRM20	Microbial decay rate coefficient: Adjusts the equation relating microbial activity to soil water, temperature and oxygen.	-	0.5	1.5	1
PRM24	Maximum depth for biological soil mixing	m	0.1	0.5	0.3
PRM25	Biological mixing efficiency: the fraction of soil material which is mixed annually.	-	0.1	0.5	0.5
PRM30	Minimum water content required to trigger denitrification, expressed as fraction of water content at field capacity	mm	0.9	1.1	1.01
PRM34	If >1, it makes soluble P runoff concentration a non-linear function of organic P concentration in the top soil layer		1	1.5	1
PRM43	Ratio of soluble C concentration in runoff to percolate		1	20	4
PRM45	Coefficient allocating slow to passive humus	-	0.001	0.05	0.05
PRM47	Slow humus transformation rate	d^{-1}	0.00041	0.00068	0.000548
PRM51	Coefficient adjusting microbial activity function in top soil layer	-	0.1	1	1
PRM57	Volatilization and nitrification partitioning coefficient	-	0.05	0.5	0.15
PRM62	Exponential coefficient regulates upward N movement by evaporation	-	0.2	2	0.5
PRM63	Upper limit of N concentration in percolating water	ppm	100	10000	9000
PRM64	Upper limit of nitrification-volatilization as a fraction of NH3 present		0	1	0.1
PRM77	Coefficient regulating p flux between labile and active pool	-	0.0001	0.001	0.0001
PRM78	Coefficient regulating p flux between active and stable pool	-	0.0001	0.001	0.0001

References

Balkovič, J., van der Velde, M., Skalsky, R., Xiong, W., Folberth, C., Khabarov, N., Smirnov, A., Mueller, N.D., Obersteiner, M., 2014. Global wheat production potentials and management flexibility under the representative concentration pathways. Global Planet. Change, 122: 107–121.

Batjes, N.H., 2006. ISRIC–WISE derived soil properties on a 5 by 5 arc-minutes global grid (version 1.1). ISRIC–World Soil Infromation, Wageningen.

Izaurralde, R.C., Williams, J.R., McGill, W.B., Rosenberg, N.J., Jakas, M.C.Q., 2006. Simulating soil C dynamics with EPIC: Model description and testing against long-term data. Ecol. Model., 192: 362–384.

Liu, J., Williams, J.R., Zehnder, A.J.B., Yang, H., 2007. GEPIC – modelling wheat yield and crop water productivity with high resolution on a global scale. Agric. Syst., 94: 478–493.

Liu, W., Yang, H., Folberth, C., Wang, X., Luo, Q., Schulin, R., 2016. Global investigation of impacts of PET methods on simulating crop–water relations for maize. Agric. For. Meteorol., 221: 164–175.

Mueller, N.D., Gerber, J.S., Johnston, M., Ray, D.K., Ramankutty, N., Foley, J.A., 2012. Closing yield gaps through nutrient and water management. Nature, 490: 254–257.

Parton, W.J., Schimel, D., Ojima, D., Cole, C.V., Bryant, R., Arnold, R., 1994. A general model for soil organic matter dynamics: sensitivity to litter chemistry, texture and management, Quantitative modeling of soil forming processes: proceedings of a symposium sponsored by Divisions S-5 and S-9 of the Soil Science Society of America in Minneapolis, Minnesota, USA, 2 Nov. 1992. Soil Science Society of America Inc., pp. 147–167.

Portmann, F.T., Siebert, S., Doll, P., 2010. MIRCA2000–Global monthly irrigated and rainfed crop areas around the year 2000: A new high-resolution data set for agricultural and hydrological modeling. Global Biogeochem. Cy., 24: GB1011.

Sacks, W.J., Deryng, D., Foley, J.A., Ramankutty, N., 2010. Crop planting dates: an analysis of global patterns. Global Ecol. Biogeogr., 19: 607–620.

Weedon, G.P., Balsamo, G., Bellouin, N., Gomes, S., Best, M.J., Viterbo, P., 2014. The WFDEI meteorological forcing data set: WATCH Forcing Data methodology applied to ERA-Interim reanalysis data. Water Resour. Res., 50: 7505–7514.

West, P.C., Gerber, J.S., Engstrom, P.M., Mueller, N.D., Brauman, K.A., Carlson, K.M., Cassidy, E.S., Johnston, M., MacDonald, G.K., Ray, D.K., Siebert, S., 2014. Leverage points for improving global food security and the environment. Science, 345: 325–328.

Williams, J.R., 1995. The EPIC model, in: Singh, V.P. (Ed.), Computer Models of Watershed hydrology. Water Resources Publications, Highlands Ranch, Colo.

Williams, J.R., Jones, C.A., Dyke, P.T., 1984. A modeling approach to determining the relationship between erosion and soil productivity. T. ASAE, 27: 129–144.

Xiong, W., Balkovic, J., van der Velde, M., Zhang, X.S., Izaurralde, R.C., Skalsky, R., Lin, E., Mueller, N., Obersteiner, M., 2014. A calibration procedure to improve global rice yield simulations with EPIC. Ecol. Model., 273: 128–139.

Chapter 4

Towards improvement of grey water footprint assessment: With an illustration for global maize cultivation

Based on

Towards improvement of grey water footprint assessment: With an illustration for global maize cultivation. Journal of Cleaner Production, 147: 1–9. (2017)

Authors

Wenfeng Liu[a], Marta Antonelli[a], Xingcai Liu[c], Hong Yang[a,b]

[a]*Eawag, Swiss Federal Institute of Aquatic Science and Technology, Ueberlandstrasse 133, CH-8600 Duebendorf, Switzerland*

[b]*Department of Environmental Sciences, University of Basel, Petersplatz 1, CH-4003 Basel, Switzerland*

[c]*Key Laboratory of Water Cycle and Related Land Surface Processes, Institute of Geographical Sciences and Natural Resources Research, Chinese Academy of Sciences, Beijing, 100101, China*

Abstract

The grey water footprint refers to the volume of water that is required to assimilate polluted water. It reflects the intensity of water pollution caused by water use for human activities. This study aims to address some major shortcomings associated with grey water footprint accounting in the literature and discuss several ways towards its improvement. Global maize production is used for illustration. The study specifically tackles three issues: the appropriate water quality standards for grey water footprint assessment; grey water footprint for multiple pollutants; and the influence of spatial resolution of the assessment on the level of grey water stress. A biophysical crop model is applied to quantify nitrogen and phosphorus losses to water in maize production on a global scale with a 0.5-degree spatial resolution. The study shows that the grey water footprint calculation is highly sensitive to the water standards applied. The results also suggest that the grey water footprint relating to nitrogen and phosphorus pollution caused by maize production alone has already exceeded their local water availability in many parts of the world. Grey water stress shows a more critical situation at the grid level than at the watershed level for maize cultivation because the former represents the local concentration whereas the latter gives the average situation of the whole watershed. This study highlights the need for standardizing the setting of water quality standards for a consistent grey water footprint assessment taking into consideration the diverse aquatic ecosystems and ambient water quality requirements across regions, as well as the presence of multiple pollutants in water bodies.

Keywords

Nitrogen and phosphorus losses; Water quality standards; Grey water stress; Global assessment; PEPIC

Highlights

Using drinking water standards for N underestimates the GWF accounting.

Taking more pollutants into account is recommended to embrace the possible GWF range.

The spatial resolution of GWF assessments influences the level of GWS.

4.1 Introduction

Nitrogen (N) and phosphorus (P) are key elements to life and are essential for crop and livestock production. During the period 1960–2010, the application of N and P fertilizers in agriculture for food production increased nine-fold and three-fold, respectively (Sutton et al., 2013). The use of fertilizers has, on the one hand, improved agricultural productivity, enabling the feeding of a growing world population while coping with the dietary shift towards an increased consumption of meat and dairy products. On the other hand, the use of fertilizers has dramatically increased the amount of N and P entering the terrestrial biosphere (Bennett et al., 2001; Vitousek et al., 2009). Nutrient losses from croplands into water bodies have caused major environmental problems, such as water quality degradation, groundwater contamination, biodiversity loss, fish deaths, and eutrophication (Galloway and Cowling, 2002; Obersteiner et al., 2013; Vitousek et al., 1997).

The need to account for the impacts of agricultural production in terms of water quantity and quality led to the development of water footprint indicators in the early 2000s (Hoekstra, 2003). The water footprint (WF) is a multidimensional indicator of consumptive water use, which accounts for green (rain) water, blue (surface and underground) water resources, and grey (polluted) water. The grey water footprint (GWF) was introduced by Hoekstra and Chapagain (2008) as a measure of the intensity of water pollution caused by water use for human activities. It is defined as the volume of water that is required to assimilate a load of pollutants to a freshwater body, based on natural background concentrations and existing ambient water quality standards (Hoekstra et al., 2011). The idea of measuring water pollution in terms of the amount of water needed to dilute pollutants can be traced back to Falkenmark and Lindh (1974), who pointed out that the amount of water required to dilute pollutants to acceptable levels is about 10–50 times the wastewater flow. The GWF indicator assumes that the gap between a water quality standard and the natural background concentration in a given water body can be used to dilute the pollution loads to meet the water quality standard. It expresses water pollution in terms of a water volume needed to dilute contaminated water to a given quality standard, so that it can be compared with water consumption.

A growing number of studies have provided GWF assessments at various geographical levels. Global GWF assessments have mainly been provided by the Water Footprint Network, e.g., Chapagain et al. (2006), Hoekstra and Mekonnen (2012), and Liu et al. (2012) (Table 4-1). Other GWF studies have been conducted at the national and regional levels (e.g., Cazcarro et al., 2016; Mekonnen et al., 2016); the river basin level (e.g., Miguel Ayala et al., 2016; Vanham and Bidoglio, 2014; Zhi et al., 2015); the city level (e.g., Manzardo et al., 2016a; Wang et al., 2013); and with a focus on specific products or crops (e.g., Ene et al., 2013; Lamastra et al., 2014;

Suttayakul et al., 2016). GWF assessments have overwhelmingly been focused on N-related loads to freshwater. Only a few considered multiple pollutants, such as N, P, COD (chemical oxygen demand), and NH4 (ammonium) (Dabrowski et al., 2009; Lu et al., 2016; Pellicer-Martinez and Martinez-Paz, 2016). Most GWF assessments used the drinking water standards (e.g., Bulsink et al., 2010; Chapagain et al., 2006; Mekonnen and Hoekstra, 2011, 2010), with a few exceptions that have used ambient water quality standards (e.g., Pellegrini et al., 2016; Pellicer-Martinez and Martinez-Paz, 2016; Zhuo et al., 2016) (Table 4-1).

It has been shown that agriculture, mainly cereal production, accounts for 75% of the global GWF related to anthropogenic N loads, with the highest contribution from Asia (Mekonnen and Hoekstra, 2015). In the period 1996–2005, GWF accounted for 15% of the global annual total water footprint (green, blue, and grey), and for 19% of global agricultural and industrial virtual water flows (Hoekstra and Mekonnen, 2012). It has also been shown that about two-thirds of world's major rivers, especially in tropical and sub-tropical areas, have a pollutant load that exceeds the basin's assimilation capacity (Liu et al., 2012). A number of studies have shown that large GWF can exacerbate water scarcity conditions (Liu et al., 2012; Mekonnen et al., 2016; Zhuo et al., 2016). Others have pointed out that the international trade of agricultural products has resulted in a globalization of agricultural pollution, which has substantially increased over the past few decades (Galloway et al., 2008; Mekonnen et al., 2016; O'Bannon et al., 2014).

The GWF indicator has been developed to describe water quality conditions and inform policies related to water pollution. However, the concept has a number of limitations that are mainly related to three aspects. First, there are significant disparities in the water standards for natural nutrient and maximum allowable concentration values used in the GWF assessment. The volume of GWF and associated values are highly sensitive to the standards chosen. This point has not been paid sufficient attention in the GWF studies and confusion often occurs. Second, GWF is generally assessed for individual pollutants, while in reality they mostly co-exist. There has been no study that specifically discussed the influences of the integration of GWF of multiple pollutants on GWF by comparing with individual pollutants. Third, the GWF studies have been conducted at different geographical levels, e.g., grid and river basin levels. However, the effects of different spatial resolutions on the GWF assessment have not been addressed. These shortcomings need to be addressed to enhance the usefulness of GWF assessment as a tool for informing sound water management and policy.

The grey water stress (GWS), which is defined as the ratio of GWF to the actual runoff with the same spatiotemporal scale, indicates the status of the assimilative capacity of the corresponding water body under the pressure of GWF, i.e. the water stress caused by GWF. The concept suggests that if the pressure of GWF is higher than the assimilation capacity, then the

GWF is environmentally unsustainable (Hoekstra et al., 2011; Mekonnen et al., 2016). It should be noted that Hoekstra et al. (2011) called this indicator the water pollution level (WPL), which was adopted by several studies (e.g., Liu et al., 2012; Mekonnen and Hoekstra, 2015). However, the concept of GWS is considered to be more explicitly in line with the concept of GWF. Therefore, this terminology is used in this study.

Table 4-1. Literature review of standards used for grey water footprint assessment.

Study area	Nitrogen		Phosphorus		References
	C_{max} (mg N L^{-1})	C_{nat} (mg N L^{-1})	C_{max} (mg P L^{-1})	C_{nat} (mg P L^{-1})	
Argentina^{R}	10 (USA)*	--	--	--	(Rodriguez et al., 2015)
Brazil^{G+W}	--	-	0.1 (Brazil)	0	(Miguel Ayala et al., 2016)
Brazil^{R}	10 (Brazil)*	0.8	--	--	(Scarpare et al., 2016)
China^{R}	12 (China)*	--	--	--	(Duan et al., 2016)
China^{W}	1 (China)$^{\#}$	0			(Liu et al., 2016a)
China^{R}	10 (USA)*	--	--	--	(Huang et al., 2012)
China^{R}	10 (China)*	0	--	--	(Lu et al., 2016)
China^{R}	1 (China)$^{\#}$	--	0.2 (China)	--	(Wang et al., 2013)
China^{R}	1 (China)$^{\#}$	0	0.2 (China)	0	(Wu et al., 2016)
China^{R}	10 (USA)*	--	--	--	(Xu et al., 2015)
China^{W}	10 (China)*	0	--	--	(Zeng et al., 2013)
China^{G+R}	1 (China)$^{\#}$	0.2	0.2 (China)	0.02	(Zhuo et al., 2016)
England^{R}	12.86 (England and Wales)$^{\#}$	6.38	0.25 (England and Wales)	0.01	(Zhang et al., 2014)
Europe^{G+R}	3.1 (Liu et al., 2012)	1.5	0.95 (Liu et al., 2012)	0.52	(Mekonnen et al., 2016)
Europe^{R}	10 (USA)*	--	--	--	(Thaler et al., 2012)
Europe^{W}	10 (USA)*	0	--	--	(Vanham and Bidoglio, 2014)
France^{G+R}	10 (USA)*	--	--	--	(Ercin et al., 2013)
Global^{R}	10 (USA)*	0	--	--	(Chapagain et al., 2006)
Global^{R}	11.3 (EU)*	--	--	--	(Chapagain and Hoekstra, 2011)
Global^{G+R}	10 (USA)*	0	--	--	(Hoekstra and Mekonnen, 2012)
Global^{W}	3.1 (Estimated)	1.5	0.95 (Estimated)	0.52	(Liu et al., 2012)
Global^{G+W}	2.9 (Canada)$^{\#}$	0.4	--	--	(Mekonnen and Hoekstra, 2015)
Global^{G+R}	10 (USA)*	0	--	--	(Mekonnen and Hoekstra, 2010)
Global^{G+R}	10 (USA)*	0	--	--	(Mekonnen and Hoekstra, 2011)
Global^{G+R}	10 (USA)*	0	--	--	(Mekonnen and Hoekstra, 2014)
Indonesia^{R}	10 (USA)*	--	--	--	(Bulsink et al., 2010)
Italy^{G+R}	10 (USA)*	0	--	--	(Aldaya and Hoekstra, 2010)
Italy^{R}	15 (Italy)$^{\#}$	0	--	--	(Pellegrini et al., 2016)
Kenya^{G+W}	10 (USA)*	0			(Mekonnen et al., 2012)
Latin America and the Caribbean^{G+R}	10 (USA)*	--	--	--	(Mekonnen et al., 2015)
New Zealand^{R}	11.3 (New Zealand)*	0–1.3			(Deurer et al., 2011)
New Zealand^{R}	11.3 (New Zealand)*	0	--	--	(Herath et al., 2013)
Morocco^{R}	10 (USA)*	--	--	--	(Schyns and Hoekstra, 2014)
Romania^{R}	10 (USA)*	--	--	--	(Ene et al., 2013)
South Africa^{R}	4 (South Africa)$^{\#}$	0.62	0.13 (South Africa)	0.06	(Dabrowski et al., 2009)
South Korea^{R}	40 (South Korea)$^{\#}$	--	4 (South Korea)	--	(Yoo et al., 2014)
Spain^{R}	11.3 (EU)*	--	--	--	(Cazcarro et al., 2016)
Spain^{R}	11.3 (EU)*	--	--	--	(Chapagain and Orr, 2009)
Spain^{W}	11.3 (EU)*	--	--	--	(Chico et al., 2013)
Spain^{R}	5.6 (Spain)$^{\#}$	--	0.13 (Spain)	--	(Pellicer-Martinez and Martinez-Paz, 2016)
Taiwan, China^{R}	10 (Taiwan)*	0	--	--	(Su et al., 2015)
Tunisia^{R}	10 (USA)*	0	--	--	(Chouchane et al., 2015)
USA^{R}	10 (USA)*	0	--	--	(Manzardo et al., 2016b)

R: Regional level; W: Watershed level; G+R: Grid and regional levels; G+W: Grid and watershed levels; *: Nitrogen standard for drinking water; #: Nitrogen standard for surface water; --: no information.

To address the above limitations in GWF accounting, a global assessment of the GWF for one of the most important cereal crops in the world, i.e. maize, is conducted for illustration. Globally, maize produces the highest crop production and ranks third on N and P consumption as well as the resulted water pollution, following wheat and rice (West et al., 2014). Considering its wide spatial coverage (Portmann et al., 2010) and relatively less diverse production conditions compared to wheat and rice, maize is selected as an illustration here. A large-scale crop model PEPIC (Liu et al., 2016b), i.e. Environmental Policy Integrated Climate (EPIC) under the Python environment (www.python.org), is applied to quantify the losses of N and P from fertilizer application on a global scale with a 0.5-degree spatial resolution. Total losses of N and P from maize croplands into water bodies are considered in the GWF assessment, as they are the major nutrients applied to crops as agrochemical fertilizers. Water quality standards are clarified and the implications of the disparities are addressed. The GWS is assessed at the grid and river basin levels to highlight the impacts of different geographical scales on the assessment. Given the importance and increasing emphasis of water management at the basin/watershed level, it is useful to provide the assessment of GWS at this level.

4.2 Methodology and data

4.2.1 Model description and input data

In this study, the EPIC model (Williams et al., 1984) was used to quantify the N and P losses from maize production. EPIC is a field-scale crop model, which was initially developed to simulate the impacts of soil erosion on soil productivity. It was then extended to simulate the complex processes in the soil–water–climate–management systems (Williams, 1995). PEPIC is a simulation framework, which is able to prepare spatial input data for EPIC, run the EPIC model, extract outputs of the simulation, and finally map the results of desired variables (Liu et al., 2016b). It has been successfully used to investigate the crop–water relations of maize and assess global N losses from major crops (Liu et al., 2016b, 2016c).

The inputs to the PEPIC model include climate, soil, digital elevation model (DEM), slope, and crop management information, e.g., planting and harvesting dates, irrigation, and fertilizer. The fertilizer inputs (including N and P) were downloaded from EarthStat (http://www.earthstat.org/). This dataset was based on Mueller et al. (2012) and West et al. (2014). Information about the other inputs can be found in (Liu et al., 2016b).

The inputs of N considered in this study include chemical fertilizer, manure, precipitation deposition, and crop residue decomposition; while the P inputs include chemical fertilizer, manure, and crop residue decomposition. On the downside, the N outputs include crop uptake, N lost to

atmosphere through denitrification and volatilization, and N lost to water bodies through surface runoff, leaching, and bounded with sediments. As for P, the outputting pathway is crop uptake, and losses go into water bodies through surface runoff, leaching, and with sediments. More details of the nutrient dynamics of the EPIC model can be found in Williams (1995) and the calculation of N losses can be found in Liu et al. (2016c). For the calculation of GWF related to N and P, the study focused on the total losses of N and P into the water bodies.

4.2.2 Grey water footprint and grey water stress

By definition (Hoekstra et al., 2011), GWF is calculated as:

$$GWF_N = 100 * L_N/(C_{max\_N} - C_{nat\_N}) \quad (4\text{-}1)$$

$$GWF_P = 100 * L_P/(C_{max\_P} - C_{nat\_P}) \quad (4\text{-}2)$$

where GWF_N [mm] and GWF_P [mm] are the grey water footprint derived from N and P loads in water bodies, respectively; L_N [kg N ha^{-1}] and L_P [kg P ha^{-1}] are the N and P concentrations, which can be estimated at different levels, e.g., grid and basin levels, as the ratios of total N [kg N] and P [kg P] loads to the whole areas of the corresponding level; C_{max_N} [mg N L^{-1}] and C_{max_P} [mg P L^{-1}] are the ambient water quality standards for N and P; C_{nat_N} [mg N L^{-1}] and C_{nat_P} [mg P L^{-1}] are the natural background concentrations of N and P in the receiving water body; 100 is for unit transformation.

In the literature, for multiple pollutants, the GWF was calculated and presented separately for each pollutant, e.g., N, P, COD, and pesticides in some studies (e.g., Dabrowski et al., 2009; Liu et al., 2016a, 2012). For an individual grid cell or a given water body, e.g., river basin, the GWF under the condition of multiple pollutants (hereby referred to as integrated GWF) should be assessed by choosing the highest GWF deriving from single pollutants (Eq. 3). A summation of GWF of individual pollutants would overestimate the total GWF because the volume of water required for diluting one pollutant can simultaneously dilute other pollutants. The highest GWF of a single pollutant can thus represent the integrated GWF for that grid cell or corresponding water body. The integrated grey water footprint is calculated as:

$$GWF_I = max(GWF_N, GWF_P) \quad (4\text{-}3)$$

where GWF_I [mm] is the integrated grey water footprint from considering the N and P loads. The total GWF is calculated as the product of GWF and the whole area. The GWS is calculated as:

$$GWS = GWF/R \quad (4\text{-}4)$$

where R is the runoff with the same spatiotemporal scale as GWF [mm]. Runoff data are produced by the Distributed Biosphere Hydrological (DBH) model forced by the Princeton global meteorological data (Liu et al., 2016d; Tang et al., 2008). For the management of a water body,

assessing the consumption of assimilative capacity caused by pollutants is important (Zhi et al., 2015). With this concept, GWS < 1 means that the water body still has excess assimilative capacity to accommodate more pollutants; GWS = 1 means all the assimilative capacity is used up; and GWS > 1 means that the pollution level has exceeded the assimilative capacity and that the water pollution is thus unsustainable. The higher the GWS, the poorer the water quality. In this study, GWS related to N (GWS_N), P (GWS_P), and their integration (GWS_I) are considered.

4.2.3 Water quality standards review

Water standards are the key information required to calculate the GWF and GWS. In different countries, these standards can vary quite substantially. An extensive literature review was conducted on the water standards used for GWF assessments related to N and P (Table 4-1). It reveals some confusion in water quality standards. From the definition of Hoekstra et al. (2011), the ambient environmental water quality standards should be applied in the GWF calculation. However, in the GWF literature to date, the USA and the EU N standards for drinking water, respectively 10 mg N L^{-1} and 11.3 mg N L^{-1}, are the most commonly used water quality standards. Among the 40 reviewed studies (which explicitly used the N-related water quality standards) in Table 4-1, 30 (75%) of them used the N drinking water quality standards. So far, no study has specifically addressed this issue. Some local standards have also been used for regional GWF assessments. It is noted that studies even adopted different standards in the same region/country. For example, in China, three standards for nitrogen were used, i.e. 1 (e.g., Wu et al., 2016), 10 (e.g., Lu et al., 2016), and 12 (Duan et al., 2016) mg N L^{-1} in the literature. Obviously, these different standards introduced significant disparities in GWF accounting. The confusion is partly related to the fact that for many countries, the information on ambient water quality standards are not available, either because they do not exist (e.g., for most African countries and less developed countries) or because of the lack of access to the data sources (e.g., for most of other countries). For P, a few papers addressed the GWF with standards varying from 0.1 to 4 mg P L^{-1} (Table 4-1).

Several national N and P standards for drinking water and ambient surface water were reviewed (Table 4-2). They show that the allowed N concentrations for surface water are generally lower than that for drinking water. This means that the estimated GWF tends to be underestimated by adopting drinking water standards, which was the case for many previous studies (as shown in Table 4-1). As P is not directly toxic for humans, drinking water standards have not been set for this pollutant. Some points to note are that in some cases the national N and P standards are not unique values but region specific. For example, the USA was divided into 13 eco-regions and there is one standard for each eco-region (https://www.epa.gov/nutrient-policy-data/ecoregional-criteria). This situation also holds for the Netherlands (Table 4-2). The way to determine surface water N standards also varies. For example, the N surface standard in Canada

(3 mg N L^{-1}) was derived from toxicity tests of aquatic species exposed to environments with different levels of nitrate (http://ceqg-rcqe.ccme.ca/download/en/197?redir=1465564929). In the USA, however, it was determined by the 25th of measured nitrate concentrations from surface water (https://www.epa.gov/nutrient-policy-data/ecoregional-criteria).

Table 4-2. National water standards for nitrogen (N) and phosphorus (P).

	N (mg N L^{-1})		TP (mg P L^{-1})
	Drinking water	Surface water	
Canada	10 (NO_3-N)[R1]	3 (NO_3-N)[R2]	0.02[R3]
China	10 (NO_3-N)[R4]	1 (TN, lakes)[R5]	0.05 (lakes)[R5] 0.2 (rivers)[R5]
EU	11.3 (NO_3-N)[R6]	5.6 (NO_3-N)[R7]	0.07–0.15[R8]
Germany	11.3 (NO_3-N)[R9]	3 (TN)[R10] 2.5 (NO_3-N)[R10]	0.15[R11]
Switzerland	5.6 (NO_3-N)[R12]	7 (TN)[R13] 5.6 (NO_3-N)[R13]	0.07[R13]
The Netherlands	11.3 (NO_3-N)[R14]	0.12–18.05 (TN)[*, R15]	0.01–2.5[*, R15]
USA	10 (NO_3-N)[R16]	0.1–1.27 (TN, lakes)[R17] 0.12–2.18 (TN, rivers)[R17]	0.008–0.038 (lakes)[R17] 0.01–0.076 (rivers)[R17]

TN: total nitrogen; TP: total phosphorus. *: the ranges are quite high because they incorporate specific goals from more than 500 water bodies.

R1: http://www.hc-sc.gc.ca/ewh-semt/pubs/water-eau/sum_guide-res_recom/index-eng.php;
R2: http://ceqg-rcqe.ccme.ca/download/en/197?redir=1465564929;
R3: http://ceqg-rcqe.ccme.ca/download/en/205?redir=1465564939;
R4: http://www.moh.gov.cn/zwgkzt/pgw/201212/33644.shtml;
R5: http://kjs.mep.gov.cn/hjbhbz/bzwb/shjbh/shjzlbz/200206/t20020601_66497.shtml;
R6: http://eur-lex.europa.eu/LexUriServ/LexUriServ.do?uri=OJ:L:1998:330:0032:0054:EN:PDF;
R7: http://eur-lex.europa.eu/legal-content/EN/TXT/PDF/?uri=CELEX:31991L0676&from=en;
R8: http://eur-lex.europa.eu/LexUriServ/LexUriServ.do?uri=OJ:L:2006:264:0020:0031:EN:PDF;
R9: http://www.gesetze-im-internet.de/bundesrecht/trinkwv_2001/gesamt.pdf;
R10: http://www.vsr-gewaesserschutz.de/33.html;
R11: http://www.vsr-gewaesserschutz.de/20.html;
R12: https://www.admin.ch/opc/en/classified-compilation/19983281/index.html#app4;
R13: http://www.modul-stufen-konzept.ch/download/ChemieD_Juni2010.pdf;
R14: http://wetten.overheid.nl/BWBR0027061/2016-01-01/0/#BijlageIII;
R15: http://www.helpdeskwater.nl/onderwerpen/wetgeving-beleid/kaderrichtlijn-water/2016-2021/;
R16: https://www.epa.gov/wqc/national-recommended-water-quality-criteria-human-health-criteria-table;
R17: https://www.epa.gov/nutrient-policy-data/ecoregional-criteria.

After careful assessment and discussions with experts in ecosystem sciences, the N standard adopted in this study for surface water is 3 mg N L^{-1}. This standard is also recommended by Franke et al. (2013). For comparison, the most commonly used N standard for drinking water (10 mg N L^{-1}) was also used for GWF calculation related to N. For P, the standard used here is 0.15 mg P L^{-1}. This standard is recommended by Germany and the EU (Table 4-2). Many previous studies assumed the natural pollutant concentration to be 0 due to a lack of data (e.g., Chapagain et al., 2006; Liu et al., 2016a; Zeng et al., 2013). However, the natural concentrations of N and P are generally higher than 0, thus such an assumption leads to an underestimation of GWF. In this study, the natural concentration was set to be 0.4 mg N L^{-1} and 0.01 mg P L^{-1} for N and P, respectively. The natural concentration for N of 0.4 mg N L^{-1} is recommended by Hoekstra et al. (2011) and Franke et al. (2013), and is also used by Mekonnen and Hoekstra (2015). As for the natural concentration of P, 0.01 mg P L^{-1}, is recommended by Franke et al. (2013). The natural

concentration was also considered to be 0 for illustrating the impacts of using different natural concentrations.

4.3 Results

4.3.1 Grey water footprint assessment

Global GWF for maize cultivation using 3 mg N L^{-1} and 0.15 mg P L^{-1} as standards with the natural concentrations of 0.4 mg N L^{-1} and 0.01 mg P L^{-1} is presented in Figure 4-1. It can be seen that GWF_P is much higher than GWF_N in many regions. The GWF_N and GWF_P also present different spatial patterns. The North China Plain, northeastern parts of China, and north central parts of the USA are the major regions with a high level of GWF_N (> 500 mm) (Figure 4-1a). While for GWF_P, not only the above mentioned regions, but also southwest parts of China, southern Mexico, and southern Brazil, as well as some parts of central Europe show a high level of GWF_P (Figure 4-1b). GWF_I presents quite a similar pattern to GWF_P (Figure 4-1c), implying that GWF_I is more related to GWF_P for maize cultivation.

The global total GWF_N for maize is 706 km^3 using the drinking water standard (10 mg N L^{-1}) and increases to 2607 km^3 using the ambient water standard (3 mg N L^{-1}) (Table 4-3). The conversion of GWF between different standards is straightforward. For example, the GWF_N with the ambient water quality standard can be obtained by multiplying 3.69, i.e. the ratio of (10−0.4) to (3−0.4), by the GWF_N calculated using the drinking water quality standard. The global GWF_P is about 2.7 times that of GWF_N. Although globally N loads are generally higher than P loads, the higher GWF_P is mainly due to the much lower value of maximum allowable concentration for P than for N. The GWF_I is only a little higher than GWF_P (4%). This indicates that GWF relating to maize production is mainly determined by P. Asia and North America contribute the largest proportion of global GWF both for N and P, while South America also contributes a high proportion of global GWF_P. At the country level, China and the USA account for the highest proportion of GWF_N, while the USA, China, and Brazil contribute the most GWF_P. For the top ten watersheds, the Mississippi plays the dominant role in contributing to GWF_N, while the Mississippi and La Plata show similar roles for GWF_P. Disparities of GWF at continental, country, and river basin levels are noticeable. For example, the GWF_P (P0.15_0.01, with 0.15 mg P L^{-1} and 0.01 mg P L^{-1} as standard and natural concentration) is about 2.2 times that of GWF_N (N3_0.4, with 3 mg N L^{-1} and 0.4 mg N L^{-1} as standard and natural concentration) in Asia, however it decreases to 1.4 times in China and only accounts for 55% of the GWF_N of the Haihe river basin.

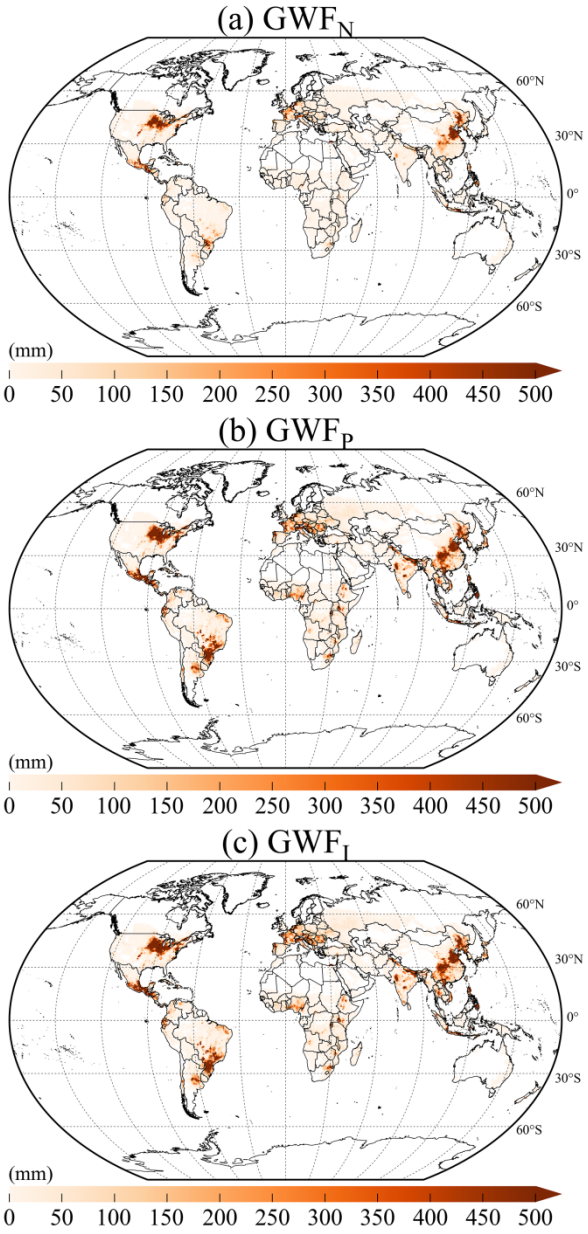

Figure 4-1. Grey water footprint (GWF) related to nitrogen (GWF_N), phosphorus (GWF_P), and their integration (GWF_I) in maize production by using 3 mg N L^{-1} and 0.15 mg P L^{-1} as the standards, and 0.4 mg N L^{-1} and 0.01 mg P L^{-1} as natural concentrations for nitrogen and phosphorus.

4.3.2 Grey water stress assessment

At the grid level, the GWS shows quite similar patterns to GWF (Figures 4-1–4-2). In the high GWF regions, GWS is generally higher than 1. For example, the GWS_N is higher than 1 in the northeastern parts of China and northeastern parts of the USA (Figure 4-2a). The high GWS in these regions implies that the assimilative capacity of the local water resource has been fully consumed and that a process of water environmental degradation is on-going. In contrast, the GWS presents an optimistic view at the watershed level, as the average values computed for a

watershed may hide the extreme values of GWS at a grid level. Most river basins present GWS lower than 0.3, except GWF_N and GWS_I in the Haihe river basin of China.

Table 4-3. The aggregated grey water footprint related to nitrogen (GWF_N), phosphorus (GWF_P), and their integration (GWF_I) in maize production at different geographical levels (km^3).

	N10_0.4[a]	N3_0.4[b]	P0.15_0.01[c]	GWF_I[d]
Continental level				
Africa	33.5	123.7	563.2	586.9
Asia	284.1	1049.1	2297.2	2459.0
Europe	75.1	277.2	666.9	681.0
N. America	236.1	871.9	2056.5	2102.7
Oceania	0.3	1.0	6.6	6.6
S. America	76.8	283.6	1395.1	1397.5
Global	706.0	2606.7	6985.5	7233.7
Top 10 maize-producing countriese				
USA	160.4	592.4	1233.4	1275.3
China	208.5	769.9	1097.3	1252.2
Brazil	54.9	202.6	1088.2	1089.2
Mexico	46.9	173.3	547.4	548.5
India	18.2	67.2	365.7	365.7
Russia	2.8	10.4	64.0	64.1
Nigeria	4.1	15.0	116.5	116.6
Argentina	8.2	30.4	125.6	125.6
Ukraine	1.8	6.6	35.5	35.5
France	25.6	94.5	123.3	131.8
Top 10 maize-producing watershedse				
Mississippi	132.6	489.8	988.0	1023.9
La Plata	44.6	164.5	843.2	843.2
Danube	11.5	42.3	144.0	144.7
Amur	37.1	137.0	113.4	158.4
Haihe	35.2	129.8	71.4	136.1
Yangtze	37.7	139.3	368.3	368.6
St Lawrence	21.4	79.1	148.1	149.7
China Coast	47.3	174.7	281.4	287.6
Ganges–Bramaputra	12.0	44.3	248.0	248.0
Yellow	22.8	84.3	63.6	91.4

[a] GWF_N with 10 mg N L^{-1} and 0.4 mg N L^{-1} as standard and natural concentration.
[b] GWF_N with 3 mg N L^{-1} and 0.4 mg N L^{-1} as standard and natural concentration.
[c] GWF_P with 0.15 mg P L^{-1} and 0.01 mg P L^{-1} as standard and natural concentration.
[d] GWF_I with 3 mg N L^{-1} and 0.15 mg P L^{-1} as the standards, and 0.4 mg N L^{-1} and 0.01 mg P L^{-1} as natural concentrations for nitrogen and phosphorus.
[e] The top 10 maize-producing countries and top 10 maize-producing watersheds are based on the maize cultivated areas.

To demonstrate the disparities of GWS due to different water quality standards and natural concentrations, different pollutants, and the integration of different pollutants, the fractions of grid number with GWS > 1 in the total grid number for maize cultivation under different conditions

were compared (Figure 4-3). The fraction for GWS_N using the ambient water quality standard (3 mg N L^{-1}) is much higher (about 5 times) than that using the drinking water quality standard (10 mg N L^{-1}), although the difference in water quality standards is only 3.3 times. Different natural concentrations also contribute to the disparities for both GWS_N and GWS_P. The fractions derived from P loads are much higher than those derived from N loads. For example, the fraction is about 2.5% for GWS_N with 3 mg N L^{-1} and 0.4 mg N L^{-1} as standard and natural concentration, while it increases to 5.1% for GWS_P with 0.15 mg P L^{-1} and 0.4 mg P L^{-1} as standard and natural concentration. When considering the integration of N and P, about 5.8% of total maize cultivation grids show GWS > 1.

4.4 Discussion

The key point addressed in this study is that there are multi-dimensional disparities of GWF assessments that prevent the indicator from providing a consistent value for water quality and being a tool for sound policy supporting in the water sector. It is here argued that improving the robustness of GWF assessments is necessary to gain a more comprehensive understanding of the impacts of human activities on water quality. To the best of our knowledge, this study is the first attempt to comprehensively address the main shortcomings of GWF accounting and to propose ways of improving it.

First, the influence of water quality standards and natural concentration levels on GWF assessment was addressed. The GWF is generally estimated using water quality standards for the receiving freshwater bodies, which can be formulated at the national (e.g., for Switzerland) or regional level (e.g., the EU Water Framework Directive). However, as these standards do not exist for all pollutants and for all countries, it is difficult to make consistent analyses in some circumstances. The choice of whether to use environmental or drinking water quality standards in GWF assessments is also a matter of great importance (Table 4-3). It is highly recommended that the standards used are verified when performing a comparison with results from different studies. Ambient water quality standards also vary considerably from one substance to another and from one country or region to another. This point needs to be addressed, as the choice of inputs and parameter values determines the major disparities in GWF assessments, as also highlighted by Mekonnen and Hoekstra (2015).

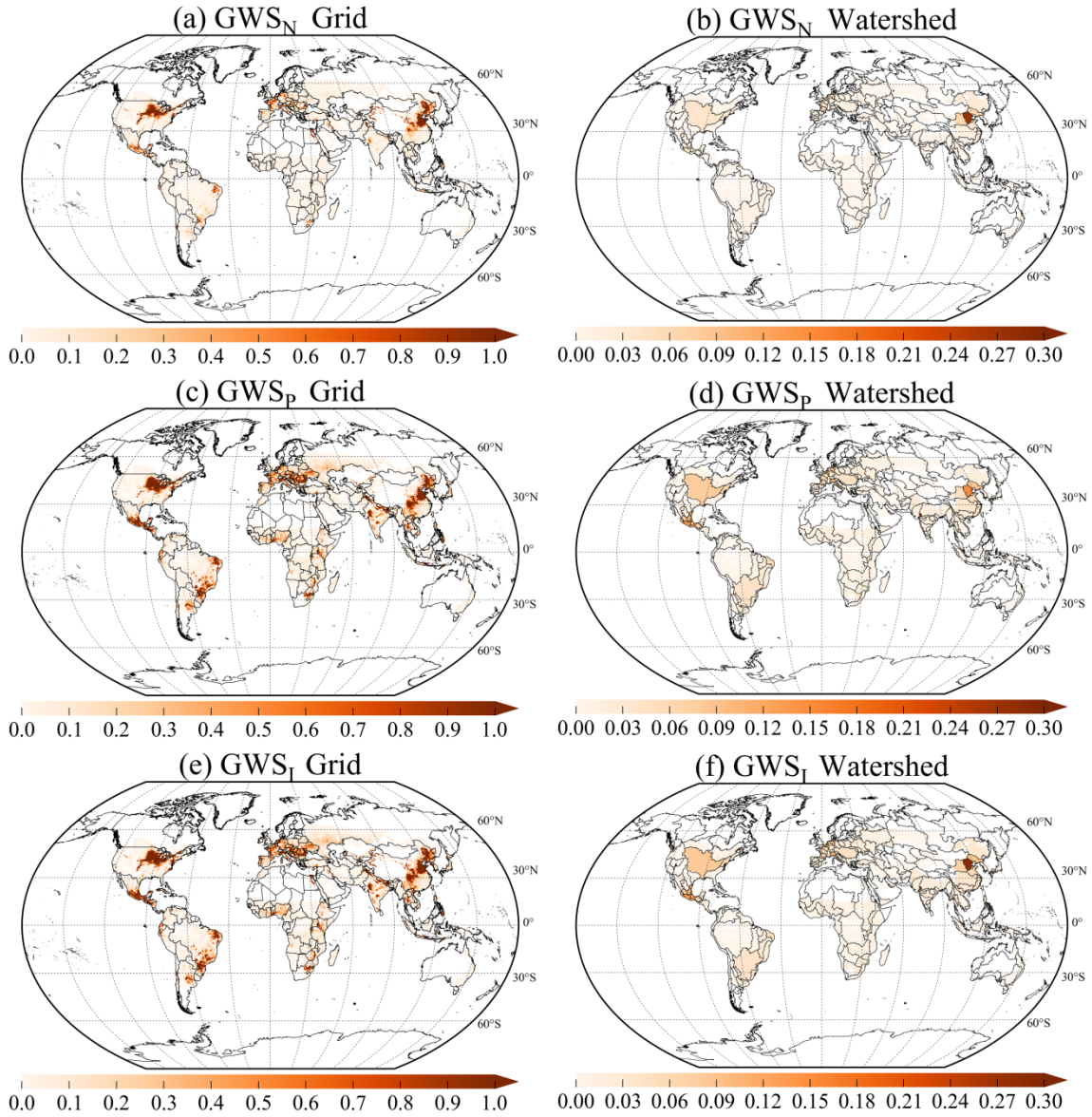

Figure 4-2. Grey water stress (GWS) related to nitrogen (GWS_N), phosphorus (GWS_P), and their integration (GWS_I) in maize production at grid and watershed levels by using 3 mg N L^{-1} and 0.15 mg P L^{-1} as standards, and 0.4 mg N L^{-1} and 0.01 mg P L^{-1} as natural concentrations for nitrogen and phosphorus.

It should be highlighted here that for N, ambient water standards are consistently higher than drinking water standards (Table 4-2). A number of water scientists from the Swiss Federal Institute for Aquatic Science and Technology (Eawag) have been consulted and a review of the relevant literature for the explanation of these differences has been conducted. It has emerged that fish, shellfish, and smaller organisms that live in water are more sensitive to N than humans are. Their small bodies make them less tolerant to the concentration of the pollutants. Therefore, the use of drinking water standards underestimates GWF (Table 4-2). The P pollution in freshwater bodies is not directly toxic to humans and animals. This is the main reason that there is generally no drinking water standard for P. It has, however, an indirect toxicity as it causes proliferation of

toxic algal blooms and results in the depletion of oxygen, which kills fish (Carpenter et al., 1998). Nitrate loads into water, in contrast, pose a direct threat for the health of humans and other mammals. High concentration of nitrate has been linked to cancers and methemoglobinemia in infants, as well as to toxic effects on livestock (e.g., abortions in cattle).

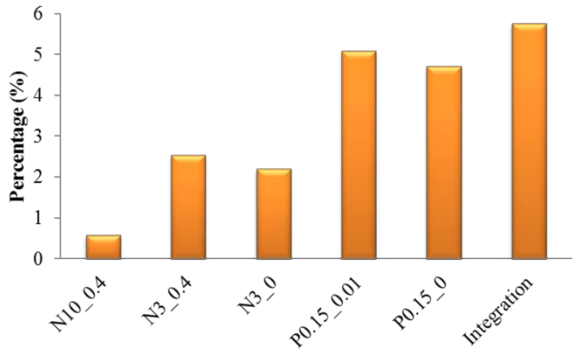

Figure 4-3. Fraction of grid number with grey water stress (GWS) higher than 1 in total grid number of maize cultivation. For X axis, N10_0.4 refers to GWS related to N (GWS_N) with 10 mg N L^{-1} and 0.4 mg N L^{-1} as standard and natural concentration; N3_0.4 refers to GWS_N with 3 mg N L^{-1} and 0.4 mg N L^{-1} as standard and natural concentration; N3_0 refers to GWS_N with 10 mg N L^{-1} and 0 mg N L^{-1} as standard and natural concentration; P0.15_0.01 refers to GWS related to P (GWS_P) with 0.15 mg P L^{-1} and 0.01 mg P L^{-1} as standard and natural concentration; P0.15_0 refers to GWS_P with 0.15 mg P L^{-1} and 0 mg P L^{-1} as standard and natural concentration; Integration is integrated GWS (GWS_I) with 3 mg N L^{-1} and 0.15 mg P L^{-1} as the standards, and 0.4 mg N L^{-1} and 0.01 mg P L^{-1} as natural concentrations for N and P.

The assumptions on natural concentration also largely influence the results of GWF analyses. As shown by Liu et al. (2012), changes in natural concentration levels can result in large disparities in GWS assessment. It is also noteworthy to say that it is not easy to account for natural concentration in a receiving body. Some studies have assumed the natural concentration to be zero. In reality, this cannot be the case, as nutrients are transported through river systems and interact with sediments. As different ecosystems respond differently to nutrient loads, to produce meaningful results, GWF assessments should be based on basin-specific values for both maximum allowable concentration and natural concentration for different nutrients. Experimental studies are needed to support more robust GWF assessments.

The second point raised in the present study is that the co-existence of multiple pollutants in water bodies (e.g. N and P, pesticides, herbicides, heavy metals, and other harmful chemical compounds) needs to be considered in GWF assessments. The majority of GWF assessments only considers anthropogenic N loads to water (e.g., Hoekstra and Mekonnen, 2012; Mekonnen and Hoekstra, 2015; O'Bannon et al., 2014) (Table 4-1), while neglecting the existence of other pollutants. In this study, an integrated GWF by considering the highest GWF of individual pollutants was explicitly illustrated using N and P losses in global maize cultivation as example.

The result demonstrates that it is important to consider P-related loads into water, as the dilution of this input is much more water intensive than the dilution of N-loads. This is because eutrophication in water bodies is more likely caused by P (Schindler et al., 2008). Therefore, the P-related water quality standards are far more stringent than those for N. It can also be argued that, as the pollutant that has the highest GWF is often unknown or cannot be determined in the water body, an aggregated water quality indicator, which takes all possible pollutants into account with a weighting factor, may be more appropriate for GWF accounting. But how to determine such an indicator deserves further investigation.

Third, this study addressed the disparities arising from the use of different spatial scales. The analysis has shown that the good condition of GWS at the basin level hides the potential negative impacts at the grid level. This is because the grid level assessment provides information on local concentration of pollution, whereas the basin level assessment gives the average concentration in the whole basin which can smooth out the high concentration in many local areas. Hence, the river basin level GWF may provide wrong information on the criticality of water pollution situation, impairing sound policy making for water resource management. Though watersheds hold the complete hydrological processes, it seems that water pollution intensity should be assessed by treating sources of pollution which are located in different parts of a basin. When the water pollution happens in the upstream of a basin, the situation may be different from if it happens in the down steam. For example, the GWS of N at Mississippi is only 0.04–0.08 when taking it as a whole area (Figure 4-2). However, a large number of grids in its northeastern parts present GSW larger than 1. It is difficult to use the downstream water resources to deal with the upstream water pollution. Therefore, assessing the GWF and GWS at the grid level should have a higher priority. The grid level was also recommended by Mekonnen and Hoekstra (2014), where they compared the green and blue water footprint at the grid, provincial, and country levels. For this reason, the current study focused on the grid level for evaluating the disparities of GWS as shown in Figure 4-3.

Finally, it should be mentioned that this study did not consider accumulation and degradation of the lost N and P in the receiving water bodies. Also, the effects of different forms of lost N and P on the aquatic ecosystem were not considered. This is because it is difficult to determine exact loads of individual forms in which the lost N and P present in water bodies due to the complex chemical and biological processes involved. For this reason, studies in grey water footprint so far have used a certain element as a proxy for N and P loads, e.g., total losses to water regardless forms and fates of the pollutant (such as in this study and many other studies, including Hoekstra and Mekonnen (2012) and Mekonnen and Hoekstra (2015). Only few have used dissolved inorganic N and P, dissolved organic N and P, and total N and P (Liu et al., 2012). It is clear that

using different forms of a certain pollution element will lead to different results of GWF. However, a detailed analysis of the fate of the lost N and P and the involved chemical and biological processes is beyond the scope of this study, but deserves further investigation in the future.

4.5 Conclusions

This study has discussed some major limitations of GWF assessment in the literature and proposed several ways towards its improvement. It provides a first exploration on how the GWF assessment can be enhanced from a methodological point of view, with an illustration for N and P loads into water relating to global maize cultivation. The insights provided can be used to investigate GWF from multiple crops and pollutants and water quality parameters. The approach taken in this study can also be used to provide a scientifically sound frame of reference for evaluating the trade-offs of importing rather than producing different crops in different locations from both a water quality and water quantity perspective. Finally, improving the scientific soundness of GWF assessments can better inform national and local governments about the pressure on water systems from agrochemical pollutants and serve as a tool for setting water pollution reduction targets based on the consumption of assimilation capacity of water bodies.

4.6 References

Aldaya, M.M., Hoekstra, A.Y., 2010. The water needed for Italians to eat pasta and pizza. Agr. Syst., 103: 351–360.

Bennett, E.M., Carpenter, S.R., Caraco, N.F., 2001. Human impact on erodable phosphorus and eutrophication: A global perspective. Bioscience, 51: 227–234.

Bulsink, F., Hoekstra, A.Y., Booij, M.J., 2010. The water footprint of Indonesian provinces related to the consumption of crop products. Hydrol. Earth Syst. Sci., 14: 119–128.

Carpenter, S.R., Caraco, N.F., Correll, D.L., Howarth, R.W., Sharpley, A.N., Smith, V.H., 1998. Nonpoint pollution of surface waters with phosphorus and nitrogen. Ecol. Appl., 8: 559–568.

Cazcarro, I., Duarte, R., Sánchez-Chóliz, J., 2016. Downscaling the grey water footprints of production and consumption. J. Clean. Prod., 132: 171–183.

Chapagain, A.K., Hoekstra, A.Y., 2011. The blue, green and grey water footprint of rice from production and consumption perspectives. Ecol. Econ., 70: 749–758.

Chapagain, A.K., Hoekstra, A.Y., Savenije, H.H.G., Gautam, R., 2006. The water footprint of cotton consumption: An assessment of the impact of worldwide consumption of cotton products on the water resources in the cotton producing countries. Ecol. Econ., 60: 186–203.

Chapagain, A.K., Orr, S., 2009. An improved water footprint methodology linking global consumption to local water resources: A case of Spanish tomatoes. J. Environ. Manage., 90: 1219–1228.

Chico, D., Aldaya, M.M., Garrido, A., 2013. A water footprint assessment of a pair of jeans: the influence of agricultural policies on the sustainability of consumer products. J. Clean. Prod., 57: 238–248.

Chouchane, H., Hoekstra, A.Y., Krol, M.S., Mekonnen, M.M., 2015. The water footprint of Tunisia from an economic perspective. Ecol. Indic., 52: 311–319.

Dabrowski, J.M., Murray, K., Ashton, P.J., Leaner, J.J., 2009. Agricultural impacts on water quality and implications for virtual water trading decisions. Ecol. Econ., 68: 1074–1082.

Deurer, M., Green, S.R., Clothier, B.E., Mowat, A., 2011. Can product water footprints indicate the hydrological impact of primary production? – A case study of New Zealand kiwifruit. J. Hydrol., 408: 246–256.

Duan, P., Qin, L., Wang, Y., He, H., 2016. Spatial pattern characteristics of water footprint for maize production in Northeast China. J. Sci. Food Agric., 96: 561–568.

Ene, S.A., Teodosiu, C., Robu, B., Volf, I., 2013. Water footprint assessment in the winemaking industry: a case study for a Romanian medium size production plant. J. Clean. Prod., 43: 122–135.

Ercin, A.E., Mekonnen, M.M., Hoekstra, A.Y., 2013. Sustainability of national consumption from a water resources perspective: The case study for France. Ecol. Econ., 88: 133–147.

Falkenmark, M., Lindh, G., 1974. How can we cope with the water resources situation by the year 2015? Ambio, 3: 114–122.

Franke, N., Hoekstra, A., Boyacioglu, H., 2013. Grey water footprint accounting: Tier 1 supporting guidelines. Value of Water Research Report Series No. 65, UNESCO-IHE, Delft, Netherlands.

Galloway, J.N., Cowling, E.B., 2002. Reactive nitrogen and the world: 200 years of change. Ambio, 31: 64–71.

Galloway, J.N., Townsend, A.R., Erisman, J.W., Bekunda, M., Cai, Z.C., Freney, J.R., Martinelli, L.A., Seitzinger, S.P., Sutton, M.A., 2008. Transformation of the nitrogen cycle: Recent trends, questions, and potential solutions. Science, 320: 889–892.

Herath, I., Green, S., Singh, R., Horne, D., van der Zijpp, S., Clothier, B., 2013. Water footprinting of agricultural products: a hydrological assessment for the water footprint of New Zealand's wines. J. Clean. Prod., 41: 232–243.

Hoekstra, A.Y. (Ed), 2003. Virtual water trade: Proceedings of the international expert meeting on virtual water trade. Value of Water Research Report Series No. 12, UNESCO-IHE, Delft, Netherlands.

Hoekstra, A.Y., Chapagain, A.K., 2008. Globalization of water: Sharing the planet's freshwater resources. Earthscan, London.

Hoekstra, A.Y., Chapagain, A.K., Aldaya, M.M., Mekonnen, M.M., 2011. The water footprint assessment manual: Setting the global standard. Earthscan, London.

Hoekstra, A.Y., Mekonnen, M.M., 2012. The water footprint of humanity. P. Natl. Acad. Sci. U.S.A., 109: 3232–3237.

Huang, J., Zhang, H., Tong, W., Chen, F., 2012. The impact of local crops consumption on the water resources in Beijing. J. Clean. Prod., 21: 45–50.

Lamastra, L., Suciu, N.A., Novelli, E., Trevisan, M., 2014. A new approach to assessing the water footprint of wine: An Italian case study. Sci. Total Environ., 490: 748–756.

Liu, C., Kroeze, C., Hoekstra, A.Y., Gerbens-Leenes, W., 2012. Past and future trends in grey water footprints of anthropogenic nitrogen and phosphorus inputs to major world rivers. Ecol. Indic., 18: 42–49.

Liu, J., Liu, Q., Yang, H., 2016a. Assessing water scarcity by simultaneously considering environmental flow requirements, water quantity, and water quality. Ecol. Indic., 60: 434–441.

Liu, W., Yang, H., Folberth, C., Wang, X., Luo, Q., Schulin, R., 2016b. Global investigation of impacts of PET methods on simulating crop-water relations for maize. Agric. For. Meteorol., 221: 164–175.

Liu, W., Yang, H., Liu, J., Azevedo, L.B., Wang, X., Xu, Z., Abbaspour, K.C., Schulin, R., 2016c. Global assessment of nitrogen losses and trade-offs with yields from major crop cultivations. Sci. Total Environ., 572: 526–537.

Liu, X., Tang, Q., Zhang, X., Leng, G., 2016d. Modeling the role of vegetation in hydrological responses to climate change, in: Tang, Q. and Oki, T. (Eds.), Terrestrial Water Cycle and Climate Change: Natural and Human-Induced Impacts. Wiley & Sons Inc., Hoboken, New Jersey, pp. 193–208.

Lu, Y., Zhang, X., Chen, S., Shao, L., Sun, H., 2016. Changes in water use efficiency and water footprint in grain production over the past 35 years: a case study in the North China Plain. J. Clean. Prod., 116: 71–79.

Manzardo, A., Loss, A., Fialkiewicz, W., Rauch, W., Scipioni, A., 2016a. Methodological proposal to assess the water footprint accounting of direct water use at an urban level: A case study of the Municipality of Vicenza. Ecol. Indic., 69: 165–175.

Manzardo, A., Mazzi, A., Loss, A., Butler, M., Williamson, A., Scipioni, A., 2016b. Lessons learned from the application of different water footprint approaches to compare different food packaging alternatives. J. Clean. Prod., 112: 4657–4666.

Mekonnen, M.M., Hoekstra, A.Y., 2010. A global and high-resolution assessment of the green, blue and grey water footprint of wheat. Hydrol. Earth Syst. Sci., 14: 1259–1276.

Mekonnen, M.M., Hoekstra, A.Y., 2011. The green, blue and grey water footprint of crops and derived crop products. Hydrol. Earth Syst. Sci., 15: 1577–1600.

Mekonnen, M.M., Hoekstra, A.Y., 2014. Water footprint benchmarks for crop production: A first global assessment. Ecol. Indic., 46: 214–223.

Mekonnen, M.M., Hoekstra, A.Y., 2015. Global gray water footprint and water pollution levels related to anthropogenic nitrogen loads to fresh water. Environ. Sci. Technol., 49: 12860–12868.

Mekonnen, M.M., Hoekstra, A.Y., Becht, R., 2012. Mitigating the water footprint of export cut flowers from the lake Naivasha basin, Kenya. Water Resour. Manage., 26: 3725–3742.

Mekonnen, M.M., Lutter, S., Martinez, A., 2016. Anthropogenic nitrogen and phosphorus emissions and related grey water footprints caused by EU-27's crop production and consumption. Water, 8: 30.

Mekonnen, M.M., Pahlow, M., Aldaya, M.M., Zarate, E., Hoekstra, A.Y., 2015. Sustainability, Efficiency and Equitability of Water Consumption and Pollution in Latin America and the Caribbean. Sustainability, 7: 2086–2112.

Miguel Ayala, L., van Eupen, M., Zhang, G., Pérez-Soba, M., Martorano, L.G., Lisboa, L.S., Beltrao, N.E., 2016. Impact of agricultural expansion on water Footprint in the Amazon under climate change scenarios. Sci. Total Environ., 569–570: 1159–1173.

Mueller, N.D., Gerber, J.S., Johnston, M., Ray, D.K., Ramankutty, N., Foley, J.A., 2012. Closing yield gaps through nutrient and water management. Nature, 490: 254–257.

O'Bannon, C., Carr, J., Seekell, D.A., D'Odorico, P., 2014. Globalization of agricultural pollution due to international trade. Hydrol. Earth Syst. Sci., 18: 503–510.

Obersteiner, M., Penuelas, J., Ciais, P., van der Velde, M., Janssens, I.A., 2013. The phosphorus trilemma. Nat. Geosci., 6: 897–898.

Pellegrini, G., Ingrao, C., Carnposeo, S., Tricase, C., Conto, F., Huisingh, D., 2016. Application of water footprint to olive growing systems in the Apulia region: a comparative assessment. J. Clean. Prod., 112: 2407–2418.

Pellicer-Martinez, F., Martinez-Paz, J.M., 2016. Grey water footprint assessment at the river basin level: Accounting method and case study in the Segura River Basin, Spain. Ecol. Indic., 60: 1173–1183.

Portmann, F.T., Siebert, S., Doll, P., 2010. MIRCA2000-Global monthly irrigated and rainfed crop areas around the year 2000: A new high-resolution data set for agricultural and hydrological modeling. Global Biogeochem. Cy., 24: GB1011.

Rodriguez, C.I., de Galarreta, V.A.R., Kruse, E.E., 2015. Analysis of water footprint of potato production in the pampean region of Argentina. J. Clean. Prod., 90: 91–96.

Scarpare, F.V., Hernandes, T.A.D., Ruiz-Correa, S.T., Kolln, O.T., Gava, G.J.D.C., dos Santos, L.N.S., Victoria, R.L., 2016. Sugarcane water footprint under different management practices in Brazil: Tiete/Jacare watershed assessment. J. Clean. Prod., 112: 4576–4584.

Schindler, D.W., Hecky, R.E., Findlay, D.L., Stainton, M.P., Parker, B.R., Paterson, M.J., Beaty, K.G., Lyng, M., Kasian, S.E.M., 2008. Eutrophication of lakes cannot be controlled by reducing nitrogen input: Results of a 37-year whole-ecosystem experiment. Proc. Natl. Acad. Sci. U.S.A., 105: 11254–11258.

Schyns, J.F., Hoekstra, A.Y., 2014. The added value of water footprint assessment for national water policy: A case study for Morocco. PLoS One, 9: e99705.

Su, M., Huang, C., Li, W., Tso, C., Lur, H.S., 2015. Water footprint analysis of bioethanol energy crops in Taiwan. J. Clean. Prod., 88: 132–138.

Suttayakul, P., H-Kittikun, A., Suksaroj, C., Mungkalasiri, J., Wisansuwannakorn, R., Musikavong, C., 2016. Water footprints of products of oil palm plantations and palm oil mills in Thailand. Sci. Total Environ., 542: 521–529.

Sutton, M.A., Bleeker, A., Howard, C., Bekunda, M., Grizzetti, B., Vries, W.d., Van Grinsven, H., Abrol, Y., Adhya, T., Billen, G., 2013. Our Nutrient World: the challenge to produce more food and energy with less pollution. Centre for Ecology and Hydrology (CEH).

Tang, Q., Oki, T., Kanae, S., Hu, H., 2008. Hydrological cycles change in the Yellow River basin during the last half of the twentieth century. J. Climate, 21: 1790–1806.

Thaler, S., Zessner, M., De Lis, F.B., Kreuzinger, N., Fehringer, R., 2012. Considerations on methodological challenges for water footprint calculations. Water Sci. Technol., 65: 1258–1264.

Vanham, D., Bidoglio, G., 2014. The water footprint of agricultural products in European river basins. Environ. Res. Lett., 9: 064007.

Vitousek, P.M., Aber, J.D., Howarth, R.W., Likens, G.E., Matson, P.A., Schindler, D.W., Schlesinger, W.H., Tilman, D., 1997. Human alteration of the global nitrogen cycle: Sources and consequences. Ecol. Appl., 7: 737–750.

Vitousek, P.M., Naylor, R., Crews, T., David, M.B., Drinkwater, L.E., Holland, E., Johnes, P.J., Katzenberger, J., Martinelli, L.A., Matson, P.A., Nziguheba, G., Ojima, D., Palm, C.A., Robertson, G.P., Sanchez, P.A., Townsend, A.R., Zhang, F.S., 2009. Nutrient imbalances in agricultural development. Science, 324: 1519–1520.

Wang, Z., Huang, K., Yang, S., Yu, Y., 2013. An input-output approach to evaluate the water footprint and virtual water trade of Beijing, China. J. Clean. Prod., 42: 172–179.

West, P.C., Gerber, J.S., Engstrom, P.M., Mueller, N.D., Brauman, K.A., Carlson, K.M., Cassidy, E.S., Johnston, M., MacDonald, G.K., Ray, D.K., Siebert, S., 2014. Leverage points for improving global food security and the environment. Science, 345: 325–328.

Williams, J.R., 1995. The EPIC model, in: Singh, V.P. (Ed.), Computer Models of Watershed hydrology. Water Resources Publications, Highlands Ranch, Colo, pp. 909–1000.

Williams, J.R., Jones, C.A., Dyke, P.T., 1984. A modeling approach to determining the relationship between erosion and soil productivity. T. ASAE, 27: 129–144.

Wu, B., Zeng, W., Chen, H., Zhao, Y., 2016. Grey water footprint combined with ecological network analysis for assessing regional water quality metabolism. J. Clean. Prod., 112: 3138–3151.

Xu, Y., Huang, K., Yu, Y., Wang, X., 2015. Changes in water footprint of crop production in Beijing from 1978 to 2012: a logarithmic mean Divisia index decomposition analysis. J. Clean. Prod., 87: 180–187.

Yoo, S.H., Choi, J.Y., Lee, S.H., Kim, T., 2014. Estimating water footprint of paddy rice in Korea. Paddy Water Environ., 12: 43–54.

Zeng, Z., Liu, J., Savenije, H.H.G., 2013. A simple approach to assess water scarcity integrating water quantity and quality. Ecol. Indic., 34: 441–449.

Zhang, G., Mathews, R.E., Frapporti, G., Mekonnen, M.M., 2014. Water footprint assessment for the Hertfordshire and north London area. Report RESE000335, Environment Agency, London, UK.

Zhi, Y., Yang, Z., Yin, X., Hamilton, P.B., Zhang, L., 2015. Using gray water footprint to verify economic sectors' consumption of assimilative capacity in a river basin: model and a case study in the Haihe River Basin, China. J. Clean. Prod., 92: 267–273.

Zhuo, L., Mekonnen, M.M., Hoekstra, A.Y., Wada, Y., 2016. Inter- and intra-annual variation of water footprint of crops and blue water scarcity in the Yellow River basin (1961-2009). Adv. Water Resour., 87: 29–41.

Chapter 5

Achieving high crop yields with low nitrogen losses in global agricultural input intensification

Based on

Achieving high crop yields with low nitrogen losses in global agricultural input intensification (submitted to Science Advances)

Authors

Wenfeng Liu[a], Hong Yang[a,b], Christian Folberth[c], Christoph Müller[d], Karim C. Abbaspour[a], Rainer Schulin[e]

[a]*Eawag, Swiss Federal Institute of Aquatic Science and Technology, Ueberlandstrasse 133, CH-8600 Duebendorf, Switzerland*

[b]*Department of Environmental Sciences, University of Basel, Petersplatz 1, CH-4003 Basel, Switzerland*

[c]*Ecosystem Services and Management Program, International Institute for Applied Systems Analysis (IIASA), Schlossplatz 1, A-2361 Laxenburg, Austria*

[d]*Potsdam Institute for Climate Impact Research, 14473 Potsdam, Germany*

[e]*ETH Zürich, Institute of Terrestrial Ecosystems, Universitätstr. 16, CH-8092 Zürich, Switzerland*

Abstract

Increasing demand for food is driving the worldwide trend of agricultural intensification using increasing fertilizer and irrigation inputs. However, there is no comprehensive knowledge about the interrelations between potential yield gains and environmental trade-offs that would enable the identification of global priority regions for further input-driven intensification. Here we explore ways of enhancing global crop yields, while avoiding significant nitrogen losses into the environment by employing a range of nitrogen and irrigation management scenarios in a global crop model. The simulated responses of yields and nitrogen losses to increased nitrogen inputs and irrigation show high spatial variations due to differences in current global agricultural inputs and agro-climatic conditions. Yields and nitrogen losses are negatively responded to nitrogen input additions. We find that avoiding further intensification in regions where ≥75% of the climatic yield potential is already achieved is key to maintaining good nitrogen use efficiencies. Depending on the intensification level, the relative increase in nitrogen losses can thus be reduced by 3–193%, while compromises in yield increase range only between 1 and 23%. This study highlights the importance of considering yield and environmental trade-offs in agricultural input intensification.

Keywords

Agricultural input intensification; Yield achievements; Nitrogen losses; Trade-offs

5.1 Introduction

With a continuously growing global population, shifts to more animal-based diets (Bodirsky et al., 2015), and possibly increasing competition in agricultural land use between food and biofuel crops (Lotze-Campen et al., 2014), modern agriculture is facing a trilemma, i.e. meeting the increasing food demand, minimizing the need for additional inputs, and limiting negative environmental impacts (Godfray et al., 2010). To feed an expected additional two billion people by 2050, global food production needs to be doubled (Tilman et al., 2011). A major challenge faced by scientists, farmers, and policy makers is to find ways to achieve this goal while keeping the environmental costs at a tolerable level (Foley et al., 2005; Godfray and Garnett, 2014; Lu et al., 2015; Sayer and Cassman, 2013).

There are in principle two different strategies to increasing agricultural food production: expansion of croplands and intensification (Matson et al., 1997). For the first option, however, suitable land resources are very limited and their conversion to cropland is increasingly constrained by other land-use purposes. In many places, croplands are actually shrinking due to encroachment by urban development (Deng et al., 2011; Lambin and Meyfroidt, 2011). The option of cropland expansion is only feasible in underdeveloped areas and often at high environmental costs such as greenhouse gas emissions and biodiversity loss from forest clearing (Foley et al., 2011). For the majority of countries and regions, intensification of crop production on existing croplands is the only way to meet the increasing demand of recent decades.

Since the Green Revolution in the 1960s, crop yields have been continuously increased, in particular through the breeding of more productive crop varieties (Bodirsky and Muller, 2014) and the intensification of land management with increasing fertilizer inputs and irrigation (Tilman et al., 2001). However, input intensification has also put substantial pressure on environmental systems. The relative increases in yield were far below that in agricultural inputs in many places (Sutton et al., 2013). The mismatch between inputs and outputs not only decreased resource use efficiency (Conant et al., 2013; Lassaletta et al., 2014; Zhang et al., 2015), but also generated serious environmental problems (Clark and Tilman, 2008; Liu et al., 2010; Liu et al., 2017; Liu et al., 2013; Schlesinger, 2009; Steffen et al., 2015). In particular, increasing inputs of mineral nitrogen (N) fertilizers have led to high N losses to the environment, causing severe eutrophication and drinking water quality problems. Hence, there is an ever more pressing need to develop pathways towards input intensification without further compromising environmental health and quality (Garnett et al., 2013; Godfray and Garnett, 2014; Pretty, 2008; Tilman et al., 2011).

Given that the yields of major crops have recently stopped increasing or even decreased in many regions of the world with high inputs (Iizumi et al., 2014; Ray et al., 2013; Ray et al., 2012; Wei et al., 2015), it seems that the benefits of additional inputs, including fertilizers and irrigation, have been exhausted in these regions, suggesting that not all regions are suitable for further input intensification. However, the scope for improved efficiency varies among different cropping systems (Carberry et al., 2013). Therefore, it is essential to identify regions where high yield returns can be obtained at low environmental costs and to explore how input intensification can be achieved in these regions most efficiently. Mauser et al. (2015) found that global food demand can be satisfied by crop production on the existing croplands, without further land clearing, and concluded that agricultural intensification is key to increasing global food production. Other studies arrived at similar conclusions (Brauman et al., 2013; Chen et al., 2014; Chen et al., 2011; Johnston et al., 2011; Mueller et al., 2014). However, previous studies have been limited in various aspects, including: a) small spatial scale, e.g. studying only a few fields in one region (Chen et al., 2014; Chen et al., 2011); b) focusing on one type of input only, either N (Chen et al., 2014) or irrigation (Brauman et al., 2013); c) no explicit consideration of environmental impacts (Johnston et al., 2011; Mauser et al., 2015); and d) ignoring interactions between agricultural inputs and environmental responses (Mueller et al., 2014).

Here we comprehensively address the agricultural trilemma by using the global agronomic model PEPIC (Liu et al., 2016b), Python-based Environmental Policy Integrated Climate (EPIC), to explore the benefits of further global agricultural input intensification in terms of increased crop yields (Y) and comparing them to expected associated N losses into the environment (N_l). We used food production units (FPU) as a spatial unit. The FPU consists of river basins and economic regions as introduced by Cai and Rosegrant (2002) and modified by Kummu et al. (2010). Focusing on N inputs (N_{in}) and irrigation water (I_w), we considered five input intensification scenarios—N25, N25+I10, N50, N50+I30, and Max—with a Baseline scenario of no additional intensification. N25 and N25+I10 represent low-level increases of N inputs only or of N and irrigation inputs in combination, while N50 and N50+I30 represent high-level increases of these inputs, respectively. In the Max scenario, N_{in} and irrigation were applied automatically by the PEPIC model without limitation. Three major cereal crops (maize, rice, and wheat) were included in the analysis. As well as looking into the increase in yield (ΔY) of the target crops and associated N losses (ΔN_l), and additional inputs requirements (ΔN_{in} and ΔI_w) between the intensification and the Baseline scenarios, we explored the relationships between ΔY and ΔN_l in response to increased N inputs (ΔN_{in}). We also assessed the incremental N use efficiency $\Delta Y/\Delta N_{in}$ and incremental environmental costs of N_l per unit of additional N_{in}, i.e. $\Delta N_l/\Delta N_{in}$.

5.2 Methods

5.2.1 Simulation model and input data

The PEPIC model (Liu et al., 2016b) was used to simulate crop growth at a daily time step and the associated nutrient dynamics on a global scale at a spatial resolution of 30 arc minutes (about 50 km at the equator). PEPIC has been used for investigating global crop–water relations of maize (Liu et al., 2016b) and assessing global N_l from the three major crops (Liu et al., 2016a). In addition, it also performed quite well in comparison to 13 other global crop models in the Agricultural Model Intercomparison and Improvement Project (AgMIP) (Müller et al., 2017; Porwollik et al., 2016). Inputs for PEPIC include longitude, latitude, elevation, slope, soil properties (e.g. layer depth, pH, bulk density, organic carbon content), climate data (precipitation, temperature, solar radiation, relative humidity, wind speed), and crop management information. As for management data, planting date, harvesting date, fertilizer, and irrigation are required. Planting and harvesting dates were obtained from the Center for Sustainability and the Global Environment (SAGE) (Sacks et al., 2010). Crop-specific fertilizer and manure application data (including N and phosphorus) were downloaded from EarthStat (http://www.earthstat.org/), which were based on Mueller et al. (2012) and West et al. (2014). Information on other input data is provided in Liu et al. (2016a; 2016b).

5.2.2 Management practices and intensification scenarios

In this study, we considered five intensification scenarios, i.e. N25, N25+I10, N50, N50+I30, and Max, in addition to the Baseline scenario (Table 5-1). A sufficient amount of phosphorus (P) was applied automatically in each scenario to eliminate the effects of P deficit on plant growth following Folberth et al. (2014). The N_{in} in the Baseline ($N_{in\text{-}base}$) were determined by the minimum value of actual N inputs ($N_{in\text{-}a}$) and automatic N inputs ($N_{in\text{-}auto}$). Here, $N_{in\text{-}base}$ was based on the EarthStat dataset and $N_{in\text{-}auto}$ was estimated by PEPIC with an automatic N fertilization without N limitation at a trigger value of 10% N stress (Balkovič et al., 2014) with the current irrigation land condition. This setting excluded the impacts of over N application on N_l in some regions (Liu et al., 2016a), since this study focused on the effects of input additions. Irrigation was applied automatically without water limitation at a trigger value of 10% water stress (Rosenzweig et al., 2014). Increased N_{in} and conversion of rainfed to irrigated cropland relative to the Baseline were considered as intensification scenarios in this study. For N_{in}, we first used PEPIC to determine the maximum N_{in} ($N_{in\text{-}max}$) by using the automatic fertilization schedule without limitation under the fully irrigated condition. This combination of fertilizer and irrigation was applied in the Max scenario. Then, the difference between $N_{in\text{-}max}$ and $N_{in\text{-}base}$, i.e. $\Delta N_{in\text{-}max}$, was calculated for each grid cell. Scenarios N25 and N25+I10 represented the lowest levels of

intensification. In N25, N inputs were increased by 25% of $\Delta N_{in\text{-}max}$ relative to the Baseline, while in N25+I10 10% of the rainfed cropland was converted to irrigated land in addition to a 25% of $\Delta N_{in\text{-}max}$ increase in N_{in}. Scenarios N50 and N50+I30 represent corresponding high-level intensification scenarios. In N50, N inputs were increased by 50% of $\Delta N_{in\text{-}max}$ relative to the Baseline, while in N50+I30 30% of the rainfed land was converted to irrigated land in addition to a 50% of $\Delta N_{in\text{-}max}$ increase in N_{in}. These levels of intensification were based on Mueller et al. (2012), who found that jointly increasing N_{in} by 30% and irrigated lands by 25% would reach productivity levels that represent 75% of the attainable yields of the year 2000. Although global constant percentage values of $\Delta N_{in\text{-}max}$ and rainfed land were used here to increase N_{in} and I_w, the actual increases in N_{in} and I_w were quite different due to the large differences in N_{in} and rainfed land area under the Baseline condition (Figures S5-1 and S5-2) and the input requirements under the Max scenario.

Table 5-1. Description of intensification scenarios in terms of increasing nitrogen (N) inputs and irrigation (I) areas.

Scenario	N inputs	Irrigation areas
Baseline	$N_{in\text{-}base}$	A_{ir}
N25	$N_{in\text{-}base} + 0.25\times\Delta N_{in\text{-}max}$	A_{ir}
N25+I10	$N_{in\text{-}base} + 0.25\times\Delta N_{in\text{-}max}$	$A_{ir} + 0.10\times A_{rf}$
N50	$N_{in\text{-}base} + 0.50\times\Delta N_{in\text{-}max}$	A_{ir}
N50+I30	$N_{in\text{-}base} + 0.50\times\Delta N_{in\text{-}max}$	$A_{ir} + 0.30\times A_{rf}$
Max	$N_{in\text{-}max}$	Full irrigation

$N_{in\text{-}base}$: $\min(N_{in\text{-}a}, N_{in\text{-}auto})$; $N_{in\text{-}a}$: actual N inputs based on EarthStat dataset; $N_{in\text{-}auto}$: optimal N inputs based on PEPIC simulation with current irrigation land condition; $N_{in\text{-}max}$: optimal N inputs based on PEPIC simulation considering current croplands with full irrigation; $\Delta N_{in\text{-}max}$: $N_{in\text{-}max} - N_{in\text{-}base}$; A_{ir} and A_{rf}: current areas for irrigation and rainfed cultivation based on MIRCA2000 dataset.

5.2.3 Definition of target variables and data analysis

Four model outputs were considered in the analysis, i.e. I_w [mm], N_{in} [kg N per ha], Y [t per ha], and N_l [kg N per ha]. N_l includes N losses into the aquatic and atmospheric environments, more information on the calculation of N_l can be found in Liu et al. (2016a). In this study, crop growth was simulated separately under rainfed and irrigated conditions. The combined outputs of each variable were calculated using the area-weighted average of irrigated and rainfed outputs (Liu et al., 2007) based on the MIRCA2000 dataset of crop-specific fractions of irrigated and rainfed land for each crop in each grid cell (Portmann et al., 2010). The combined results were aggregated to FPU (Cai and Rosegrant, 2002; Kummu et al., 2010), continental, and global levels. Subsequently, the differences of each variable between the intensification scenarios and the Baseline were calculated, i.e. differences of I_w (ΔI_w), differences of N_{in} (ΔN_{in}), differences of Y (ΔY), and differences of N_l (ΔN_l). For FPUs with $\Delta Y < 1\%$ of Baseline Y, outputs under the intensification scenarios were treated as the same values of the Baseline to exclude possible errors due to minor responses. After this treatment, ΔI_w, ΔN_{in}, ΔY, and ΔN_l were re-evaluated. The ratios

of ΔY to ΔN_{in} ($\Delta Y/\Delta N_{in}$) and ΔN_l to ΔN_{in} ($\Delta N_l/\Delta N_{in}$) were calculated to explore the responses of Y and N_l to N_{in} additions under different intensification scenarios.

The FPUs with different degrees of yield gap closure, i.e. 70%, 75%, 80%, 85%, 90%, and 95% of Y_{max} achieved with each management scenario were also identified. To reveal the importance of regions with high $\Delta Y/\Delta N_{in}$ and low $\Delta N_l/\Delta N_{in}$, the responses of ΔY to ΔN_l were investigated by intensifying the FPUs with an order of ascending $\Delta N_l/\Delta N_{in}$ and descending $\Delta Y/\Delta N_{in}$.

5.3 Results

5.3.1 Yield benefits

The simulated responses of crop yields Y to increased N_{in} and I_w showed high spatial variations, with very large effects in some regions, but only minor ones in other areas (Figure 5-1 and S5-3). These benefits also showed different spatial patterns among the three crops, but were rather similar among the different scenarios for each crop. Areas with high ΔY for maize and rice were found to be concentrated mainly in the southern parts of Africa and South America, where the Baseline Y was quite low and differences in N_{in} between the Max and Baseline scenarios were very high. In addition to these regions, parts of eastern Europe and the Middle East also showed large ΔY for wheat. For other regions, particularly China and India, only small ΔY were predicted for the three crops. Globally, the average ΔY in the five scenarios ranged between 20 and 53% for maize, 10 and 20% for rice, and 27 and 72% for wheat (Tables 5-2 and S5-1). Yields responded mainly to increased N inputs and less to intensified irrigation. Increased N inputs were found to substantially increase irrigation water use efficiency (defined as yield per unit of applied I_w), while the effects of I_w additions on N use efficiency (defined as yield per unit of applied N_{in}) were quite small (Tables S5-2 and S5-3). Meanwhile, to achieve high Y benefits, significant increases in the input of these resources were required (Tables S5-4 and S5-5).

5.3.2 Nitrogen losses into the environment

The simulations predicted that Y benefits from N_{in} and I_w intensification would result in substantial ΔN_l around the world, with increases varying between 20 and 236% for maize, 14 and 96% for rice, and from 28 to 278% for wheat among the five scenarios (Table 5-2). ΔN_l was particularly high in Africa, Oceania, and South America for maize and rice, and in Africa, Europe, Oceania, and South America for wheat (Table S5-6). The overall geographical distribution patterns were very similar to those for the respective ΔY (Figures 5-2 and S5-4), but there were also major differences. Large ΔN_l were predicted in Southeast Asia for all three crops and in the

eastern parts of the USA for wheat, while Y are not expected to increase significantly in these regions. While increasing N inputs always increased N losses, increased irrigation reduced N losses in some regions relative to the Baseline scenario, because the plants that grow better under irrigation took up more N.

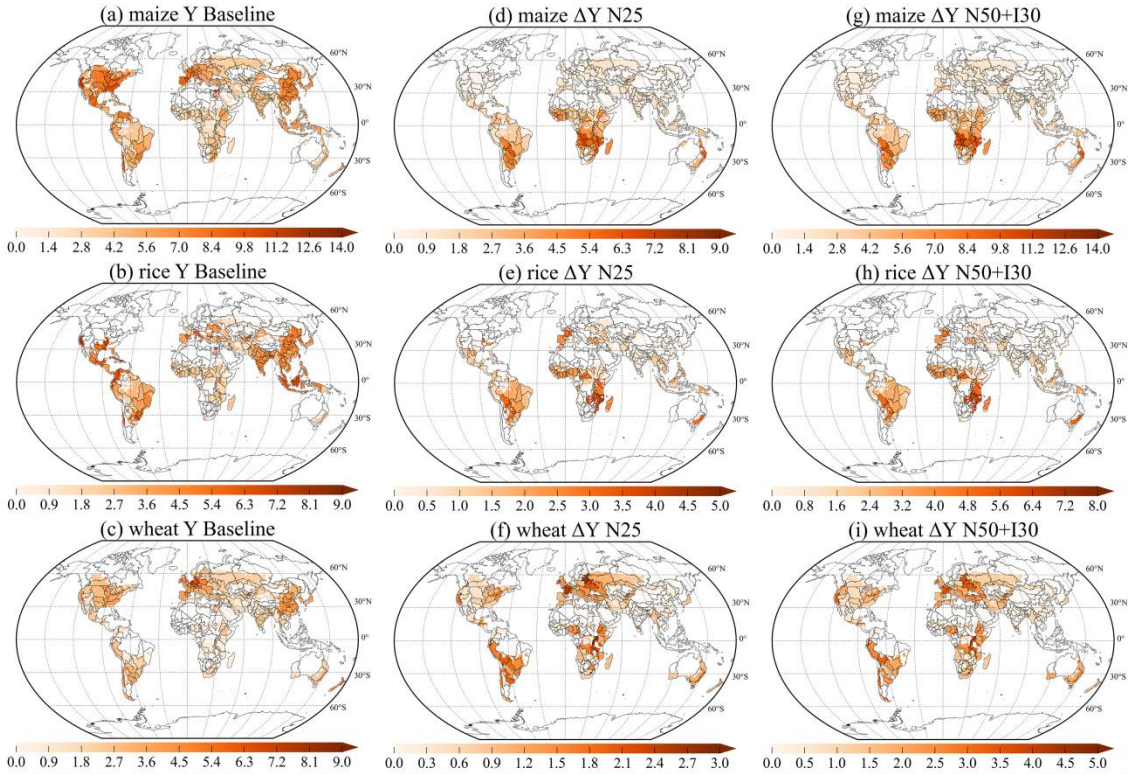

Figure 5-1. Yield (Y) in Baseline (a, b, c) and changes in Y (ΔY) [t per ha] between N25 (d, e, f) and Baseline, as well as between N50+I30 (g, h, i) and Baseline. Information for scenarios N25+I10, N50, and Max are presented in Figure S5-3.

5.3.3 Relationship between yield increases and nitrogen losses

The incremental N use efficiency, expressed in terms of the ratio $\Delta Y/\Delta N_{in}$, and the incremental environmental costs of increased N_l, expressed as the ratio $\Delta N_l/\Delta N_{in}$, demonstrated opposite spatial distribution patterns at the FPU level (Figures S5-5 and S5-6). China and India showed quite high incremental N loss-to-input ratios. For maize cultivation, the eastern parts of the USA also had a high $\Delta N_l/\Delta N_{in}$ ratio. The $\Delta Y/\Delta N_{in}$ ratio showed clear negative linear relationships to the $\Delta N_l/\Delta N_{in}$ ratio for all three crops in all five intensification scenarios (Figure 5-3). The positions of individual FPU along the relationships between incremental Y and N loss was closely related to the magnitude of additional N input. In contrast, the intensification of irrigation had little effect, as these relationships showed little difference between the scenarios without and with irrigation, i.e. between N25 and N25+I10 and between N50 and N50+I30, respectively. The negative slopes of these relationships indicate that there is a win–win situation if further input

intensification concentrates on regions where additional inputs have the highest incremental N use efficiency, as these are also the regions with the smallest additional N losses.

Table 5-2. Global average irrigation water (I_w) [mm], nitrogen inputs (N_{in}) [kg N per ha], yields (Y) [t per ha], and total nitrogen losses (N_l) [kg N per ha] under Baseline and different intensification scenarios. All croplands are intensified.

	maize				rice				wheat			
	I_w	N_{in}	Y	N_l	I_w	N_{in}	Y	N_l	I_w	N_{in}	Y	N_l
Baseline	50.2	110.4	6.3	75.3	41.3	115.0	4.5	102.0	44.7	79.0	2.7	51.5
N25	50.2	148.3	7.6	90.1	41.3	138.2	5.0	116.4	44.8	123.1	3.4	66.5
N25+I10	62.0	156.6	7.7	95.6	42.2	138.2	5.0	115.7	55.6	123.6	3.5	66.1
N50	50.2	183.9	8.1	110.8	41.3	163.1	5.2	135.5	44.8	162.5	3.6	90.8
N50+I30	87.0	202.0	8.5	121.8	44.0	163.2	5.2	134.9	78.4	166.5	3.9	89.4
Max	173.0	356.3	9.7	253.3	50.1	235.1	5.4	199.6	156.9	296.0	4.6	194.6

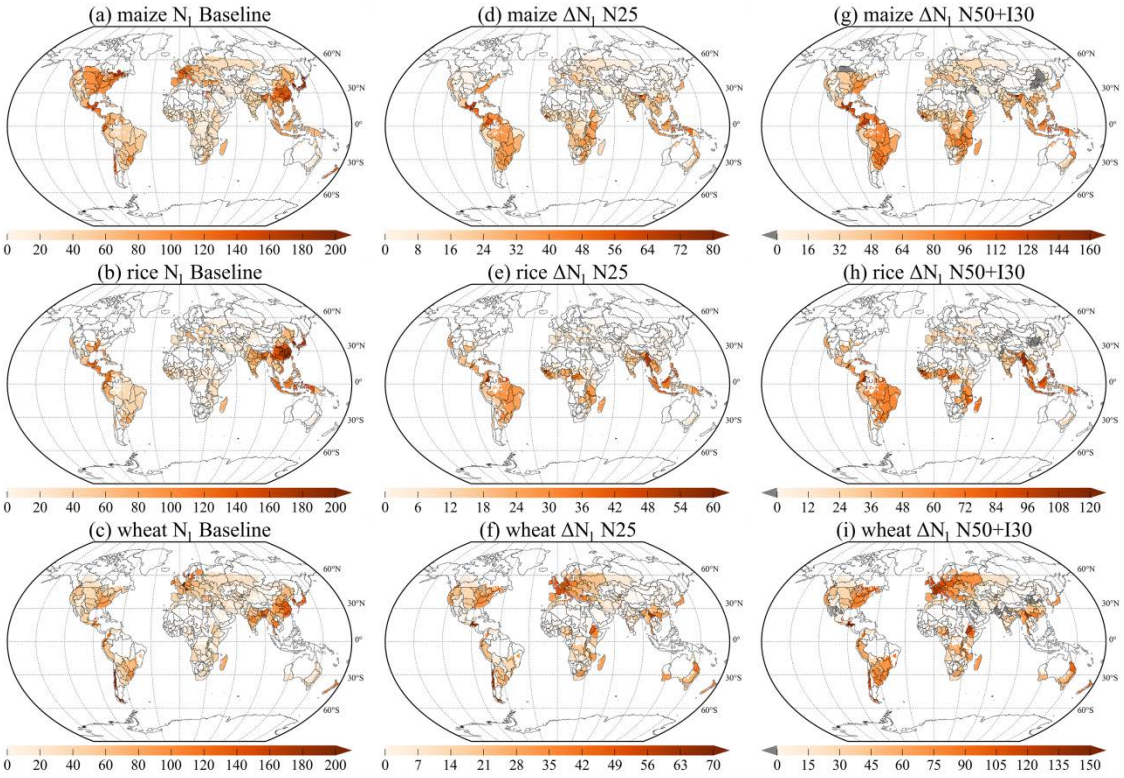

Figure 5-2. Nitrogen losses (N_l) in Baseline (a, b, c) and changes in Nl (ΔN_l) [kg N per ha] between N25 (d, e, f) and Baseline, as well as between N50+I30 (g, h, i) and Baseline. Information for scenarios N25+I10, N50, and Max are presented in Figure S5-4.

In most FPUs with a high $\Delta N_l/\Delta N_{in}$ ratio (> 0.7) and a low $\Delta Y/\Delta N_{in}$ ratio, mainly in China, India, western Europe, and eastern USA (Figures S5-3 and S5-4), Y has already obtained a high level (e.g. 75%) of what could be achieved in the Max scenario, Y_{max}, before intensification under each scenario (Figure 5-3). This means that significant N_l can be avoided by stopping further increases of N_{in} and I_w applications in such FPUs. This condition was found to be especially

common in rice cultivation, where about 84% of the cropland presently under rice cultivation produced 75% of Y_{max} in the Baseline scenario (Table S5-7). For wheat and maize, the respective percentages were 43% and 36%. The regions showing low yield gap were mainly located in east Asia, central Europe and the eastern USA for maize, eastern and southeastern Asia for rice, and China and India for wheat (Figure 5-4). In the N50+I30 scenario, only small fraction of croplands did not achieve 75% of the Y_{max}.

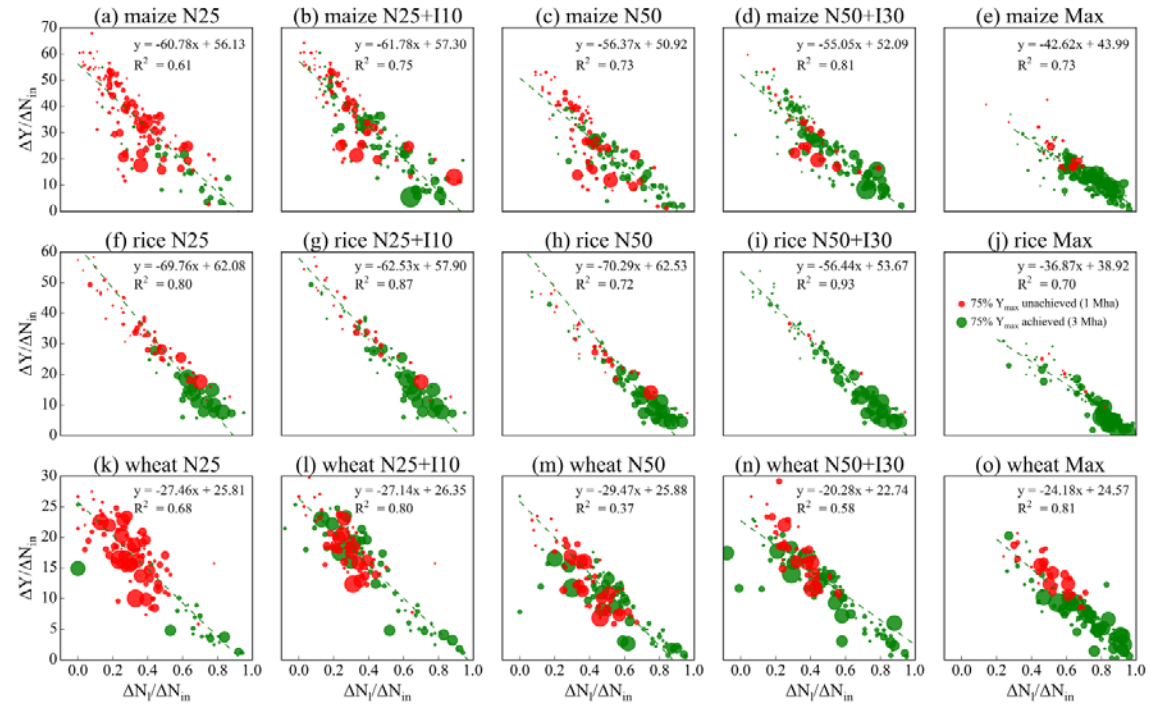

Figure 5-3. Relationships between $\Delta Y/\Delta N_{in}$ [kg grain per kg N] and $\Delta N_l/\Delta N_{in}$ [-] under different intensification scenarios at the food production unit (FPU) level. ΔY: differences in yields (Y) between intensification scenarios and Baseline; ΔN_{in}: differences in nitrogen inputs (N_{in}) between intensification scenarios and Baseline; ΔN_l: differences in total nitrogen losses (N_l) between intensification scenarios and Baseline. The FPUs with the smallest areas (for a total of 1% of global total cropland areas of each crop) are not shown. Sizes represent cropland areas for each FPU. Green circles represent the FPUs with 75% of maximum Y (Y_{max}) achieved before the corresponding scenario with an intensification order of Baseline, N25, N25+I10, N50, N50+I30, and Max; red circles represent the FPUs without 75% of Y_{max} achieved. Equations represent the linear relationship between $\Delta Y/\Delta N_{in}$ and $\Delta N_l/\Delta N_{in}$ (points with negative $\Delta N_l/\Delta N_{in}$ are not included for regression analysis); the R^2 is the coefficient of determination of equation.

5.3.4 Frontier lines for intensifying croplands on a global scale

Based on the negative relationship between $\Delta Y/\Delta N_{in}$ and $\Delta N_l/\Delta N_{in}$, we constructed frontier lines of cumulative ΔY against cumulative ΔN_l, ordering the FPU by ascending $\Delta N_l/\Delta N_{in}$ and descending $\Delta Y/\Delta N_{in}$ (Figure 5-5). Starting with FPU high in ΔY and low in ΔN_l, these lines decrease in slope as ΔY decreases, while ΔN_l increases. This is particularly notable for scenarios N50, N50+I30, and Max. Furthermore, the frontier lines show a large difference between the Max

and the other scenarios, indicating the high environmental costs versus small benefits of further intensifying crop production when the level of intensification is already high. Avoiding intensification in the FPUs with $\Delta N_l/\Delta N_{in} > 0.7$ can significantly reduce the ΔN_l, especially for the Max scenario (Figure 5-5a, c, e).

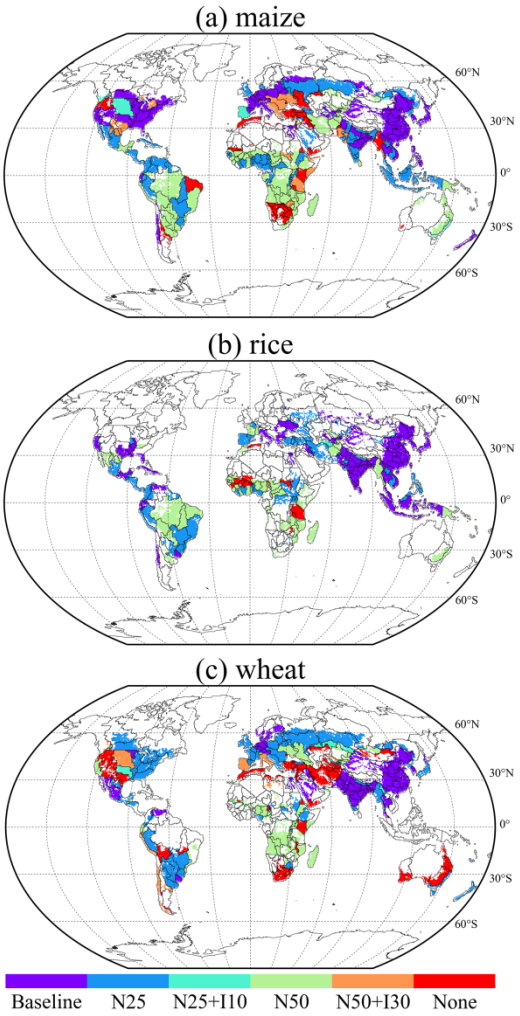

Figure 5-4. Distribution of the scenario with 75% of maximum yields (Y_{max}) achieved. Scenario definition refers to Table 5-1; Y_{max} is estimated by the PEPIC model under the Max scenario; None means FPU cannot achieve 75% of Y_{max} under the scenarios of Baseline, N25, N25+I10, N50, and N50+I30.

An important strategy for limiting the increase in N_l with little compromise on Y increase is to avoid further intensification in FPUs, where high levels of Y_{max} have been achieved, which we here define as a threshold of 75% (Figure 5-5b, d, f). With this restriction, simulated incremental N losses were reduced from 15–178 [kg N per ha] to 13–33 [kg N per ha] (this reduction representing 3–193% of the Baseline N_l) for maize; from 14–98 [kg N per ha] to 5–10 [kg N per ha] (the reduction representing 9–86% of the Baseline N_l) for rice; and from 15–143 [kg N per ha] to 13–44 [kg N per ha] (the reduction representing 4–192% of the Baseline N_l) for wheat, depending on the scenario. Expected ΔY were reduced by only 0.0–1.5 [t per ha] (corresponding

to 1–23% of the Baseline Y) for maize; 0.2–0.5 [t per ha] (corresponding to 4–12% of the Baseline Y) for rice; and 0.0–0.5 [t per ha] (corresponding to 1–19% of the Baseline Y) for wheat (Table 5-3), and the frontier lines lay very close together for the different scenarios. Furthermore, the results also show that much less N and water resources are required to achieve the same increase in yield with a strategy in which further intensification is limited to cropland where the yield gap is still comparatively large than with indiscriminate further intensification. In addition to restricting intensification to FPU with yield levels of <75% Y_{max}, we performed the analogous analysis setting the restriction level at 70%, 80%, 85%, 90%, and 95% of Y_{max} (Figure S5-7). Similar trends for ΔY and ΔN_l were found for these levels as with the level of 75% Y_{max}. However, the trade-offs between Y achievements and N_l increases were different using the different target levels.

5.4 Discussion

The high spatial variations of the responses of Y and N_l to increased N_{in} and I_w inputs of the three crops were mainly due to differences in these inputs in the Baseline scenario chosen to represent the current situation of N fertilization and irrigation intensity, and thus to differences in what the scenarios actually are. Regions with a high level of N inputs generally respond with low incremental N use efficiency $\Delta Y/\Delta N_{in}$ but high incremental N loss costs $\Delta N_l/\Delta N_{in}$ to further intensification (Figure S5-8). This is in agreement with previous studies. When N_{in} is already high, the yield benefits of additional N_{in} are quite low (Lassaletta et al., 2014), while the potential of N losses tends to be high (Bodirsky and Muller, 2014). Compared to N inputs, most regions showed low ΔY in response to more irrigation in all three crops maybe due to the low-level increases in irrigated croplands (Figure S5-9). The different responses of Y to I_w are mainly due to different fractions of irrigated lands to total cultivated lands and the differences in irrigation requirements under Baseline management by considering all croplands as irrigated cultivation (Figure S5-10). A low irrigation requirement indicates that rainfall is generally sufficient for crop growth, and so there are low benefits from increased irrigation. This explanation generally holds for maize cultivation in south-eastern China and central Africa, for rice cultivation in south-eastern China and central parts of South America, and for wheat cultivation in southern India and central Africa. On the other hand, there is only limited opportunity to further increasing Y by taking additional land under irrigation where a large fraction of the cropland is already under irrigation. This condition especially holds for rice cultivation (Figure S5-10d). On land where yields are already close to what can be achieved for the maximum N and irrigation water inputs, further increasing their intensity can produce only minor benefits, while the environmental costs and the

consumption of resources become ever more significant. Such regions need to be identified and excluded from further intensification and sufficient data should be provided to take this action.

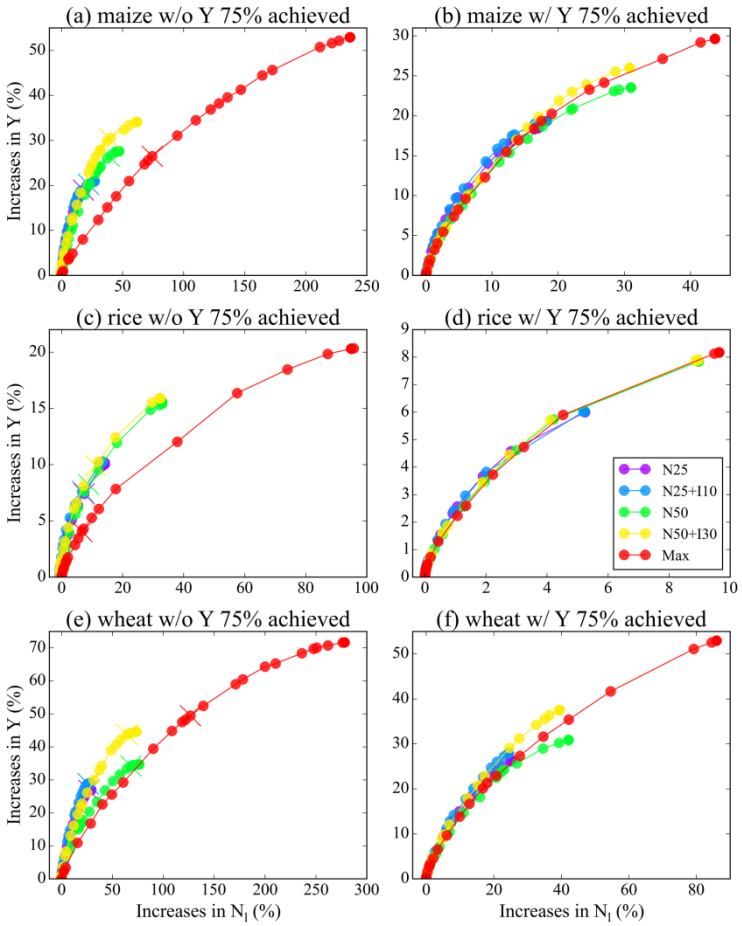

Figure 5-5. Percentage increases in global average yields (Y) and nitrogen losses (N_l) in different intensification scenarios without (w/o) considering 75% of maximum Y (Y_{max}) achieved (left panel) and with (w/) considering 75% of Y_{max} achieved (right panel). Considering 75% of Y_{max} achieved means the intensification scenario for the food production unit (FPU) with 75% of Y_{max} achieved uses the first scenario among Baseline, N25, N25+I10, N50, and N50+I30, which achieved 75% of Y_{max}. Points in each curve are derived by intensifying FPUs with an ascending order of $\Delta N_l/\Delta N_{in}$ and a descending order of $\Delta Y/\Delta N_{in}$ on the basis of Figure 5-3. Crosses in subplots a, c, and e present the maximum increases of Y and N_l by stopping intensifying the FPUs with $\Delta N_l/\Delta N_{in} > 0.7$. For better visualization, every 10 points between the first and last points are plotted for each curve.

Based on our simulations, it was not possible to double the production of the three crops on the current cropland area even if there was no limit on N fertilizer application and irrigation, especially in rice production (Table 5-2). Similar findings were reported by Mueller et al. (2014), who estimated production potentials close to 100% of maximum attainable Y through nutrients and irrigation management. Therefore, other measures should be considered to further increase yields, such as breeding more productive varieties (Khush, 2001), change of cropping intensities (Challinor et al., 2015), and better allocation on a global scale of crops to cultivated land (Mauser

et al., 2015) among others. Combining these measures with better N and irrigation management can be expected to further increase Y_{max} and strengthen the responses of Y to N_{in} and I_w in currently high Y regions. Hence, a comprehensive assessment including these options should be the focus of further research.

Table 5-3. Global average irrigation water (I_w) [mm], nitrogen inputs (N_{in}) [kg N per ha], yields (Y) [t per ha], and total nitrogen losses (N_l) [kg N per ha] under different intensification scenarios. Only croplands without achieving 75% of maximum Y are intensified.

	maize				rice				wheat			
	I_w	N_{in}	Y	N_l	I_w	N_{in}	Y	N_l	I_w	N_{in}	Y	N_l
N25	50.2	145.2	7.5	88.1	41.3	125.2	4.8	107.3	44.8	120.2	3.4	64.5
N25+I10	57.1	146.7	7.6	89.1	41.7	125.2	4.8	107.3	52.8	120.3	3.4	64.1
N50	51.5	164.2	7.8	98.6	41.3	130.8	4.9	111.1	45.8	136.3	3.5	73.2
N50+I30	64.6	165.8	8.0	98.5	41.6	130.8	4.9	111.1	63.4	138.6	3.7	71.8
Max	80.9	179.9	8.2	108.2	42.3	131.8	4.9	111.8	97.0	175.5	4.1	95.7

Intensifying all croplands to a high level would require a considerable increase in N_{in} and I_w inputs (Figures S5-1 and S5-2 and Tables S5-4 and S5-5). However, inputs cannot be increased without limit and they are associated with significant environmental impacts. While there is sufficient N in the atmosphere for practically unlimited industrial production of mineral N fertilizer, the energy required for it is likely to set an upper limit. Already about 2% of the world's energy use is used for the production of reactive N (Sutton et al., 2013). Moreover, there is still a long way to go for many developing countries, mainly in Africa and South America, to afford enough nutrients for their croplands. In comparison to N, freshwater is a much more limited resource and its spatiotemporal distribution is already very uneven for natural reasons (Oki and Kanae, 2006). That is why we set lower levels of irrigated land expansion. While we found that by expanding the irrigated areas maize and wheat yields could be increased substantially in the western USA and western and central Asia (Figure S5-9), the available water resources set a rather low upper limit to this option (Elliott et al., 2014). An estimated four billion people suffer from severe water scarcity for at least one month per year (Mekonnen and Hoekstra, 2016). Further expansion of irrigation agriculture hence bears the risk of worsening this problem. Therefore, it will be vital to increase the efficiency of irrigation (Jagermeyr et al., 2015; Jagermeyr et al., 2016) and fertilizer (Zhang et al., 2015) applications. As shown here, one strategy to achieve this is to avoid further intensification in regions where yields are already very high and to concentrate intensification efforts instead on regions with currently low yields and inefficient use of these resources.

Mueller et al. (2012) have already explored trade-offs between excess N (differences between N inputs and crop taking up N) and crop production using frontier lines. The difference between the study here and their study is that we also used frontier lines to explore the benefits of

avoiding further intensification in regions where yields are already close to their potential maximum levels, i.e. 70–95% of Y_{max} (Figures 5-5 and S5-7). The frontier lines reveal consistent trends, but differences also exist. In particular, the separation of frontier lines for the six scenarios was more pronounced when targeting for a high yield level than for a low yield level, highlighting the environmental costs of achieving a high level of Y by input intensification. On the other hand, the ΔN_l may be reduced if setting a low target level. But then the increases in Y will also be less. Thus, it is important to find a level at which these effects are in a desirable balance. In the end, setting such a target level is a political decision.

We also recognize some limitations of the approach taken. Firstly, the results were based on simulations with just one crop model. Thus, model-related uncertainties cannot be considered. Such uncertainties could be high in the simulation of crop growth and associated nutrient dynamics (Bassu et al., 2014; Li et al., 2015). Performing the same analysis with different models would give explicit information on the potential influence of modelling uncertainties on the results (Martre et al., 2015). Secondly, we did not consider the impacts of climate change and adaptation strategies, which are also important factors affecting future food security, although their uncertainties are also high (Pugh et al., 2016; Ray et al., 2015; Rosenzweig et al., 2014). Thirdly, as the purpose of this study is to investigate the yield potentials of input intensification, associated environmental trade-offs, and their regional differences, we only considered several levels of intensification (low, high, and maximum) in order to reduce the computation time. A full range of N and irrigation intensification scenarios would help to identify the optimal intensification level. Coping with these factors was beyond the scope of this study and will be subject to future research.

5.5 References

Balkovič, J. et al., 2014. Global wheat production potentials and management flexibility under the representative concentration pathways. Global Planet. Change, 122: 107–121.

Bassu, S. et al., 2014. How do various maize crop models vary in their responses to climate change factors? Global Change Biol., 20(7): 2301–2320.

Bodirsky, B.L. and Muller, C., 2014. Robust relationship between yields and nitrogen inputs indicates three ways to reduce nitrogen pollution. Environ. Res. Lett., 9(11): 111005.

Bodirsky, B.L. et al., 2015. Global food demand scenarios for the 21st century. PLoS One, 10(11): e0139201.

Brauman, K.A., Siebert, S. and Foley, J.A., 2013. Improvements in crop water productivity increase water sustainability and food security—a global analysis. Environ. Res. Lett., 8(2): 024030.

Cai, X.M. and Rosegrant, M.W., 2002. Global water demand and supply projections part – 1. A modeling approach. Water Int., 27(2): 159–169.

Carberry, P.S. et al., 2013. Scope for improved eco-efficiency varies among diverse cropping systems. Proc. Natl. Acad. Sci. U.S.A., 110(21): 8381–8386.

Challinor, A.J., Parkes, B. and Ramirez-Villegas, J., 2015. Crop yield response to climate change varies with cropping intensity. Global Change Biol., 21(4): 1679–1688.

Chen, X. et al., 2014. Producing more grain with lower environmental costs. Nature, 514(7523): 486–9.

Chen, X.P. et al., 2011. Integrated soil–crop system management for food security. Proc. Natl. Acad. Sci. U.S.A., 108(16): 6399–6404.

Clark, C.M. and Tilman, D., 2008. Loss of plant species after chronic low-level nitrogen deposition to prairie grasslands. Nature, 451(7179): 712–715.

Conant, R.T., Berdanier, A.B. and Grace, P.R., 2013. Patterns and trends in nitrogen use and nitrogen recovery efficiency in world agriculture. Global Biogeochem. Cycles, 27(2): 558–566.

Deng, J.S., Qiu, L.F., Wang, K., Yang, H. and Shi, Y.A.Y., 2011. An integrated analysis of urbanization-triggered cropland loss trajectory and implications for sustainable land management. Cities, 28(2): 127–137.

Elliott, J. et al., 2014. Constraints and potentials of future irrigation water availability on agricultural production under climate change. Proc. Natl. Acad. Sci. U.S.A., 111(9): 3239–3244.

Folberth, C. et al., 2014. Effects of ecological and conventional agricultural intensification practices on maize yields in sub-Saharan Africa under potential climate change. Environ. Res. Lett., 9(4): 044004.

Foley, J.A. et al., 2005. Global consequences of land use. Science, 309(5734): 570–574.

Foley, J.A. et al., 2011. Solutions for a cultivated planet. Nature, 478: 337–342.

Garnett, T. et al., 2013. Agriculture. Sustainable intensification in agriculture: premises and policies. Science, 341(6141): 33–4.

Godfray, H.C.J. et al., 2010. Food Security: The challenge of feeding 9 billion people. Science, 327(5967): 812–818.

Godfray, H.C.J. and Garnett, T., 2014. Food security and sustainable intensification. Philos. Trans. R. Soc. London, Ser. B, 369(1639) : 20120273.

Iizumi, T. et al., 2014. Historical changes in global yields: major cereal and legume crops from 1982 to 2006. Global Ecol. Biogeogr., 23(3): 346–357.

Jagermeyr, J. et al., 2015. Water savings potentials of irrigation systems: global simulation of processes and linkages. Hydrol. Earth Syst. Sci., 19(7): 3073–3091.

Jagermeyr, J. et al., 2016. Integrated crop water management might sustainably halve the global food gap. Environ. Res. Lett., 11(2): 025002.

Johnston, M. et al., 2011. Closing the gap: global potential for increasing biofuel production through agricultural intensification. Environ. Res. Lett., 6(3): 034028.

Khush, G.S., 2001. Green revolution: the way forward. Nat. Rev. Genet., 2(10): 815–822.

Kummu, M., Ward, P.J., de Moel, H. and Varis, O., 2010. Is physical water scarcity a new phenomenon? Global assessment of water shortage over the last two millennia. Environ. Res. Lett., 5(3): 034006.

Lambin, E.F. and Meyfroidt, P., 2011. Global land use change, economic globalization, and the looming land scarcity. Proc. Natl. Acad. Sci. U.S.A., 108(9): 3465–3472.

Lassaletta, L., Billen, G., Grizzetti, B., Anglade, J. and Garnier, J., 2014. 50 year trends in nitrogen use efficiency of world cropping systems: the relationship between yield and nitrogen input to cropland. Environ. Res. Lett., 9(10): 105011.

Li, T. et al., 2015. Uncertainties in predicting rice yield by current crop models under a wide range of climatic conditions. Global Change Biol., 21(3): 1328–1341.

Liu, J., Williams, J.R., Zehnder, A.J.B. and Yang, H., 2007. GEPIC – modelling wheat yield and crop water productivity with high resolution on a global scale. Agric. Syst., 94(2): 478–493.

Liu, J. et al., 2010. A high-resolution assessment on global nitrogen flows in cropland. Proc. Natl. Acad. Sci. U.S.A., 107(17): 8035–40.

Liu, W., Antonelli, M., Liu, X. and Yang, H., 2017. Towards improvement of grey water footprint assessment: With an illustration for global maize cultivation. J. Cleaner Prod., 147: 1–9.

Liu, W. et al., 2016a. Global assessment of nitrogen losses and trade-offs with yields from major crop cultivations. Sci. Total Environ., 572: 526–537.

Liu, W.F. et al., 2016b. Global investigation of impacts of PET methods on simulating crop–water relations for maize. Agric. For. Meteorol., 221: 164–175.

Liu, X. et al., 2013. Enhanced nitrogen deposition over China. Nature, 494(7438): 459–62.

Lotze-Campen, H. et al., 2014. Impacts of increased bioenergy demand on global food markets: an AgMIP economic model intercomparison. Agr. Econ., 45(1): 103–116.

Lu, Y. et al., 2015. Addressing China's grand challenge of achieving food security while ensuring environmental sustainability. Sci. Adv., 1(1): e1400039.

Martre, P. et al., 2015. Multimodel ensembles of wheat growth: many models are better than one. Global Change Biol., 21(2): 911–925.

Matson, P.A., Parton, W.J., Power, A.G. and Swift, M.J., 1997. Agricultural intensification and ecosystem properties. Science, 277(5325): 504–509.

Mauser, W. et al., 2015. Global biomass production potentials exceed expected future demand without the need for cropland expansion. Nat. Commun., 6: 8946.

Mekonnen, M.M. and Hoekstra, A.Y., 2016. Four billion people facing severe water scarcity. Sci. Adv., 2(2): e1500323.

Mueller, N.D. et al., 2012. Closing yield gaps through nutrient and water management. Nature, 490(7419): 254–257.

Mueller, N.D. et al., 2014. A tradeoff frontier for global nitrogen use and cereal production. Environ. Res. Lett., 9(5): 054002.

Müller, C. et al., 2017. Global gridded crop model evaluation: benchmarking, skills, deficiencies and implications. Geosci. Model Dev., 10(4): 1403–1422.

Oki, T. and Kanae, S., 2006. Global hydrological cycles and world water resources. Science, 313(5790): 1068–1072.

Portmann, F.T., Siebert, S. and Doll, P., 2010. MIRCA2000–Global monthly irrigated and rainfed crop areas around the year 2000: A new high-resolution data set for agricultural and hydrological modeling. Global Biogeochem. Cycles, 24: GB1011.

Porwollik, V. et al., 2016. Spatial and temporal uncertainty of crop yield aggregations. Eur. J. Agron. doi: 10.1016/j.eja.2016.08.006

Pretty, J., 2008. Agricultural sustainability: concepts, principles and evidence. Philos. Trans. R. Soc. London, Ser. B, 363(1491): 447–465.

Pugh, T.A. et al., 2016. Climate analogues suggest limited potential for intensification of production on current croplands under climate change. Nat. Commun., 7: 12608.

Ray, D.K., Gerber, J.S., MacDonald, G.K. and West, P.C., 2015. Climate variation explains a third of global crop yield variability. Nat. Commun., 6: 5989.

Ray, D.K., Mueller, N.D., West, P.C. and Foley, J.A., 2013. Yield trends are insufficient to double global crop production by 2050. PLoS One, 8(6): e66428.

Ray, D.K., Ramankutty, N., Mueller, N.D., West, P.C. and Foley, J.A., 2012. Recent patterns of crop yield growth and stagnation. Nat. Commun., 3: 1293.

Rosenzweig, C. et al., 2014. Assessing agricultural risks of climate change in the 21st century in a global gridded crop model intercomparison. Proc. Natl. Acad. Sci. U.S.A., 111(9): 3268–3273.

Sacks, W.J., Deryng, D., Foley, J.A. and Ramankutty, N., 2010. Crop planting dates: an analysis of global patterns. Global Ecol. Biogeogr., 19(5): 607–620.

Sayer, J. and Cassman, K.G., 2013. Agricultural innovation to protect the environment. Proc. Natl. Acad. Sci. U.S.A., 110(21): 8345–8348.

Schlesinger, W.H., 2009. On the fate of anthropogenic nitrogen. Proc. Natl. Acad. Sci. U.S.A., 106(1): 203–208.

Steffen, W. et al., 2015. Planetary boundaries: Guiding human development on a changing planet. Science, 347(6223): 1259855.

Sutton, M., A. et al., 2013. Our Nutrient World: the challenge to produce more food and energy with less pollution. Centre for Ecology and Hydrology (CEH).

Tilman, D., Balzer, C., Hill, J. and Befort, B.L., 2011. Global food demand and the sustainable intensification of agriculture. Proc. Natl. Acad. Sci. U.S.A., 108(50): 20260–20264.

Tilman, D. et al., 2001. Forecasting agriculturally driven global environmental change. Science, 292(5515): 281–284.

Wei, X. et al., 2015. Is yield increase sufficient to achieve food security in China? PLoS One, 10(2): e0116430.

West, P.C. et al., 2014. Leverage points for improving global food security and the environment. Science, 345(6194): 325–328.

Zhang, X. et al., 2015. Managing nitrogen for sustainable development. Nature, 528(7580): 51–59.

Supplementary information for

Achieving high crop yields with low nitrogen losses in global agricultural input intensification

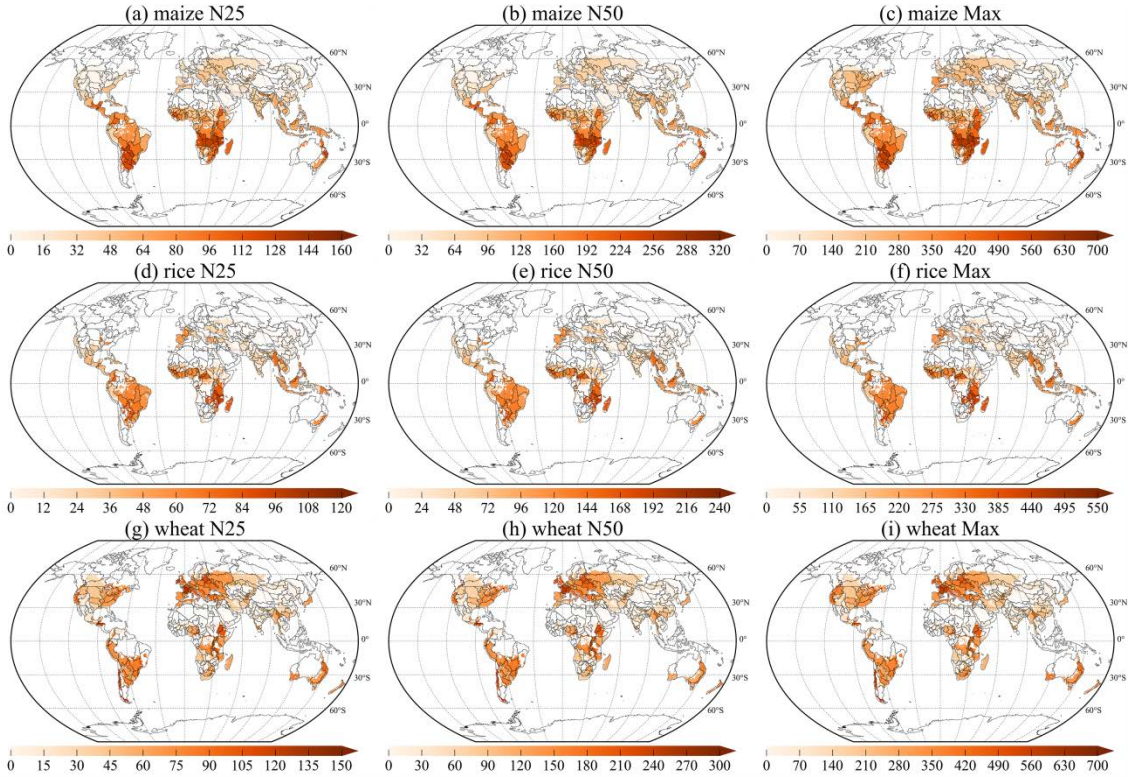

Figure S5-1. Changes of nitrogen inputs (ΔN_{in}) [kg N per ha] between N25 (a, d, g), N50 (b, e, h), Max (c, f, i) and Baseline.

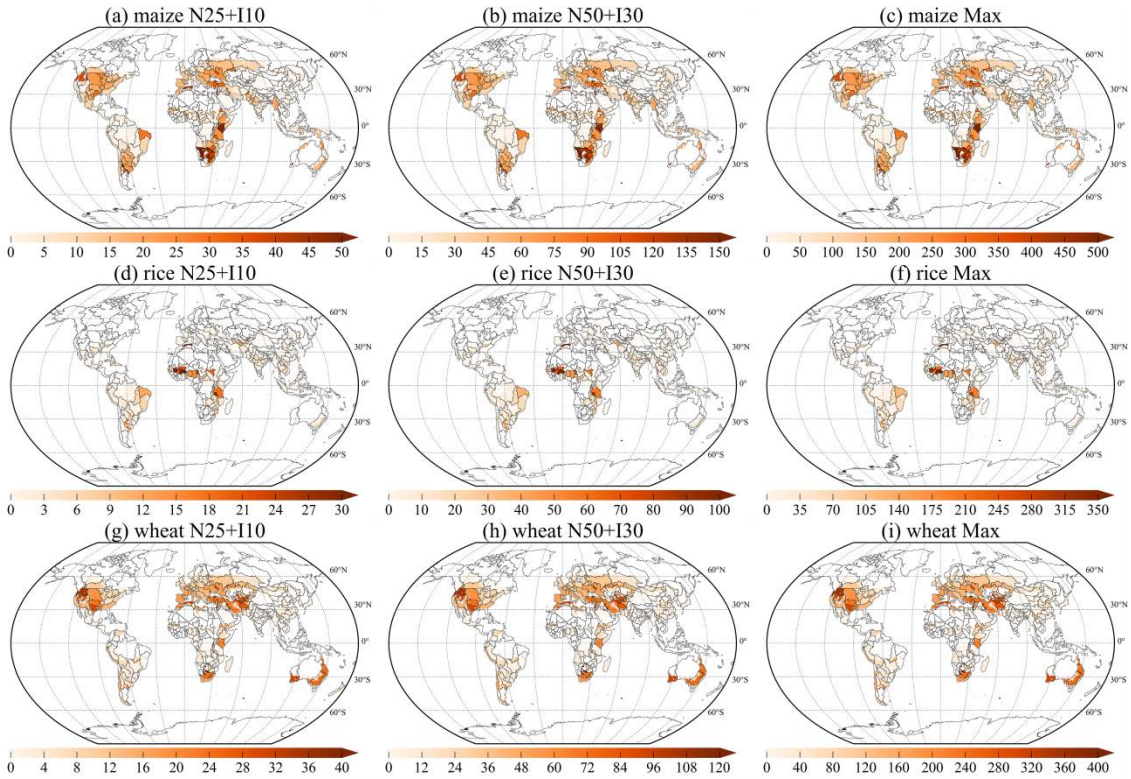

Figure S5-2. Changes in irrigation water (ΔI_w) [mm] between N25+I10 (a, d, g), N50+I30 (b, e, h), Max (c, f, i) and Baseline.

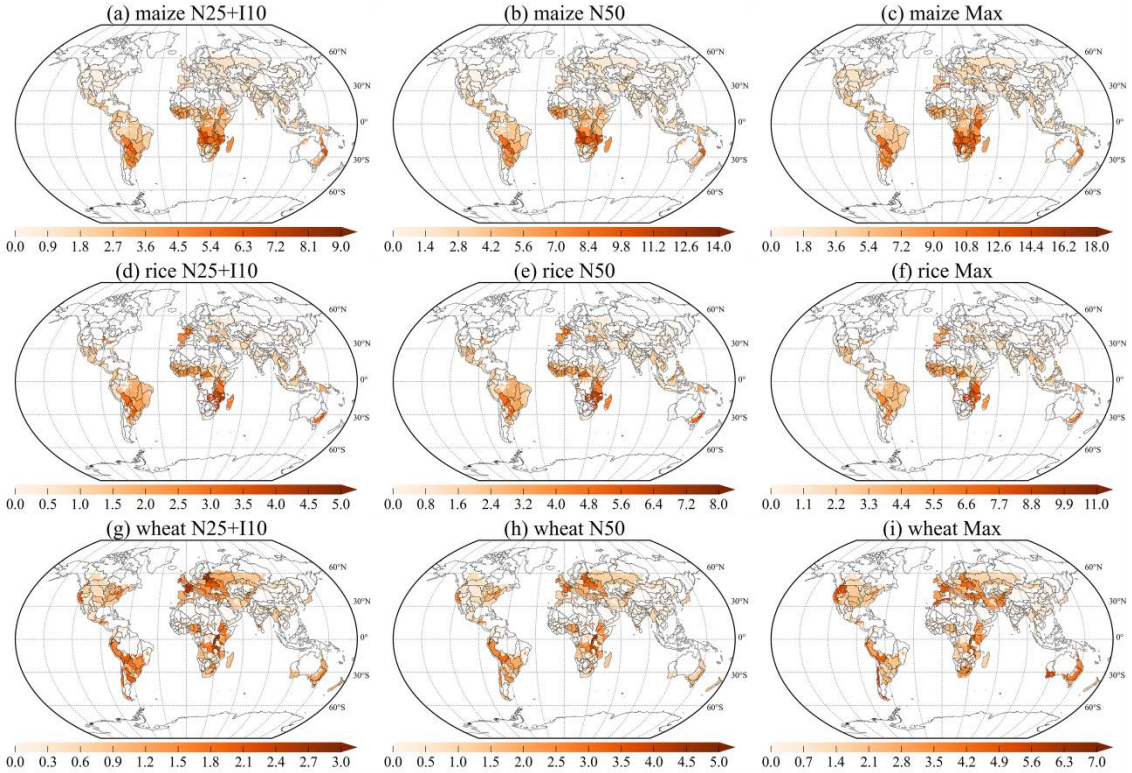

Figure S5-3. Changes in yields (ΔY) [t per ha] between N25+I10 (a, d, g), N50 (b, e, h), Max (c, f, i) and Baseline.

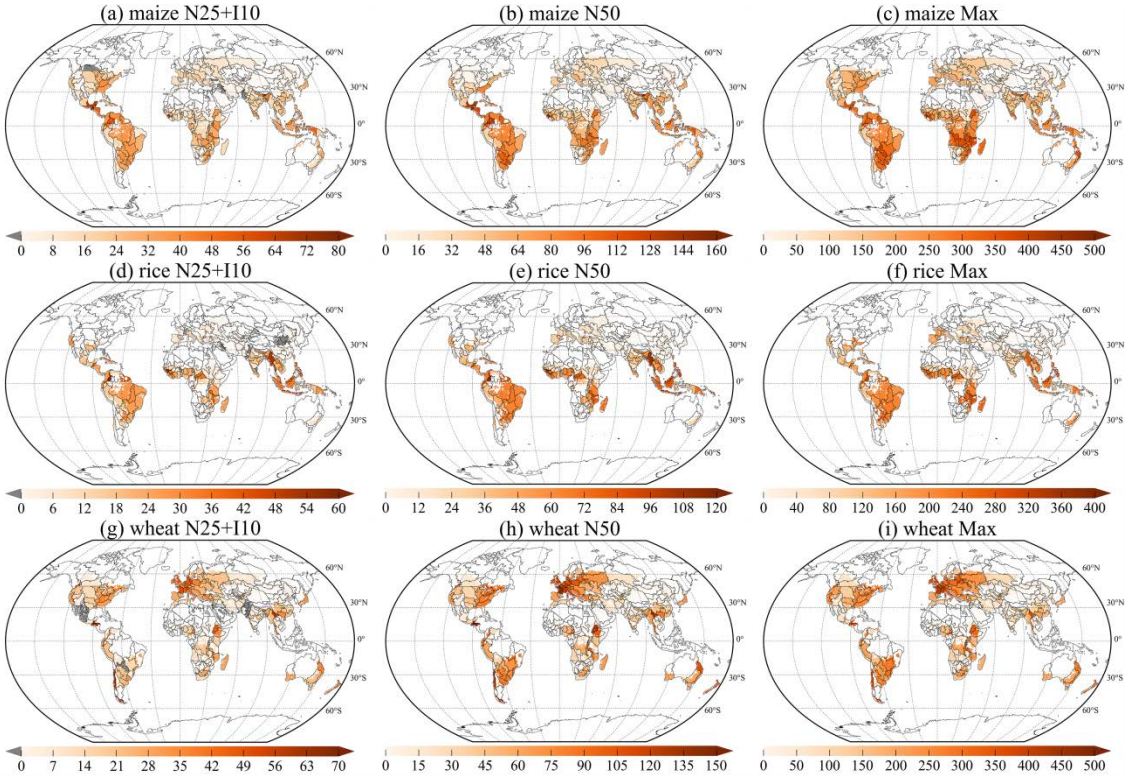

Figure S5-4. Changes in nitrogen losses (ΔN_l) [kg N per ha] between N25+I10 (a, d, g), N50 (b, e, h), Max (c, f, i) and Baseline.

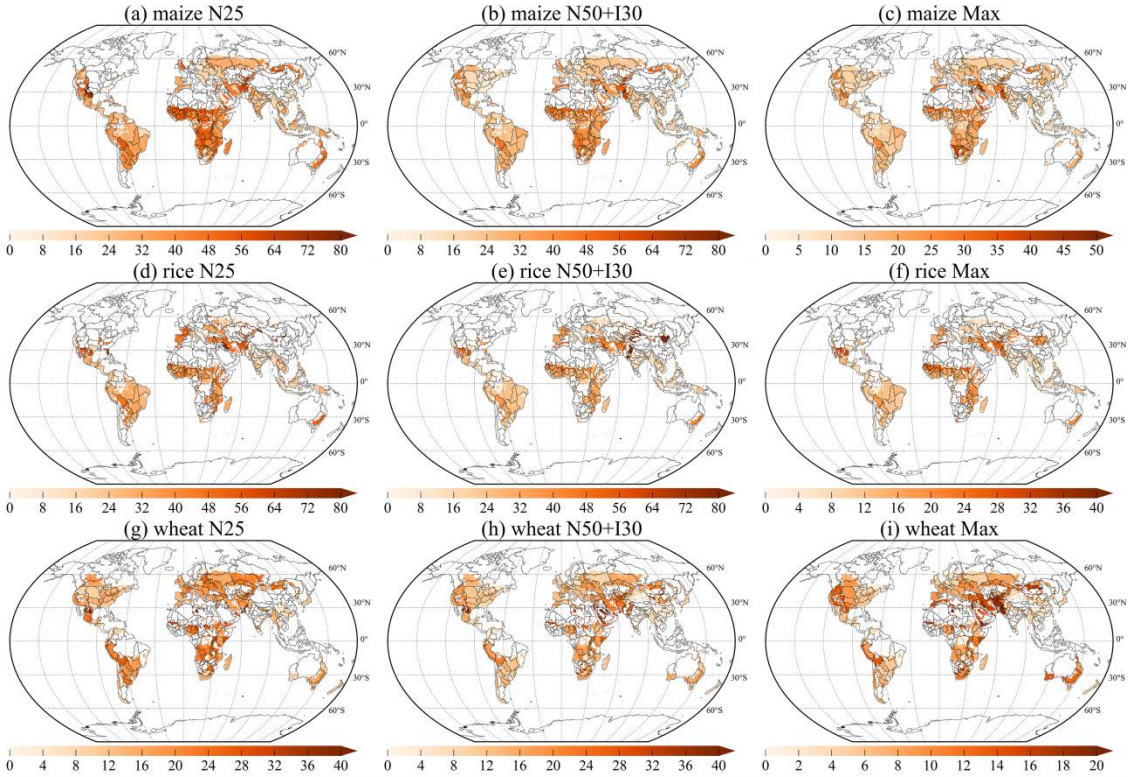

Figure S5-5. Spatial distribution of $\Delta Y/\Delta N_{in}$ [kg grain per kg N] in the intensification scenarios N25 (a, d, g), N50+I30 (b, e, h), and Max (c, f, i). ΔY: differences in yields (Y) between intensified scenarios and Baseline; ΔN_{in}: differences in nitrogen inputs (N_{in}) between intensified scenarios and Baseline.

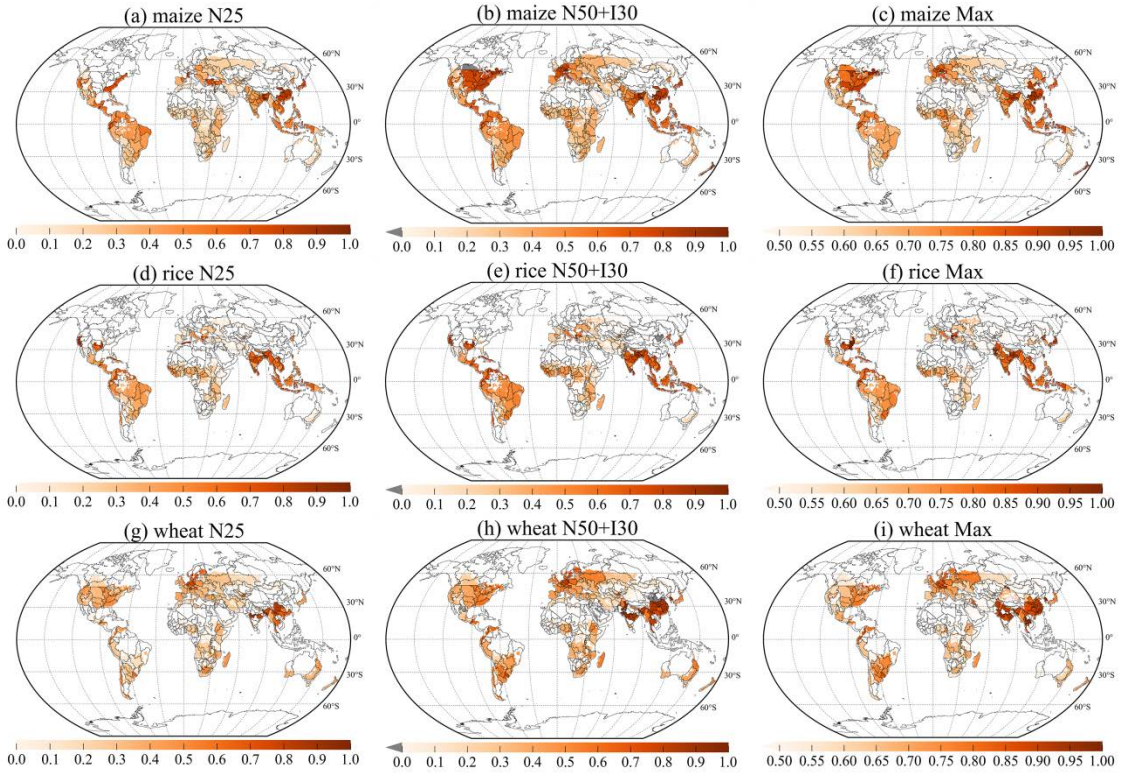

Figure S5-6. Spatial distribution of $\Delta N_l/\Delta N_{in}$ [-] in the intensification N25 (a, d, g), N50+I30 (b, e, h), and Max (c, f, i). ΔN_l: differences in total nitrogen losses (N_l) between intensification scenarios and Baseline; ΔN_{in}: differences in nitrogen inputs (N_{in}) between intensification scenarios and Baseline.

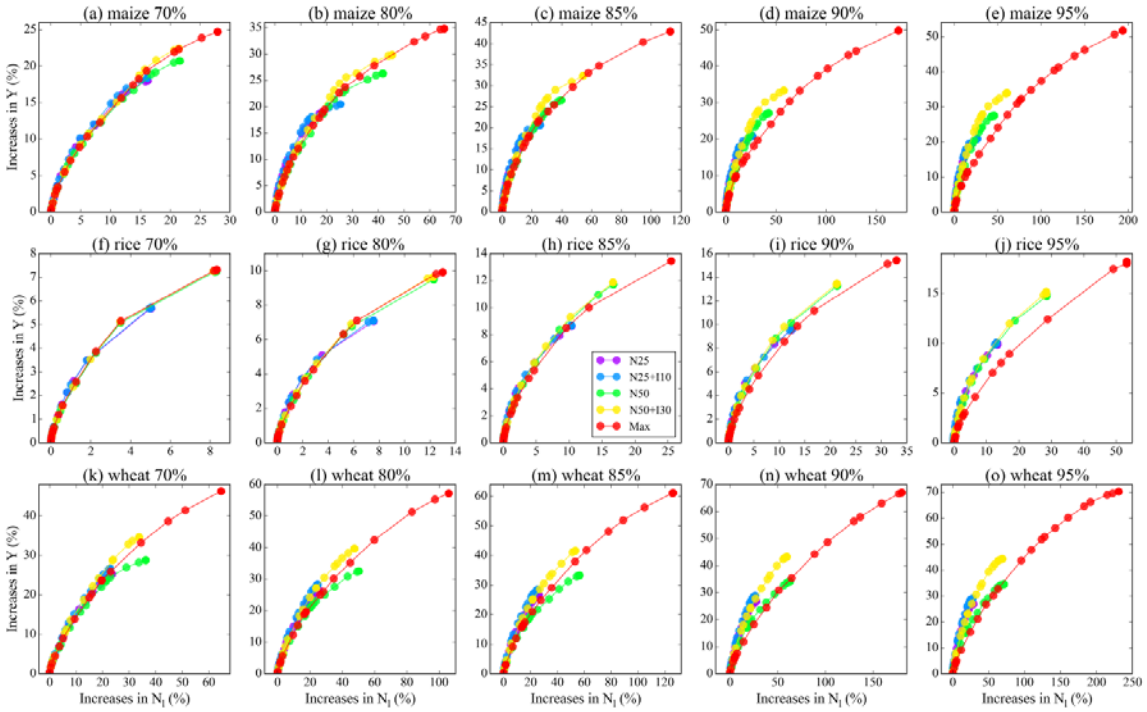

Figure S5-7. Percentage changes in global average yields (Y) and nitrogen losses (N_l) in different intensified scenarios considering 70%, 80%, 85%, 90% and 95% of maximum Y (Y_{max}) achieved. Considering each level of Y_{max} achieved means the intensification scenario for the food production unit (FPU) with corresponding level of Y_{max} achieved uses the first scenario among Baseline, N25, N25+I10, N50, and N50+I30, which has achieved the corresponding level of Y_{max}. Points in each curve are derived by intensifying FPUs with an ascending order of $\Delta N_l/\Delta N_{in}$ and a descending order of $\Delta Y/\Delta N_{in}$ on the basis of Figure 5-3. For better visualization, every 10 points between the first and last points are plotted for each curve.

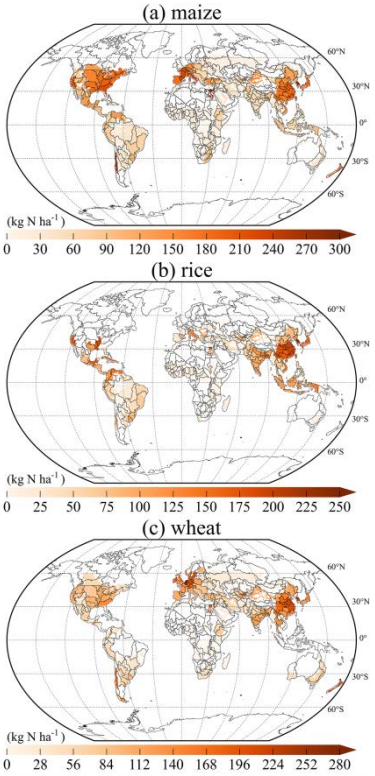

Figure S5-8. Spatial distribution of nitrogen inputs in Baseline ($N_{in\text{-}base}$) [kg N per ha].

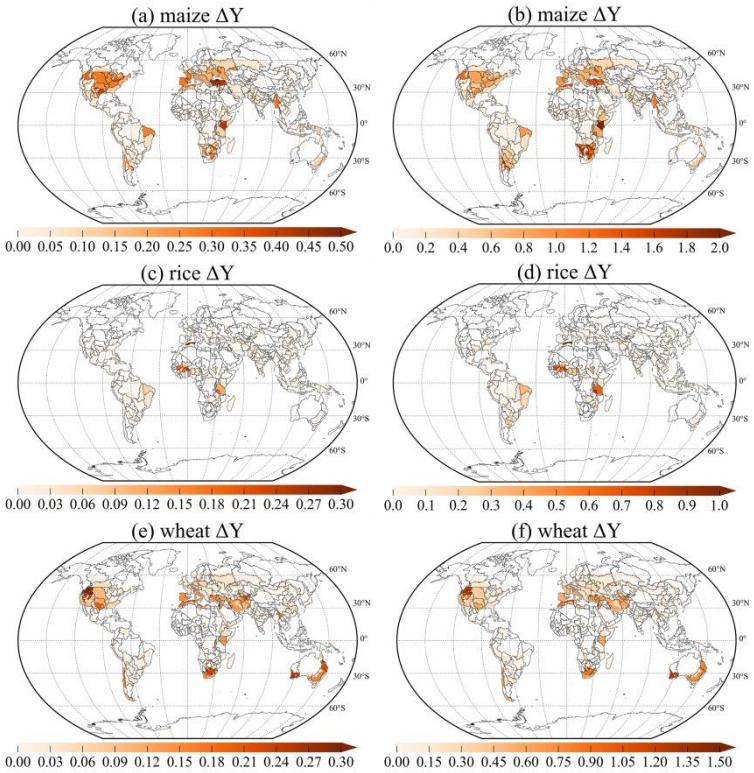

Figure S5-9. Changes of yields (ΔY) [t per ha] due to irrigated land expansions considering the ΔY between N25+I10 and N25 (a, c, e) as well as between N50+I30 and N50 (b, d, f).

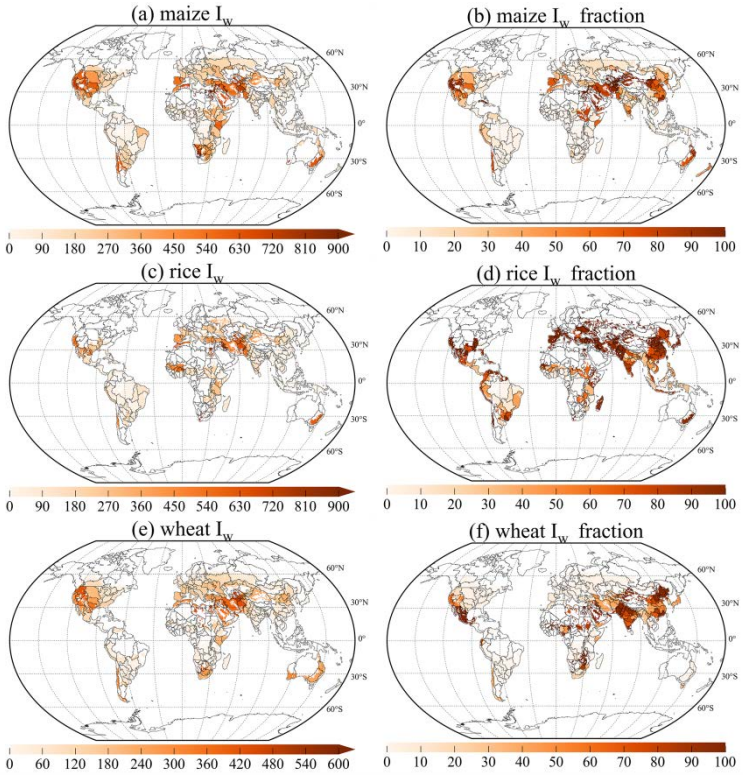

Figure S5-10. Irrigation water (I_w) [mm] for maize (a), rice (c), and wheat (e); and fraction of irrigated land to total cultivated land (I_w fraction) [%] for maize (b), rice (d), and wheat (f). The I_w was estimated by PEPIC considering all the croplands as irrigated land with nitrogen fertilization in Baseline.

Table S5-1. Average yields [t per ha] under different conditions. Description of each scenario refers to Table 5-1.

Crop	Continent	Baseline	N25	N25+I10	N50	N50+I30	Max
maize	Africa	3.9	7.2	7.3	8.8	9.3	11.2
	Asia	6.3	6.7	6.7	6.9	7.0	7.3
	Europe	6.0	6.7	6.8	6.8	7.4	8.8
	N. America	8.2	8.7	8.9	8.9	9.6	11.2
	Oceania	4.6	8.2	8.3	10.1	10.4	11.5
	S. America	5.5	8.5	8.5	9.9	10.1	11.2
rice	Africa	2.9	4.9	4.9	6.1	6.2	7.1
	Asia	4.5	4.9	4.9	5.1	5.1	5.2
	Europe	4.8	6.3	6.3	6.9	6.9	7.0
	N. America	6.5	6.9	6.9	7.0	7.1	7.2
	Oceania	2.6	5.6	5.6	7.6	7.7	8.4
	S. America	4.6	6.2	6.2	7.0	7.1	7.5
wheat	Africa	2.0	3.0	3.1	3.3	3.9	5.8
	Asia	2.3	2.6	2.7	2.8	2.9	3.4
	Europe	3.5	5.0	5.0	5.4	5.6	6.3
	N. America	3.1	3.7	3.7	3.8	4.1	5.0
	Oceania	1.9	2.9	3.1	3.1	4.0	6.6
	S. America	3.1	4.7	4.7	5.0	5.0	5.3

Table S5-2. Average irrigation water use efficiency [kg grain per mm irrigation water] under different conditions. Description of each scenario refers to Table 5-1.

Crop	Continent	Baseline	N25	N25+I10	N50	N50+I30	Max
maize	Global	126.5	150.7	124.0	161.4	97.8	56.1
	Africa	88.7	163.8	120.8	198.2	99.1	53.6
	Asia	102.4	109.6	105.7	112.2	95.9	73.0
	Europe	145.5	160.9	118.6	163.1	80.6	42.3
	N. America	128.9	136.0	109.2	140.3	81.9	46.4
	Oceania	16.1	28.6	28.0	35.0	32.9	29.9
	S. America	834.7	1295.1	549.5	1506.8	302.8	116.3
rice	Global	108.6	119.6	117.2	125.4	118.3	107.6
	Africa	27.2	46.2	44.0	57.0	49.8	42.5
	Asia	130.1	139.9	137.8	145.0	138.6	129.1
	Europe	17.5	22.7	22.7	25.0	25.0	25.1
	N. America	31.4	33.1	33.0	33.9	33.5	32.9
	Oceania	4.7	10.2	10.2	13.9	13.8	14.4
	S. America	121.1	164.0	150.8	183.7	145.5	102.6
wheat	Global	59.9	76.0	62.2	80.6	49.4	29.3
	Africa	24.0	35.8	30.9	39.5	28.8	22.0
	Asia	30.3	34.7	32.4	36.5	30.2	23.1
	Europe	780.7	1107.1	274.9	1194.6	122.9	44.4
	N. America	187.2	221.0	116.7	230.6	65.6	29.0
	Oceania	938.1	1413.9	108.9	1478.7	49.0	24.7
	S. America	572.8	873.1	466.3	924.4	258.1	100.3

Table S5-3. Average nitrogen use efficiency [kg grain per kg nitrogen] under different conditions. Description of each scenario refers to Table 5-1.

Crop	Continent	Baseline	N25	N25+I10	N50	N50+I30	Max
maize	Global	57.5	51.0	49.0	44.0	42.1	27.2
	Africa	93.7	58.8	59.4	45.1	46.8	26.3
	Asia	52.8	48.7	48.8	43.9	44.4	32.3
	Europe	63.4	52.4	52.0	44.7	44.5	28.6
	N. America	50.3	47.8	42.7	44.5	37.8	26.1
	Oceania	62.0	55.1	55.3	46.4	46.4	25.3
	S. America	80.9	55.9	56.1	41.6	42.4	23.6
rice	Global	39.1	35.9	35.9	31.9	32.0	23.1
	Africa	100.8	56.2	56.4	41.5	42.3	23.2
	Asia	37.8	34.8	34.8	31.2	31.2	23.1
	Europe	72.4	60.2	60.2	48.7	48.7	27.6
	N. America	42.0	39.1	39.1	35.8	35.9	22.2
	Oceania	164.0	72.8	72.8	55.0	55.0	26.8
	S. America	71.1	50.9	51.1	39.0	39.4	22.3
wheat	Global	34.0	27.6	28.0	22.2	23.3	15.5
	Africa	34.1	24.6	25.7	19.6	22.6	16.5
	Asia	27.2	25.2	25.4	22.5	23.1	17.1
	Europe	43.3	30.2	30.5	22.1	22.9	13.6
	N. America	39.7	29.9	30.5	24.0	25.2	16.5
	Oceania	36.5	22.9	24.3	17.7	21.6	16.1
	S. America	53.9	34.4	34.5	23.1	23.4	13.1

Table S5-4. Average irrigation water [mm] under different conditions. Description of each scenario refers to Table 5-1.

Crop	Continent	Baseline	N25	N25+I10	N50	N50+I30	Max
maize	Africa	44.1	44.2	60.7	44.2	93.7	209.1
	Asia	61.3	61.3	63.8	61.3	73.0	100.7
	Europe	41.4	41.5	57.7	41.5	91.6	209.2
	N. America	63.7	63.8	81.4	63.8	116.8	240.5
	Oceania	287.9	288.3	296.9	289.0	317.5	383.9
	S. America	6.5	6.6	15.5	6.6	33.5	96.3
rice	Africa	106.4	106.4	112.3	106.4	124.4	166.5
	Asia	34.9	34.9	35.5	34.9	36.6	40.5
	Europe	276.2	276.4	276.6	276.5	276.9	278.1
	N. America	207.2	207.2	208.3	207.3	210.5	219.5
	Oceania	545.1	545.9	549.8	545.9	557.1	584.2
	S. America	37.9	37.9	41.3	37.9	48.5	73.3
wheat	Africa	83.1	83.1	100.8	83.2	137.1	263.8
	Asia	75.9	76.0	82.2	76.0	97.2	146.6
	Europe	4.5	4.5	18.2	4.5	45.7	141.9
	N. America	16.5	16.5	32.0	16.5	62.9	171.2
	Oceania	2.1	2.1	28.7	2.1	82.1	268.9
	S. America	5.4	5.4	10.1	5.4	19.6	52.7

Table S5-5. Average nitrogen inputs [kg N per ha] under different conditions. Description of each scenario refers to Table 5-1.

Crop	Continent	Baseline	N25	N25+I10	N50	N50+I30	Max
maize	Africa	41.8	123.1	123.5	194.1	198.5	426.6
	Asia	118.9	137.9	138.0	156.9	157.7	227.7
	Europe	95.0	127.3	131.5	151.2	165.8	309.5
	N. America	163.2	181.6	207.9	201.2	252.8	426.9
	Oceania	74.6	149.6	150.1	218.0	225.0	453.0
	S. America	67.5	151.9	152.2	237.3	239.3	474.2
rice	Africa	28.7	87.5	87.5	146.1	146.4	304.4
	Asia	120.3	140.5	140.5	162.6	162.7	226.4
	Europe	66.6	104.0	104.0	141.8	141.9	252.9
	N. America	155.0	175.6	175.6	196.5	196.6	325.2
	Oceania	15.6	76.6	76.9	138.0	139.7	315.4
	S. America	64.5	122.1	122.1	178.7	178.9	336.6
wheat	Africa	58.5	120.9	121.5	167.0	174.9	351.7
	Asia	84.7	104.5	105.1	123.4	127.0	197.6
	Europe	80.6	164.1	164.2	243.0	245.2	463.2
	N. America	77.7	122.0	122.4	158.9	163.8	300.8
	Oceania	53.0	128.0	128.6	173.4	186.0	410.6
	S. America	57.1	136.2	136.2	215.1	215.4	402.1

Table S5-6. Average nitrogen losses [kg N per ha] under different conditions. Description of each scenario refers to Table 5-1.

Crop	Continent	Baseline	N25	N25+I10	N50	N50+I30	Max
maize	Africa	33.5	56.0	55.6	89.8	88.6	276.2
	Asia	76.2	86.1	86.0	100.0	98.3	161.0
	Europe	68.6	79.7	82.1	95.8	102.4	220.7
	N. America	104.1	114.4	133.2	127.8	165.9	315.9
	Oceania	49.1	66.1	65.9	96.0	98.4	286.0
	S. America	64.5	96.6	96.3	141.0	139.5	342.1
rice	Africa	40.8	62.8	62.5	96.3	95.2	228.2
	Asia	106.3	119.8	119.2	137.6	137.0	194.6
	Europe	50.7	60.3	60.2	80.9	80.9	181.8
	N. America	94.4	108.3	108.1	125.3	125.0	247.6
	Oceania	17.3	27.5	27.4	46.0	46.1	203.9
	S. America	61.6	87.7	87.5	125.2	124.3	268.0
wheat	Africa	33.2	51.9	50.1	77.3	71.3	191.3
	Asia	57.2	63.6	63.6	73.3	73.4	126.8
	Europe	52.3	82.3	81.7	133.4	131.4	326.7
	N. America	44.6	60.4	59.8	81.2	80.5	191.2
	Oceania	24.8	51.5	49.2	87.9	77.5	223.7
	S. America	55.6	76.1	75.4	135.2	133.2	312.0

Table S5-7. Fraction [%] of croplands with 75% of maximum yields achieved to the total croplands under different conditions. Description of each scenario refers to Table 5-1.

Scenario	maize	rice	wheat
Baseline	43.9	83.8	36.0
N25	66.2	92.0	61.6
N25+I10	71.9	92.0	68.0
N50	78.9	99.4	74.9
N50+I30	93.9	99.4	80.7

Chapter 6

Resource conservation and pollution reduction in the context of global food trade and agricultural intensification

Based on

Resource conservation and pollution reduction in the context of global food trade and agricultural intensification (submitted to Science Advances)

Authors

Wenfeng Liu[a], Hong Yang[a,b], Yu Liu[c,d], Matti Kummu[e], Arjen Y. Hoekstra[f,g], Junguo Liu[h], Rainer Schulin[i]

[a]*Eawag, Swiss Federal Institute of Aquatic Science and Technology, Ueberlandstrasse 133, CH-8600 Duebendorf, Switzerland*

[b]*Department of Environmental Sciences, University of Basel, Petersplatz 1, CH-4003 Basel, Switzerland*

[c]*Institutes of Science and Development, Chinese Academy of Sciences, Beijing 100190, China*

[d]*School of Public Policy and Management, University of Chinese Academy of Sciences, Beijing 100049, China*

[e]*Water & Development Research Group, Aalto University, Tietotie 1E, 02150 Espoo, Finland*

[f]*Twente Water Centre, University of Twente, Enschede, The Netherlands*

[g]*Institute of Water Policy, Lee Kuan Yew School of Public Policy, National University of Singapore, Singapore*

[h]*School of Environmental Science and Engineering, South University of Science and Technology of China, Xueyuan Road 1088, Nanshan Districit, Shenzhen, 518055, Shenzhen, China*

[i]*ETH Zürich, Institute of Terrestrial Ecosystems, Universitätstr. 16, CH-8092 Zürich, Switzerland*

Abstract

Global food trade entails virtual flows of agricultural resources and environmental pollution across country boundaries. Existing studies largely focus on water resources but lack a comprehensive evaluation of environmental impacts associated with food trade. Here, we performed a global-scale assessment of the impacts of international food trade on blue water use, total water use, and nitrogen (N) inputs in agriculture and on N losses from agriculture to water and the total environment for the three major crops (maize, rice, and wheat). Blue water use refers to the blue water footprint of crop production, and total water use to the sum of the blue and green water footprint. Besides the baseline simulations around the year 2000, we explored the impacts of an agricultural intensification scenario, in which particularly countries with low N and irrigation inputs under the baseline in crop production enhance crop yields by increasing those inputs. For these purposes, we combined a crop model with the Global Trade Analysis Project (GTAP) model. For the first time we found that food exports generally occurred from regions with lower resource use intensities to regions with higher ones. This resulted that food trade globally conserved a large amount of agricultural resources as well as reduced substantial N losses. The trade-related conservation in blue water use reached 85 km^3 yr^{-1} accounting for more than half of total blue water use for producing the three crops. Food exported from the USA contributed the largest proportion of global resource conservation and N loss reduction, but also emitted substantial export-associated N losses in its own territory. Under the intensification scenario, the converging resource use and N loss intensities across countries result in a more level playing field; crop trade volume will generally decrease, and global resource conservation and pollution reduction associated with international trade will reduce accordingly. The study provides useful information to understand the implications on international crop trade and resources use and pollution patterns of agricultural intensification in the world's least developed regions.

Keywords

Food trade; Resource conservation; Pollution reduction; Agricultural intensification

6.1 Introduction

Global food trade is associated with virtual flows of water resources between trading countries. Water resources are to a greater or lesser extent bound to the place where they occur, but the possibility to use them for producing export products makes them global (Hoekstra, 2017). It has been estimated that around the year 2000 the volume of virtual water flowing throughout the world as a result of international food trade amounted to one-fifth of total water consumption for agricultural production (Hoekstra and Mekonnen, 2012). With the expansion of international trade, virtual water trade has been increasing during the past few decades (Antonelli et al., 2017; Dalin et al., 2012; Kastner et al., 2014). The influence of international food trade on water resources utilization across trade partners has been intensively studied (Hoekstra and Hung, 2005; Porkka et al., 2017; Zhao et al., 2015).

In addition to water, other agricultural resources as well as environmental quality are influenced by international food trade. In particular, impacts on nutrients such as nitrogen (N) (Lassaletta et al., 2016; Oita et al., 2016) and phosphorus (Nesme et al., 2016), land (Fader et al., 2011), water pollution (O'Bannon et al., 2014; Wan et al., 2016), CO_2 emissions (Feng et al., 2013; Peters et al., 2011), aerosols (Lin et al., 2016; Lin et al., 2014), and fine particulate matter ($PM_{2.5}$) (Zhang et al., 2017) have been studied. For instance, it was estimated that about a quarter of global N emissions were driven by demand for international trade in 2010 (Oita et al., 2016).

International food trade could serve to conserve global resources and alleviate environmental degradation if food were to be exported from regions with lower resource uses and pollution intensities to regions with higher resource uses and pollution intensities. Whereas the impacts of food trade on water conservation have been widely studied (Chapagain et al., 2006; Konar et al., 2016; Yang et al., 2006), the effects of food trade on conserving other resources and reducing environmental pollution are still largely unclear (Dalin and Rodriguez-Iturbe, 2016). Furthermore, investigations of trade impacts on resource uses and pollution have mainly been conducted by considering one metric at a time, e.g. either water or N (Dalin et al., 2017; Oita et al., 2016). Only a few studies so far have attempted to investigate such impacts through considering multiple aspects in some regions. For example, Martinez-Melendez and Bennett (2016) explored the benefits of food trade between the USA and Mexico taking impacts on land, water, and N fertilizer resources, as well as on nitrous oxide (N_2O) emissions into consideration and concluded that the trade between the two countries reduced the environmental costs of agriculture. Zhao et al. (2016) included water, chemical oxygen demand (COD), and ammoniacal nitrogen (NH_3-N) to explore the burden shifting of water quantity and quality stress from Shanghai, the largest megacity in China, to its domestic trading partners. A comprehensive and integrated assessment of environmental impacts of food trade through a multi-metric research is still absent on a global

scale. Such assessment is essential for improving our understanding of the impacts through providing a more general picture (MacDonald et al., 2012; Yang et al., 2013).

Here, for the first time we performed a comprehensive global-scale investigation of trade effects on agricultural resources and N emissions to the environment, comparing the baseline situation around the year 2000 to a scenario of agricultural intensification. Using the grid-based crop model PEPIC, i.e. Python-based Environmental Policy Integrated Climate (Liu et al., 2016a), we simulated agricultural blue water use (BWU), total water use (TWU) and N inputs (N_{in}), as well as N losses from agriculture to water (N_w) and the total environment (N_t) for the three major crops—maize, rice, and wheat. BWU refers to the evapotranspiration (ET) of irrigation water from the crop field, also referred to as blue water consumption or blue water footprint. TWU refers to total ET, i.e. the sum of ET of irrigation water (blue water) and rainwater (green water). To investigate the impacts of trade on these aspects, we first estimated resource use intensities and N loss intensities, calculated as a ratio of resource uses and N losses to crop yields. Gross virtual resource flows between countries and export-associated N losses were then calculated by multiplying international food trade volumes with respective resource use intensities and N loss intensities in the exporting countries. Finally, resource conservation through international food trade was obtained by multiplying exported food volumes with the difference between resource use intensities in food importing countries and exporting countries. In the case of reduction in N losses through international food trade, N loss intensities were used instead of resource use intensities.

In addition to these baseline calculations, we also considered an agricultural intensification scenario, N25I10, in which we assume an increase of N inputs by 25% of the differences between maximum N inputs and baseline N inputs (here baseline N over-application was eliminated) and a conversion of 10% of rainfed croplands into irrigated cultivation. Under the N25I10 scenario, the increases in N- input and irrigation area were therefore larger in the regions with low N-input and a high rainfed fraction in the baseline than in regions with high N-input and a high irrigated fraction in the baseline. Therefore, global spatial patterns of irrigation and N inputs were more balanced in the N25I10 scenario than in the baseline. The purpose of this scenario analysis was to illustrate possible impacts of agricultural intensification, which is advocated for achieving larger crop yields and production enhancement in low-input regions (Mueller et al., 2012), on global resource conservation and environmental impacts. The trends demonstrated in this scenario reflect a general situation under any other agricultural intensification. The Global Trade Analysis Project (GTAP) (Hertel, 1997) was used to estimate bilateral food trade under the N25I10 scenario, by inputting GTAP with relative changes of yields between N25I10 and baseline. Then, resource

conservation and reduction in N losses due to food trade were evaluated for the N25I10 scenario, similar to the baseline.

6.2 Methods

6.2.1 The PEPIC model

The crop model PEPIC (Liu et al., 2016a) was used to simulate crop yields, crop water consumption, and N dynamics at a spatial resolution of 30 arc minutes for the baseline and N25I10 scenario. The PEPIC model is a grid-version of the EPIC model (Williams, 1995; Williams et al., 1984). EPIC simulates soil–water–climate–management processes related to crop growth at a daily step. Previous investigations showed that PEPIC performed well in representing global crop yields and N losses (Liu et al., 2016a; Liu et al., 2016b). The PEPIC model also contributed to the Global Gridded Crop Model Intercomparison (GGCMI) (Elliott et al., 2015), which is part of the Agricultural Model Intercomparison and Improvement Project (AgMIP) (Rosenzweig et al., 2013). The performance of PEPIC in simulating historical yield variability at the country level compared well with the other 13 global crop models involved in the GGCMI (Müller et al., 2017; Porwollik et al., 2016).

Inputs for the PEPIC model include a digital elevation model (DEM), slope, climate (Weedon et al., 2014), soil (Batjes, 2006), and crop management practices, e.g. irrigation area, fertilizer inputs, and planting and harvesting dates (Sacks et al., 2010). For the baseline, irrigated and rainfed cultivation areas were based on the MIRCA2000 dataset (Portmann et al., 2010). Fertilizer inputs of phosphorus (P) and N (including chemical mineral fertilizer and manure) were obtained from the EarthStat dataset (http://www.earthstat.org) (Mueller et al., 2012; West et al., 2014) (Table S6-1). Irrigation was applied automatically when water deficits for a crop exceeded 10% of water requirements without water limitation (Folberth et al., 2016). P was applied before planting based on Balkovič et al. (2014), while N ($N_{in\text{-}base}$ based on the EarthStat dataset) was applied three times with equal amount during the whole growth season (Liu et al., 2016b). For the N25I10 scenario, irrigation was applied in the same way as in the baseline scenario, but converting 10% of rainfed croplands into irrigated cultivation. P was applied automatically by PEPIC without limitation to avoid the P deficiency that would limit plant growth (Folberth et al., 2014). N was applied automatically, triggered by 10% N stress (Liu et al., 2016b). To determine N inputs in the N25I10 scenario, maximum N inputs with baseline irrigation condition ($N_{in\text{-}base\text{-}max}$) and maximum N inputs with full irrigation condition ($N_{in\text{-}full\text{-}max}$) were first estimated using PEPIC triggered by 10% N stress without N limitation. The minimum value of $N_{in\text{-}base}$ and $N_{in\text{-}base\text{-}max}$ was treated as $N_{in\text{-}base\text{-}limit}$ to eliminate baseline N over-application. The difference of $N_{in\text{-}full\text{-}max}$ and $N_{in\text{-}}$

$_{base\text{-}limit}$ was calculated as ΔN_{in} (Figure S6-1). Finally, N inputs in the N25I10 scenario were estimated by $N_{in\text{-}base\text{-}limit} + 0.25 \times \Delta N_{in}$ (Table S6-1). Therefore, the N25I10 scenario combines the effects of N input intensification and avoidance of N overuse. It should be noted that the idea of the designed intensification scenario is to propose a relatively balanced agricultural condition in terms of N and irrigation inputs. The N25I10 scenario is therefore an illustration of such idea.

6.2.2 The GTAP model

The GTAP model is a multi-sector and multi-region general equilibrium global trade model with constant returns to scale and perfect competition, considering capital, land, natural resources, skilled labour, and unskilled labour as production factors (Hertel, 1997). It provides a detailed description of the demand and supply for each sector and each region. The GTAP model has been widely used to investigate the impacts of changes in yields on international trade (Konar et al., 2013; Konar et al., 2016; Liu et al., 2014). In GTAP, yield improvements due to agricultural input intensification affect food trade through changing food production and food price. Here, the GTAP v6 database, which refers to the year 2001, was used because the land-use data and the EarthStat fertilizer data under the baseline were mainly related to the period 1998–2002. Percentage differences in trade value (in million US dollars) between N25I10 (price effects on final trade value were eliminated) and baseline were generated based on the GTAP simulations. The average gross bilateral exported food volumes (EFV) [t yr^{-1}] of the three crops between 1998 and 2002 were obtained from FAOSTAT (http://www.fao.org/faostat/en/#home). Country-specific food EFV was then aggregated to 96 regions defined in the GTAP v6 database (Tables S6-2 and S6-3). Final EFV under the N25I10 scenario was calculated as the product of EFV of the baseline and the percentage differences of trade value between N25I10 and baseline.

6.2.3 Variable descriptions

The variables used in this study include crop yield (Y) [t ha^{-1}], BWU [mm], TWU [mm], N_{in} [kg N ha^{-1}], N_w [kg N ha^{-1}], and N_t [kg N ha^{-1}]. TWU refers to growing season evapotranspiration. BWU is the part of the total growing season evapotranspiration derived from surface- and ground-water. It was calculated based on Liu et al. (2009). N_w is N loss with surface runoff, leaching and erosion. N_t is the sum of N_w and N loss to the atmosphere (Liu et al., 2016b).

In order to assess gross virtual resource export, and N losses associated with food export, we first calculated resource use intensities and N loss intensities relative to crop yields at the country level aggregated from grid level using area-weighted averages:

$$BWUI = 10 * BWU/Y \quad (6\text{-}1)$$

$$TWUI = 10 * TWU/Y \quad (6\text{-}2)$$

$$N_{in}I = N_{in}/Y \quad (6\text{-}3)$$

$$N_wI = N_w/Y \quad (6\text{-}4)$$

$$N_tI = N_t/Y \quad (6\text{-}5)$$

where BWUI [$m^3\ t^{-1}$], TWUI [$m^3\ t^{-1}$], $N_{in}I$ [kg N t^{-1}], N_wI [kg N t^{-1}], and N_tI [kg N t^{-1}] are blue water use intensity, total water use intensity, N input intensity, water N loss intensity, and total N loss intensity, respectively. The 10 is used for unit transformation. Then, gross virtual BWU, TWU, and N_{in} export, as well as N_w, and N_t associated with export were obtained by multiplying EFV with the corresponding intensities:

$$BWUExp_{e,i} = BWUI_e * EFV_{e,i} \quad (6\text{-}6)$$

$$TWUExp_{e,i} = TWUI_e * EFV_{e,i} \quad (6\text{-}7)$$

$$N_{in}Exp_{e,i} = N_{in}I_e * EFV_{e,i} \quad (6\text{-}8)$$

$$N_wExp_{e,i} = N_wI_e * EFV_{e,i} \quad (6\text{-}9)$$

$$N_tExp_{e,i} = N_tI_e * EFV_{e,i} \quad (6\text{-}10)$$

where $BWUExp_{e,i}$ [m^3], $TWUExp_{e,i}$ [m^3], $N_{in}Exp_{e,i}$ [kg N] are gross virtual resource export from exporting country, e, to importing country, i, for BWU, TWU, and N_{in}, respectively; $N_wExp_{e,i}$ [kg N] and $N_tExp_{e,i}$ [kg N] are export-associated N_w and N_t. On the basis of the intensity differences between importing and exporting countries, resource conservation and pollution reduction through food trade were calculated using the following equations:

$$BWUCon_{e,i} = (BWUI_i - BWUI_e) * EFV_{e,i} \quad (6\text{-}11)$$

$$TWUCon_{e,i} = (TWUI_i - TWUI_e) * EFV_{e,i} \quad (6\text{-}12)$$

$$N_{in}Con_{e,i} = (N_{in}I_i - N_{in}I_e) * EFV_{e,i} \quad (6\text{-}13)$$

$$N_wRed_{e,i} = (N_wI_i - N_wI_e) * EFV_{e,i} \quad (6\text{-}14)$$

$$N_tRed_{e,i} = (N_tI_i - N_tI_e) * EFV_{e,i} \quad (6\text{-}15)$$

where $BWUCon_{e,i}$ [m^3], $TWUCon_{e,i}$ [m^3], $N_{in}Con_{e,i}$ [kg N], $N_wRed_{e,i}$ [kg N], and $N_tRed_{e,i}$ [kg N] are BWU conservation, TWU conservation, N_{in} conservation, N_w reduction, and N_t reduction through food trade from exporting country, e, to importing country, i, respectively. A positive value of the five variables means resource conservation or pollution reduction, while a negative value means increase in resource consumption or pollution emission. Finally, global resource conservation through food trade was calculated as the sum of resource conservation resulting from the entire trade and global N loss reduction as the sum of N losses avoided due to

international trade of the respective crop, compared to the hypothetical situation with no trade, in which the import of crops would be replaced by equivalent amounts of additional crop production in the importing countries.

6.3 Results

6.3.1 Virtual resource export and global conservation through food trade

Global trade in the three crops in the year around 2000 involved a total gross virtual resource export of 14 $km^3\ yr^{-1}$, 221 $km^3\ yr^{-1}$, and 5621 Gg (Gg = 10^9 g) N yr^{-1} for BWU, TWU, and N_{in}, respectively (Table 6-1), accounting for 8%, 12%, and 10%, respectively, of the total consumption of these resources (Table S6-4). Rice contributed the largest percentage of gross virtual BWU export (46%), while wheat contributed the largest percentages of gross virtual TWU export (64%) and gross virtual N_{in} export (58%). The USA contributed most to gross virtual resource export, accounting for 40%, 30%, and 34% of global gross virtual resource export for BWU, TWU, and N_{in}, respectively (Figure 6-1). Because the USA was the major crop exporter for maize and wheat (Figure S6-2), the gross virtual resource export of BWU, TWU, and N_{in} from the USA was also the biggest for these two crops (Figures S6-3–S6-5). As for rice, Pakistan exported the largest virtual BWU, while Thailand exported the largest virtual TWU and China exported the largest virtual N_{in} (Figure S6-4). Regarding specific trade links, food exported from the USA to Japan was responsible for the largest bilateral virtual flow of BWU, TWU and N_{in} (Figure 6-1).

Table 6-1. Global gross virtual resource export to importing countries and resource conservation through food trade for maize, rice, and wheat under the baseline and N25I10 scenario. BWU: blue water use; TWU: total water use; N_{in}: nitrogen inputs.

Scenario	Variable	Gross virtual resource export to importing countries				Resource conservation through food trade			
		maize	rice	wheat	sum	maize	rice	wheat	sum
Baseline	BWU ($km^3\ yr^{-1}$)	4.2	6.3	3.3	13.8	24.9	36.7	23.4	85.0
	TWU ($km^3\ yr^{-1}$)	53.0	26.8	141.2	221.0	41.7	42.1	21.0	104.8
	N_{in} (Gg N yr^{-1})	1623	748	3251	5621	515	453	1366	2333
N25I10	BWU ($km^3\ yr^{-1}$)	4.1	2.4	6.2	12.6	14.7	29.1	30.4	74.3
	TWU ($km^3\ yr^{-1}$)	40.9	11.8	115.0	167.7	11.8	27.8	27.8	67.5
	N_{in} (Gg N yr^{-1})	1642	320	4646	6608	332	-54	593	871

We further found that these virtual resource exports generally occurred from regions with lower resource use intensities to regions with higher ones, while only a few links flowed in the opposite direction (Figures 6-1 and S6-3–S6-5). It indicated that most trade links did conserve global resources. Global resource conservation through trade in the three crops totalled up to 85

$km^3\ yr^{-1}$, 105 $km^3\ yr^{-1}$, and 2333 Gg N yr^{-1} for BWU, TWU, and N_{in}, respectively (Table 6-1). The resource conservation was particularly high for BWU. Total global BWU conserved through food trade was six times the total gross virtual export of BWU and accounted for 51% of the global BWU consumption for the three crops (Table S6-4). This means that the importing countries on average used much more blue water to produce a unit of these crops than the exporting countries. Also, global TWU and N_{in} conservation through food trade reached half of their total gross virtual export. Global N_{in} conservation through food trade was almost equivalent to the total N_{in} consumption in Africa and Oceania for the three crops. Rice trade conserved most BWU (43%) and TWU (40%), while wheat trade conserved most N_{in} (59%). Crop export to the Middle East presented the highest potential for conserving global resources, while crop export from the USA contributed the largest fractions of global conservation of the three resources (Figure 6-1).

6.3.2 Global pollution reduction through food trade and export-associated N losses

Similar to resource conservation, global food trade reduced agricultural N losses in most bilateral trading links, with only a few links increasing N losses (Figure 6-2). This means that most exporting countries produced the three crops wasting less N fertilizer than the importing countries. The total N losses reduced through food trade were 1924 Gg N yr^{-1} for N_w and 2211 Gg N yr^{-1} for N_t for all three crops together (Table 6-2). The main contribution came from international wheat trade. The USA, Australia, and Canada were the top three contributors, together accounting for 80% and 75% of total N_w and N_t reduction, respectively. The USA contributed the largest N_w and N_t reduction with maize and wheat trade, while Thailand reduced the most N losses with rice trade (Figures S6-6–S6-8). Trade from the USA to Japan led to the largest N loss reduction associated with a single bilateral trade flow (Figures 6-2b and 6-2d). Rice exported from China mainly resulted in increases in N losses (Figure S6-7).

The simulation results indicate that global food trade conserved resources and reduced environmental pollution from N losses in terms of global totals, but the exported crops were still associated with substantial N losses to the environment in the exporting countries. This part of N losses were environmental burden shifts from food importing countries to food exporting countries. Total export-associated N losses related to the three crops reached 1914 Gg N yr^{-1} and 3681 Gg N yr^{-1} for N_w and N_t, respectively (Table 6-2), accounting for about 7% and 8% of the respective total N losses for the production of the three crops (Table S6-4). Wheat alone accounted for more than half of the global N_w and N_t losses associated with the production of the three crops for export, with respective fractions of 54% and 59%. The USA, France, and China were the major emitters of N losses associated with food export, together emitting more than half

of the N_w and N_t on their territories. In particular, the USA alone accounted for about one-third of export-associated N losses (Figures 6-2a and 6-2c).

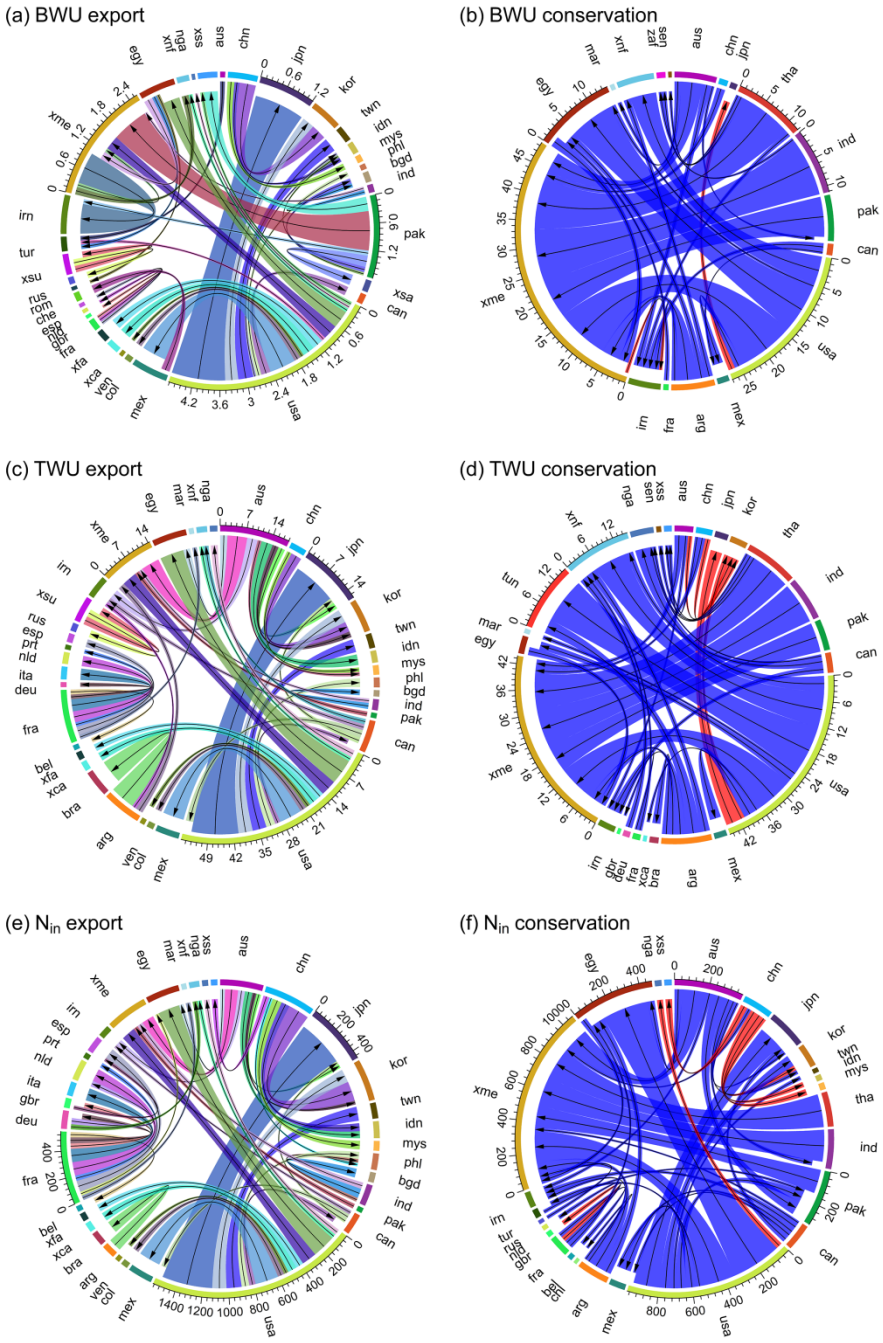

Figure 6-1. Gross virtual resource export to importing countries and resource conservation through trade in the three crops under the baseline. BWU: blue water use (km^3 yr^{-1}); TWU: total water use (km^3 yr^{-1}); N_{in}: nitrogen inputs (Gg N yr^{-1}). Arrows point to food importing countries; blue beams represent resource conservation in subplots b, d, and f, while red beams represent increases in resource consumption; the links with volumes less than 0.5% of the global total are disregarded; numbers outside arcs show total volume of export and conservation for major trading countries. Regions are defined in Tables S6-2 and S6-3.

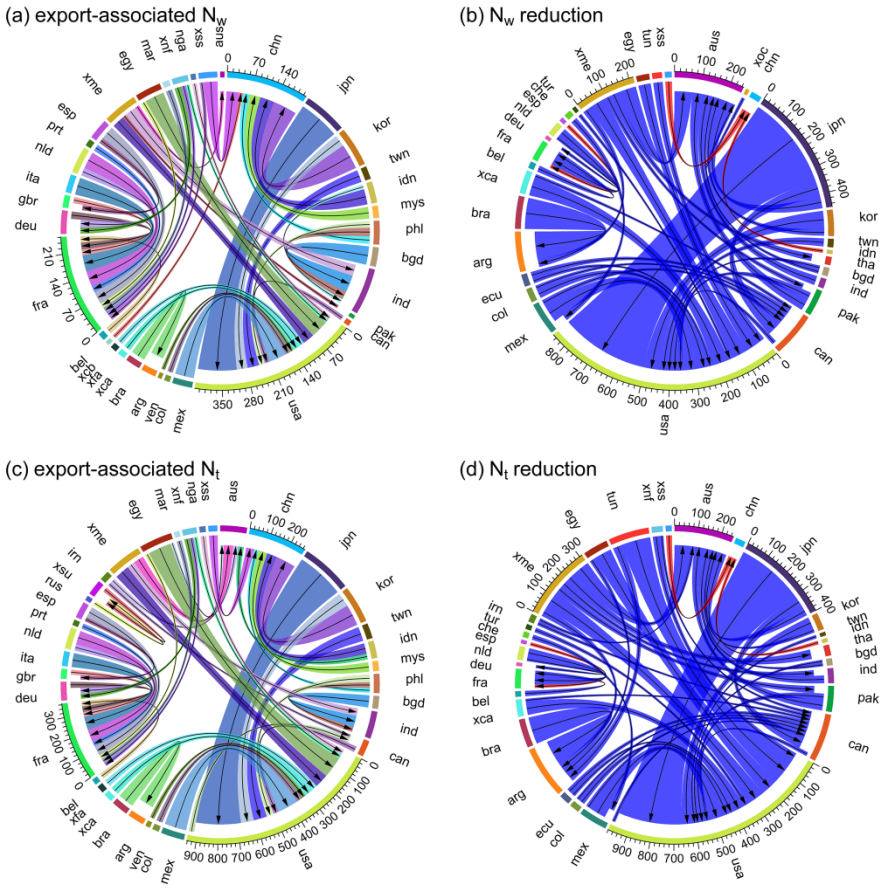

Figure 6-2. Export-associated nitrogen (N) losses in exporting countries and reduction in N losses through trade in three crops under the baseline. N_w: N losses to water (Gg N yr^{-1}); N_t: N losses to the total environment (Gg N yr^{-1}). Arrows point to food exporting countries; blue beams represent reduction in N losses in subplots b and d, while red beams represent increases in N losses; the links with volumes less than 0.5% of the global total are disregarded; numbers outside arcs show total volume of export-associated N losses and reduction in N losses for major trading countries. Regions are defined in Tables S6-2 and S6-3.

6.3.3 Impacts of agricultural intensification

Based on our PEPIC and GTAP simulations, agricultural intensification according to the N25I10 scenario would increase global crop production (Table S6-4) and decrease trade volumes in most trade links (Figure S6-2), especially for maize and rice, due to the relatively large increases in crop yields in importing countries with low-input crop production. But it would also largely increase maize export in Argentina and wheat export in Australia, mainly because of their significant yield increases under the N25I10 scenario and their important roles in exporting the two crops in the world. Consequently, global gross virtual water export and export-associated N losses would generally decrease in the N25I10 scenario compared to the baseline scenario, while the flow of virtual N_{in} would generally increase (Figures S6-9 and S6-10, Tables 6-1 and 6-2). The exceptions are that export-associated N_w would slightly increase for maize, that N_{in} would

largely decrease for rice, and that BWU would increase and N_{in} decrease for wheat. Agricultural intensification would also reduce export-associated N losses in some food exporting countries under the N25I10 scenario, e.g. China and India (Figure S6-10).

Table 6-2. Global export-associated nitrogen (N) losses in exporting countries and reduction in N losses through trade in maize, rice, and wheat under the baseline and N25I10 scenario. N_w: N losses to water; N_t: N losses to the total environment.

Scenario	Variable	Export-associated N losses in exporting countries				N loss reduction through food trade			
		maize	rice	wheat	sum	maize	rice	wheat	sum
baseline	N_w (Gg N yr^{-1})	534	344	1036	1914	638	64.8	1221	1924
	N_t (Gg N yr^{-1})	1026	499	2156	3681	826	125	1260	2211
N25I10	N_w (Gg N yr^{-1})	559	141	779	1479	431	0.2	983	1415
	N_t (Gg N yr^{-1})	1000	216	2080	3297	486	28.0	991	1505

Global resource conservation and N loss reduction through food trade could largely decline under the N25I10 scenario relative to the baseline, except resource conservation in BWU and TWU would increase for wheat (Tables 6-1 and 6-2). In particular, total N_{in} conservation of the three crops would decrease from 2333 Gg N yr^{-1} in the baseline to 871 Gg N yr^{-1} in the N25I10 scenario. Conservation in N_{in} for rice would become negative, indicating that global rice trade leads to increased consumption of N inputs. This is mainly due to substantial decreases in N_{in} conservation through food exported to the Middle East, where the major rice producer Iraq avoided N over-application and therefore N_{in} use intensity was reduced for the whole Middle East (Figure S6-13f). The declines in the contributions to resource conservation and N loss reduction were particularly large for the USA (Figures S6-9 and S6-10). For example, conservation in TWU through trade in the three crops drops from 40 km^3 yr^{-1} in the baseline to only 8 km^3 yr^{-1} in the N25I10 scenario in the USA. The major contributors of resource conservation and N loss reduction through global food trade would also change for each crop (Figures S6-11–S6-16).

6.4 Discussion

Previous studies found that global food trade could conserve TWU for crop production (Konar et al., 2013; Oki and Kanae, 2004), which is consistent with this study. Furthermore, we clearly presented that a large amount of BWU was conserved through food trade globally, reaching half of the total BWU consumption for producing the three crops. This is particularly important for managing global water resources, as TWU includes the dominant fraction of water resources from precipitation and soil moisture, which is difficult to use for other purpose (Rockström et al., 2009). To our best knowledge, also this study for the first time demonstrated that global food trade conserved N inputs and reduced N losses. This assessment largely improved

our understanding of the benefits of global food trade in terms of resource conservation and pollution reduction.

However, resource conservation and N loss reduction associated with global food trade were achieved at the expense of increased resource consumption and extra environmental pollution in the exporting countries. While, as found in this study, global food trade conserved substantial BWU, virtual water export has placed significant pressure on blue water sustainability in many exporting countries (Dalin and Conway, 2016; Dalin et al., 2014; Hoekstra and Mekonnen, 2016; Marston et al., 2015), particularly groundwater depletion induced by international food export (Dalin et al., 2017). For instance, about 9% of Japan's domestic cereal supply relied on water resources from overexploited aquifers in the USA (Marston et al., 2015). Continuous depletion of blue water resources, associated with an increasing burden of environmental degradation, is challenging virtual water trade (Zhao et al., 2016). From this point of view, reducing the virtual water export and pollution associated with food trade in the USA would reduce the pressure on its water resources and environment. This could partially explain why there are fewer and fewer countries exporting food (Porkka et al., 2013).

Our estimations of virtual water trade are comparable with previous studies. For example, Liu et al. (2009) concluded that around 6% of virtual water trade originated from BWU in 2000, consistent with our estimation. The total virtual TWU export of the three crops in this study (221 $km^3\ yr^{-1}$ under the baseline) is quite close to the estimate of Hanasaki et al. (2010) (213 $km^3\ yr^{-1}$ in 2000). Also the crop-specific comparison matches very well, i.e. 56, 35, 122 $km^3\ yr^{-1}$ for maize, rice, and wheat in Hanasaki et al. (2010) vs. 53, 27, 141 $km^3\ yr^{-1}$, respectively, in this study. However, due to a lack of crop-specific data on virtual N_{in} export and export-associated N losses, we could not compare our estimations of these variables with other studies. This calls for more integrated assessments of environmental impacts of international food trade by taking multi-metrics into consideration (Dalin and Rodriguez-Iturbe, 2016; MacDonald et al., 2015).

The N25I10 scenario included the effects of intensification in irrigation and N inputs and avoidance of N over-application. Therefore, crop yields and consumption in BWU and TWU would increase. Also, N_{in} would increase and more N would be lost to the environment in regions that under-applied N in the baseline. However, changes in resource use intensities and N loss intensities between N25I10 and baseline were quite different for different countries, due to different input intensification levels considered by the N25I10 scenario and different agro-climatic yield potentials (Mueller et al., 2012). Generally, resource use intensities and N loss intensities would converge across countries in the intensification scenario compared to the baseline situation (Tables S6-5–S7). Combining the decreased export volumes in most food trade links (Figure S6-2), input intensification according to the N25I10 scenario could largely reduce

global resource conservation and N loss reduction associated with food trade. Still, input intensification creates a more level playing field. It improves crop yields, reduces the need for import and enhances self-sufficiency and food security, particularly for the lowest performing countries in Africa (Sanchez, 2010). Another positive outcome of input intensification would be the reduced resource consumption and exported-associated N losses for the major exporting countries.

In order to investigate the impact of agricultural intensification on crop trade, we used percentage increases in yields derived from improved N and irrigation management as input to run the GTAP model. While there are other factors (e.g. population, policy, and technology) that can affect food trade (Dalin et al., 2015), only considering changes in yields is a common practice in using GTAP in order to reduce the complexity of the simulation (Konar et al., 2013; Konar et al., 2016). With this approach, we isolated the influence of increased N and irrigation inputs, particularly in countries with low inputs in the baseline, on global food trade by keeping other factors unchanged. Our main research objective was achieved. Including other factors, which may change trade picture, deserves more detailed research in the future.

6.5 Conclusions

In this study, we combined the PEPIC model with the GTAP model to investigate the impacts of international trade in three major crops on resource uses and N losses in the baseline year 2000 and an intensification scenario regarding increased N and irrigation inputs. For the first time we systematically demonstrated that global food trade did reduce N losses and conserve a large amount of N inputs and water resources. In particular, conservation in BWU through food trade accounted for more than half of the total BWU consumption for producing the three crops. This suggests that enlarging food trade could further improve these benefits. However, it brings challenges in enhancing self-sufficiency and food security for the lowest performing countries. Agricultural intensification improves crop yields and holds the key to address the challenges. However, as a result of the converging resource use and pollution intensities across countries, resource conservation and pollution reduction associated with international food trade will decline under the intensification scenario. The study provides useful information to understand the implications of international food trade and agricultural intensification on resource uses and pollution patterns.

6.6 References

Antonelli, M., Tamea, S. and Yang, H., 2017. Intra-EU agricultural trade, virtual water flows and policy implications. Sci. Total Environ., 587–588: 439–448.

Balkovič, J. et al., 2014. Global wheat production potentials and management flexibility under the representative concentration pathways. Global Planet. Change, 122: 107–121.

Batjes, N.H., 2006. ISRIC–WISE derived soil properties on a 5 by 5 arc-minutes global grid (version 1.1), ISRIC – World Soil Infromation, Wageningen.

Chapagain, A.K., Hoekstra, A.Y. and Savenije, H.H.G., 2006. Water saving through international trade of agricultural products. Hydrol. Earth Syst. Sc., 10(3): 455–468.

Dalin, C. and Conway, D., 2016. Water resources transfers through southern African food trade: water efficiency and climate signals. Environ. Res. Lett., 11(1): 035012.

Dalin, C., Hanasaki, N., Qiu, H.G., Mauzerall, D.L. and Rodriguez-Iturbe, I., 2014. Water resources transfers through Chinese interprovincial and foreign food trade. Proc. Natl. Acad. Sci. U.S.A., 111(27): 9774–9779.

Dalin, C., Konar, M., Hanasaki, N., Rinaldo, A. and Rodriguez-Iturbe, I., 2012. Evolution of the global virtual water trade network. Proc. Natl. Acad. Sci. U.S.A., 109(16): 5989–94.

Dalin, C., Qiu, H., Hanasaki, N., Mauzerall, D.L. and Rodriguez-Iturbe, I., 2015. Balancing water resource conservation and food security in China. Proc. Natl. Acad. Sci. U.S.A., 112(15): 4588–4593.

Dalin, C. and Rodriguez-Iturbe, I., 2016. Environmental impacts of food trade via resource use and greenhouse gas emissions. Environ. Res. Lett., 11(3): 035012.

Dalin, C., Wada, Y., Kastner, T. and Puma, M.J., 2017. Groundwater depletion embedded in international food trade. Nature, 543(7647): 700–704.

Elliott, J. et al., 2015. The Global Gridded Crop Model Intercomparison: data and modeling protocols for Phase 1 (v1.0). Geosci. Model Dev., 8(2): 261–277.

Fader, M. et al., 2011. Internal and external green–blue agricultural water footprints of nations, and related water and land savings through trade. Hydrol. Earth Syst. Sc., 15(5): 1641–1660.

Feng, K.S. et al., 2013. Outsourcing CO_2 within China. Proc. Natl. Acad. Sci. U.S.A., 110(28): 11654–11659.

Folberth, C. et al., 2016. Uncertainty in soil data can outweigh climate impact signals in global crop yield simulations. Nat. Commun., 7: 11872.

Folberth, C. et al., 2014. Effects of ecological and conventional agricultural intensification practices on maize yields in sub-Saharan Africa under potential climate change. Environ. Res. Lett., 9(4): 044004.

Hanasaki, N., Inuzuka, T., Kanae, S. and Oki, T., 2010. An estimation of global virtual water flow and sources of water withdrawal for major crops and livestock products using a global hydrological model. J. Hydrol., 384(3–4): 232–244.

Hertel, T.W., 1997. Global trade analysis: modeling and applications. Cambridge university press.

Hoekstra, A.Y., 2017. Water footprint assessment: Evolvement of a new research field. Water Resour. Manage. doi:10.1007/s11269-017-1618-5

Hoekstra, A.Y. and Hung, P.Q., 2005. Globalisation of water resources: international virtual water flows in relation to crop trade. Global Environ. Change, 15(1): 45–56.

Hoekstra, A.Y. and Mekonnen, M.M., 2012. The water footprint of humanity. Proc. Natl. Acad. Sci. U.S.A., 109(9): 3232–3237.

Hoekstra, A.Y. and Mekonnen, M.M., 2016. Imported water risk: the case of the UK. Environ. Res. Lett., 11(5): 055002.

Kastner, T., Erb, K.H. and Haberl, H., 2014. Rapid growth in agricultural trade: effects on global area efficiency and the role of management. Environ. Res. Lett., 9(3): 034015.

Konar, M., Hussein, Z., Hanasaki, N., Mauzerall, D.L. and Rodriguez-Iturbe, I., 2013. Virtual water trade flows and savings under climate change. Hydrol. Earth Syst. Sc., 17(8): 3219–3234.

Konar, M., Reimer, J.J., Hussein, Z. and Hanasaki, N., 2016. The water footprint of staple crop trade under climate and policy scenarios. Environ. Res. Lett., 11(3): 035006.

Lassaletta, L. et al., 2016. Nitrogen use in the global food system: past trends and future trajectories of agronomic performance, pollution, trade, and dietary demand. Environ. Res. Lett., 11(9): 095007.

Lin, J. et al., 2016. Global climate forcing of aerosols embodied in international trade. Nat. Geosci., 9(10): 790–794.

Lin, J.T. et al., 2014. China's international trade and air pollution in the United States. Proc. Natl. Acad. Sci. U.S.A., 111(5): 1736–1741.

Liu, J., Hertel, T.W., Taheripour, F., Zhu, T.J. and Ringler, C., 2014. International trade buffers the impact of future irrigation shortfalls. Global Environ. Change, 29: 22–31.

Liu, J., Zehnder, A.J.B. and Yang, H., 2009. Global consumptive water use for crop production: The importance of green water and virtual water. Water Resour. Res., 45(5): W05428.

Liu, W. et al., 2016a. Global investigation of impacts of PET methods on simulating crop–water relations for maize. Agric. For. Meteorol., 221: 164–175.

Liu, W. et al., 2016b. Global assessment of nitrogen losses and trade-offs with yields from major crop cultivations. Sci. Total Environ., 572: 526–537.

MacDonald, G.K., Bennett, E.M. and Carpenter, S.R., 2012. Embodied phosphorus and the global connections of United States agriculture. Environ. Res. Lett., 7(4): 044024.

MacDonald, G.K. et al., 2015. Rethinking agricultural trade relationships in an era of globalization. Bioscience, 65(3): 275–289.

Marston, L., Konar, M., Cai, X.M. and Troy, T.J., 2015. Virtual groundwater transfers from overexploited aquifers in the United States. Proc. Natl. Acad. Sci. U.S.A., 112(28): 8561–8566.

Martinez-Melendez, L.A. and Bennett, E.M., 2016. Trade in the US and Mexico helps reduce environmental costs of agriculture. Environ. Res. Lett., 11(5): 055004.

Mueller, N.D. et al., 2012. Closing yield gaps through nutrient and water management. Nature, 490(7419): 254–257.

Müller, C. et al., 2017. Global gridded crop model evaluation: benchmarking, skills, deficiencies and implications. Geosci. Model Dev., 10(4): 1403–1422.

Nesme, T., Roques, S., Metson, G.S. and Bennett, E.M., 2016. The surprisingly small but increasing role of international agricultural trade on the European Union's dependence on mineral phosphorus fertiliser. Environ. Res. Lett., 11(2): 025003.

O'Bannon, C., Carr, J., Seekell, D.A. and D'Odorico, P., 2014. Globalization of agricultural pollution due to international trade. Hydrol. Earth Syst. Sc., 18(2): 503–510.

Oita, A. et al., 2016. Substantial nitrogen pollution embedded in international trade. Nat. Geosci., 9(2): 111–115.

Oki, T. and Kanae, S., 2004. Virtual water trade and world water resources. Water Sci. Technol., 49(7): 203–209.

Peters, G.P., Minx, J.C., Weber, C.L. and Edenhofer, O., 2011. Growth in emission transfers via international trade from 1990 to 2008. Proc. Natl. Acad. Sci. U.S.A., 108(21): 8903–8908.

Porkka, M., Guillaume, J.H.A., Siebert, S., Schaphoff, S. and Kummu, M., 2017. The use of food imports to overcome local limits to growth. Earth's Future. doi:10.1002/2016EF000477

Porkka, M., Kummu, M., Siebert, S. and Varis, O., 2013. From food insufficiency towards trade dependency: A historical analysis of global food availability. PLoS One, 8(12): e82714.

Portmann, F.T., Siebert, S. and Doll, P., 2010. MIRCA2000–Global monthly irrigated and rainfed crop areas around the year 2000: A new high-resolution data set for agricultural and hydrological modeling. Global Biogeochem. Cycles, 24: GB1011.

Porwollik, V. et al., 2016. Spatial and temporal uncertainty of crop yield aggregations. Eur. J. Agron. doi: 10.1016/j.eja.2016.08.006

Rockström, J. et al., 2009. Future water availability for global food production: The potential of green water for increasing resilience to global change. Water Resour. Res., 45: W00A12.

Rosenzweig, C. et al., 2013. The Agricultural Model Intercomparison and Improvement Project (AgMIP): Protocols and pilot studies. Agric. For. Meteorol., 170: 166–182.

Sacks, W.J., Deryng, D., Foley, J.A. and Ramankutty, N., 2010. Crop planting dates: an analysis of global patterns. Global Ecol. Biogeogr., 19(5): 607–620.

Sanchez, P.A., 2010. Tripling crop yields in tropical africa. Nat. Geosci., 3(5): 299–300.

Wan, L.Y., Cai, W.J., Jiang, Y.K. and Wang, C., 2016. Impacts on quality-induced water scarcity: drivers of nitrogen-related water pollution transfer under globalization from 1995 to 2009. Environ. Res. Lett., 11(7): 074017.

Weedon, G.P. et al., 2014. The WFDEI meteorological forcing data set: WATCH Forcing Data methodology applied to ERA-Interim reanalysis data. Water Resour. Res., 50(9): 7505–7514.

West, P.C. et al., 2014. Leverage points for improving global food security and the environment. Science, 345(6194): 325–328.

Williams, J.R., 1995. The EPIC model. In: V.P. Singh (Editor), Computer Models of Watershed hydrology. Water Resources Publications, Highlands Ranch, Colo.

Williams, J.R., Jones, C.A. and Dyke, P.T., 1984. A modeling approach to determining the relationship between erosion and soil productivity. Trans. ASAE, 27(1): 129–144.

Yang, H., Pfister, S. and Bhaduri, A., 2013. Accounting for a scarce resource: virtual water and water footprint in the global water system. Curr. Opin. Environ. Sustainability, 5(6): 599–606.

Yang, H., Wang, L., Abbaspour, K.C. and Zehnder, A.J.B., 2006. Virtual water trade: an assessment of water use efficiency in the international food trade. Hydrol. Earth Syst. Sc., 10(3): 443–454.

Zhang, Q. et al., 2017. Transboundary health impacts of transported global air pollution and international trade. Nature, 543(7647): 705–709.

Zhao, X. et al., 2016. Burden shifting of water quantity and quality stress from megacity Shanghai. Water Resour. Res., 52(9): 6916–6927.

Zhao, X. et al., 2015. Physical and virtual water transfers for regional water stress alleviation in China. Proc. Natl. Acad. Sci. U.S.A., 112(4): 1031–1035.

Supplementary information for

Resource conservation and pollution reduction in the context of global food trade and agricultural intensification

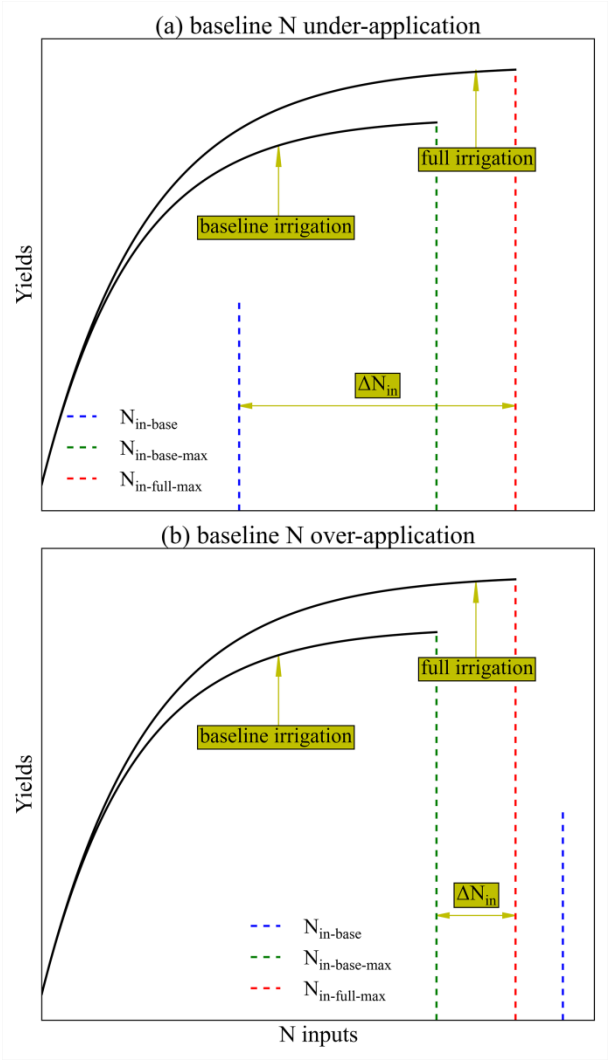

Figure S6-1. Conceptual description for obtaining the maximum increases in nitrogen (N) inputs under baseline N under-application condition (a) and baseline N over-application condition (b). $N_{in\text{-}base}$: baseline N inputs based on EarthStat dataset; $N_{in\text{-}base\text{-}max}$: maximum N inputs based on PEPIC simulation with baseline irrigation condition; $N_{in\text{-}full\text{-}max}$: maximum N inputs based on PEPIC simulation with full irrigation condition. $\Delta N_{in} = N_{in\text{-}full\text{-}max} - N_{in\text{-}base\text{-}limit}$, where $N_{in\text{-}base\text{-}limit} = min(N_{in\text{-}base}, N_{in\text{-}base\text{-}max})$.

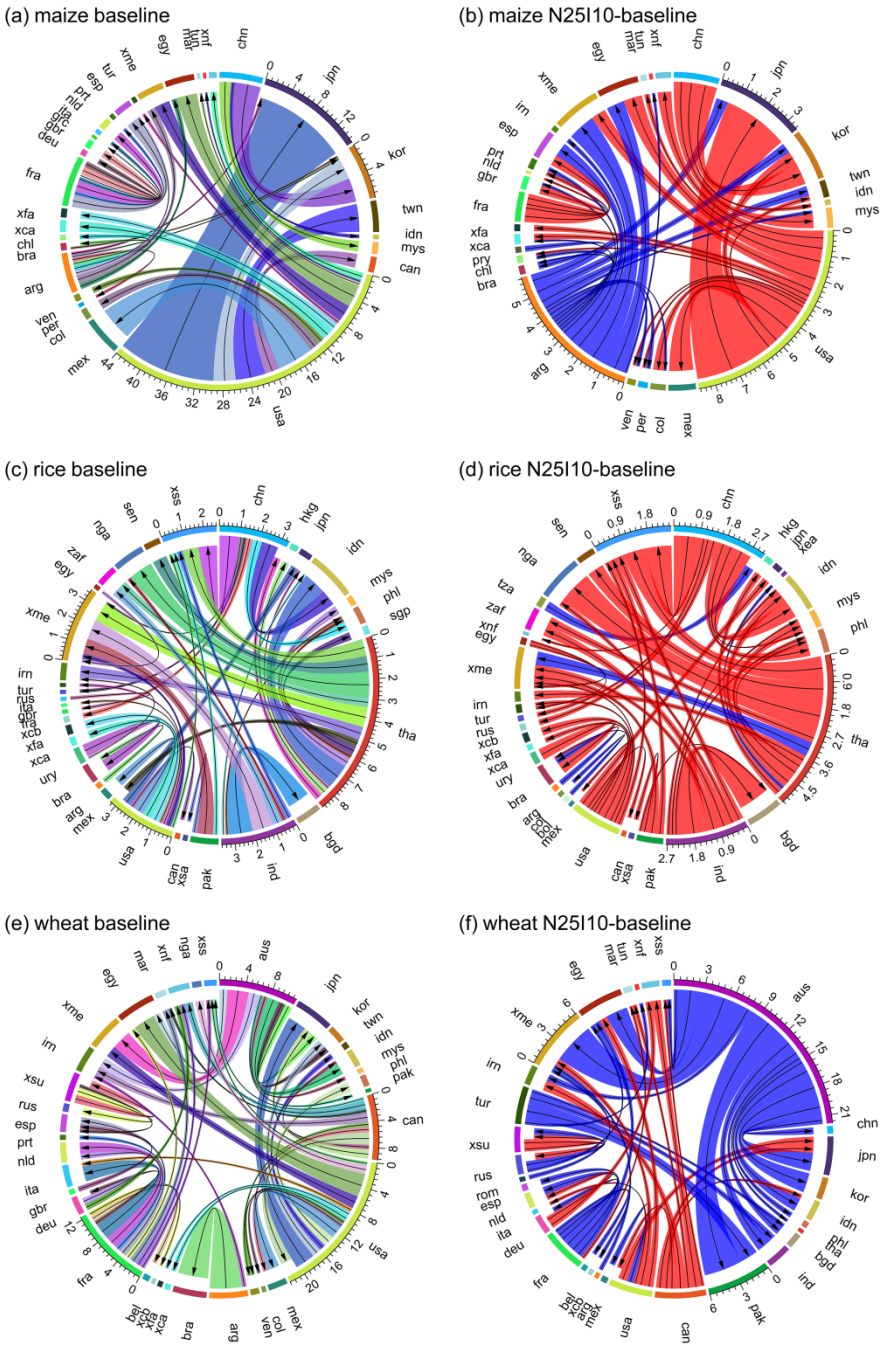

Figure S6-2. Food export volume (Tg yr^{-1}) for maize, wheat and rice under baseline and differences between N25I10 and baseline. Arrows point to food importing countries; blue beams represent increases in export volume in subplots b, d, and f, while red beams represent decreases in export volume; the links with volumes less than 0.5% of the global total are disregarded; numbers outside arcs show total trade volume for major trading countries. Regions are defined in Tables S6-2 and S6-3.

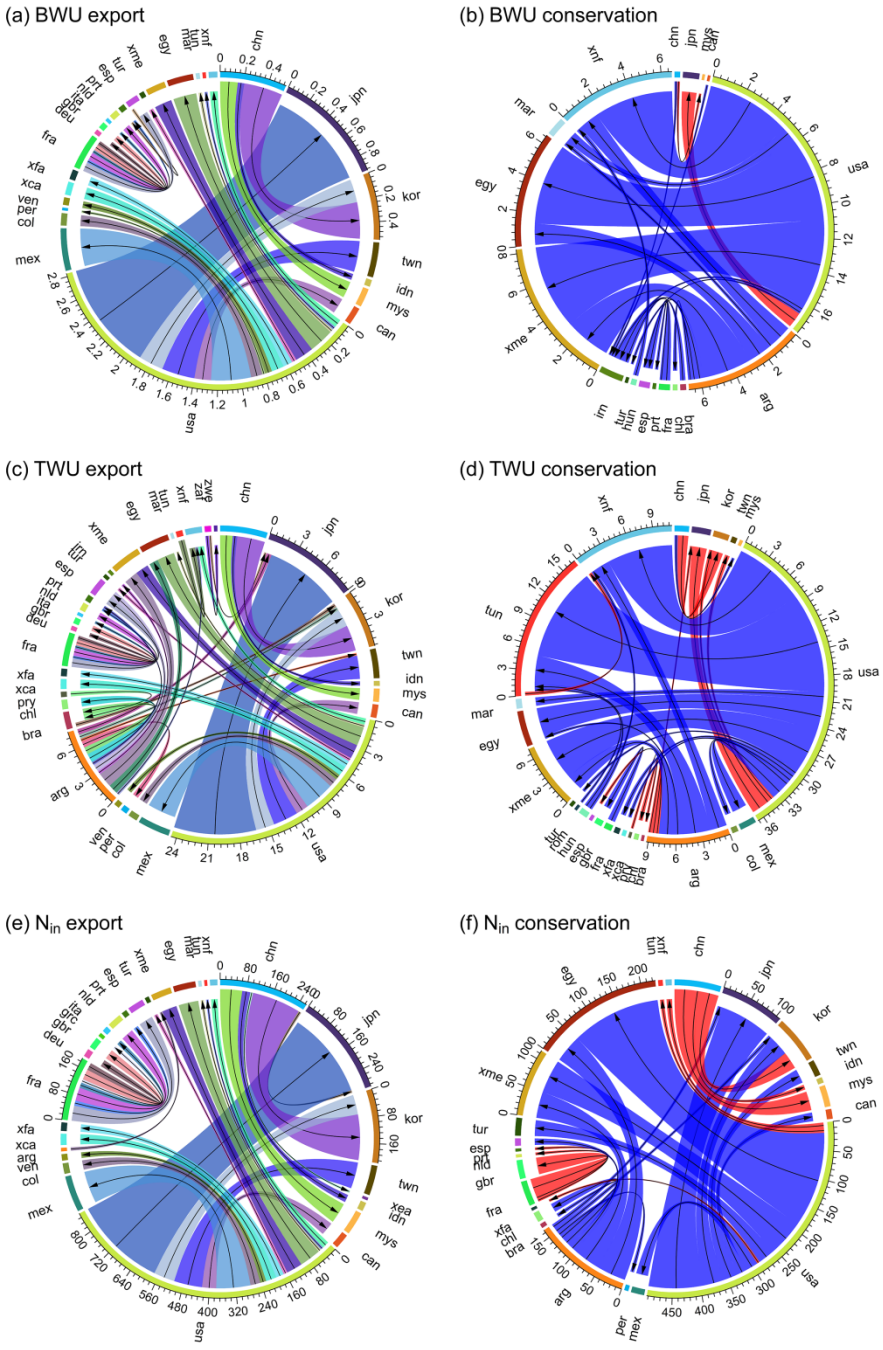

Figure S6-3. Gross virtual resource export to importing countries and resource conservation through trade in maize under the baseline. BW: blue water (km^3 yr^{-1}); TWU: total water use (km^3 yr^{-1}); N_{in}: nitrogen inputs (Gg N yr^{-1}). Arrows point to food importing countries; blue beams represent resource conservation in subplots b, d, and f, while red beams represent increases in resource consumption; the links with volumes less than 0.5% of the global total are disregarded; numbers outside arcs show total volume of export and conservation for major trading countries. Regions are defined in Tables S6-2 and S6-3.

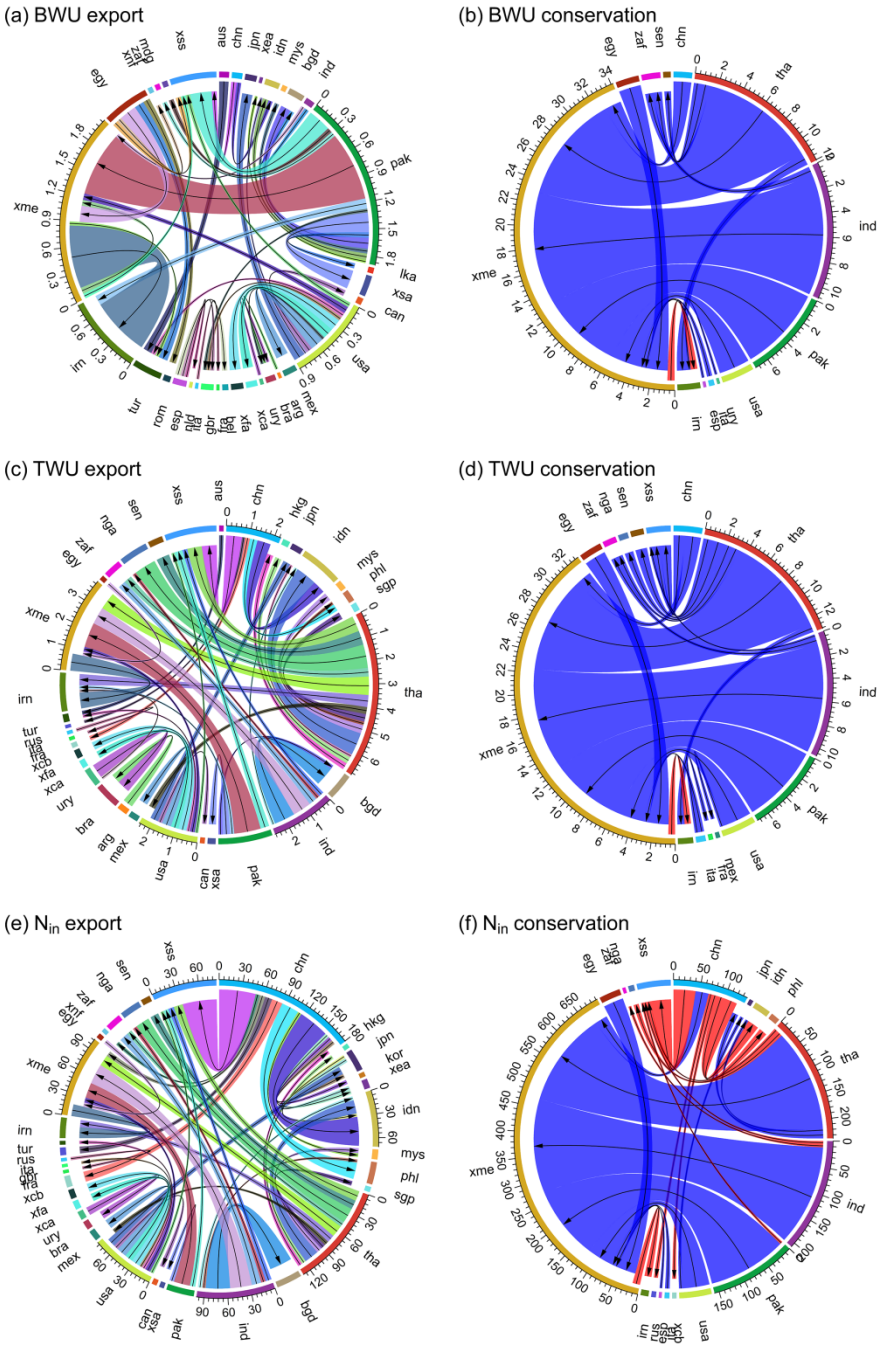

Figure S6-4. Gross virtual resource export to importing countries and resource conservation through trade in rice under the baseline. BW: blue water (km^3 yr^{-1}); TWU: total water use (km^3 yr^{-1}); N$_{in}$: nitrogen inputs (Gg N yr^{-1}). Arrows point to food importing countries; blue beams represent resource conservation in subplots b, d, and f, while red beams represent increases in resource consumption; the links with volumes less than 0.5% of the global total are disregarded; numbers outside arcs show total volume of export and conservation for major trading countries. Regions are defined in Tables S6-2 and S6-3.

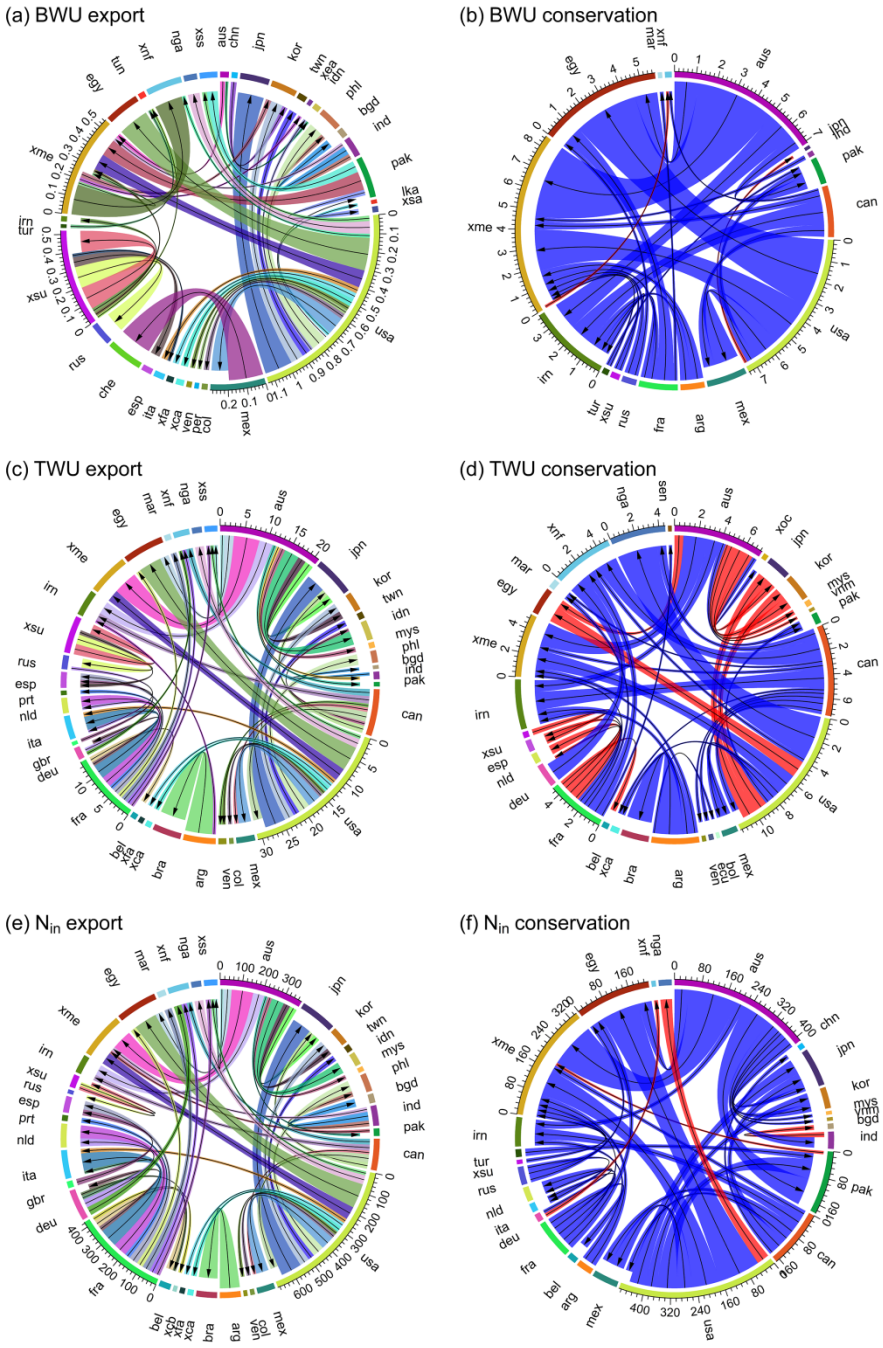

Figure S6-5. Gross virtual resource export to importing countries and resource conservation through trade in wheat under the baseline. BW: blue water (km^3 yr^{-1}); TWU: total water use (km^3 yr^{-1}); N_{in}: nitrogen inputs (Gg N yr^{-1}). Arrows point to food importing countries; blue beams represent resource conservation in subplots b, d, and f, while red beams represent increases in resource consumption; the links with volumes less than 0.5% of the global total are disregarded; numbers outside arcs show total volume of export and conservation for major trading countries. Regions are defined in Tables S6-2 and S6-3.

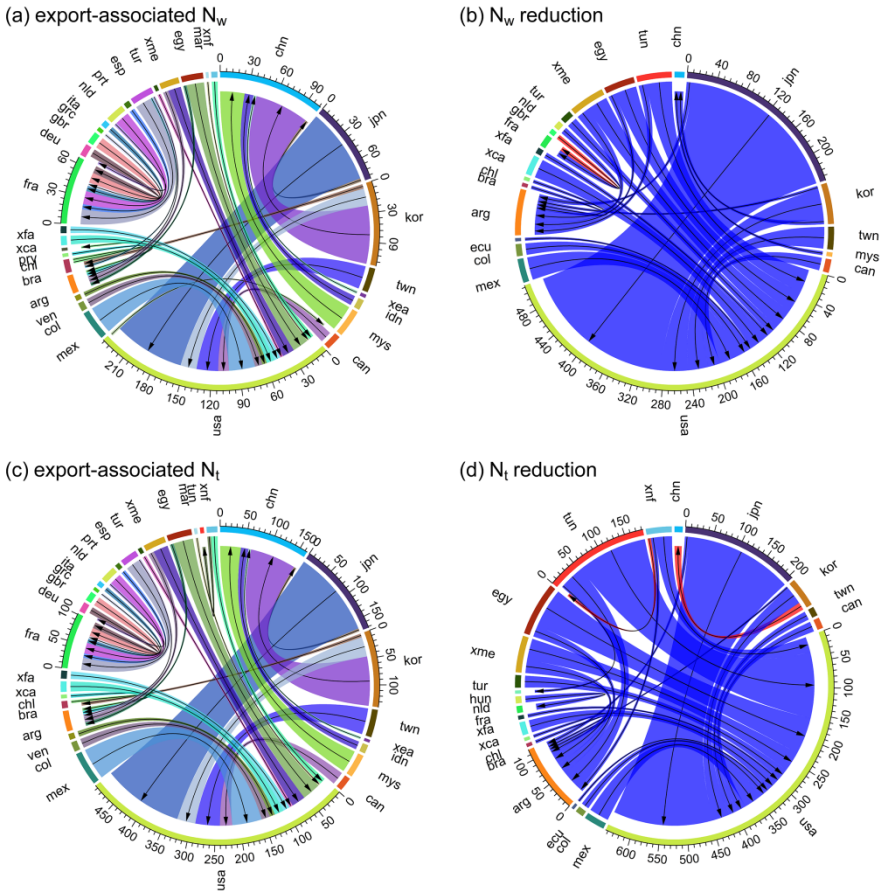

Figure S6-6. Export-associated nitrogen (N) losses in exporting countries and reduction in N losses through trade in maize under the baseline. N_w: N losses to water (Gg N yr^{-1}); N_t: N losses to the total environment (Gg N yr^{-1}). Arrows point to food exporting countries; blue beams represent reduction in N losses in subplots b and d, while red beams represent increases in N losses; the links with volumes less than 0.5% of the global total are disregarded; numbers outside arcs show total volume of exported-associated N losses and reduction in N losses for major trading countries. Regions are defined in Tables S6-2 and S6-3.

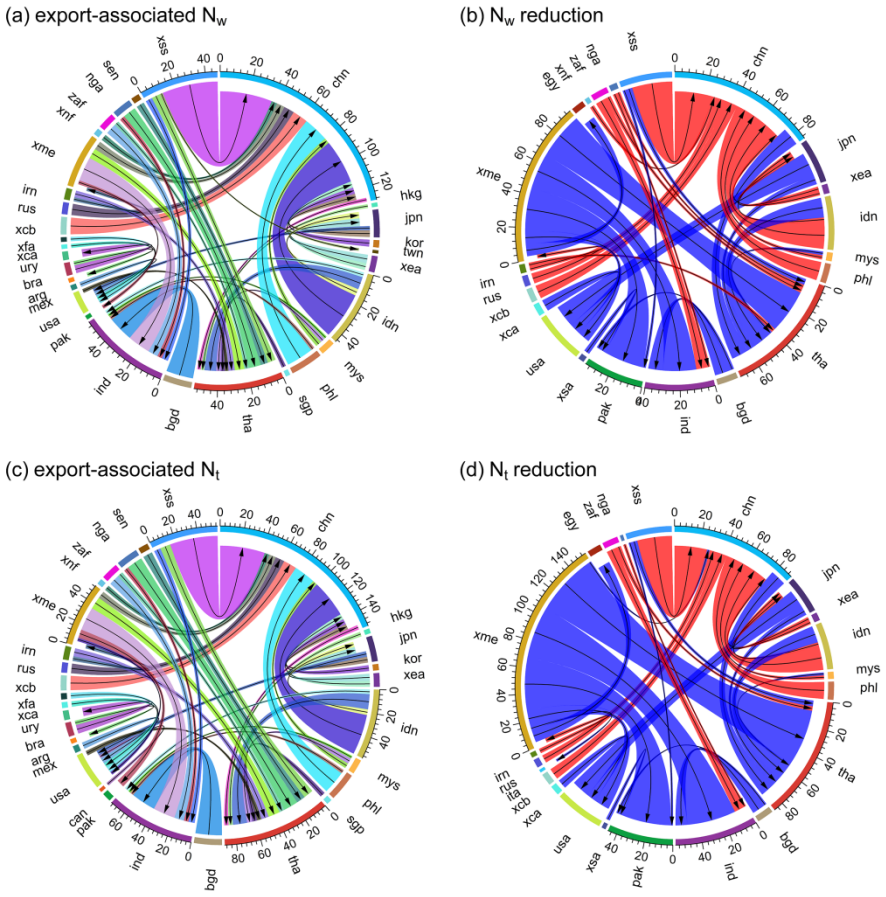

Figure S6-7. Export-associated nitrogen (N) losses in exporting countries and reduction in N losses through trade in rice under the baseline. N_w: N losses to water (Gg N yr^{-1}); N_t: N losses to the total environment (Gg N yr^{-1}). Arrows point to food exporting countries; blue beams represent reduction in N losses in subplots b and d, while red beams represent increases in N losses; the links with volumes less than 0.5% of the global total are disregarded; numbers outside arcs show total volume of exported-associated N losses and reduction in N losses for major trading countries. Regions are defined in Tables S6-2 and S6-3.

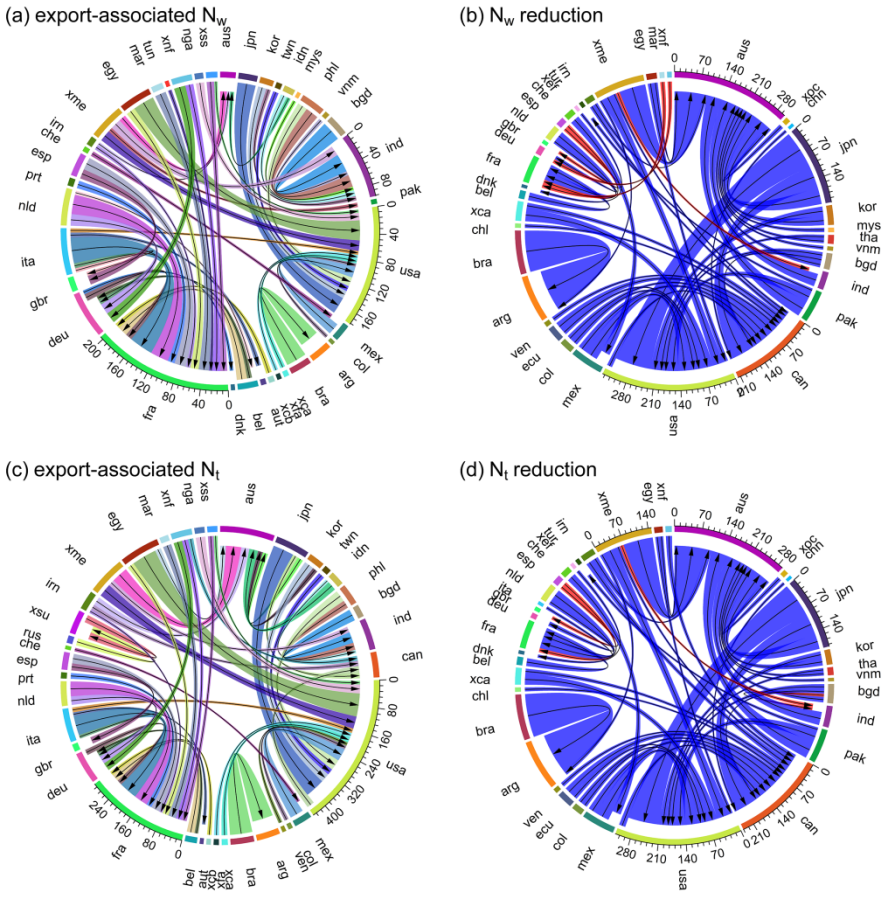

Figure S6-8. Export-associated nitrogen (N) losses in exporting countries and reduction in N losses through trade in wheat under the baseline. N_w: N losses to water (Gg N yr^{-1}); N_t: N losses to the total environment (Gg N yr^{-1}). Arrows point to food exporting countries; blue beams represent reduction in N losses in subplots b and d, while red beams represent increases in N losses; the links with volumes less than 0.5% of the global total are disregarded; numbers outside arcs show total volume of exported-associated N losses and reduction in N losses for major trading countries. Regions are defined in Tables S6-2 and S6-3.

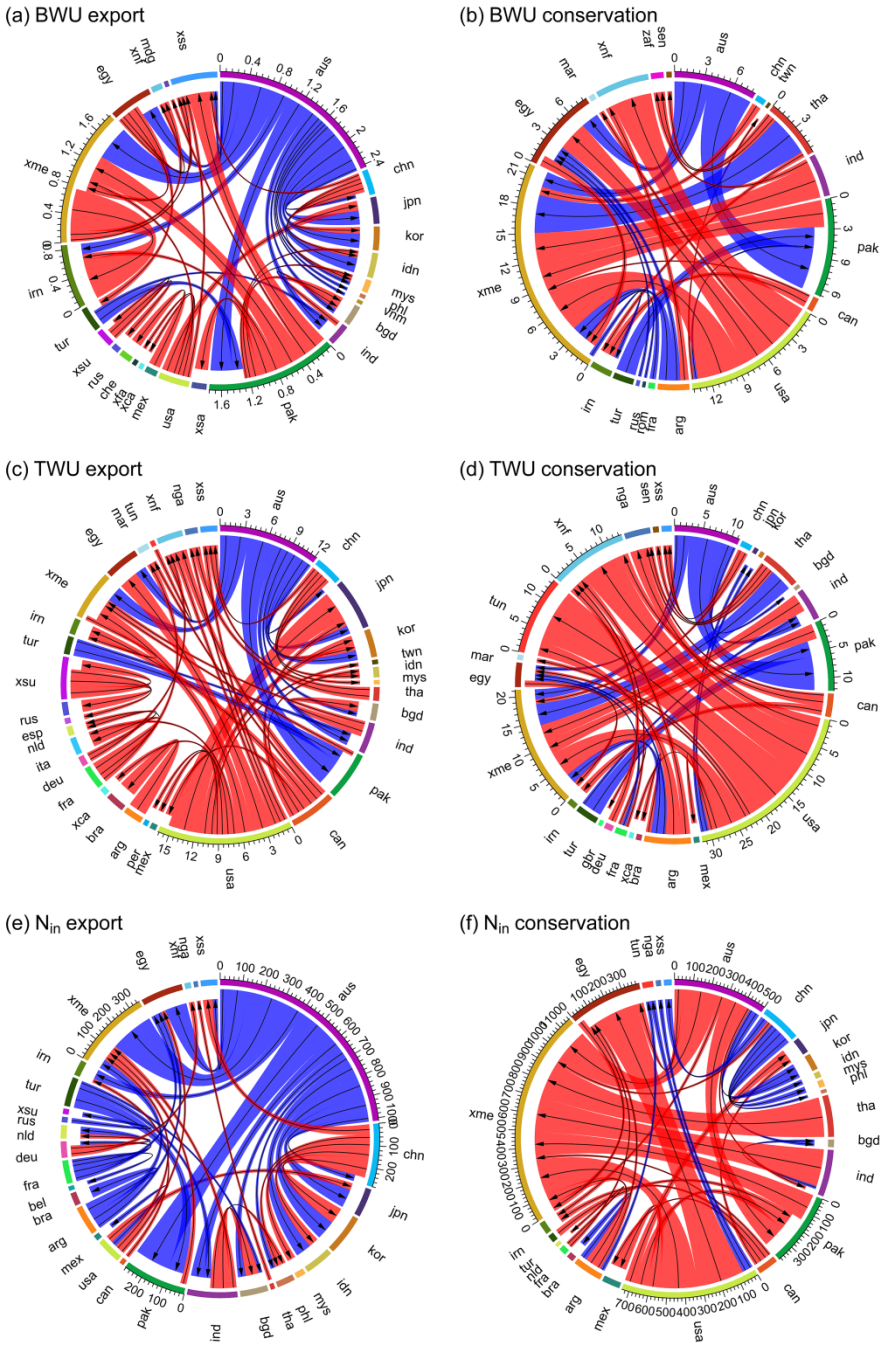

Figure S6-9. Differences of gross virtual resource export to importing countries and resource conservation through trade in the three crops between N25I10 and baseline. BW: blue water (km^3 yr^{-1}); TWU: total water use (km^3 yr^{-1}); N_{in}: nitrogen inputs (Gg N yr^{-1}). Arrows point to food importing countries; blue beams represent increases in gross virtual resource export and red beams show decreases in gross virtual resource export in subplots a, c, and e; blue beams represent increases in resource conservation and red beams show decreases in resource conservation in subplots b, d, and f; the links with volumes less than 0.5% of the global total are disregarded; numbers outside arcs show total volume of export and conservation for major trading countries. Regions are defined in Tables S6-2 and S6-3.

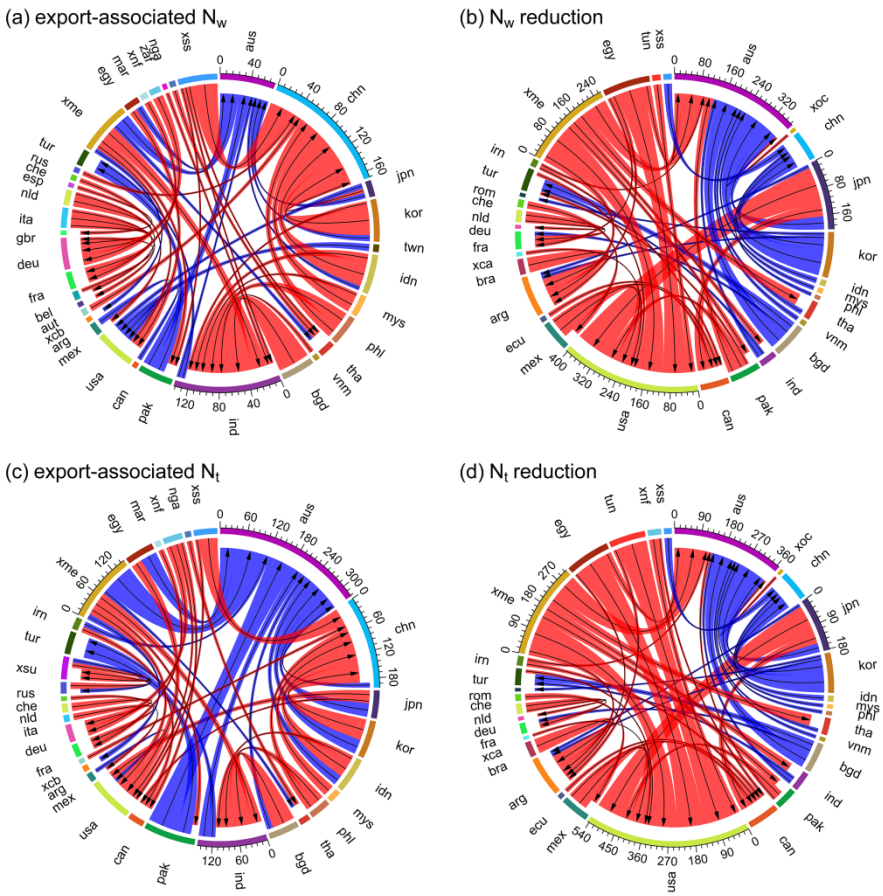

Figure S6-10. Differences of export-associated nitrogen (N) losses in exporting countries and N loss reduction through trade in the three crops between N25I10 and baseline. N_w: N losses to water (Gg N yr^{-1}); N_t: N losses to the total environment (Gg N yr^{-1}). Arrows point to food exporting countries; blue beams represent increases in export-associated N losses and red beams show decreases in export-associated N losses in subplots a and c; blue beams represent increases in N loss reduction and red beams show decreases in N loss reduction in subplots b and d; the links with volumes less than 0.5% of global total are disregarded; numbers outside arcs show total volume of export-associated N losses and N loss reduction for major trading countries. Regions are defined in Tables S6-2 and S6-3.

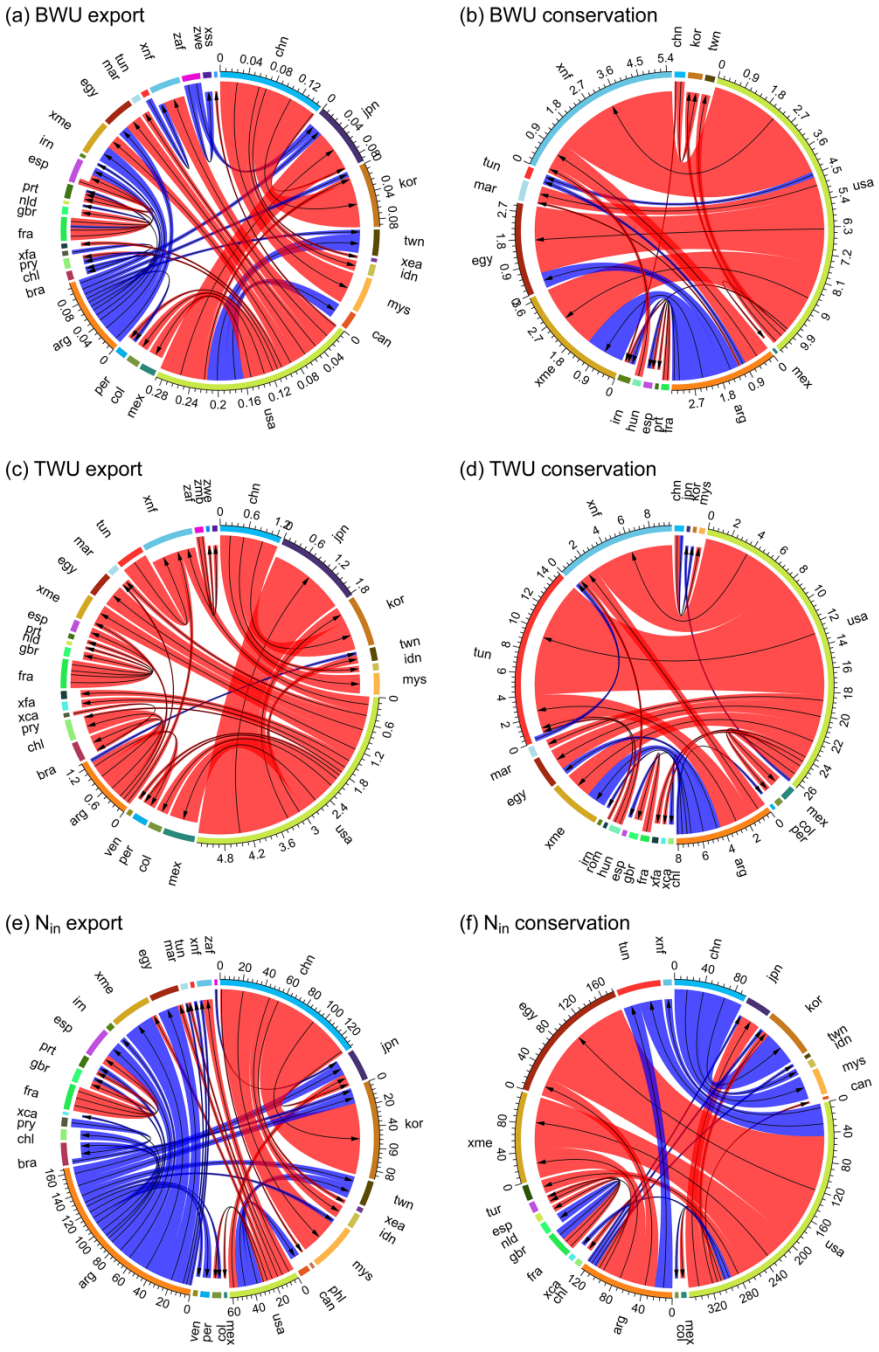

Figure S6-11. Differences of gross virtual resource export to importing countries and resource conservation through trade in maize between N25I10 and baseline. BW: blue water (km^3 yr^{-1}); TWU: total water use (km^3 yr^{-1}); N_{in}: nitrogen inputs (Gg N yr^{-1}). Arrows point to food importing countries; blue beams represent increases in gross virtual resource export and red beams show decreases in gross virtual resource export in subplots a, c, and e; blue beams represent increases in resource conservation and red beams show decreases in resource conservation in subplots b, d, and f; the links with volumes less than 0.5% of the global total are disregarded; numbers outside arcs show total volume of export and conservation for major trading countries. Regions are defined in Tables S6-2 and S6-3.

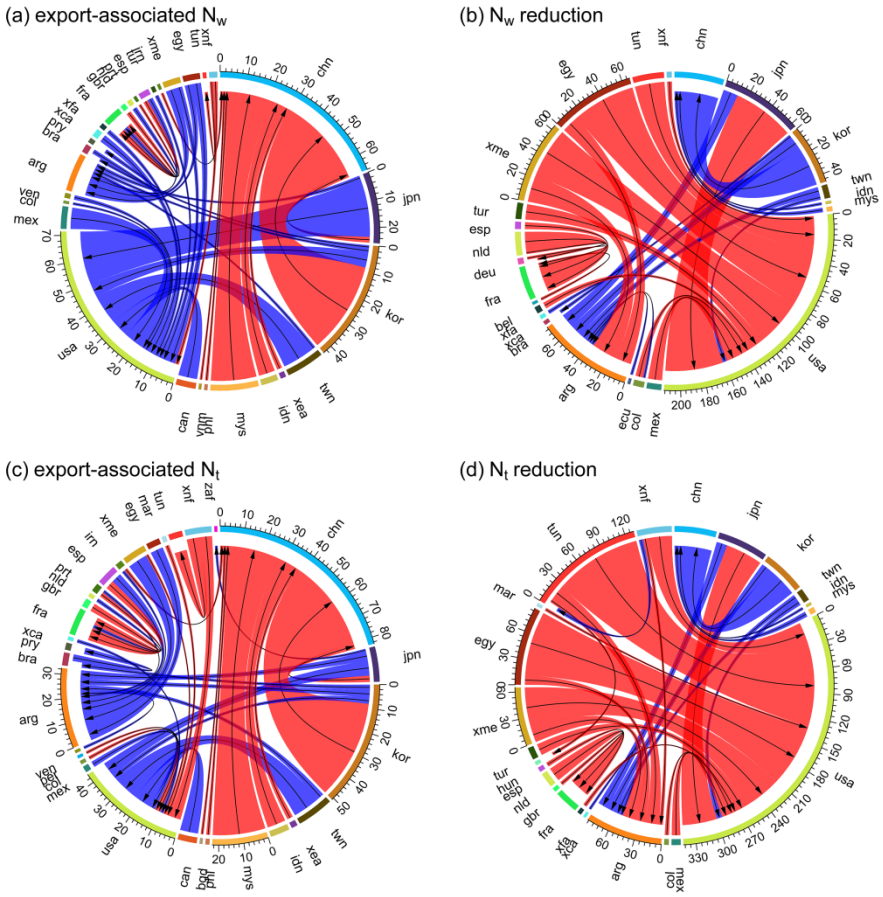

Figure S6-12. Differences of export-associated nitrogen (N) losses in exporting countries and N loss reduction through trade in maize between N25I10 and baseline. N_w: N losses to water (Gg N yr^{-1}); N_t: N losses to the total environment (Gg N yr^{-1}). Arrows point to food exporting countries; blue beams represent increases in export-associated N losses and red beams show decreases in export-associated N losses in subplots a and c; blue beams represent increases in N loss reduction and red beams show decreases in N loss reduction in subplots b and d; the links with volumes less than 0.5% of global total are disregarded; numbers outside arcs show total volume of export-associated N losses and N loss reduction for major trading countries. Regions are defined in Tables S6-2 and S6-3.

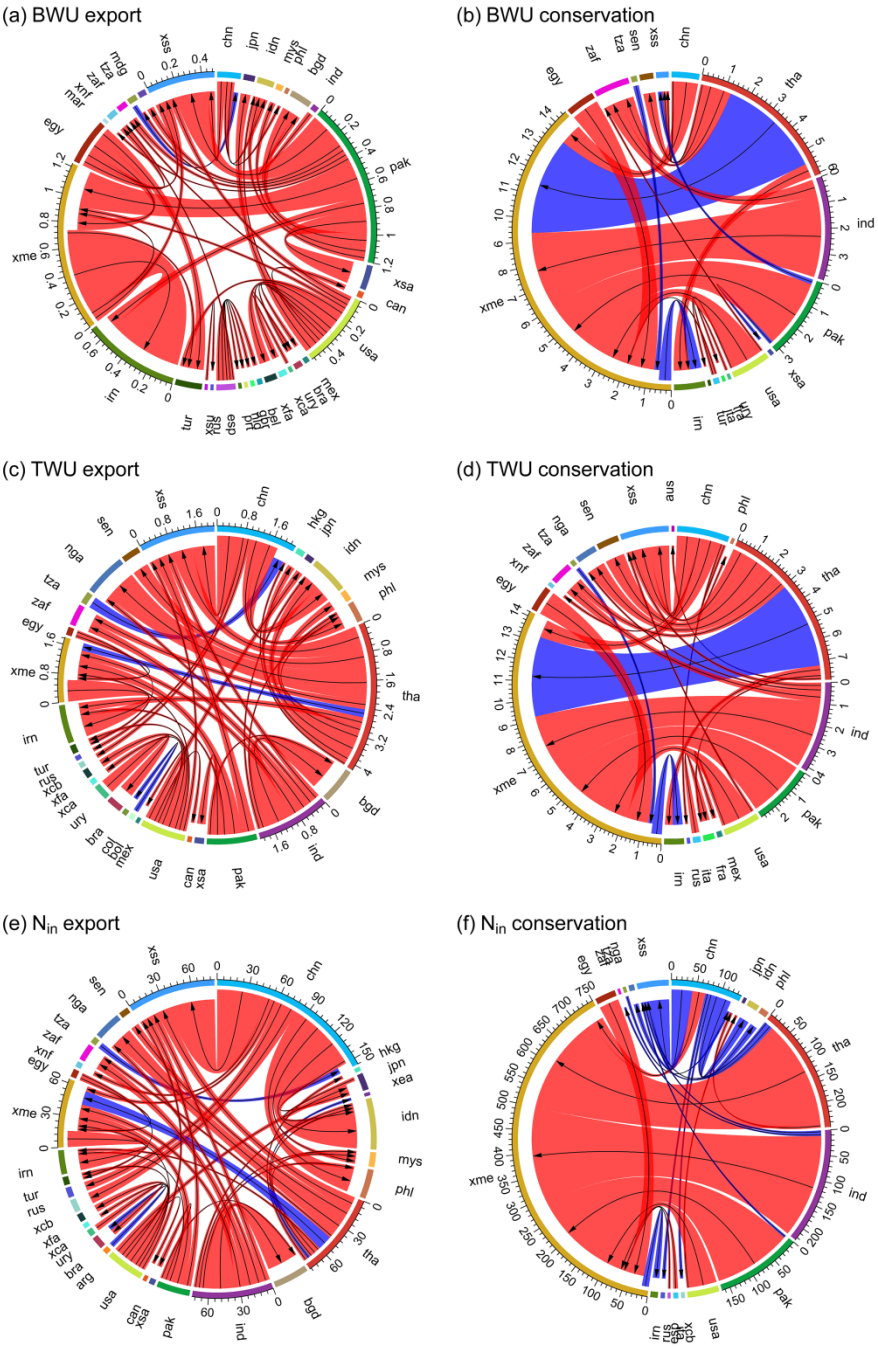

Figure S6-13. Differences of gross virtual resource export to importing countries and resource conservation through trade in rice between N25I10 and baseline. BW: blue water (km^3 yr^{-1}); TWU: total water use (km^3 yr^{-1}); N_{in}: nitrogen inputs (Gg N yr^{-1}). Arrows point to food importing countries; blue beams represent increases in gross virtual resource export and red beams show decreases in gross virtual resource export in subplots a, c, and e; blue beams represent increases in resource conservation and red beams show decreases in resource conservation in subplots b, d, and f; the links with volumes less than 0.5% of the global total are disregarded; numbers outside arcs show total volume of export and conservation for major trading countries. Regions are defined in Tables S6-2 and S6-3.

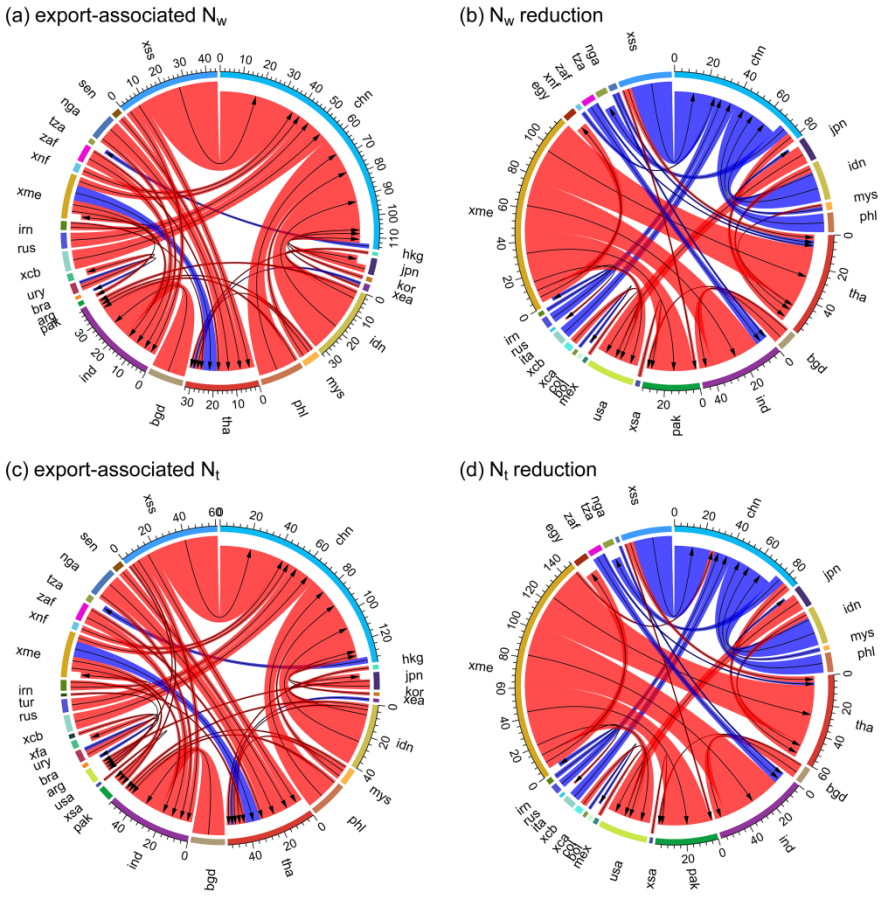

Figure S6-14. Differences of export-associated nitrogen (N) losses in exporting countries and N loss reduction through trade in rice between N25I10 and baseline. N_w: N losses to water (Gg N yr^{-1}); N_t: N losses to the total environment (Gg N yr^{-1}). Arrows point to food exporting countries; blue beams represent increases in export-associated N losses and red beams show decreases in export-associated N losses in subplots a and c; blue beams represent increases in N loss reduction and red beams show decreases in N loss reduction in subplots b and d; the links with volumes less than 0.5% of global total are disregarded; numbers outside arcs show total volume of export-associated N losses and N loss reduction for major trading countries. Regions are defined in Tables S6-2 and S6-3.

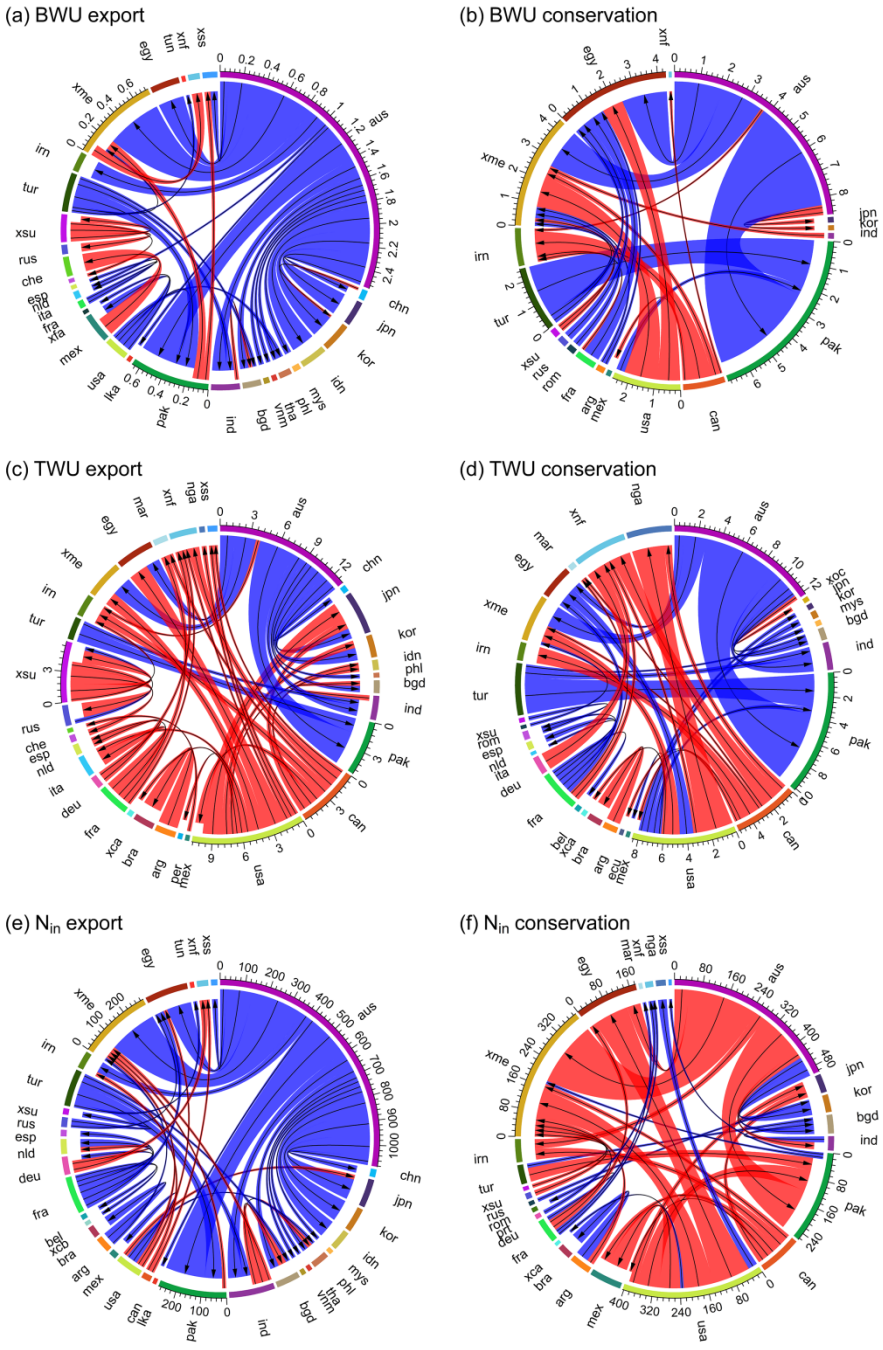

Figure S6-15. Differences of gross virtual resource export to importing countries and resource conservation through trade in wheat between N25I10 and baseline. BW: blue water (km^3 yr^{-1}); TWU: total water use (km^3 yr^{-1}); N_{in}: nitrogen inputs (Gg N yr^{-1}). Arrows point to food importing countries; blue beams represent increases in gross virtual resource export and red beams show decreases in gross virtual resource export in subplots a, c, and e; blue beams represent increases in resource conservation and red beams show decreases in resource conservation in subplots b, d, and f; the links with volumes less than 0.5% of the global total are disregarded; numbers outside arcs show total volume of export and conservation for major trading countries. Regions are defined in Tables S6-2 and S6-3.

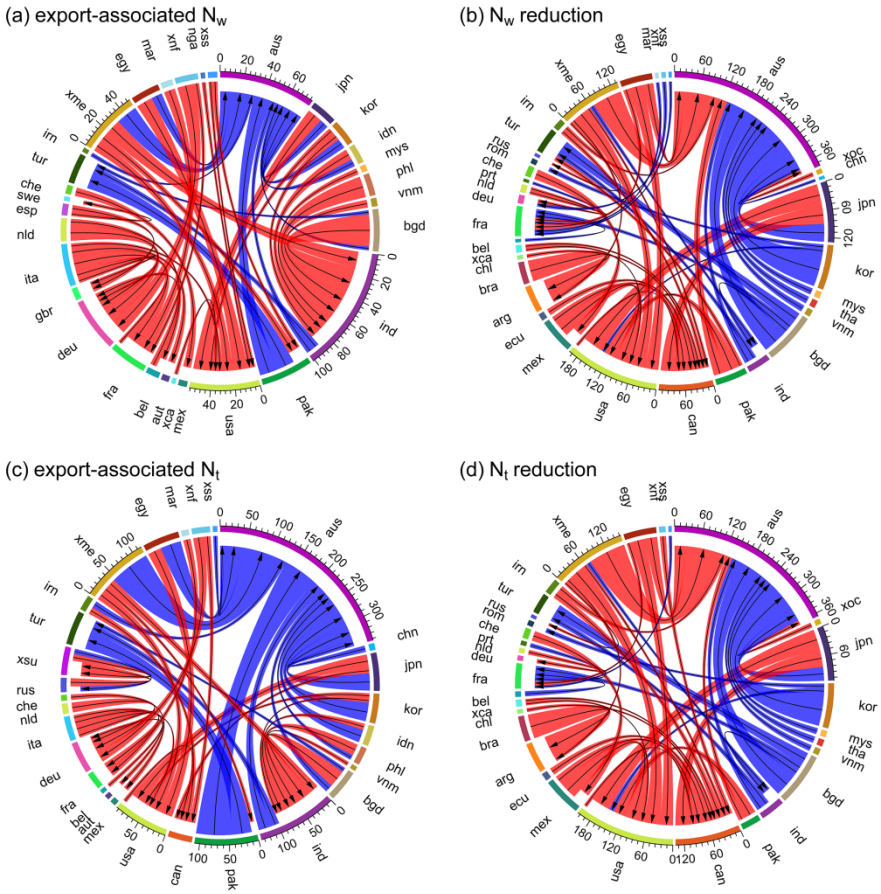

Figure S6-16. Differences of export-associated nitrogen (N) losses in exporting countries and N loss reduction through trade in wheat between N25I10 and baseline. N_w: N losses to water (Gg N yr^{-1}); N_t: N losses to the total environment (Gg N yr^{-1}). Arrows point to food exporting countries; blue beams represent increases in export-associated N losses and red beams show decreases in export-associated N losses in subplots a and c; blue beams represent increases in N loss reduction and red beams show decreases in N loss reduction in subplots b and d; the links with volumes less than 0.5% of global total are disregarded; numbers outside arcs show total volume of export-associated N losses and N loss reduction for major trading countries. Regions are defined in Tables S6-2 and S6-3.

Table S6-1. Description of the baseline and N25I10 scenario in terms of increasing nitrogen (N) inputs and irrigation (I) areas.

Scenario	N inputs	Irrigation areas	Rainfed areas
baseline	$N_{in\text{-}base}$	A_{ir}	A_{rf}
N25I10	$N_{in\text{-}base\text{-}limit} + 0.25\times\Delta N_{in}$	$A_{ir} + 0.10\times A_{rf}$	$0.9\times A_{rf}$

$N_{in\text{-}base}$ is actual N inputs based on the EarthStat dataset; $N_{in\text{-}base\text{-}limit} = \min(N_{in\text{-}base}, N_{in\text{-}base\text{-}max})$, where $N_{in\text{-}base\text{-}max}$ is maximum N inputs based on PEPIC simulation with baseline irrigation condition; $\Delta N_{in} = N_{in\text{-}full\text{-}max} - N_{in\text{-}base\text{-}limit}$, where $N_{in\text{-}full\text{-}max}$ is maximum N inputs based on PEPIC simulation with full irrigation condition; A_{ir} and A_{rf} are baseline irrigation and rainfed cultivation areas based on the MIRCA2000 dataset.

Table S6-2. Description of the 96 regions in the GTAP model.

Num.	Abb.	Name	Num.	Abb.	Name
1	aus	Australia	49	irl	Ireland
2	nzl	New Zealand	50	ita	Italy
3	xoc	Rest of Oceania	51	lux	Luxembourg
4	chn	China	52	nld	Netherlands
5	hkg	Hong Kong	53	prt	Portugal
6	jpn	Japan	54	esp	Spain
7	kor	SouthKorea	55	swe	Sweden
8	twn	Taiwan	56	che	Switzerland
9	xea	Rest of East Asia	57	xef	Rest of European Free Trade Area
10	khm	Cambodia	58	xer	Rest of Europe
11	idn	Indonesia	59	alb	Albania
12	mys	Malaysia	60	bgr	Bulgaria
13	phl	Philippines	61	hrv	Croatia
14	sgp	Singapore	62	cyp	Cyprus
15	tha	Thailand	63	cze	Czech Republic
16	vnm	Vietnam	64	hun	Hungary
17	xse	Rest of Southeast Asia	65	mlt	Malta
18	bgd	Bangladesh	66	pol	Poland
19	ind	India	67	rom	Romania
20	pak	Pakistan	68	svk	Slovakia
21	lka	Sri Lanka	69	svn	Slovenia
22	xsa	Rest of South Asia	70	est	Estonia
23	can	Canada	71	lva	Latvia
24	usa	United States of America	72	ltu	Lithuania
25	mex	Mexico	73	rus	Russian Federation
26	xna	Rest of North America	74	xsu	Rest of Former Soviet Union
27	bol	Bolivia	75	tur	Turkey
28	col	Colombia	76	irn	Iran
29	ecu	Ecuador	77	xme	Rest of Middle East
30	per	Peru	78	egy	Egypt
31	ven	Venezuela	79	mar	Morocco
32	arg	Argentina	80	tun	Tunisia
33	bra	Brazil	81	xnf	Rest of North Africa
34	chl	Chile	82	bwa	Botswana
35	pry	Paraguay	83	zaf	South Africa
36	ury	Uruguay	84	xsc	Rest of South African Customs Union
37	xsm	Rest of South America	85	mwi	Malawi
38	xca	Rest of Central America	86	mus	Mauritius
39	xfa	Rest of Free Trade Area of the Americas	87	moz	Mozambique
40	xcb	Rest of the Caribbean	88	tza	Tanzania
41	aut	Austria	89	zmb	Zambia
42	bel	Belgium	90	zwe	Zimbabwe
43	dnk	Denmark	91	xsd	Rest of Southern African Development Community
44	fin	Finland	92	mdg	Madagascar
45	fra	France	93	nga	Nigeria
46	deu	Germany	94	sen	Senegal
47	gbr	United Kingdom	95	uga	Uganda
48	grc	Greece	96	xss	Rest of Sub-Saharan Africa

Table S6-3. Definition of regions in the GTAP model.

Name	Countries
Rest of Oceania	American Samoa, Cook Islands, French Polynesia, Fiji, Federated States of Micronesia, Guam, Kiribati, Marshall Islands, Nauru, New Caledonia, Norfolk Islands, Northern Mariana Islands, Niue, Palau, Papua New Guinea, Samoa, Solomon Islands, Tokelau, Tonga, Tuvalu, Vanuatu, Wallis & Futuna
Rest of East Asia	Democratic People's Republic of Korea, Macau, Mongolia
Rest of Southeast Asia	Brunei Darussalam, Lao People's Democratic Republic, Myanmar, Timor-Leste
Rest of South Asia	Afghanistan, Bhutan, Maldives, Nepal
Rest of North America	Bermuda, Greenland, Saint Pierre & Miquelon
Rest of South America	Falkland Islands, French Guiana, Guyana, Suriname
Rest of Central America	Belize, Costa Rica, El Salvador, Guatemala, Honduras, Nicaragua, Panama
Rest of Free Trade Area of the Americas	Antigua & Barbuda, Bahamas, Barbados, Dominica, Dominican Republic, Grenada, Haiti, Jamaica, Puerto Rico, Saint Kitts & Nevis, Saint Lucia, Saint Vincent & the Grenadines, Trinidad & Tobago, USA Virgin Islands
Rest of the Caribbean	Anguilla, Aruba, Cayman Islands, Cuba, Guadeloupe, Martinique, Montserrat, Netherlands Antilles, Turks & Caicos, UK Virgin Islands
Rest of European Free Trade Area	Iceland, Liechtenstein, Norway
Rest of Europe	Andorra, Bosnia & Herzegovina, Faroe Islands, Gibraltar, Macedonia, Monaco, San Marino, Serbia & Montenegro
Rest of Former Soviet Union	Armenia, Azerbaijan, Belarus, Georgia, Kazakhstan, Kyrgyzstan, Moldova, Tajikistan, Turkmenistan, Ukraine, Uzbekistan
Rest of Middle East	Bahrain, Iraq, Israel, Jordan, Kuwait, Lebanon, Oman, Palestinian Territory, Qatar, Saudi Arabia, Syrian Arab Republic, United Arab Emirates, Yemen
Rest of North Africa	Algeria, Libya
Rest of South African Customs Union	Lesotho, Namibia, Swaziland
Rest of Southern African Development Community	Angola, The Democratic Republic of Congo, Seychelles
Rest of Sub-Saharan Africa	Benin, Burkina Faso, Burundi, Cameroon, Cape Verde, Central African Republic, Chad, Comoros, Congo, Cote d´Ivoire, Djibouti, Equatorial Guinea, Eritrea, Ethiopia, Gabon, Gambia, Ghana, Guinea, Guinea-Bissau, Kenya, Liberia, Mali, Mauritania, Mayotte, Niger, Reunion, Rwanda, Saint Helena, Sao Tome & Principe, Sierra Leone, Somalia, Sudan, Togo

Table S6-4. Global total resource consumption, nitrogen (N) losses, crop production, and gross food export for maize, rice, wheat, and sum of the three crops under the baseline and N25I10 scenario. BWU: blue water use; TWU: total water use; N_{in}: nitrogen inputs; N_w: nitrogen losses to water; N_t: nitrogen losses to the total environment; Prod: crop production.

Scenario	Variable	maize	rice	wheat	sum
baseline	BWU (km^3 yr^{-1})	57.1	45.8	63.9	166.8
	TWU (km^3 yr^{-1})	617.1	545.9	689.4	1852.4
	N_{in} (Gg N yr^{-1})	17867.8	20493.7	20919.4	59280.8
	N_w (Gg N yr^{-1})	6802.8	13653.1	8603.1	29058.9
	N_t (Gg N yr^{-1})	12454.6	17285.7	14288.4	44028.7
	Prod (Tg yr^{-1})	781.6	684.2	518.8	1984.6
N25I10	BWU (km^3 yr^{-1})	69.0	46.6	78.6	194.2
	TWU (km^3 yr^{-1})	629.7	546.8	704.9	1881.5
	N_{in} (Gg N yr^{-1})	23062.7	21138.9	25880.3	70081.8
	N_w (Gg N yr^{-1})	8323.8	13504.3	6220.0	28048.1
	N_t (Gg N yr^{-1})	15467.9	17719.6	13781.9	46969.4
	Prod (Tg yr^{-1})	949.6	764.0	727.1	2440.8

Table S6-5. Resource use intensities and nitrogen (N) loss intensities for maize under the baseline and N25I10 scenario. BWUI: blue water use intensity; TWUI: total water use intensity; $N_{in}I$: nitrogen input intensity; N_wI: water nitrogen loss intensity; N_tI: total nitrogen loss intensity; --: no information.

	BWUI (m^3 t^{-1})		TWUI (m^3 t^{-1})		$N_{in}I$ (kg N t^{-1})		N_wI (kg N t^{-1})		N_tI (kg N t^{-1})	
	baseline	N25I10	baseline	N25I10	baseline	N25I10	baseline	N25I10	baseline	N25I10
aus	688.0	289.0	1609.5	664.4	9.3	15.3	1.0	1.2	4.5	4.3
nzl	47.5	49.2	502.3	503.3	29.3	26.9	14.1	12.8	19.7	18.7
xoc	0.0	1.4	1869.9	610.1	2.0	16.4	25.4	10.1	31.8	13.5
chn	87.4	91.0	725.6	727.2	39.4	27.6	15.6	8.7	24.9	18.3
hkg	--	--	--	--	--	--	--	--	--	--
jpn	0.8	1.3	440.6	419.1	26.3	29.8	21.1	23.9	24.9	28.0
kor	0.0	0.0	402.0	400.0	30.7	33.7	17.6	22.7	21.1	26.4
twn	0.0	0.0	425.5	404.2	25.6	30.2	12.0	16.5	15.0	20.3
xea	0.3	0.2	612.7	435.0	19.8	20.7	13.4	13.4	16.6	16.0
khm	0.0	0.0	1369.7	799.9	11.2	22.9	10.3	13.8	16.6	20.1
idn	14.4	22.1	826.5	651.0	24.6	28.8	19.6	20.1	27.0	28.9
mys	0.0	2.8	941.1	635.0	18.2	26.2	18.9	17.1	24.7	23.8
phl	0.0	0.1	793.0	620.6	19.2	25.5	15.9	18.9	22.3	26.5
sgp	--	--	--	--	--	--	--	--	--	--
tha	0.0	0.2	809.1	695.9	19.7	25.1	7.7	11.1	15.0	20.0
vnm	0.8	1.6	686.3	654.2	31.3	35.9	15.9	22.0	22.4	29.9
xse	22.7	47.6	1072.0	749.4	21.1	33.8	25.0	21.2	35.1	33.5
bgd	0.0	0.0	911.0	711.9	28.0	33.6	35.6	35.7	44.0	43.8
ind	18.6	24.1	1000.0	811.1	20.4	25.7	9.3	10.4	17.0	19.5
pak	186.5	181.2	624.9	582.5	18.9	17.4	2.9	2.9	6.4	6.6
lka	0.0	6.3	1418.9	780.2	12.9	24.2	13.2	13.3	19.3	19.2
xsa	534.0	312.5	1599.9	927.9	14.3	22.1	12.4	12.1	17.8	17.6
can	5.9	16.3	476.4	473.9	27.0	29.6	13.2	16.6	19.8	23.2
usa	63.7	74.3	562.4	546.8	19.6	23.8	5.3	8.5	11.4	14.8
mex	65.6	56.8	900.5	717.2	23.7	27.4	11.2	13.2	18.1	20.9
xna	--	--	--	--	--	--	--	--	--	--
bol	30.4	20.3	2910.0	977.5	6.6	18.2	2.8	2.1	11.4	8.4
col	1.8	2.5	1000.2	668.8	18.1	26.0	15.5	17.3	20.6	23.3
ecu	59.4	60.6	816.9	718.3	26.6	28.5	27.2	31.2	35.7	40.6
per	95.0	81.5	803.8	659.4	20.6	21.6	9.7	7.8	17.0	15.5
ven	17.7	16.0	773.6	627.6	22.5	27.3	5.8	8.9	11.6	16.2
arg	5.9	13.0	1140.3	545.7	7.8	16.3	4.2	3.8	8.7	7.9
bra	0.5	7.2	1046.0	717.4	19.1	24.8	11.8	11.9	18.4	19.1
chl	345.9	348.8	486.2	486.7	29.0	25.4	10.3	7.8	16.1	14.0
pry	0.3	16.6	2859.9	1008.5	9.4	23.5	15.9	11.0	23.0	16.9
ury	12.6	15.5	1099.5	525.0	9.7	17.2	7.6	6.1	12.2	10.4
xsm	0.0	1.7	967.4	606.7	19.3	24.3	15.7	13.7	22.5	20.5
xca	0.7	1.4	830.6	613.3	21.4	31.0	20.8	26.9	24.9	31.4
xfa	5.0	10.0	1049.0	649.0	15.8	22.1	11.6	11.2	16.7	16.9
xcb	0.6	0.4	705.6	483.7	10.1	15.3	5.7	5.5	10.4	10.3
aut	0.1	1.8	450.1	451.1	21.5	22.5	7.8	9.8	13.4	15.3
bel	1.0	5.8	499.1	493.4	34.4	27.8	20.4	13.7	26.1	19.6

Table S6-5. Continued.

	BWUI (m^3 t^{-1})		TWUI (m^3 t^{-1})		$N_{in}I$ (kg N t^{-1})		N_wI (kg N t^{-1})		N_tI (kg N t^{-1})	
	baseline	N25I10	baseline	N25I10	baseline	N25I10	baseline	N25I10	baseline	N25I10
dnk	18.4	13.1	1049.8	619.3	0.0	8.4	1.8	1.7	9.8	7.8
fin	1.0	8.7	533.8	526.9	3.2	5.1	5.2	4.9	15.6	15.2
fra	43.1	49.4	471.2	456.0	26.0	27.9	9.2	11.1	14.2	16.4
deu	0.9	5.1	499.8	499.8	23.6	22.8	10.3	9.4	16.8	15.9
gbr	0.0	2.8	1170.7	607.1	0.0	8.3	3.8	2.2	11.3	6.8
grc	311.4	296.3	555.8	521.9	24.4	23.2	5.6	5.2	10.9	11.1
irl	0.0	0.0	999.7	742.3	0.0	5.3	6.8	5.0	14.2	11.3
ita	84.6	85.9	436.5	425.5	23.6	25.8	7.1	9.8	11.4	14.5
lux	0.0	12.2	491.7	491.5	40.4	32.9	20.7	13.8	25.5	18.5
nld	1.9	5.2	619.9	511.5	22.6	17.4	15.2	6.7	21.8	13.3
prt	367.9	257.3	698.1	480.9	17.7	18.8	5.0	3.7	9.1	7.8
esp	279.0	269.7	566.8	532.3	26.0	21.6	7.4	4.3	12.1	9.5
swe	5.9	3.3	1294.9	612.1	0.0	9.2	0.9	0.5	8.1	4.8
che	0.1	0.4	464.9	450.0	23.5	25.6	16.9	17.6	20.9	21.8
xef	--	--	--	--	--	--	--	--	--	--
xer	2.6	20.1	656.8	508.9	10.9	18.3	2.6	3.8	8.3	10.3
alb	366.8	302.2	958.8	772.6	22.9	28.6	4.6	7.2	12.0	16.7
bgr	56.6	92.9	1932.3	1195.6	9.7	28.0	3.7	4.3	23.6	23.1
hrv	0.6	22.5	948.8	821.6	24.9	32.1	7.5	11.1	16.5	22.0
cyp	837.7	373.9	1962.5	748.4	0.1	24.5	1.4	2.1	21.5	16.9
cze	0.0	3.7	501.6	499.5	15.3	18.5	3.3	5.6	9.9	12.0
hun	1.1	16.3	524.5	495.5	14.2	18.1	1.5	2.7	8.2	9.6
mlt	--	--	--	--	--	--	--	--	--	--
pol	1.8	7.4	526.6	513.6	16.2	15.4	6.3	4.5	13.5	11.6
rom	18.4	43.2	1096.0	892.5	14.8	23.0	3.9	4.7	16.3	18.7
svk	5.9	12.2	545.2	502.6	12.0	16.8	1.9	3.7	7.6	9.8
svn	1.3	5.2	450.7	451.3	27.0	28.0	12.6	15.7	17.6	20.8
est	8.5	14.7	893.5	632.4	2.4	9.1	2.4	2.2	9.5	8.1
lva	2.2	19.8	1294.9	1050.4	13.4	19.9	4.0	4.3	17.3	16.9
ltu	1.8	13.8	1335.7	1007.9	8.9	17.3	2.7	3.2	14.8	14.8
rus	87.1	99.2	1470.2	1125.4	6.4	17.8	3.0	3.4	19.6	18.1
xsu	278.3	238.9	1496.4	1142.5	12.4	20.6	2.4	2.6	18.2	16.9
tur	348.9	360.3	1198.8	1084.1	67.1	41.9	28.1	11.8	45.5	29.1
irn	1626.1	1344.3	2060.1	1694.3	24.2	19.4	3.6	1.2	12.3	9.9
xme	2193.3	1689.2	2643.4	2030.8	45.6	18.4	17.2	1.9	27.0	10.4
egy	1603.1	1172.5	1624.0	1187.7	70.9	32.3	14.7	0.4	33.2	13.6
mar	1551.2	781.0	2649.6	1296.9	18.6	22.8	1.6	1.3	18.1	13.0
tun	0.0	648.6	27602.9	3336.9	1.4	100.7	85.9	39.7	309.7	92.5
xnf	4556.2	1224.3	7955.8	2009.0	10.1	25.1	6.4	3.1	38.5	17.7
bwa	6.4	135.4	3117.6	1385.3	17.4	29.5	0.5	0.7	15.2	13.8
zaf	31.0	95.5	1702.0	1192.9	29.6	38.5	4.4	5.1	18.4	21.8
xsc	18.4	42.9	1954.2	1015.5	14.9	22.6	10.3	7.5	19.0	15.8
mwi	0.1	8.4	2049.8	783.9	9.2	20.6	3.8	2.9	10.0	9.8
mus	--	--	--	--	--	--	--	--	--	--

Table S6-5. Continued.

	BWUI (m^3 t^{-1})		TWUI (m^3 t^{-1})		$N_{in}I$ (kg N t^{-1})		N_wI (kg N t^{-1})		N_tI (kg N t^{-1})	
	baseline	N25I10	baseline	N25I10	baseline	N25I10	baseline	N25I10	baseline	N25I10
moz	2.8	7.7	2867.7	807.8	2.2	18.6	9.3	4.8	17.6	10.5
tza	24.5	51.5	2368.8	973.2	7.3	27.1	7.8	9.0	21.5	20.1
zmb	1.0	15.0	1712.8	765.1	8.2	20.2	4.7	3.8	12.3	11.5
zwe	12.1	46.0	1553.6	840.6	17.5	25.9	5.3	4.1	12.9	13.0
xsd	0.1	2.0	2080.3	681.9	2.0	16.9	4.3	2.9	13.1	9.4
mdg	0.0	3.6	2517.8	827.9	5.4	21.7	37.0	14.8	44.8	19.8
nga	0.5	2.6	1182.2	680.2	10.8	18.0	4.8	3.9	11.4	10.5
sen	3.8	5.4	1165.9	749.5	12.9	18.2	4.2	4.9	10.4	11.1
uga	0.0	6.4	1416.6	789.2	9.2	17.8	3.6	3.5	11.4	10.8
xss	54.4	59.0	1560.1	827.3	13.1	21.5	5.3	4.8	13.1	12.8

Table S6-6. Resource use intensities and nitrogen (N) loss intensities for rice under the baseline and N25I10 scenario. BWUI: blue water use intensity; TWUI: total water use intensity; $N_{in}I$: nitrogen input intensity; N_wI: water nitrogen loss intensity; N_tI: total nitrogen loss intensity; --: no information.

	BWUI (m^3 t^{-1})		TWUI (m^3 t^{-1})		$N_{in}I$ (kg N t^{-1})		N_wI (kg N t^{-1})		N_tI (kg N t^{-1})	
	baseline	N25I10	baseline	N25I10	baseline	N25I10	baseline	N25I10	baseline	N25I10
aus	1867.9	838.6	3210.6	1435.9	6.9	13.5	0.5	0.4	6.1	4.4
nzl	--	--	--	--	--	--	--	--	--	--
xoc	0.0	0.4	2251.6	1005.7	0.3	23.6	23.1	21.9	27.6	25.4
chn	61.5	61.6	695.0	693.3	49.0	36.5	35.6	25.2	42.3	32.2
hkg	--	--	--	--	--	--	--	--	--	--
jpn	7.1	6.7	637.8	635.0	42.7	35.5	38.8	31.8	44.8	37.8
kor	7.9	8.3	622.5	623.1	48.5	41.6	35.4	31.6	40.3	36.6
twn	0.7	1.0	695.2	612.7	26.5	28.1	13.6	13.6	17.4	18.0
xea	0.3	0.3	706.2	640.1	27.4	25.7	16.5	16.7	21.8	21.0
khm	16.2	16.5	1214.6	781.1	10.6	18.3	7.5	8.9	11.4	12.8
idn	1.3	1.2	717.8	603.0	20.8	24.7	16.0	17.8	20.7	22.9
mys	3.5	2.9	818.7	652.6	18.0	22.6	11.2	13.0	15.1	17.3
phl	0.4	0.4	1002.4	721.6	14.0	20.8	12.1	14.3	15.9	18.4
sgp	--	--	--	--	--	--	--	--	--	--
tha	2.1	2.7	786.7	679.5	15.5	19.8	6.4	8.9	10.7	13.7
vnm	0.0	0.0	689.4	657.4	27.8	29.4	18.6	19.8	24.0	25.6
xse	0.2	0.1	1206.6	789.9	10.0	24.2	17.8	22.9	21.9	26.6
bgd	0.0	0.0	711.8	671.2	27.1	29.3	22.6	24.2	27.4	29.6
ind	43.6	42.7	758.6	722.9	27.3	27.3	14.5	15.2	19.5	20.7
pak	945.1	923.3	1391.9	1359.4	26.3	17.9	3.0	1.0	9.0	6.2
lka	22.1	21.9	655.7	613.3	23.4	27.0	11.3	14.2	15.2	18.7
xsa	123.9	98.8	962.1	765.2	17.5	24.0	17.8	20.3	21.6	24.3
can	--	--	--	--	--	--	--	--	--	--
usa	285.3	280.1	782.7	767.4	25.7	28.6	6.0	11.1	11.2	17.0
mex	582.4	429.9	1485.0	1068.0	16.1	18.1	6.8	6.6	12.1	11.3
xna	--	--	--	--	--	--	--	--	--	--
bol	11.6	7.4	2516.1	929.4	0.9	13.2	3.0	2.6	8.4	6.0
col	17.9	15.1	745.7	612.6	18.7	23.1	13.9	15.4	17.4	19.4
ecu	5.7	5.5	740.5	615.0	15.6	20.0	17.2	17.2	21.4	22.0
per	363.3	303.8	889.4	735.4	16.1	17.4	9.6	8.9	14.5	13.7
ven	45.1	44.6	585.9	578.4	24.4	27.1	7.1	10.3	11.7	15.4
arg	126.6	80.0	1598.4	956.8	10.4	17.0	9.8	8.8	14.2	13.4
bra	23.1	21.1	1047.7	722.4	12.6	18.9	6.9	8.1	10.9	12.4
chl	621.0	586.6	889.0	839.5	18.1	20.7	4.3	5.8	9.8	12.7
pry	77.2	37.2	1798.8	898.7	7.9	17.8	6.6	5.1	10.2	8.5
ury	61.1	49.7	945.7	767.2	17.3	20.5	8.1	8.5	12.4	13.5
xsm	0.0	0.0	883.5	659.7	15.8	22.3	8.8	12.3	12.0	15.6
xca	14.2	10.6	795.2	627.7	23.0	26.3	22.5	22.2	27.6	27.4
xfa	63.0	54.7	681.6	582.8	17.4	20.9	4.3	6.1	7.9	10.6
xcb	0.0	5.4	789.0	732.6	22.0	25.3	8.1	11.4	13.6	17.8
aut	--	--	--	--	--	--	--	--	--	--
bel	60.4	31.8	1867.4	982.3	0.1	8.8	1.5	0.8	8.9	6.0

Table S6-6. Continued.

	BWUI (m^3 t^{-1})		TWUI (m^3 t^{-1})		$N_{in}I$ (kg N t^{-1})		N_wI (kg N t^{-1})		N_tI (kg N t^{-1})	
	baseline	N25I10	baseline	N25I10	baseline	N25I10	baseline	N25I10	baseline	N25I10
dnk	--	--	--	--	--	--	--	--	--	--
fin	--	--	--	--	--	--	--	--	--	--
fra	940.1	336.2	2801.7	1003.3	0.1	11.6	8.0	2.3	14.8	5.9
deu	62.8	29.6	1979.6	955.0	0.1	9.6	5.0	2.5	13.1	7.8
gbr	--	--	--	--	--	--	--	--	--	--
grc	466.0	430.2	849.0	783.4	17.5	20.1	1.7	4.1	7.0	10.5
irl	--	--	--	--	--	--	--	--	--	--
ita	175.6	155.4	763.4	676.4	22.0	23.2	6.5	7.8	11.7	13.0
lux	--	--	--	--	--	--	--	--	--	--
nld	--	--	--	--	--	--	--	--	--	--
prt	838.6	420.9	1694.2	845.2	4.9	12.3	6.0	2.9	12.3	7.4
esp	862.2	507.3	1486.7	875.2	9.4	13.3	1.6	0.9	7.0	5.1
swe	--	--	--	--	--	--	--	--	--	--
che	--	--	--	--	--	--	--	--	--	--
xef	--	--	--	--	--	--	--	--	--	--
xer	232.2	219.7	732.8	688.7	13.6	16.3	2.6	4.0	9.0	11.5
alb	285.2	260.7	712.9	651.6	14.1	19.8	1.3	3.9	5.5	9.9
bgr	174.0	176.5	726.6	721.8	24.7	22.7	8.3	7.3	16.0	16.0
hrv	--	--	--	--	--	--	--	--	--	--
cyp	--	--	--	--	--	--	--	--	--	--
cze	--	--	--	--	--	--	--	--	--	--
hun	66.7	69.2	731.8	733.8	18.5	17.6	5.0	5.0	14.1	14.2
mlt	--	--	--	--	--	--	--	--	--	--
pol	7.4	6.2	912.1	763.7	8.5	9.8	3.7	1.3	10.2	8.1
rom	264.6	226.9	994.0	842.6	8.4	10.7	1.2	1.2	8.6	8.6
svk	0.0	0.0	782.1	724.5	5.2	9.4	3.6	4.7	11.0	13.3
svn	270.6	107.4	2586.0	1082.3	0.1	12.6	27.6	9.9	34.4	14.1
est	--	--	--	--	--	--	--	--	--	--
lva	--	--	--	--	--	--	--	--	--	--
ltu	--	--	--	--	--	--	--	--	--	--
rus	501.2	355.2	1461.8	1016.6	6.0	9.1	4.3	2.0	12.8	8.7
xsu	1004.1	887.9	1359.3	1200.8	18.2	17.1	3.0	1.4	9.9	8.5
tur	933.1	612.9	1473.9	968.3	10.0	14.4	1.3	1.0	6.4	5.8
irn	1498.3	1249.0	1816.7	1514.2	17.1	14.9	2.4	0.8	9.0	7.2
xme	9550.5	9144.7	9925.8	9504.2	211.0	3.5	34.9	2.5	56.2	16.4
egy	916.9	907.7	940.5	931.1	28.9	22.5	0.9	0.4	10.4	8.7
mar	2611.0	1002.8	3348.7	1285.6	0.4	11.1	0.8	0.4	7.3	3.8
tun	--	--	--	--	--	--	--	--	--	--
xnf	0.0	363.1	2402.7	1817.6	19.9	17.3	10.6	8.5	38.7	30.9
bwa	1867.3	830.3	3609.5	1594.4	6.9	13.5	0.3	0.2	4.0	3.5
zaf	1602.6	1230.2	1989.0	1524.8	14.5	16.3	0.0	0.1	3.2	3.7
xsc	923.4	321.8	3472.5	1206.2	4.5	13.9	6.7	3.6	11.5	6.7
mwi	11.3	12.4	1260.5	746.9	12.3	19.4	3.9	4.9	7.0	8.7
mus	--	--	--	--	--	--	--	--	--	--

Table S6-6. Continued.

	BWUI (m^3 t^{-1})		TWUI (m^3 t^{-1})		$N_{in}I$ (kg N t^{-1})		N_wI (kg N t^{-1})		N_tI (kg N t^{-1})	
	baseline	N25I10	baseline	N25I10	baseline	N25I10	baseline	N25I10	baseline	N25I10
moz	17.1	8.6	2718.2	852.9	1.1	15.0	4.3	3.9	9.2	6.9
tza	217.7	112.5	2540.2	968.3	1.8	17.8	7.4	6.3	16.0	12.2
zmb	356.3	139.2	2544.3	965.6	1.6	14.4	3.3	3.3	9.2	7.4
zwe	410.5	175.7	2607.3	1110.0	7.1	17.3	6.3	4.6	10.4	8.5
xsd	45.8	25.5	1176.1	654.3	2.2	12.4	3.5	4.7	9.5	9.3
mdg	180.7	81.8	1925.2	888.3	5.4	17.7	21.5	14.7	26.4	18.3
nga	2.2	16.5	1430.2	763.0	7.2	16.7	4.5	5.6	9.5	10.0
sen	773.7	455.5	2216.4	1290.5	10.7	16.4	6.0	5.9	10.1	9.4
uga	0.0	0.7	1186.6	643.2	3.9	12.2	2.5	2.1	8.2	6.9
xss	188.4	107.9	1696.5	897.7	6.4	17.2	11.0	10.7	16.1	14.8

Table S6-7. Resource use intensities and nitrogen (N) loss intensities for wheat under the baseline and N25I10 scenario. BWUI: blue water use intensity; TWUI: total water use intensity; $N_{in}I$: nitrogen input intensity; N_wI: water nitrogen loss intensity; N_tI: total nitrogen loss intensity; --: no information.

	BWUI (m^3 t^{-1})		TWUI (m^3 t^{-1})		$N_{in}I$ (kg N t^{-1})		N_wI (kg N t^{-1})		N_tI (kg N t^{-1})	
	baseline	N25I10	baseline	N25I10	baseline	N25I10	baseline	N25I10	baseline	N25I10
aus	8.7	71.4	1633.9	972.3	30.6	41.1	3.2	3.7	15.0	15.6
nzl	0.0	3.1	764.6	554.0	40.4	40.8	21.8	17.3	28.1	23.5
xoc	0.0	1.8	3323.7	1080.5	0.1	32.5	56.1	21.3	67.5	26.3
chn	177.7	179.0	972.0	958.8	50.8	44.2	17.4	13.7	27.1	24.7
hkg	--	--	--	--	--	--	--	--	--	--
jpn	0.7	0.2	1023.4	738.7	47.9	47.3	41.8	30.9	49.6	38.5
kor	8.7	11.1	658.7	659.0	55.8	61.5	26.2	35.6	33.2	44.3
twn	--	--	--	--	--	--	--	--	--	--
xea	4.5	18.6	1396.4	974.6	14.0	22.8	7.5	3.9	18.0	11.7
khm	0.0	0.0	1353.7	1282.0	78.2	72.9	57.3	52.2	65.9	60.7
idn	--	--	--	--	--	--	--	--	--	--
mys	0.0	1.6	966.4	935.8	45.4	56.8	19.3	30.2	25.3	37.0
phl	--	--	--	--	--	--	--	--	--	--
sgp	--	--	--	--	--	--	--	--	--	--
tha	0.0	0.3	1190.0	1123.2	60.9	63.4	43.9	46.6	51.4	54.1
vnm	0.0	0.0	922.8	916.0	57.5	63.4	30.6	37.9	37.8	45.8
xse	6.3	4.0	2003.0	1119.1	11.2	35.0	45.7	35.1	55.0	41.3
bgd	0.0	0.0	1522.3	1499.8	61.8	67.4	56.9	65.4	67.2	75.9
ind	117.9	122.4	1770.3	1748.2	100.4	47.0	73.6	29.1	86.6	41.6
pak	1177.6	1163.9	2490.1	2448.6	192.1	31.6	81.1	7.0	96.9	22.2
lka	--	--	--	--	--	--	--	--	--	--
xsa	896.8	531.5	2655.5	1435.4	28.0	36.6	15.8	9.4	28.4	19.7
can	3.6	18.8	1085.1	877.7	19.8	26.2	1.6	1.7	11.6	11.3
usa	50.1	68.8	1406.4	1081.9	31.8	35.6	8.9	6.7	20.5	18.0
mex	685.9	571.0	1757.3	1475.2	54.6	29.1	27.0	7.8	38.6	16.7
xna	--	--	--	--	--	--	--	--	--	--
bol	0.0	18.5	3494.6	1118.4	2.4	26.3	10.2	4.5	21.6	9.4
col	0.0	0.0	1087.3	836.9	30.2	41.9	34.6	34.8	40.4	40.7
ecu	3.1	1.7	2502.9	1237.1	3.5	32.3	89.9	58.2	101.7	64.9
per	0.0	8.9	1203.1	767.8	19.2	28.3	13.0	10.2	19.4	15.9
ven	0.0	25.5	1534.2	1335.3	32.2	31.2	18.4	13.6	27.7	23.1
arg	1.3	5.3	1131.2	724.3	18.5	26.9	6.2	5.7	13.4	12.5
bra	0.2	1.0	1577.3	932.4	17.1	32.9	28.1	18.0	36.1	24.4
chl	330.7	197.8	1066.5	605.2	48.4	44.9	55.5	32.2	65.0	40.1
pry	0.0	0.4	2231.6	1075.1	14.8	32.4	41.0	16.2	48.7	21.0
ury	0.0	0.2	1042.1	905.8	28.4	38.7	15.3	19.5	22.9	29.0
xsm	--	--	--	--	--	--	--	--	--	--
xca	0.0	0.7	1888.0	1110.4	34.1	54.5	47.8	47.7	53.2	51.8
xfa	--	--	--	--	--	--	--	--	--	--
xcb	--	--	--	--	--	--	--	--	--	--
aut	0.1	4.3	845.2	630.1	39.8	39.0	19.8	12.1	27.9	21.5
bel	0.0	7.3	657.8	577.9	60.8	58.1	35.7	28.2	43.3	37.8

Table S6-7. Continued.

	BWUI (m^3 t^{-1})		TWUI (m^3 t^{-1})		$N_{in}I$ (kg N t^{-1})		N_wI (kg N t^{-1})		N_tI (kg N t^{-1})	
	baseline	N25I10	baseline	N25I10	baseline	N25I10	baseline	N25I10	baseline	N25I10
dnk	6.0	8.9	843.2	527.3	41.1	36.7	21.6	8.4	31.1	17.7
fin	0.0	2.9	792.9	651.6	41.4	39.1	27.4	20.5	42.8	34.9
fra	1.8	13.2	1180.5	644.0	34.2	36.1	15.4	9.9	23.1	16.6
deu	0.1	6.0	802.1	598.2	40.1	39.5	17.6	10.3	25.8	19.3
gbr	0.1	3.6	896.7	535.4	36.6	34.7	17.9	9.0	25.9	16.5
grc	13.3	19.9	992.9	580.6	31.8	32.5	13.8	6.7	21.5	13.5
irl	0.0	2.4	1086.4	565.5	47.6	40.9	32.0	15.2	39.7	21.0
ita	17.3	31.2	1080.3	652.3	39.1	42.8	17.2	11.8	26.4	21.8
lux	0.0	22.1	1218.1	652.1	54.3	42.3	27.8	11.4	34.5	18.4
nld	0.0	4.9	750.7	572.7	50.7	44.2	28.6	16.1	39.0	26.0
prt	115.9	117.7	1405.9	873.5	45.3	57.9	15.1	16.7	29.8	31.7
esp	19.8	29.4	820.9	574.2	30.7	33.6	6.3	4.0	13.6	11.8
swe	0.0	5.1	727.1	511.9	60.5	49.8	41.9	21.4	52.1	32.6
che	0.0	0.1	2090.7	878.7	88.0	48.1	116.2	51.1	124.4	56.4
xef	0.0	5.2	1056.3	545.1	94.2	53.2	107.3	41.7	123.6	54.3
xer	0.0	12.5	1535.8	788.6	24.7	31.0	11.1	6.5	21.5	14.5
alb	13.8	12.6	1114.4	558.4	40.0	36.7	31.9	15.2	38.1	20.6
bgr	3.3	15.3	1162.1	704.3	27.8	30.5	10.2	5.0	20.8	13.8
hrv	0.2	11.4	1545.9	846.4	37.5	40.6	20.8	16.8	28.6	23.5
cyp	1748.8	565.7	3321.4	1071.9	0.1	24.9	1.7	0.4	17.7	7.4
cze	0.0	2.9	862.5	596.8	37.0	35.9	16.4	7.4	24.6	16.0
hun	1.2	12.2	975.8	710.5	26.9	30.7	6.7	3.9	17.1	13.9
mlt	--	--	--	--	--	--	--	--	--	--
pol	0.2	6.6	988.4	614.3	33.1	34.5	16.5	8.0	27.0	17.2
rom	22.6	28.0	1602.4	836.6	18.2	25.9	7.0	3.6	18.4	11.7
svk	2.2	8.7	1203.8	663.7	31.8	32.2	18.3	6.8	28.1	14.6
svn	0.5	5.9	1364.3	841.1	50.1	48.7	38.3	28.3	45.8	35.6
est	0.0	4.1	1412.1	591.1	31.1	30.4	19.4	5.0	30.5	12.3
lva	0.0	6.3	2216.3	728.6	7.1	27.5	8.1	5.2	22.4	12.4
ltu	0.0	4.2	1863.3	691.0	15.3	27.3	10.3	4.1	22.3	11.1
rus	9.9	21.8	1523.0	962.7	10.4	25.0	3.4	3.7	16.4	14.7
xsu	99.4	85.5	1710.5	1045.8	15.3	24.9	3.3	2.2	17.9	14.1
tur	92.5	85.0	1514.7	867.8	39.1	40.7	14.4	8.3	26.2	19.0
irn	810.2	577.6	2239.3	1474.3	46.2	39.7	9.6	3.8	24.3	16.3
xme	1166.5	785.4	2271.5	1496.9	75.9	33.6	24.5	4.3	38.7	15.1
egy	964.2	935.7	1018.3	988.1	66.7	41.2	12.9	0.5	23.4	10.8
mar	181.0	144.2	1573.0	855.6	25.6	37.7	4.2	3.7	19.9	16.2
tun	72.7	90.9	1540.2	979.4	38.5	44.3	7.6	6.9	21.8	20.3
xnf	124.2	138.1	2437.1	1104.2	27.1	40.5	5.9	3.1	23.2	16.9
bwa	535.1	287.0	2713.9	1273.0	16.9	33.3	1.5	3.8	9.5	10.0
zaf	193.2	174.6	1366.4	904.2	31.1	37.0	7.0	6.0	17.1	16.7
xsc	49.9	45.9	1681.6	796.7	18.0	27.7	4.8	3.0	11.6	9.0
mwi	0.0	16.1	3938.1	1279.0	19.3	43.9	13.9	13.7	22.8	21.1
mus	--	--	--	--	--	--	--	--	--	--

Table S6-7. Continued.

	BWUI (m^3 t^{-1})		TWUI (m^3 t^{-1})		$N_{in}I$ (kg N t^{-1})		N_wI (kg N t^{-1})		N_tI (kg N t^{-1})	
	baseline	N25I10	baseline	N25I10	baseline	N25I10	baseline	N25I10	baseline	N25I10
moz	0.0	1.6	2852.3	1177.8	3.1	32.4	68.7	40.0	85.2	47.8
tza	0.0	8.0	2362.5	962.6	2.4	25.6	8.9	6.5	20.7	12.7
zmb	81.5	34.1	3002.7	1118.6	5.0	32.1	56.0	29.9	73.0	37.6
zwe	--	--	--	--	--	--	--	--	--	--
xsd	7.2	4.6	2966.6	1073.5	0.3	28.1	18.2	13.0	30.7	18.8
mdg	0.0	6.6	3907.3	1311.0	3.7	43.4	148.1	68.3	167.4	75.5
nga	68.2	30.7	3997.5	1590.8	4.5	27.7	7.6	9.3	16.2	13.5
sen	0.0	13.2	2758.3	1783.4	2.2	14.4	2.3	2.0	14.0	9.5
uga	0.0	4.8	3062.1	1112.7	0.9	23.3	6.6	3.5	17.3	8.8
xss	74.2	61.1	1477.3	916.4	23.5	37.3	8.0	11.4	15.4	18.3

Chapter 7

General conclusions and outlook

7.1 General conclusions

The major goal of this study was to analyse the global water–food–environment–trade nexus in the context of agricultural input intensification. With this aim, we developed and applied a grid-based crop model PEPIC, which facilitates the implementation of EPIC on large scales, and combined it with a global trade model GTAP for the analysis. The study explored the trade-offs between water consumption, nitrogen (N) losses, and yields for the baseline of the year 2000 and several agricultural intensification scenarios regarding irrigation and N managements, and analysed the impacts of global food trade on resource conservation and pollution reduction.

The PEPIC model was first used to investigate uncertainties associated with the selection of five different potential evapotranspiration (PET) estimation methods in simulating crop–water relations. For the first time it showed that the choice of different PET estimation methods can lead to significant uncertainties in simulating crop–water relations globally. These impacts were particularly high for water-related variables, but less on crop yields, mainly because crop yields are indirectly linked to the PET estimation. The uncertainties related to the PET methods differed with water availability. The understanding of these uncertainties is particularly important for projecting impacts of future climate change on water and food security, where PET is the basis for the projection. Generally, using the Penman–Monteith estimation method, the PEPIC model provided the best crop yields estimates relative to statistics. Therefore, the Penman–Monteith method was also used in the following sections of the study.

Global crop-specific assessment showed that total N losses to the environment reached 44 Tg N yr^{-1} in 2000 for the three major crops—maize, rice and wheat—with two-thirds of these being lost to water bodies. N losses were found to be concentrated in some hot-spot regions for certain crops, e.g. China and the USA for maize, and China and India for rice and wheat. At the country level, N loss intensity—a ratio of N losses to crop yields—demonstrated substantial variations, indicating potentials to reduce N losses and increase crop yields through redistributing N inputs and avoiding N over-use. For lowest performing countries, there were high potentials to increase

crop yields through applying more N inputs, particularly in Africa. It highlights the importance of input intensification for the under-performed regions.

The grey water footprint (GWF) is an indicator of water pollution intensity. In this study, the agricultural GWF was calculated using N and phosphorus (P) loads to water caused by global maize cultivation. The GWF for P was much higher than that for N, which was mainly because P-related water quality standards are far more stringent than those for N. Assessment of grey water stress showed that GWF related to N and P loads from maize cultivation alone has exceeded local water availability in many parts of the world, especially in the north-eastern parts of China and north central parts of the USA, indicating serious degradation of water quality. This assessment showed that crop production not only directly consumes a large amount of water resources, but also causes water pollution, which requires substantial water resources to dilute the polluted water to meet the ambient water quality standard. The GWF expresses water pollution in terms of water volume needed to dilute contaminated water to a given quality standard, so that it can be compared with water consumption. However, more effort is needed to standardise this methodology.

After assessing the global N losses and crop yields trade-offs for the three major crops, potentials in yield achievements and possible changes in N losses were investigated for five agricultural intensification scenarios regarding increased irrigation areas and N inputs. It was found that increases in crop yields and N losses were particularly high in the southern hemisphere, due to their low irrigation and N inputs under the baseline. On the other hand, yields presented minor benefits in high resource application regions with large incremental N losses relative to N input additions. These high input regions generally have achieved a high level of agro-climatic yield potentials under the baseline. Hence, avoiding intensification in these high yield regions can significantly alleviate N losses and crop yields trade-offs. For instance, by only intensifying regions with baseline yields lower than 75% of yield potentials, relative increases in N losses can be reduced by 3–193%, while relative increases in yields will only decrease by 1–23%.

The last part of the study demonstrated that global food trade provided positive influences on the environmental impacts of crop production. Global agricultural resources conserved 85 km^3 yr^{-1} of blue water use, 105 km^3 yr^{-1} of total water use, and 2333 Gg N yr^{-1} of N inputs for the three major crops. Conservation in blue water use was particularly high, accounting for more than 50% of total blue water use for the three crops. In addition to resource conversation, substantial N losses were also reduced due to food trade, reaching about 1923 and 2210 Gg N yr^{-1} for N losses to water and the total environment. These benefits of global food trade were because resource use intensities and pollution intensities were generally lower in major food exporting countries than most food importing countries. However, global food trade also resulted in substantial resource

losses and export-associated N losses for the food exporting countries, especially in the USA. The GTAP model was used to simulate the trade patterns under an agricultural intensification scenario, in which particularly low-input countries under the baseline enhance crop yields by increasing N and irrigation inputs. It suggests that global resource conservation and N loss reduction would decline, due to converging resource use and N loss intensities across countries. Agricultural intensification can increase global food supply but compromise the benefits of global food trade in terms of water conservation and N loss reduction.

7.2 Limitations

Due to time constraints, only three major crops, i.e. maize, rice and wheat, were included for the analysis in the study. Although these three crops play a dominant role in providing dietary calories (62%), and consuming N inputs (61%) and irrigation water use (70%) of the 17 most commonly produced crops (West et al., 2014), more crops should be considered in future research. For example, another 10% of total N inputs for the 17 crops were applied to barley and soybean and about 20% of additional global irrigation water use was consumed by cotton and sugarcane. Including these crops can give a more complete picture of global agricultural challenges and hence help to propose effective mitigation strategies.

Limited by the crop-specific data availability, such as nutrient inputs (Mueller et al., 2012; West et al., 2014), irrigated and rainfed cultivation areas (Portmann et al., 2010), and crop planting and harvesting dates (Sacks et al., 2010), the analysis in the study was based on the year 2000. This is actually a general limitation for the current global large-scale crop modelling (Müller et al., 2017). There have been increasing global N inputs (Liu et al., 2016) and expanding irrigated areas (Alexandratos and Bruinsma, 2012) in recent years, implying more serious challenges faced with agriculture to date. There is an urgent need to update the analysis to a more recent timeline, e.g. 2010 or even 2015. It, therefore, calls for actions to share and develop more detailed crop-specific input database for supporting global large-scale crop simulations. The EarthStat database (http://www.earthstat.org), which provides a large number of basic agricultural input datasets, is one of the excellent examples. But much more effort is still required to overcome the data constraints.

Another significant environmental impact of agricultural production—greenhouse gas (GHG) emissions (Parton et al., 2015)—is not considered in this study. This is mainly due to the fact that simulation routines related to GHG emissions are not included in the public version of the EPIC model (Gerik et al., 2015). Recent efforts have focused on developing new routines for EPIC to estimate GHG emissions, such as CO_2, CH_4, and N_2O (Izaurralde et al., 2012). An integrated

investigation of influences of agricultural production on water pollution and climate change can provide a complete view of agricultural environmental impacts. Therefore, GHG emissions should be explicitly considered in further research when the new version of EPIC is available.

7.3 Outlook

Looking forward, there are three ways that could further strengthen our abilities to investigate the agricultural trilemma using large-scale crop models: comprehensive evaluation of model performance, determining N inputs trough balancing N uptakes and N losses, and adopting alternative cropping systems, e.g. integrated production (IP) systems (Figure 7-1).

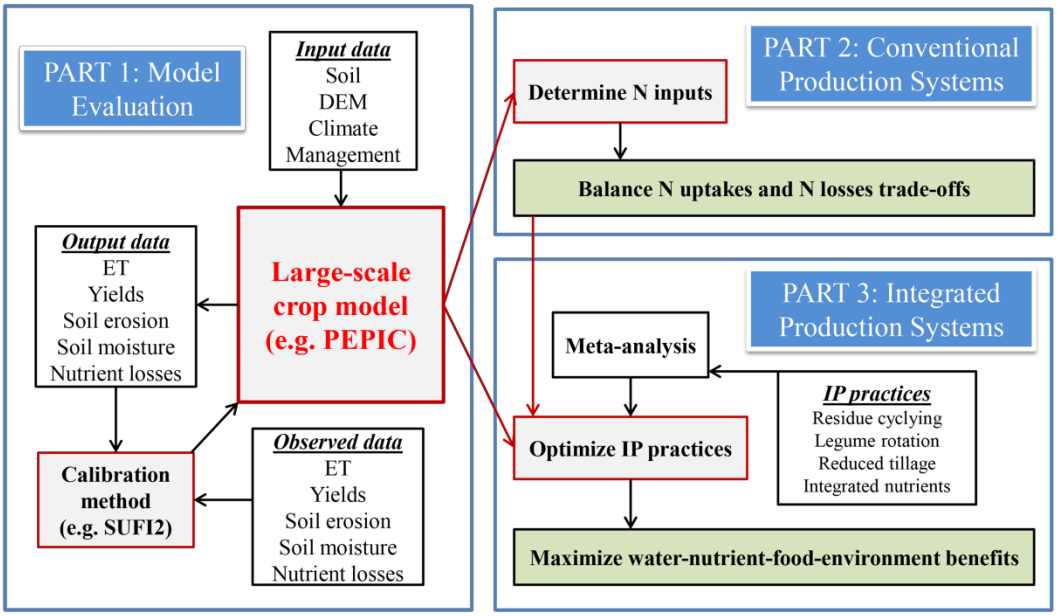

Figure 7-1. Conceptual framework for the future research.

Currently, large-scale crop models have been mainly evaluated by comparing estimated yields at national or sub-national scale with statistical data (Balkovič et al., 2013; Deryng et al., 2011; Folberth et al., 2012). The ability of large-scale crop models to predict other target variables or to simulate processes such as ET, soil moisture and erosion, and nutrient dynamics, was rarely tested against observed data, due to lack of reported spatial data. In order to provide a robust research tool, it is important to conduct a comprehensive calibration and validation of large-scale crop models on simulating multiple processes and variables related to environmental impacts by adopting an automatic calibration method (Abbaspour, 2011).

In addition to avoiding over-use of N, redistributing global N inputs patterns, and intensifying N through a more efficient pathway, there is another strategy for addressing N challenges: determining N inputs by simultaneously balancing N uptakes and N losses and

thereby optimizing trade-offs. Three steps are involved in obtaining the balanced N inputs: 1) applying N inputs with an incremental step, saying 5, 10, 15, … kg N ha^{-1}; 2) drawing response curves of N uptakes and N losses relative to N inputs; 3) deriving the balanced N inputs when marginal increase of N uptakes ($MarN_{up}$) equals to marginal increase of N losses ($MarN_{loss}$) from the response curves. This way of estimating the balanced N inputs is based on the idea that when N inputs exceed the balanced level, more N will be lost to environment other than being uptake by crops. It should be noted that yields obtained using this method may be lower than actual yields in some regions, due to currently excessive N application. In order to ensure sufficient food supply, maintaining a minimum level of current high yields should also be considered before adopting the strategy for determining the balanced N inputs.

This study mainly focused on conventional production systems, which rely on extensive external inputs, e.g. water, nutrient, and pesticides. Besides conventional cropping systems, a number of alternative cropping systems are being developed all over the world to address the agricultural challenges, particularly IP systems. IP systems use a variety of crop management practices, e.g. crop residue utilization (Turmel et al., 2015), conservation tillage (Van den Putte et al., 2010), legume-based crop rotation (Reckling et al., 2016), and integrated nutrient management (Wu and Ma, 2015). IP systems can refer to a variety of production systems, e.g. low-input production systems (Giuliano et al., 2016), legume-based cropping systems (Drinkwater et al., 1998), biologically diversified farming systems (Kremen and Miles, 2012), and eco-efficient agriculture (Keating et al., 2010). It is not clear what sorts of crop management practices and regions are most or least beneficial for adopting the IP systems on a global scale. Hence, a meta-analysis can be employed to identify the most commonly used IP practices. Then, a robust large-scale crop model can help to determine the potentials of the IP practices on maximizing global water–nutrient–food–environment benefits. Although it is still a big challenge to simulate detailed IP systems on a global scale, it should be one of the major research directions in the future.

7.4 References

Abbaspour, K.C., 2011. SWAT–CUP: SWAT calibration and uncertainty programs, Eawag, Dübendorf, Switzerland.

Alexandratos, N. and Bruinsma, J., 2012. World agriculture towards 2030/2050: the 2012 revision, ESA Working paper Rome, FAO.

Balkovič, J. et al., 2013. Pan-European crop modelling with EPIC: Implementation, up-scaling and regional crop yield validation. Agric. Syst., 120: 61–75.

Deryng, D., Sacks, W.J., Barford, C.C. and Ramankutty, N., 2011. Simulating the effects of climate and agricultural management practices on global crop yield. Global Biogeochem. Cycles, 25: GB2006.

Drinkwater, L.E., Wagoner, P. and Sarrantonio, M., 1998. Legume-based cropping systems have reduced carbon and nitrogen losses. Nature, 396(6708): 262–265.

Folberth, C., Gaiser, T., Abbaspour, K.C., Schulin, R. and Yang, H., 2012. Regionalization of a large-scale crop growth model for sub-Saharan Africa: Model setup, evaluation, and estimation of maize yields. Agric. Ecosyst. Environ., 151: 21–33.

Gerik, T. et al., 2015. EPIC User's Manual Version 0810, Blackland Research and Extension Center, Temple, Texas.

Giuliano, S. et al., 2016. Low-input cropping systems to reduce input dependency and environmental impacts in maize production: A multi-criteria assessment. Eur. J. Agron., 76: 160–175.

Izaurralde, R.C., McGill, W.B. and Williams, J.R., 2012. Development and application of the EPIC model for carbon cycle, greenhouse gas mitigation, and biofuel studies, Managing Agricultural Greenhouse Gases, pp. 293–308.

Keating, B.A. et al., 2010. Eco-efficient Agriculture: concepts, challenges, and opportunities. Crop Sci., 50(2): S109–S119.

Kremen, C. and Miles, A., 2012. Ecosystem services in biologically diversified versus conventional farming systems: benefits, externalities, and trade-Offs. Ecol. Soc., 17(4): 40.

Liu, W. et al., 2016. Global assessment of nitrogen losses and trade-offs with yields from major crop cultivations. Sci. Total Environ., 572: 526–537.

Mueller, N.D. et al., 2012. Closing yield gaps through nutrient and water management. Nature, 490(7419): 254–257.

Müller, C. et al., 2017. Global gridded crop model evaluation: benchmarking, skills, deficiencies and implications. Geosci. Model Dev., 10(4): 1403–1422.

Parton, W.J. et al., 2015. Measuring and mitigating agricultural greenhouse gas production in the US Great Plains, 1870-2000. Proc. Natl. Acad. Sci. U.S.A., 112(34): E4681–E4688.

Portmann, F.T., Siebert, S. and Doll, P., 2010. MIRCA2000–Global monthly irrigated and rainfed crop areas around the year 2000: A new high-resolution data set for agricultural and hydrological modeling. Global Biogeochem. Cycles, 24: GB1011.

Reckling, M. et al., 2016. A cropping system assessment framework-Evaluating effects of introducing legumes into crop rotations. Eur. J. Agron., 76: 186–197.

Sacks, W.J., Deryng, D., Foley, J.A. and Ramankutty, N., 2010. Crop planting dates: an analysis of global patterns. Global Ecol. Biogeogr., 19(5): 607–620.

Turmel, M.S., Speratti, A., Baudron, F., Verhulst, N. and Govaerts, B., 2015. Crop residue management and soil health: A systems analysis. Agric. Syst., 134: 6–16.

Van den Putte, A., Govers, G., Diels, J., Gillijns, K. and Demuzere, M., 2010. Assessing the effect of soil tillage on crop growth: A meta-regression analysis on European crop yields under conservation agriculture. Eur. J. Agron., 33(3): 231–241.

West, P.C. et al., 2014. Leverage points for improving global food security and the environment. Science, 345(6194): 325–328.

Wu, W. and Ma, B.L., 2015. Integrated nutrient management (INM) for sustaining crop productivity and reducing environmental impact: A review. Sci. Total Environ., 512: 415–427.

Acknowledgements

Time finally goes to the end of my PhD study in Switzerland. After crossing a number of research mountains during the past four years, I am very grateful to many people.

First and foremost, I would like to express my sincerest gratitude to my supervisor Prof. Hong Yang for giving me the opportunity to work on this project. I appreciate your generosity for allowing me to work with freedom. You guided me as to how to work as a scientist and how to write a scientific paper in a logic and systematic way. It is a treasure that I will benefit from for the whole of my academic career. I was deeply impressed by your selfless support in my personal life. I am very grateful to my supervisor at ETH Zurich—Prof. Rainer Schulin. Without your insightful guidance and contribution, this study would not have been possible. I also thank you for your kindness in supporting me in applying for research funding from different sources.

I'd like to thank Dr. Karim C. Abbaspour for your great help in solving many technical issues and valuable discussions in writing scientific papers. I also thank Dr. Michael Obersteiner for serving as an external examiner and dedicating your precious time to reading this dissertation and attending my defence. Thanks also go to Prof. Emmanuel Frossard for chairing the defence despite your busy work schedule.

I would like to thank many other scientists. Dr. Christian Folberth provided valuable suggestions on developing the PEPIC model and writing scientific papers. Dr. Xiuying Wang answered many specific questions regarding the EPIC model. Prof. Zongxue Xu and Prof. Junguo Liu are acknowledged for helpful discussions during the project. I thank Dr. Marta Antonelli, Dr. Ligia B. Azevedo, Prof. Arjen Y. Hoekstra, Dr. Matti Kummu, Dr. Qunying Luo, Dr. Xingcai Liu, Dr. Yu Liu, and Dr. Christoph Müller for providing valuable inputs in preparing research papers. In addition, I'd like to thank Dr. Juraj Balkovič and Dr. Rastislav Skalský for giving me helpful support during my attendance at the Young Scientists Summer Program at IIASA.

I would like to thank EAWAG for funding this PhD project. The World Food System Center at ETH Zurich is appreciated for providing me with the Ambassadors award to visit IIASA. I also thank the Swiss Society of Hydrology and Limnology for supporting me in presenting the research findings from the PhD project at the 8th International Congress on Environmental Modelling and Software at Toulouse, France.

I would like to thank my office mates Dr. Jonas Šukys, Dr. Xu Zhao, Dr. Dong Hua, and Prof. Hamid Reza Moradi for providing a nice working atmosphere and interesting discussions. I also thank all other colleagues at SIAM department. I appreciate Lorenz Ammann for translating the summary of this dissertation and Karin Ghilardi for managing all administration issues. The IT support of EAWAG, especially from Canan Aglamaz and Franz Werder, is acknowledged. I thank the Hypatia cluster team at EMPA, Dr. Daniele Passerone and Patrik Burkhalter, for extensive support with running the simulations.

I would like to thank all the Chinese friends I met here: Yang Yue, Xinping Luo, Jun Zheng, Tianyun Huang, Xiaomei Li, Yigang Yan, Xu He, Pu Shi, Huifang Ma, Yaohui Bai, Yujie Men, Shiyong Wang, Jia Liu, Zhengqian Liu, An Ding, Suxiao Li, and Fan Fu, among others. I really appreciate the good time with all of you. There are a lot of precious memories.

Last but not least, I want to thank my family and friends for providing generous support during the last 30 years. Especially my grandma, I miss you. It is a tough road towards a PhD degree. I would like to express the deepest gratitude to my wife—Yang Bai. Without your understanding and support, I could not make such a big difference.

前路漫漫，吾将求索！

Dübendorf, Switzerland

14.08.2017